Assessing the Impact of Benzalkonium Chlorides on the Gut Microbiome and Liver Metabolism

Vanessa Andrea Lopez

A dissertation submitted in partial fulfillment of the requirements for the degree of:

Doctor of Philosophy

University of Washington

2024

Reading Committee:

Libin Xu, Chair

Julia Y. Cui

Rheem A. Totah

Program Authorized to Offer Degree:

Medicinal Chemistry

University of Washington

Abstract

Assessing the Impact of Benzalkonium Chlorides on the Gut Microbiome and Liver Metabolism

Vanessa Andrea Lopez

Chair of the Supervisory Committee:

Libin Xu

Medicinal Chemistry

Benzalkonium Chlorides (BACs) are highly effective disinfectants, widely used in consumer, clinical, food processing and agricultural settings. Recently, the Food and Drug Administration (FDA) called for additional safety data on BACs. Additionally, the recent COVID-19 pandemic has resulted in increased concentrations of BACs being detected in human blood samples as well as residential dust samples. Importantly, environmental toxicant exposure and the effects on the resident gut microbiome is becoming increasingly recognized as a unique mechanism of understanding human health and disease. The gut-liver axis is a unique, bidirectional link that has become recognized for the role it has in liver disease and impairment of liver function. We hypothesize is that exposure to BACs can impact the resident microbiome, which will lead to alterations in transcriptomic, sterol, lipid, and xenobiotic metabolism of the liver. In this dissertation, I describe a comprehensive animal study that elucidated BAC exposure effects on gut

microbiome composition and diversity, unconjugated bile acid (BA) pools in biological extracts, and BAC and BAC metabolite profiles. Additionally, I report a thorough and comprehensive quantitation analysis of BAC and BAC metabolite distribution throughout brain, lung, blood, spleen, kidney, liver, duodenum, jejunum, ileum, large intestine, feces and urine in male and female BAC exposed mice. Next, I share a comprehensive multiomics analyses of BAC-induced changes to endogenous and exogenous metabolism in livers of BAC exposed mice including transcriptomics, sterolomics, lipidomics and cytochrome p450 activity. Finally, I conclude with overall conclusions and implications of this work, and provide insight into future studies that should be conducted. Together, this dissertation provides a comprehensive and rigorous comprehension of environmental toxicant exposure risk to human health by elucidating mechanisms by which BAC-exposure disrupts gut microbiome composition and diversity, and endogenous and exogenous metabolism in the liver.

Acknowledgements

Thank you Libin for believing in my potential, and for your mentorship. Thank you for supporting my interests and providing me the best opportunities to grow as a public speaker, a writer, a mentor, a scientist and a leader. I couldn't have been felt more grateful when I was able to join the BAC project. Studying environmental toxicant exposure was exactly what I wanted to do. Thank you for supporting my development as a toxicologist and thank you for believing in my dreams of staying in academia.

Thank you to my reading committee members Julia and Rheem. I was ecstatic to ask you two to read, give commentary and a close eye on my thesis. I have admired you both for your rigorous science, and professorship, I am so honored this work has your close attention. Thank you also, to my committee members Kelly, Shijie and the late Qingcheng. I have learned so much from you.

Thank you to the incredible lab members of the Xu lab; past and present, Hideaki, Kelly, Josi, Amy,Quynh, Dylan, Emily, Marie, Noelle, Ryan N. Linxi, Tianwei, and especially Ryan S. I am eternally grateful to have spent the last 6 years of work in the lab with you all. Thank you for all the hours we've spent in lab together, the walks around the department when we need a break (Marie), the talks, the group meetings, the laughs, the happy hours, the conversations; all of it.

Thank you to my undergrads Gabby and Sydney. Thank you for trusting me as your mentor for your first lab experiences. You have made the experiments more fun, and I look back on all of our days together with so much joy and nostalgia.

Thank you to the faculty and staff of the MedChem department. Thank you Abhi for recruiting me at SACNAS in 2017, my life changed that day. Thank you Bill for run ins in the hallway and

for always asking how I'm doing. Thank you Sarah Lenti for being a constant the past 6 years, you make the department so much brighter.

Thank you Sally, I am thanking the stars everyday that I had you throughout grad school. I will miss peeking into each others labs to see if we were busy, the lunch times together, the talks that lasted hours, the laughs, the walks, all of it. Thank you for your continued friendship. My Seattle sister.

Thank you Ryan Seguin. The first person and last person I worked with. You have made me a better scientist. Thank you for your continued mentorship, friendship, laughs, and advice. I have treasured our time together and our shared perspectives. May the seagulls forever be looking over us.

Thank you to my former teachers and mentors. Mr. Wulff, Dr. Wyels, Dr. Hampton and Dr. Awad. Thank you for seeing potential in me, for your continued support, for believing in me and for giving me so much confidence to dream big. Thank you, thank you, thank you.

Lauren, thank you for being part of my chosen family here in Seattle. Meeting you made my life in Seattle complete. Thank you for your consistency, devotion and commitment to our friendship.

Lourdes, thank you for your cooked meals, suggestions of background noise, accommodations to my stressed self, and continued support throughout this journey. Thank you for your company when I'm nervous and for listening to my practice talks…even if you fall asleep.

My family, thank you for your continued support. I miss seeing most of you every weekend, but I get through when I remember just how proud and happy you are. Thank you Araceli for challenging me to dream big, thank you Tio Ramon for your consistency in showing up for me, thank you Tio Mando for always motivating me to dream bigger (I will always cherish seeing

you every weekend and telling you how college was that week), thank you Tia Luz and Carla for always seeing my potential, wanting the best for me and for your support, thank you Tio Chavo for being so supportive when I was deciding to come to UW, thank you Arianna, Alex, Joe, Piri and Mandito for encouraging me during every point of this journey.

Gracias Abuelita y Abuelito por su amor y bendiciones. Siempre tendre tus ultimas palabras para mi antes de irme. “Buena suerte buen furturo y que Dios te cuide”

Especially thank you to my mom, dad and sister. Mom, thank you for being so supportive of me coming to Seattle, even when I know it was hard. Thank you for being the best role model of being a Latina in stem. Thank you for always texting me to see how my days were going. Thank you for always finding the way to visit for my birthday. Nan, I could not have had this journey without you. Thank you for visiting me every 3 months the past 6 years. Thank you for the weekly phone calls. Thank you for coming when I asked for specific dates that I knew I’d be stressed during. Thank you for believing in me and for never letting me forget it. T, thank you for your visits to Seattle. Thank you for rooting for me always. Thank you for lifting me up when times got hard and for making sure I always remembered to have fun.

Sammy, thank you for being the most unexpected but heaven-sent blessing. You are the light of my life, I can’t wait to see what the next chapter of our life brings.

Table of Contents

Abbreviations	
Acyl CoA Cholesterol Acyltransferases	ACAT
Acute-on-Chronic Liver Failure	ACLF
Acetonitrile	ACN
Atherosclerotic Cardiovascular Disease	ACVD
Atopic Dermatitis	AD
Aryl Hydrocarbon Receptor	AhR
Acetaminophen	APAP
Apical Sodium Dependent Bile Acid Transporter	ASBT
Bile Acid-CoA	BAAT
Benzalkonium Chlorides	BACs
Bile Acids	BAs
Bile Salt Export Pump	BSEP
Bile Salt Hydrolase	BSH
Collision Gas	CAD
Constitutive Androstane Receptor	CAR
Chenodeoxycholic Acid	CDCA
Collision Energy	CE
Ceramide	Cer
Chronic Heart Failure	CHF
Chronic Kidney Disease	CKD
Coronavirus Disease 19	COVID-19
Colorectal Cancer	CRC
Curtain Gas	CUR
Collision Cell Exit Potential	CXP
Cytochrome P450	Cyp
Cytidine Diphosphate	CDP
Deoxycholic Acid	DCA
Diacylglycerol-O-acyltransferases	DGATs
Dehydrocholesterol	DHC
Dehydroxysterol Reductase	DHCR
Dehydrodesmosterol	DHD
Diacylglycerol	DAG
Drug Metabolizing Enzymes	DMEs
Declustering Potential	DP
Dextrorphan	DXO
Entrance Potential	EP
Environmental Protection Agency	EPA
Electrospray Ionization	ESI

Fatty Acids	FAs
Food and Administration	FDA
Flavin-Containing Monooxygenases	FMO
Farnesoid X Receptor	FXR
Gastrointestinal	GI
Glucosylceramide	GlcCer
Gene Ontology	GO
Ion Source Gas 1	GS1
Ion Source Gas 2	GS2
Glutathione	GSH
Glutathione-S-transferases	GSTs
Hepatocellular Carcinoma	HCC
Hydrophilic Interaction Liquid Chromatography	HILIC
3-Hydroxy-3-Methylglutaryl Coenzyme A Reductase	HMGCR
Hydroxysteroid Dehydrogenases	HSDHs
Ileal Bile Acid-Binding Protein	IBABP
Inflammatory Bowel Disease	IBD
Irritable Bowel Syndrome	IBS
Immunoglobulin A	IgA
Interleukin	IL
Ion Spray Voltage	IS
Internal Standard	IS
Lauric Acid	LA
Liquid Chromatography	LC
Lithocholic Acid	LCA
Low-Density Lipoprotein Receptors	LDLR
Low-Density Lipoprotein Receptor	LDLR
Lowest Observable Adverse Effect Limit	LOAEL
Lipopolysaccharide	LPS
Liver X Receptors	LXR
Lysophosphatidylcholine	LPC
mass-to-charge	m/z
Microbial-Associated Molecular Patterns	MAMPs
Muricholic Acid	MCA
Midazolam	MDZ
Methanol	MeOH
Myocardial Infarction	MI
Multidrug Resistance-Associated Proteins	MRPs
Sodium	Na
Non-Alcoholic Fatty Liver Disease	NAFLD

N-acetyltransferase Domain	Natd
N-acetyltransferase Family Member	Natf
Arylamine N-acetyltransferases	NATs
NAD(P)H: Quinone Oxidoreductases	NQOs
Nuclear Receptor	NR
Na -taurocholate Cotransporting Polypeptide	NTCP
Organic Anion-Transporting Polypeptide 2	OATP
Osteoporosis	OP
Organic Solute Transporter	OST
Principal Coordinate Analysis	PCoA
Phosphatic Acid	PA
Phosphatidylcholine	PC
Phosphatidylglycerol	PG
Phosphatidylinositol	PI
Phosphatidylserine	PS
Phosphatidylethanolamine	PE
Peroxisome Proliferator-Activated Receptor	PPAR
Pregnane X Receptor	PXR
Quadrupole Mass Filter	Q
Quaternary Ammonium Compounds	QACs
Rheumatoid Arthritis	RA
SREBP Cleavage-Activating Protein	SCAP
Short-Chain Fatty Acid	SCFA
Small Heterodimer Partner	SHP
Sphingomyelin	SM
Sterol Regulatory Element Binding Proteins	SREBP
Selective Reaction Monitoring	SRM
Standard Deviation	Stdev
Temperature	TEM
Tumor Necrosis Factor	TNF
Time-Of-Flight	TOF
Ursodeoxycholic Acid	UDCA
Ultra-High Performance Liquid Chromatography Trandem Mass Spectrometry	UHPLC-MS/MS
Urinary Stone Disease	USD
Vitamin D Receptor	VDR
Very Low-Density Lipoprotein	VLDL

Chapter 1 Introduction

1.1 Dissertation Overview

The work in this dissertation is centered on understanding environmental toxicant exposure effects on the gut-liver axis. Benzalkonium Chlorides (BACs) are highly effective antimicrobial compounds, widely used in consumer, clinical, food processing and agricultural settings. Recently, the Food and Drug Administration (FDA) called for additional safety data on BACs and increasing evidence demonstrates BACs are present in the majority of human blood samples- and that the levels are increasing. Environmental toxicant exposure effects on the gut microbiome is becoming more recognized as a novel mechanism of host health and disease state. The gut microbiome elicits its overall health effects by participating in various axes, broadly termed gut-organ axis. The gut-liver axis is a unique, bidirectional link that has become recognized for the role it has in liver disease and impairment of liver function. Our hypothesis is that exposure to BACs can impact the resident microbiome, which will lead to alterations in transcriptomic, sterol, lipid, and xenobiotic metabolism of the liver.

To address this work, this thesis is divided into five chapters. **Chapter 1** will provide a comprehensive overview on BAC regulation, biochemical mechanism of action and toxicity. Additionally, **Chapter 1** will provide background information on the liver and its role in endogenous and exogenous metabolism; as well as the gut microbiome and its role in understanding host health and disease. Lastly, **Chapter 1** will define the gut liver axis, its implication in health and disease state and how the bidirectional, tight links between the gut and liver communicate. In **Chapter 2**, I describe a comprehensive animal study that elucidated BAC exposure effects on gut microbiome composition and diversity, unconjugated bile acid (BA) pools

in biological extracts, and BAC and BAC metabolite profiles. In **Chapter 3**, I share the first comprehensive dataset that elucidates BAC metabolite distribution throughout brain, lung, blood, spleen, kidney, liver, duodenum, jejunum, ileum, large intestine, feces and urine in male and female BAC exposed mice. In **Chapter 4**, I demonstrate a comprehensive multiomics analyses of BAC-induced changes to the liver- including transcriptomics, sterolomics, lipidomics, and cytochrome p450 activity assays on mouse liver microsomes made of control and BAC-exposed mice. Finally, in **Chapter 5**, I discuss overall conclusions of this thesis work, and future studies that should be conducted. Together, this thesis provides a rigorous understanding of environmental toxicant exposure risks to human health.

1.2 Benzalkonium Chlorides

Benzalkonium Chlorides (BACs) belong to a class of quaternary ammonium compounds (QACs); a broad array of chemicals used as antimicrobials, surfactants, and preservatives (Arnold *et al.*, 2023). BAC structures are comprised of a central ammonium ion with a permanent positive charge that bonds to alkyl chains ranging from C8-C18 (Arnold *et al.*, 2023) **(Figure 1.1)**. QAC function, performance, and toxicity are influenced by the length of the alkyl chain and the nature of bonded substituents (Arnold *et al.*, 2023). QACs are widely distributed in hand sanitizers, surfaces, hand and disinfecting wipes, personal care products, and pesticides. Production volumes of many QACs are high in the US, with over 1 million pounds produced or imported annually. (Arnold *et al.*, 2023). A recent Canadian commerce described approximately 800 QACs (Arnold *et al.*, 2023). Previous studies demonstrate from all QACs tested by various groups, BACs- C12, C14, and C16 were detected at the highest concentrations relative to other QACs (Merchel Piovesan Pereira and Tagkopoulos, 2019). BACs are the active ingredient in domestic (fabric softeners, personal care, and cosmetic products like shampoos, conditioners, and body lotions),

agricultural (tools, vehicles, insecticides), industrial (food processing and hospital settings), clinical (nasal sprays and eye drops) and consumer settings (Arnold *et al.*, 2023; Merchel Piovesan Pereira and Tagkopoulos, 2019) **(Figure 1.2)**.

BACs are directly applied to eating utensils, egg shells, milking equipment and udders, and medical instruments (US EPA, 2006). BACs have also been reported on various food products, including fruits and vegetables, grapefruit seed extracts, and dairy products. The median and maximum levels of BACs in milk were 0.15 and 6.7 mg/kg respectively, and were higher in milk-based ice cream levels were higher at 0.22 and 22 mg/kg (Takeoka *et al.*, 2005; The Federal Institute for Risk Assessment (BfR) of Germany, 2012; Slimani *et al.*, 2017). BACs have also been detected as an unpermitted ingredient in food additives applied in meat products (Kröckel *et al.*, 2003).

BACs are widely used as disinfectants because of their effectiveness as broad-spectrum antimicrobials. The mechanism of action is dependent on both the disruption of the membrane bilayers by the alkyl chains and the disruption of the positively charged nitrogen ion (Merchel Piovesan Pereira and Tagkopoulos, 2019) **(Figure 1.3)**. The COVID-19 pandemic has led to excessive usage of BAC-containing disinfecting chemicals that has resulted in increased environmental exposure to BACs well above pre-pandemic levels. For example, the quantitation of QACs in indoor residential dust suggests an almost doubling of the levels of BACs during COVID-19 relative to pre-COVID-19 (Zheng *et al.*, 2020) and median levels of BACs in human blood increased 2.7-fold during the COVID-19 pandemic relative to pre-COVID-19 (Zheng *et al.*, 2021a).

Recently, BACs C12-C18 were detected in surface waters from Europe, Asia, and North America (Mohapatra *et al.*, 2023; Arnold *et al.*, 2023). Sediment cores in aquatic environments are meaningful in reconstructive long-term temporal trends in QAC contamination (Arnold *et al.*, 2023). BACs were first observed in sediments in the 1950s, and had peaks within the 1960s through 1980s (Arnold *et al.*, 2023). Furthermore, data within aquatic sediment demonstrated that within BAC structures, C12 BAC was observed at the greatest abundance (Mohapatra *et al.*, 2023; Arnold *et al.*, 2023). Within indoor environments, QACs are capable of binding to dust and are persistent on surfaces after spraying, leading to exposure routes like unintended hand-to-mouth contact after touching disinfected hard surfaces. **A recent model study found hand-to-mouth contact contributed the most to exposure** (D. Li *et al.*, 2020).

Despite the widespread usage of QACs, most have not undergone rigorous regulatory assessment for adverse human health effects, nor basic parameters like quantitative data on uses and volumes, toxicity, and exposure (Arnold *et al.*, 2023). However, BACs specifically are currently regulated in the United States by the Environmental Protection Agency (EPA) and the Food and Drug Administration (FDA) (Merchel Piovesan Pereira and Tagkopoulos, 2019). In 2016, the FDA banned 19 active ingredients, like triclosan and triclocarban in consumer hand rub antiseptics, hand and body wash, and healthcare antiseptics (US FDA, 2016b; Merchel Piovesan Pereira and Tagkopoulos, 2019; Arnold *et al.*, 2023) because there was insufficient evidence of their safety. Notably, the original rule included BACs, but they were removed from decisions and were granted deferral letters as requested by manufacturers (Arnold *et al.*, 2023). Decisions to postpone action regarding BAC regulation were implemented based on a lack of sufficient data in the literature (Merchel Piovesan Pereira and Tagkopoulos, 2019). Interestingly, however, BACs are used as frequent replacements for banned compounds like triclosan (Arnold *et al.*, 2023). Thus,

there have been many studies focused on understanding BAC toxicity in the literature highlighting BAC toxicity in both animal and human subjects. Work by Sreevidya et al demonstrated BACs are comparably toxic as Triclosan in C. elegans, had greater toxicity to zebrafish embryos, and were capable of inducing neurotoxicity in fish embryos (Sreevidya *et al.*, 2018).

Given the ubiquitous environmental presence of BACs, humans may be chronically and systemically exposed by several routes: direct dermal/eye contact, inhalation, and ingestion (US FDA, 2016b) **(Figure 1.4)**. Furthermore, animal studies demonstrate BACs are orally bioavailable and distributed broadly throughout tissues. After a single dose/ intravenous injection of BACs to rats (7mg/kg), BACs were found to be widely distributed in various tissues, with the highest levels in the kidney, then lung and spleen, serum, liver, and brain 30 minutes after administration (Xue *et al.*, 2002). After oral administration (250 mg/kg), BAC levels reached their highest concentrations for most of the tissues after 24 hours (liver was 2 hours) with the following levels kidney (5.25µg/g) > lung (2.75 µg/g) > liver (0.72 µg/g) > blood (0.34 µg/g) (Xue *et al.*, 2004). Oral dosage of radiolabeled BACs led to 87-99% of BACs being excreted through the feces, a third of which were metabolites (Luz *et al.*, 2020).

Notably, the literature suggests that BACs are absorbed into the body and that exposure within human populations is significant. For example, BACs are readily detectable in human blood following acute oral ingestion (Xue *et al.*, 2002; Mishima-Kimura *et al.*, 2018). BACs are extremely persistent. In a fatal ingestion case, BACs were quantified at 245-264 nM in the blood 18 days post-ingestion (Mishima-Kimura *et al.*, 2018). We have even reported BACs were detectable in the blood of 80% of human participants who had BAC concentration levels in the 10-150 nM range (Hrubec *et al.*, 2021a). BACs C12-C16 have been quantified in breast milk collected from women in the US (Zheng *et al.*, 2022). More recently, we have detected both BACs and BAC

metabolites in five human fecal samples, reaching over 1 µM in total BAC concentrations (Nguyen *et al.*, 2024). Biochemically, BACs elicit their mode of action by perturbing and disrupting the membrane bilayers by the alkyl chains of the BAC structure (**Figure 1.3**), which leads to the disruption of the cellular membrane.

Currently, BACs are classified by the EPA as toxicity category II by oral and inhalation routes, signifying moderate toxicity. Work has demonstrated when BACs are administered by intratracheal instillation in mice, led to histological evidence of diffuse congestion, hemorrhage, necrotizing alveolar wall and fibrin thrombus in small vessels (Lee and Park, 2019). Furthermore, patients with stable bronchial asthma have been susceptible to BAC induced bronchoconstriction (Lee and Park, 2019; Lee and Kim, 2007), and thus, effects of BACs are under current investigation of their effects on bronchoconstriction, which is ultimately hypothesized to play an interference in respiration or cardiac function (Lee and Park, 2019). Furthermore, BACs are categorized as toxicity category III (slightly toxic) via dermal route, and are considerably irritating to the eyes and skin (US EPA, 2006; Merchel Piovesan Pereira and Tagkopoulos, 2019).Various studies have demonstrated BACs are capable of various ocular damage including reduced nerve fiber density, increased inflammatory cell infiltration, and aqueous tear production after treatment to neuroflourescent mouse eyes with BACs (Sarkar *et al.*, 2012). Dose-dependent BAC exposure demonstrated ocular surface epithelial changes that are aligned with features of dry eye disease in C57BL/6 mice and cultivated primary mouse corneo-limbal epithelial cells (Zhang *et al.*, 2020). In vitro models have demonstrated BACs cause DNA changes in respiratory epithelial cells even at concentrations commonly used in commercially available nasal preparations (Deutschle *et al.*, 2006).

Occupational BAC exposure is associated with increased risks of asthma as well as allergic eye and skin reactions in humans (Gonzalez *et al.*, 2014; Baudouin *et al.*, 1999; Robinson *et al.*, 2017). In mice, chronic consumption of BAC-containing food (60 and 120 mg/kg/day) was responsible for significant decreases in fertility as well as increased dam mortality (Melin *et al.*, 2014, 2016). Recent evidence has shown that an environmentally relevant QAC mixture that included BACs. led to significantly increased incidences of neural tube defects in mice that were ambiently exposed compared to those in a QAC-free facility (Hrubec *et al.*, 2017). Our lab has previously demonstrated C10- and C12-BACs are potent inhibitors of 3β-hydroxysterol-Δ 7 -reductase (DHCR7) in cholesterol biosynthesis at nM concentrations and that all BACs disrupt lipid homeostasis in neuronal cell lines (Herron *et al.*, 2016; Hines *et al.*, 2017). Additionally, our lab has previously shown that cholesterol biosynthesis and lipid metabolism are altered in neonatal mouse brains exposed to BACs in utero (Herron *et al.*, 2019).

1.3 Liver

The liver is home to the highest concentrations of cytochrome P450 enzymes- membrane-bound hemeproteins that play pivotal roles in bile acid biosynthesis, homeostasis of steroid hormones, vitamin metabolism, metabolism of unsaturated fatty acids, cholesterol biosynthesis, and metabolism of foreign compounds (Jaeschke, 2015; Esteves *et al.*, 2021) **(Figure 1.5)**. Within a human lifetime, we are exposed to 1-3 million various foreign compounds, or xenobiotics, a term that describes chemical substances that are foreign to life, such as drugs, pesticides, cosmetics, flavorings, fragrances, industrial chemicals and environmental pollutants (Esteves *et al.*, 2021; Patterson *et al.*, 2010). Effective detoxification and subsequent of foreign compounds is crucial in avoiding the accumulation of toxic compound levels, which could interfere with cellular homeostasis, and cellular and tissue damage (Esteves *et al.*, 2021). Thus, having a comprehensive

understanding of in vivo xenobiotic mentalism is essential in understanding and predicting health risk through bioavailability, and bioaccumulation following chemical exposure (Esteves *et al.*, 2021).

The metabolism and subsequent cellular excretion of xenobiotics are heavily dependent on Phase I and Phase II drug-metabolizing enzymes (DMEs). Phase I enzymes are primarily composed of the CYP superfamily- however flavin-containing monooxygenases (FMOs), NAD(P)H: quinone oxidoreductases (NQOs), amine oxidases, alcohol dehydrogenases, esterases, peroxidases are all capable of catalyzing the oxidation, reduction and hydrolyses of primarily lipophilic xenobiotics (Esteves *et al.*, 2021). CYPs can catalyze various biotransformation reactions like aliphatic, aromatic, and N-hydroxylation, epoxidation, oxygenation, dehydrogenation, dehalogenation, and N-, O- and S-dealkylation (Esteves *et al.*, 2021). The typical CYP-mediated monooxygenation reaction is defined by the incorporation of one oxygen atom into the substrate ($RH + O_2 + 2e^- + 2H^+ \rightarrow ROH + H_2O$) (Esteves *et al.*, 2021). The increased polarity of primarily lipophilic xenobiotics after Phase I reactions provides Phase II enzymes the opportunity to perform conjugation reactions. This is exemplified by the understanding that Phase II enzymes are capable of interacting directly with the parent compound, however, phase I metabolites are primarily conjugated with charged species like amino acids, methyl and/or acetyl groups (Esteves *et al.*, 2021).

Substantially, CYPs have been found to be involved in the majority of enzymatic reactions within the metabolism of xenobiotics (Esteves *et al.*, 2021). Furthermore, 15 isoforms belonging to CYP families 1, 2, and 3 account for up to 80 % of all Phase I metabolism of clinically used drugs, and up to 90% are involved in the biotransformation of environmental chemicals. Among the 15 isoforms, CYP1A2, CYP2C9, CYP2D6, and CYP3A4/5 are reported to account for roughly

72% of all CYP-mediated metabolism of clinically marketed drugs (Esteves *et al.*, 2021). *Members of the CYP4 family are important for the ω-oxidation of endogenous fatty acids and eicosanoids and are also involved in xenobiotic metabolism- this includes CYP4A11, CYPF2, and CYP4F12* (Esteves *et al.*, 2021).

We have elucidated the metabolic pathway of BACs by CYPs in human liver microsomes (HLMs) and recombinant CYPs (R. P. Seguin *et al.*, 2019).We reported that CYPs 2D6, 4F2, 4F11, and 4F12 are the major metabolizing enzymes of BACs. CYPs 4F2 and 4F11 are responsible for (ω)-hydroxyl metabolite formation, and CYP2D6 and CYP4F12 are responsible for (ω-1)-hydroxyl metabolite formation (R. P. Seguin *et al.*, 2019). The primary (ω)- and (ω-1)-hydroxyl metabolites are oxidized to metabolites (ω,ω-1)-dihydroxy, (ω-1)-ketone and (ω)-carboxylic acid (R. P. Seguin *et al.*, 2019).

The liver is also vital in the regulation of lipid distribution (lipid metabolism and transport) throughout the body (Seebacher *et al.*, 2020; Ten Hove *et al.*, 2020). Lipids play valuable roles in serving as building blocks of cellular membranes, energy storage, cellular signaling, and pre-cursors for hormones (Seebacher *et al.*, 2020). Thus, maintenance of cellular and systemic lipid levels is imperative for physiological homeostasis (Wang and Tontonoz, 2018). Hepatocytes synthesize, store, and secrete lipids to maintain whole-body lipid homeostasis (Seebacher *et al.*, 2020). Excessive lipid accumulation is defined in NAFLD, and obesity (Seebacher *et al.*, 2020) and perturbations of lipid metabolism are associated with various disease states like diabetes, atherosclerosis, cancer, steatosis, cirrhosis and hepatocellular carcinoma and neurodegenerative diseases (Wang and Tontonoz, 2018; Ten Hove *et al.*, 2020). Lipids are classified into eight categories a) fatty acyls b) glycerolipids c) glycerophospholipids d) sphingolipids e) sterol lipids f) prenol lipids g) saccharolipids and h) polyketides (Ten Hove *et al.*, 2020). Hepatocytes utilize

various sources of lipids that depend on their metabolic state (Seebacher *et al.*, 2020). Regardless of the source, fatty acids are esterified into either cholesterol esters by acyl CoA cholesterol acyltransferases (ACATs 1 and 2) or triglycerides by diacylglycerol-O-acyltransferases (DGATs 1 and 2). Triglycerides can then be stored into lipid droplets and mobilized, or can be re-esterified and packed into VLDL particles for secretion, or can be channeled into mitochondrial beta-oxidation (Seebacher *et al.*, 2020). If used for mitochondrial beta-oxidation, the resulting acetyl-CoA can be used as a building block for cholesterol synthesis (Seebacher *et al.*, 2020). Important to consider, NRs like liver X receptors (LXR), FXR, and PPARs, have been documented to respond to changes in cellular levels of endogenous lipid ligands by regulating the expression of genes that encode proteins involved in lipid metabolism (Seebacher *et al.*, 2020). Lastly, the liver is the principal site for cholesterol homeostasis maintenance (Trapani, 2012). Examples of cholesterol homeostasis maintenance mechanisms include biosynthesis by 3-hydroxy-3-methylglutaryl coenzyme A reductase (HMGCR) activity, low-density lipoprotein receptors (LDLR) uptake, lipoprotein release in the blood, storage by esterification with fatty acids, and degradation and conversion into bile acids (BAs) (Trapani, 2012).

1.4 The Gut Microbiome

The resident gut microbiota encompasses the consortium of commensal, symbiotic, and pathogenic microorganisms including bacteria, archaea, viruses, fungi, eukarya, protozoa, and bacteriophages (Thursby and Juge, 2017; Hills *et al.*, 2019; Fan and Pedersen, 2021; Barko *et al.*, 2018). The microbiome encompasses all genomic content of described microorganisms inhabiting the gastrointestinal tract (Thursby and Juge, 2017; Hills *et al.*, 2019). The collection of all intestinal microbial genes within an individual is more than an order of magnitude higher in gene number than the human genome (Fan and Pedersen, 2021). The gut microbiome has co-evolved with the

host for thousands of years and thus has formed a mutually intricate and beneficial relationship (Thursby and Juge, 2017). The microbiome participates in various physiological functions such as harvesting energy, protecting against pathogens, strengthening the gut integrity, maintaining the integrity of the mucosal barrier, providing nutrients to the host, shaping intestinal epithelium, and regulating host immunity- all of which are beneficial to the host (Thursby and Juge, 2017). The gut microbiota composition in microbial communities is functionally redundant compared to other bodily sites (Thursby and Juge, 2017). Interestingly, a study investigating an extensive catalog of human gut microbiomes revealed evidence of country-specific microbial signatures. The study suggests that the gut microbiome is shaped, in part, by environmental factors and genetics. However, despite differences in microbiota composition between groups, the functional redundancy identified within the catalog of human gut microbiomes suggests similar protein and metabolite profiles (Thursby and Juge, 2017). Suggestions in the field have been proposed for defining a "core microbiota" - a proposed set of the same organisms present in all individuals- ; however, the current discussion is centered on whether the core microbiota should be defined at the functional level rather than the organismic level (Thursby and Juge, 2017). While gut bacterial diversity and richness alone are not indicators of healthy microbiota alone; high taxa diversity, and high microbial gene richness are considered characteristics of a healthy gut microbial community (Fan and Pedersen, 2021).

The gastrointestinal microbiome has become increasingly recognized as an invaluable contributor to human (host) health because of the symbiotic relationship between the host and the gut microbiome. This symbiosis has been linked to positive contributions to overall host health- examples include immunity, nutrition, and human development (Eloe-Fadrosh and Rasko, 2013). When normal microbiota composition is disrupted, or there's an imbalance in the composition

and/or function (dysbiosis), the community of gut microbiota cannot perform their essential physiological, unique metabolic functions (Hills *et al.*, 2019; Saxami *et al.*, 2023). Gut microbiome dysbiosis can lead to the degradation of mucin along the gut epithelial cells, disruption of the gut's protective barrier, and increased permeability (Saxami *et al.*, 2023). Thus, abundant epidemiological and metagenomic data tie gut microbiome dysbiosis to many human diseases, such as obesity, asthma, some cancers, chronic GI diseases, neurodevelopmental disorders, heart disease, and even autism (Barko *et al.*, 2018; Thursby and Juge, 2017). The microbiome has become a recognized predictor of health and disease, and the composition of the microbiome is believed to be a better indicator of body mass index (BMI), cholesterol and blood glucose levels, and cardiac health than genetic factors (Koontz *et al.*, 2019). Microbiome composition is predictive of disease severity in cirrhosis patients, microbiome composition of amniotic fluid is a predictor of preterm birth, and maternal exposure to pollutants is associated with alterations in infant microbiome development (Koontz *et al.*, 2019; Naspolini *et al.*, 2022).

Increasing evidence has acknowledged the effects of environmental toxicant exposure on the microbiome is associated with host health and **potential** disease pathology. Gut microbiome toxicity can include functional damage defined as changes in bacterial metabolites, loss of bacterial diversity, effects on energy metabolism and effects on energy homeostasis (Tu *et al.*, 2020). These functional gut microbiome alterations may directly and indirectly influence host health- an increasingly appreciated mechanism of environmental toxicant toxicity (Turesky and Lu, 2020). For example, disorders like celiac disease, obesity, allergies and type 2 diabetes may be mediated by low-dose chronic toxic effects on the microbiome, as exemplified by cases like obesity from the use of antibiotics (Koontz *et al.*, 2019). Various groups have demonstrated exposure to toxicants like arsenic, cadmium and nickel have different changes to the microbiota (Koontz *et al.*,

2019; Tu *et al.*, 2020). For example, alcoholic injury is primarily caused by oxidative metabolite formation in the liver that leads to degradation (Koontz *et al.*, 2019). However, increasing evidence has signified that gut leakage, translocation of bacteria and bacterial metabolites, bacterial overgrowth and dysbiosis leads to observed health effects as well as heightens the inflammatory state of the liver (Koontz *et al.*, 2019). Importantly, exposure to arsenic has been shown to alter gut microbiota composition and the subsequent alterations have been associated with changes in lipid, vitamin, and bile acid metabolism; as well as oxidative stress (Chiu *et al.*, 2020). Significantly, arsenic exposure is a persistent problem in humans through ingestion of contaminated waters. Accordingly, a Bangladesh population has been reported to have altered microbiome due to arsenic exposure by infected waters, which has resulted in overproduction of bacteria Citrobacter, whose species which has been associated with various health problems like respiratory diseases, sepsis, inflamed GI and urinary tract infections (Chiu *et al.*, 2020). Furthermore, data has shown a significant association between arsenic exposure, Citrobacter and vascular intima-media thickness (IMT). IMT is used as a subclinical marker for atherosclerosis. Thus, arsenic exposure effects on the resident gut microbiome may play a pivotal role in the development of atherosclerosis.

There have been various examples highlighting the role environmental toxicant exposures have on resident gut microbiota and the implications for host health. For example, high levels of phthalate (plasticizer commonly used in detergents, personal care products and children's toys) exposure at birth alters gut microbiota composition, and the resulting changes have been associated with enhanced immunoglobulin M responses against hepatitis B vaccination; evidence for a phthalate-induced gut microbial immune response to vaccination effect (Chiu *et al.*, 2020). Persistent organic pollutant, polychlorinated biphenyls (PCBs) cause functional changed in GI

physiology, Immunology and gut microbiota composition (Chiu *et al.*, 2020). Perfluorochemicals (commonly used in nonstick cookware), like polyfluorobutane substance (PFBS) exposure in male fish had increased abundance of bacteria positively correlated with altered tight junction protein expression- a marker of epithelial barrier integrity, as well as hyperactive immune responses. Furthermore, female fish had severely impaired lipid metabolism demonstrated by decreased levels of triglycerides and fatty acids (Chiu *et al.*, 2020). Exposure to polybrominated diphenyl ethers like BDE-47 (flame retardant), show evidence of reduced diversity of gut microbiota composition and impaired glucose homeostasis in male mice. Additionally, studies show exposure to BDE-47 and BDE-99 lead to altered gut microbial taxa and amino acid and carbohydrate metabolism (Chiu *et al.*, 2020).

There are five categories of bacterial metabolizing compounds including azoreductases, nitroreductases, β- reductases, sulfatases and β-lyases. Considerably, microbes have the ability to metabolize chemicals and as such, increasing evidence depicts metabolism of environmental chemicals by microbes can affect the toxicity of exposed chemical on the host (Koontz *et al.*, 2019). This is exemplified by ethanol metabolism by gut microbes to generate acetaldehyde, which has been linked to rectal cancer development (Koontz *et al.*, 2019). Importantly, toxicity of the gut microbiome alters the bacterial metabolite profile, influencing host metabolism and physiology (Tu *et al.*, 2020). Various bacterial metabolites are signaling molecules by binding to receptors and activating signaling cascades (Tu *et al.*, 2020). For example, short-chain fatty acids (SCFAs) bind to cellular receptors like G-protein-coupled receptors (GPCRs), and bile acids (BAs) bind to GPCR TGR5 and nuclear receptor farnesoid X receptor (FXR). For example, both SCFAs and BAs can bind to GPCR43 and TGR5 to modulate secretion of glucagon-like peptide (GLP-1), exhibiting a valuable role of gut microbiome in insulin secretion, glucose homeostasis and potentially risk of

diabetes. Another example includes tryptophan metabolites produced by bacteria like indole 3-propionic acid and indol-3-acetic acid that activates nuclear receptors aryl hydrocarbon receptor (AHR) and pregnane X receptor (PXR), regulating intestinal immune cells and barrier functions. Furthermore, reductions in bacterial tryptophan metabolism are suggested to contribute to Inflammatory Bowel Disease (IBD), and AHR activation is involved in IBD (Tu *et al.*, 2020).

1.5 The Gut-Liver Axis

The gastrointestinal microbiome elicits its role in overall health effects by participating in crosstalk communications with the host. This is evidenced by recent work signifying the bidirectional interactions between the gut microbiome and other organs- called the "gut-organ axis" (Saxami *et al.*, 2023). The gut microbiome can communicate bidirectionally with various organs via signaling pathways as well as direct chemical interactions between the host and microorganisms (Saxami *et al.*, 2023). Gut microbes are capable of synthesizing a variety of bioactive compounds, and these microbial metabolites can further communicate with organs throughout the body allowing them to connect to the hormone, immune, and metabolic systems of the host (Ahlawat *et al.*, 2021). These interactions enable the complex interactions between the gut microbiome and the host immune system to influence body functions in other organs, thus resulting in the "-axis" formation between said organ and the gut microbiome (Ahlawat *et al.*, 2021). Various work has established vital relationships and consequences within host health in axes like the gut-immune-axis, gut-bone-axis, gut-brain axis, gut-skin axis, gut-kidney axis, gut-heart axis, and gut-liver axis (Levy *et al.*, 2017; Ahlawat *et al.*, 2021) **(Figure 1.6)**. These unique crosstalk relationships have been implicated in various disease states. For example, the gut-bone axis in rheumatoid arthritis (RA) and osteoporosis (op); the gut-brain axis is implicated in autism spectrum disorders, Parkinson's disease, and Alzheimer's; the gut-skin axis in eczema, atopic

dermatitis (ad) and acne vulgaris; the gut-kidney in urinary stone disease (USD), nephrolithiasis, and chronic kidney disease (CKD); the gut-heart axis in chronic heart failure (CHF), atherosclerotic cardiovascular disease (ACVD), myocardial infarction (MI) and hypertension; the gut-liver axis in non-alcoholic fatty liver disease (NAFLD), cirrhosis and acute-on-chronic liver failure (ACLF) (Ahlawat *et al.*, 2021).

Crosstalk between the gut and liver has become increasingly recognized by parallel rises in occurrences of liver diseases and GI and immune disorders (A. Tripathi *et al.*, 2018). For example, the gut-liver axis is implicated in diseases like NAFLD, cirrhosis, alcohol-associated liver disease, and hepatocellular carcinoma where patients have intestinal microbiota composition changes (A. Tripathi *et al.*, 2018). The gut and the liver communicate through tight bidirectional links including the biliary tract, portal vein, as well as systemic circulation (A. Tripathi *et al.*, 2018). Examples of communicative interactions between the gut and the liver are described in the following a) the liver releases BAs and other bioactive mediators into the biliary tract as well as systemic circulation b) endogenous (BAs and amino acids) and exogenous (diet and environmental exposure) substrates metabolites from both the host and the microorganisms in the intestine travel to the liver through the portal vein and can subsequently influence liver function (A. Tripathi *et al.*, 2018) (**Figure 1.7**). The liver transports bile salts and antimicrobial molecules like immunoglobulin A (IgA) to the intestinal lumen via the biliary tract- a process that controls bacterial overgrowth (A. Tripathi *et al.*, 2018). Additionally, host and/or microbial metabolites and microbial-associated molecular patterns (MAMPs) from the gut- can translocate to the liver through the portal vein. Systemic circulation is also a key mechanism for communication between the gut and liver, exemplified by the transportation of liver metabolites of endogenous and xenobiotic substances to the intestine (A. Tripathi *et al.*, 2018)

BAs are imperative signaling molecules for intermediary metabolism within the gut-liver axis (C. Y. Li *et al.*, 2018). BAs are synthesized from cholesterol in the endoplasmic reticulum of hepatocytes by microsomal cytochrome p450 proteins (Chen *et al.*, 2021). There are two well-established biosynthetic pathways a) the neutral classical pathway and b) the acidic alternative pathway (Chen *et al.*, 2021). The liver is the only organ that carries out the classic BA synthetic pathway; however, the alternative pathway is present in not just the liver but also the brain, adrenal glands, and macrophages (Chen *et al.*, 2021). Within rodents, the alternative pathway may account for up to 50% of BA synthesis, however in humans, only 3-18% of newly synthesized BAs in humans are formed from the alternative pathway (Chen *et al.*, 2021). Within the classical synthesis pathway, the cholesterol 7-α-hydroxylase (CYP7A1) metabolizes cholesterol into 7α-hydroxycholesterol, which is then converted to 7α-hydroxy-4-cholesten-3-one (C4)- the precursor for primary BAs. Importantly, CYP7A1 controls the rate of BA synthesis within the classical pathway, versus CYP7B1(Chen *et al.*, 2021; Fuchs and Trauner, 2022). The classical pathway accounts for at least 75% of BA production (Chen *et al.*, 2021). The classical pathway yields distinct primary BAs, cholic acid (CA), and chenodeoxycholic acid (CDCA) from cholesterol in human hepatocytes (Chen *et al.*, 2021; Fuchs and Trauner, 2022). CYP7A1 and CYP7B1 are both important for the classical pathway; however, CYP7B1 is only relevant in the neutral pathway (Fuchs and Trauner, 2022). In rodents, a rodent-specific enzyme called sterol-6B-hydroxylase (CYP2C70) converts CDCA to α- and β-muricholic acid (MCA) (Chen *et al.*, 2021); furthermore, CYP2C70 hydroxylates ursodeoxycholic acid (UDCA) to β-MCA (Chen *et al.*, 2021). The alternative pathway produces CDCA via CYP7B1 and is initiated by CYP27A1 (Chen *et al.*, 2021). Within hepatocytes, BAs are then conjugated to amino acids glycine or taurine through enzymes bile acid-CoA synthase and bile acid-CoA: amino acid N-acyltransferase (BAAT), a

process that makes them negatively charged molecules and thus, allows them efficient uptake and excretion across cell membranes for secretion into the bile by transporters, bile salt export pump (BSEP) and multidrug resistance-associated proteins (MRPs) (Chen *et al.*, 2021; Fuchs and Trauner, 2022; Stellaard and Lütjohann, 2021). BAAT allows for BAs to retain amphipathic structure which is crucial for lipid emulsification in the acidic environment of the duodenum (Fuchs and Trauner, 2022). If BA accumulation is excessive, it can be excreted by basolateral export systems of the liver mediated by members of the MRP and sodium-independent organic anion-transporting polypeptide 2 (OATP2) transporters. These taurine and glycine-conjugated primary BAs are deconjugated and 7α-dehydroxylated to form secondary BAs deoxycholic acid (DCA) and lithocholic acid (LCA) once they reach the intestine via the resident gut bacterial bile salt hydrolase and gut bacterial 7α-dehydroxylase removes the 7α-hydroxyl group (Chen *et al.*, 2021; Fuchs and Trauner, 2022; Stellaard and Lütjohann, 2021).

In humans, CA, CDCA, and DCA encompass more than 90% of the total BA pool size (Stellaard and Lütjohann, 2021). Within the terminal ileum, up to 95% of BAs are efficiently reabsorbed at the brush border membrane via the ASBT transporter (Fuchs and Trauner, 2022). They are subsequently transported through enterocytes via the IBABP through to the basolateral membrane and then exported via OSTα/β) to the portal vein back to the liver. Once in the liver, the conjugated BAs are taken up by NA+-dependent active transport mechanisms, and the unconjugated BAs are taken up by OATP1B1 and OATP1B3 (Fuchs and Trauner, 2022) **(Figure 1.9)**. BAs participate in a process called enterohepatic circulation of BAs which describes the process in which BAs are recycled up to 12 times per day between hepatocytes in the liver and enterocytes in the intestine (Mertens *et al.*, 2017).

BAs are vital for their role in assisting physiological functions like nutrient absorption, biliary secretion of lipids, toxic metabolites and xenobiotics, metabolism of glucose and lipids and energy expenditure in peripheral tissues (Schneider *et al.*, 2018; Hild *et al.*, 2021; Li and Chiang, 2012). There are major physiological functions of BAs that are established (Hofmann, 1999). Formation of BAs from cholesterol in the liver leads to cholesterol moving from hepatocyte to the intestinal lumen, ultimately leading to the elimination of cholesterol via feces. Defects within the conversion of cholesterol to BAs can cause severe hepatic and systemic disease states (Hofmann, 1999). Additionally, BAs promote dietary lipid absorption because of their role in solubilizing dietary lipids and thus accelerating lipid absorption. Hinderance of such activity leads to fat-soluble vitamins like (A, D, E and K) and phospholipids not being absorbed and deficiencies occurring (Hofmann, 1999). BAs have become increasingly recognized for their role as signaling molecules that bind to nuclear receptors which are important for regulation of BA, glucose and lipid homeostasis (Asgharpour *et al.*, 2015). Alterations in bile acid homeostasis and processes can lead to dysregulation of energy balance, increased inflammation and fibrosis of the liver (Chow *et al.*, 2017). As a result, BAs have been implicated as targets for NAFLD and NASH drug therapies (Chow *et al.*, 2017).

BAs additionally act as hormone-like signaling molecules because they serve as ligands to nuclear receptors (NRs), like farnesoid X receptor (FXR), pregnane X receptor (PXR), constitutive androstane receptor (CAR), and the vitamin D receptor (VDR) (Fuchs and Trauner, 2022). By binding to the NRs, BAs can control their own transport and metabolism, lipid and glucose metabolism, and innate and adaptive immunity (Fuchs and Trauner, 2022). For example, FXR induces BSEP, which actively secretes BAs into bile as well as MDR2 and 3 and ABCG5/8 and MRP3 and MRP4, facilitating hepatic BA export route (Fuchs and Trauner, 2022).

Unconjugated and conjugated primary BAs like CA, CDCA, DCA, UDCA, TCA, and TCDCA are taken up by transporters like BSEP, MRP2, MDR3 and OATP2 in hepatocytes. At the terminal ileum, unconjugated BAs are reabsorbed by ASBT into enterocytes and then secreted by basolateral BA transporters OSTα/β into the portal circulation. After this, BAs are taken up by NTCP and OATP1 into hepatocytes (Chen *et al.*, 2021).

After primary BAs are transported into the intestinal lumen, the microbiota has direct influences on the BA pool composition, secondary BA formation, and hydrophobicity of the BA pool (Stellaard and Lütjohann, 2021). This is recognized by a few key examples. Firstly, conjugated primary BAs are hydrolyzed by bile salt hydrolases (BSH). BSH is a cytoplasmic enzyme that has been recognized in microbiota like Bacteroides, Clostridium, Lactobacillus, and Bifidobacterium. There are reports of up to 29% of 693 bacterial genomes containing bile salt hydrolase genes. Secondly, following deconjugation, free BAs are metabolized to secondary BAs with dehydroxylation by bacteria like Clostridium and Eubacterium (Chen *et al.*, 2021).

Furthermore, deconjugation, dehydrogenation, and epimerization are dependent on hydroxysteroid dehydrogenases (HSDHs). Of the same 693 bacterial genomes mentioned previously, there was the detection of the 3α-, 3β-, 7β- and 12α HSDHs in 17, 12, 3, and 6% of the genomes (Stellaard and Lütjohann, 2021). HSDH oxidation is followed by epimerization reactions to the respective α and β hydroxyls. These products can only be mediated by clostridium bacteria (Stellaard and Lütjohann, 2021). Distinguishably, microbial metabolism of BAs results in increased diversity as well as a more hydrophobic BA pool, and as such, changes in intestinal microbial compositional shifts the biological modification of BAs (Chen *et al.*, 2021).

Within the liver, BA synthesis is regulated by nuclear receptor-FXR signaling pathways. FXR participates in negative feedback regulation through a) FXR-bound fibroblast growth factor 19/15 (FGF19 in humans; FGF15 in mice) within the ileum and small heterodimer partner (SHP) in the liver (Chen *et al.*, 2021). For example, FXR binds easily to other nuclear receptors to form small heterodimers that induce expression of SHP which subsequently antagonizes the effects of the CYP7A1 promoter, and establishes CYP7A1 suppression (Chen *et al.*, 2021; Stellaard and Lütjohann, 2021). BA synthesis is regulated at the first step in the process by a negative feedback mechanism included by BAs themselves (Stellaard and Lütjohann, 2021). Secondly, the regulation of BA synthesis is closely related to enterohepatic circulation wherein, the gut senses the BA pool and sends signals to the liver. FXR can influence BA transport because of its role in regulating the expression of transporters in the enterohepatic circulation- examples include BSEP, MDR3, and IBABP (Chen *et al.*, 2021).

Additionally, BAs also activate cell surface G-protein coupled receptor TGR5. Particularly, BAs LCA, DCA, CDCA and CA (Li and Chiang, 2012). Moreso, within the intestine secondary BAs LCA and DCA activate TGR5 (Chiang and Ferrell, 2018). Furthermore, taurine conjugation of BAs increases the affinity for TGR5, and glycine conjugation has a negligible impact on TGR5 affinity (Holter *et al.*, 2020). TGR5 is important in regulating bile acid pool and synthesis. For example, several studies have indicated that TGR5 may regulate BA profile by selective downregulation of hepatic Cyp8b1 expression (Holter *et al.*, 2020). Activation of TGR5 has been shown to protect the liver from BA overload during liver regeneration and markedly decreases LPS-induced cytokine production in primary macrophages. Recent reports demonstrate TGR5 may be involved in the regulation of CYP7B1, a male-predominant gene in the alternative BA synthesis pathway. Additionally, other findings suggest TGR5 signaling may upregulate the

alternative pathway of BA synthesis by stimulating expression of Cyp7b1 and Cyp27a1, leading to a decrease in the hydrophobicity of the BA pool (Holter *et al.*, 2020). An imbalance or disruption in BA homeostasis and signaling can elicit a cascade of host immune responses relevant to the progression of liver diseases like NAFLD and the progression of HCC (A. Tripathi *et al.*, 2018; Fuchs and Trauner, 2022). Impairment in BA homeostasis can also contribute to the pathogenesis of irritable bowel syndrome (IBS), inflammatory bowel disease (IBD), and colorectal cancer (CRC) (Fuchs and Trauner, 2022). Furthermore, TGR5 has additionally been shown to play a pivotal role in lipid deposition. For example, high fat diet (HFD)-fed male whole body Tgr5-/- mice exhibited increased lipid deposition compared with male wild-type mice (Vassileva *et al.*, 2010). More studies have shown treatment with agonists of TGR5, like INT-777 and RDX8940 decreased plasma free fatty acids and decreased hepatic triglyceride and cholesterol levels in HFD- and western-diet fed mice respectively (Holter *et al.*, 2020).

Importantly, the gut microbiome and the liver communicate to modify hepatic xenobiotic biotransformation and nutrient homeostasis (C. Y. Li *et al.*, 2018). Specifically, the gut microbiome has become increasingly recognized as a of xenobiotic biotransformation by regulation of drug-metabolizing enzymes (DMEs), including cytochromes P450 (CYPs) (C. Y. Li *et al.*, 2018). The gut microbiome has been reported to modulate the activities of NRs that are responsible for roles in regulating drug-metabolizing enzymes (DMEs), such as PXR, CAR and PPARα (Selwyn, Cui, *et al.*, 2015; Selwyn *et al.*, 2016; Selwyn, Cheng, *et al.*, 2015; Fu *et al.*, 2017; Cui and Klaassen, 2016). Transcriptional activation is described as the main process of CYP gene induction (Esteves *et al.*, 2021) **(Table 1.1)**. Several reports have defined various roles of NRs in mediating the induction of CYPs; for example, the aryl hydrocarbon receptor (AhR)-CYP1 genes; PXR- CYP2A6, 2B, 2C, and 3A genes; and finally, CAR-CYP1A, 2A6, 2B, 2C8, 2C9 and

3A4 genes (Esteves *et al.*, 2021). PXR positively regulates Cyp3a genes, CAR positively regulates Cyp2b genes and negatively regulates Cyp2c and Cyp4 genes and CAR and PPARs positively regulate Cyp4 genes within the liver (Selwyn, Cui, *et al.*, 2015; Cui and Klaassen, 2016). *Mice free of gut microbiota, i.e., germ-free (GF) mice have altered expression of Cyp genes compared to conventional (CV) mice* (Selwyn, Cui, *et al.*, 2015; Selwyn *et al.*, 2016; Cui and Klaassen, 2016). For example, GF mice have downregulation of Cyp3a genes and upregulation of Cyp4 genes, suggesting inhibition of PXR and activation of PPARα, relative to CV mice (Selwyn, Cui, *et al.*, 2015; Selwyn *et al.*, 2016; Cui and Klaassen, 2016). Additionally, GF mice have downregulated cholesterol and lipids (triglycerides and phospholipids) within the liver (Zhong *et al.*, 2015). Gut bacteria can directly metabolize cholesterol as well as directly and indirectly influence host lipid metabolism (Molinero *et al.*, 2019; Johnson *et al.*, 2020; Ghazalpour *et al.*, 2016).

Various groups have identified the role environmental toxicant exposure has on gut-liver axis and implications for health and disease. The microbiome has been defined as the first interface between the environment and almost all metabolic, biochemical, endocrine, and signaling pathways influencing the onset and progression of NAFLD (Di Ciaula *et al.*, 2020). For example, dietary exposure Bisphenol-A (BPA) increases lipid content and fat accumulation in the liver while simultaneously altering gut microbiome composition in mouse models (Di Ciaula *et al.*, 2020). In female C57BL/6 mice, oral exposure to polychlorinated biphenyl 126 (PCB126), affected gut microbiota composition, promoted dyslipidemia and NAFLD (Di Ciaula *et al.*, 2020). Another example demonstrates that in mouse models, chow diet with enrichment of six commonly used pesticides developed glucose intolerance and liver steatosis as well as perturbations of gut microbiota that correlated to altered urinary concentration of microbiota-related metabolites (Di Ciaula *et al.*, 2020). Sub-chronic exposure to Cadmium (Cd) in drinking water increased hepatic

triacylglycerol and liver inflammation, and changes in energy metabolism were paralleled by decreases in Firmicutes and y-proteobacteria in the gut microbiome. Additionally, another mouse study demonstrated low dose Cd exposure in early life leads to metabolic alterations developed together with altered microbiota composition (Di Ciaula *et al.*, 2020). Evidence has indicated that BPA causes dysbiosis that leads to the accumulation of hepatic lipids and steatosis, and that BPA-induced hepatic steatosis was related to the activation of the gut-liver axis (Di Ciaula *et al.*, 2020; Feng *et al.*, 2020). Furthermore, chemicals like the pesticide dichlorodiphenyldichloroethylene (DDE) cause dysbiosis that has strongly correlated with altered blood levels of phospholipids and triacylglycerols (Di Ciaula *et al.*, 2020). Additionally, chemical tetrachlorodibenzo-p-dioxin (TCDD) leads to dysbiosis related to the disruption of the enterohepatic cycle which is characterized by depletion of fecal BAs and increased intestinal permeability (Di Ciaula *et al.*, 2020). A recent study demonstrated that DBP was capable of causing disordered lipid metabolism in the liver, altered structure and composition of the gut microbiota composition and activated immune pathways to cause inflammation in the liver (Xiong *et al.*, 2020). Another study demonstrated low-dose Cd exposure affects intestinal permeability, altered composition of gut microbiota, allowed Cd accumulation in the liver and altered normal functions of multiple metabolic pathways (Liu *et al.*, 2020).

Chapter 1 Figures

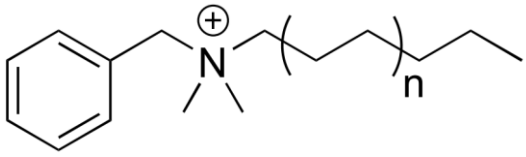

Figure 1.1 Benzalkonium Chloride (BAC) Structure.

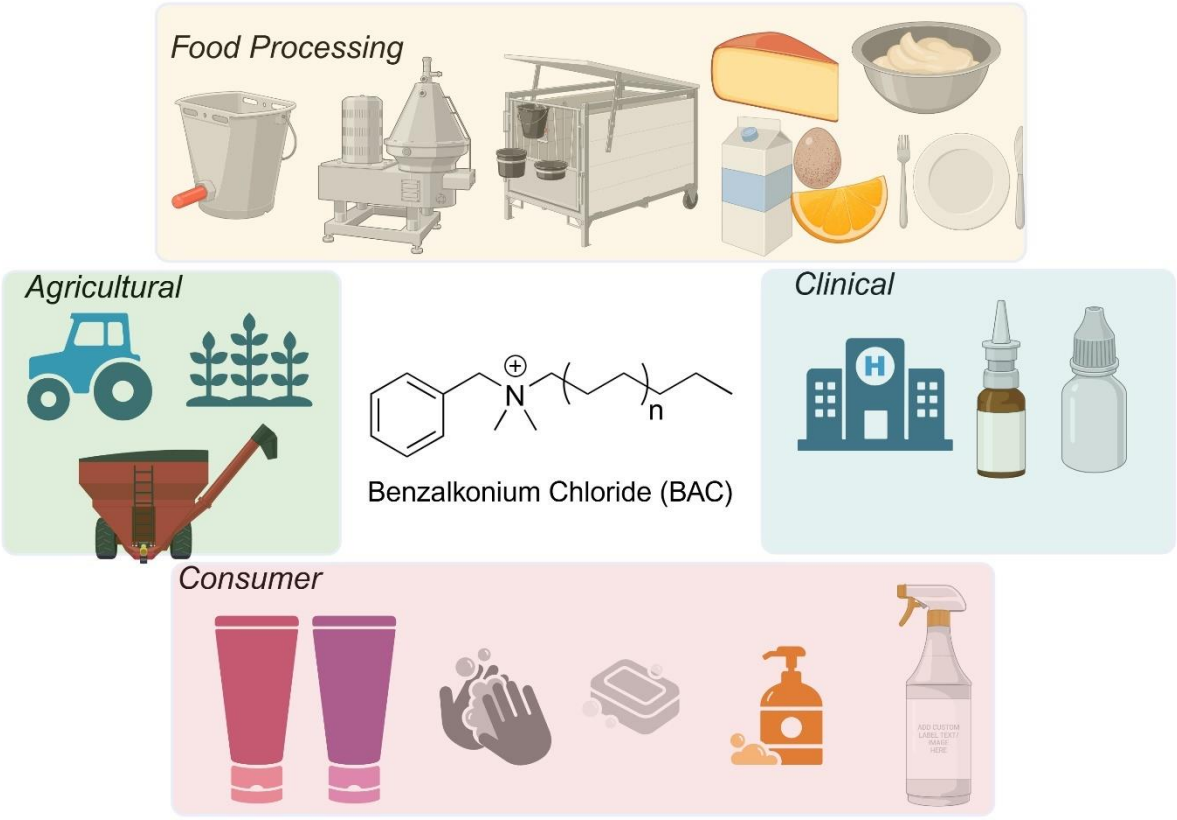

Figure 1.2 Examples of BAC Usage.

Made with BioRender.

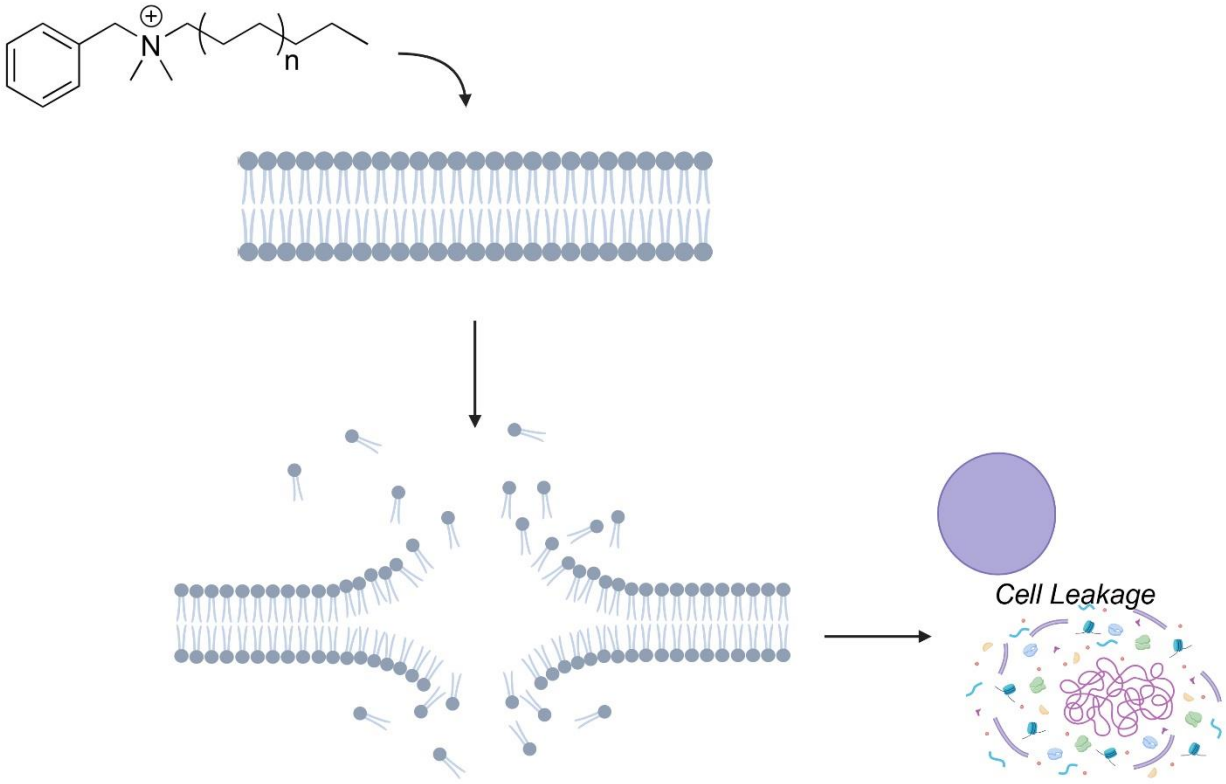

Figure 1.3 Mechanism of BAC Disruption.

Made with BioRender.

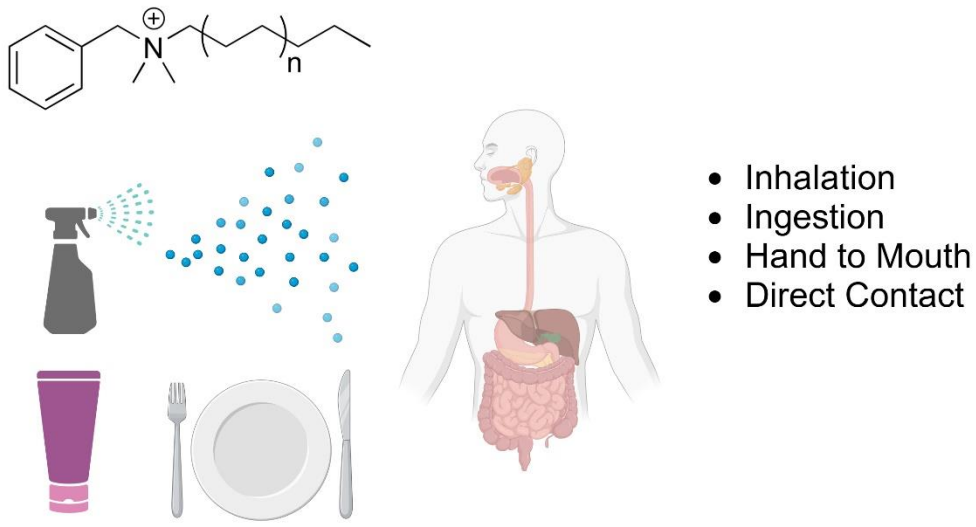

Figure 1.4 BAC Exposure Routes.

Made with BioRender.

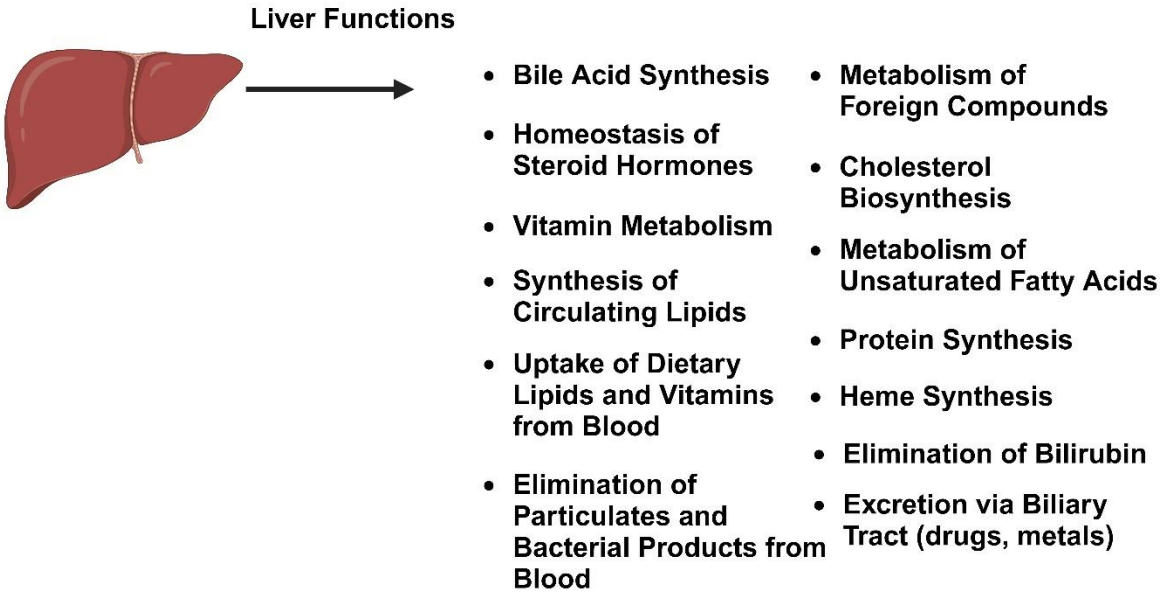

Figure 1.5 Liver Functions.

Made with BioRender.

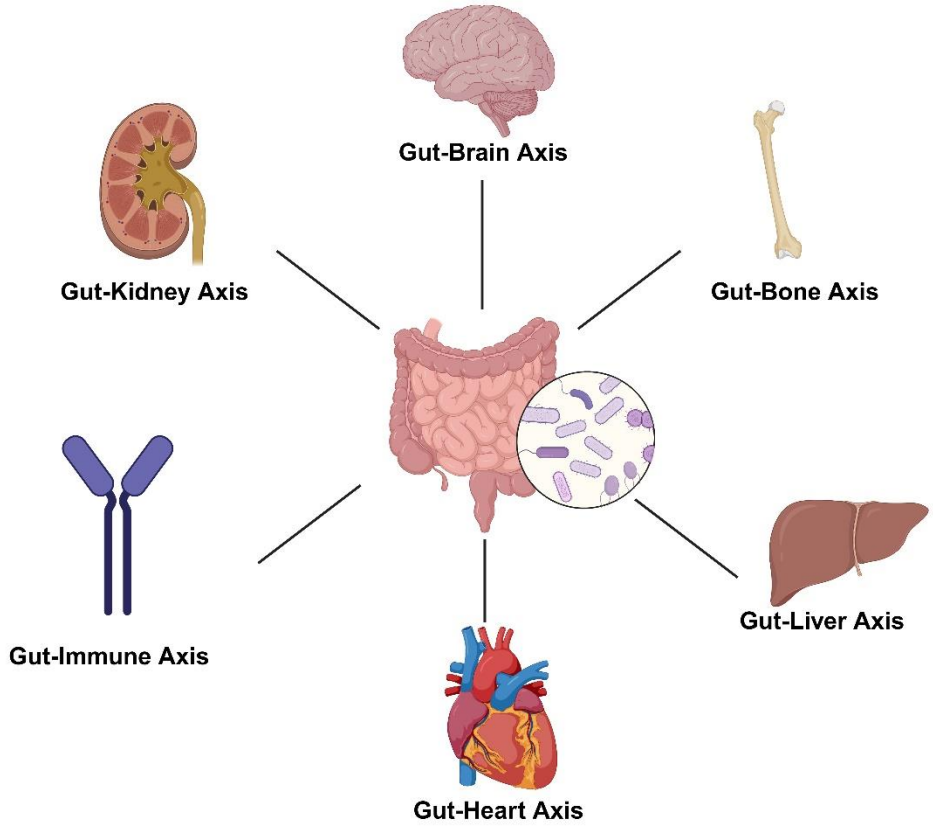

Figure 1.6 Gut-Organ Axis Examples.

Made with BioRender.

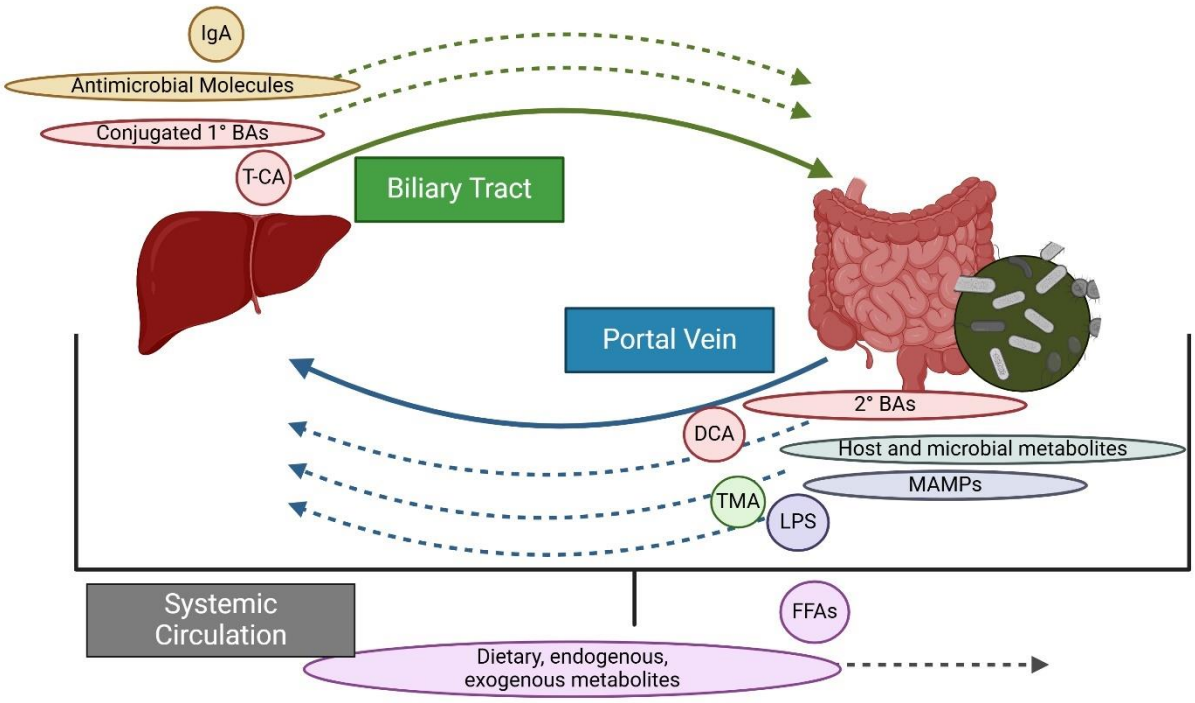

Figure 1.7 The Gut-Liver Axis.

Made with BioRender.

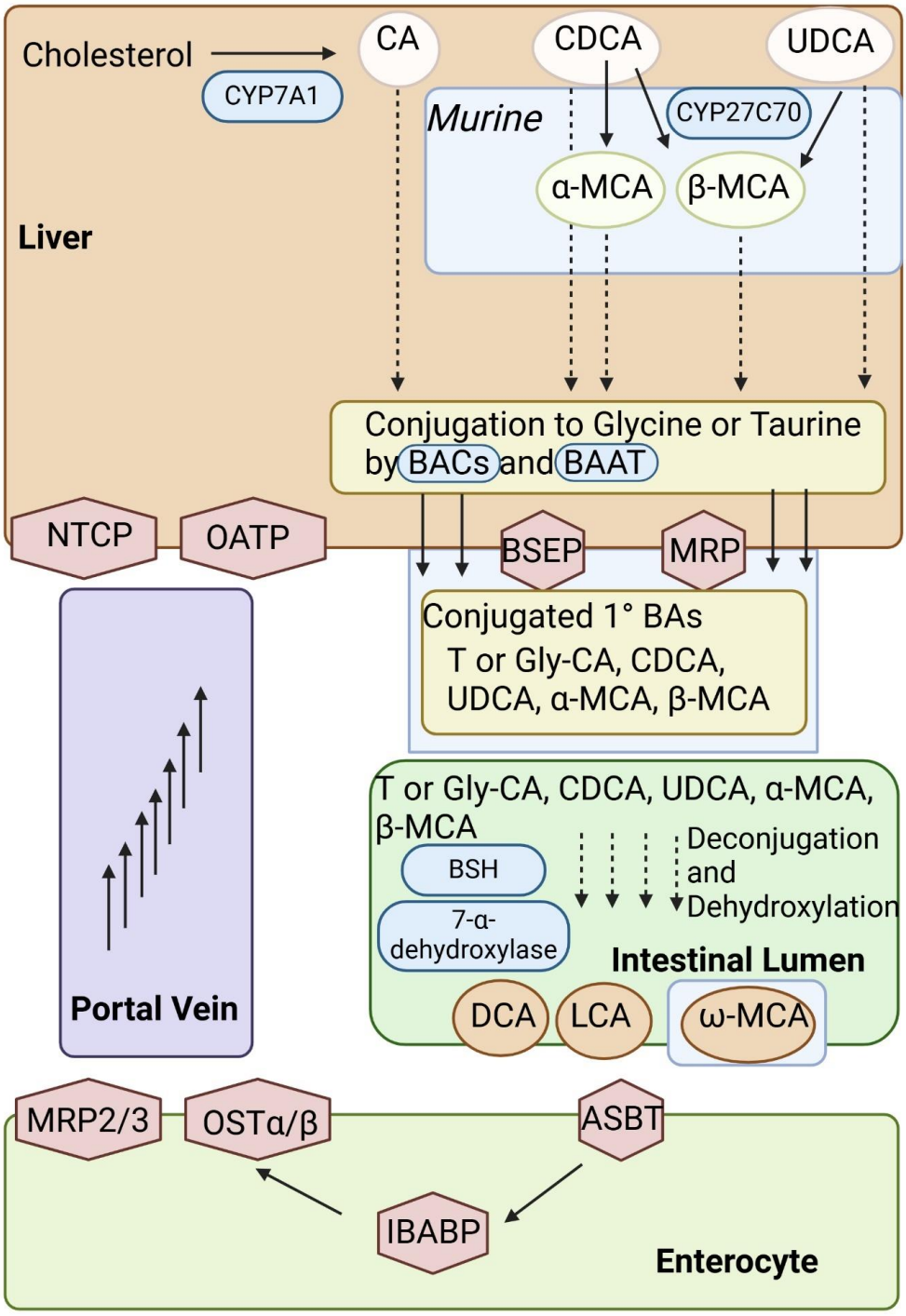

Figure 1.8 Example of Enterohepatic Circulation of BAs.

Made with BioRender.

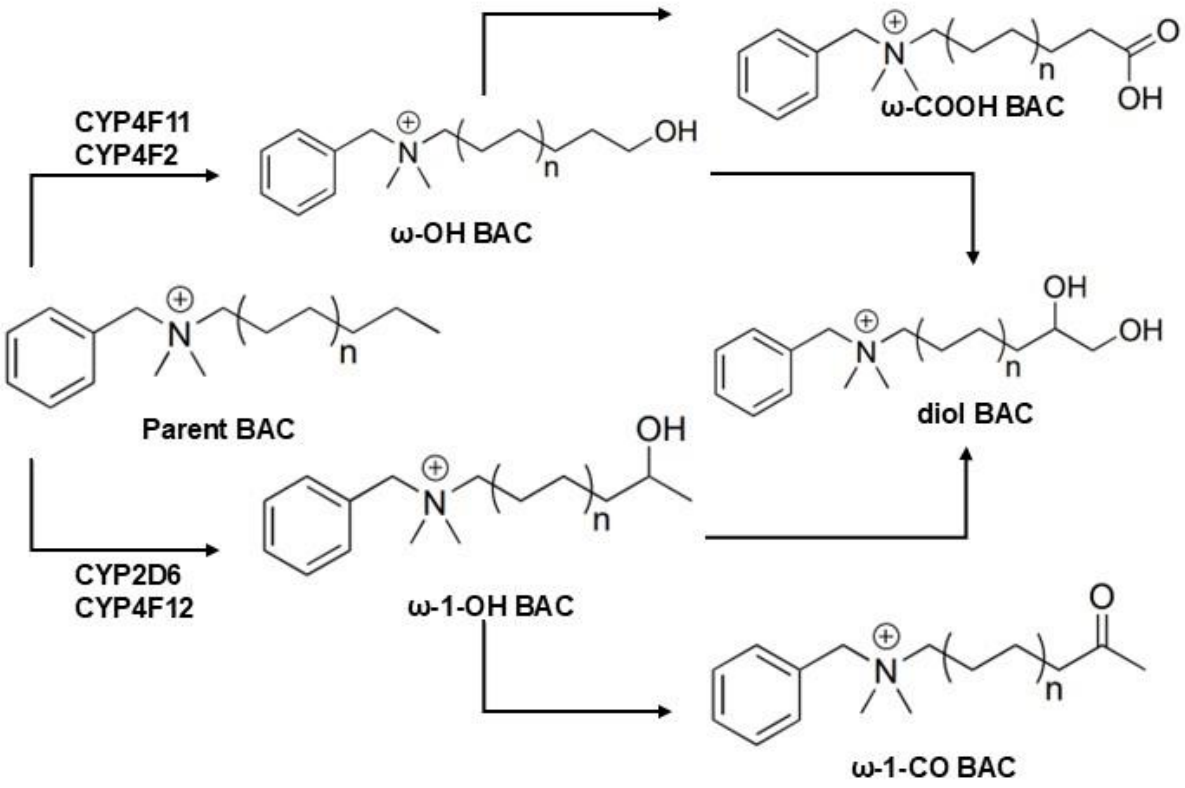

Figure 1.9 Metabolism of BACs by P450.

Chapter 1 Tables

Table 1.1 Induction and Suppression of CYPs by NRs in Human and Mouse.

1. (Hrycay and Bandiera, 2009)
2. (Abraham *et al.*, 2002)
3. (Kapelyukh *et al.*, 2019)
4. (Kwon *et al.*, 2021)
5. (Hakkola *et al.*, 2020)
6. (Chiang *et al.*, 2001)
7. (Goodwin *et al.*, 2000a)

Table 1.1 Induction and Suppression of CYPs by NRs

(+) represents induction; (-) represents suppression; unless otherwise denoted, all data is in liver. (O): Ovary; (D): Duodenum; (K): Kidney

Nuclear Receptor	CYP Genes Human	Cyp Genes Mouse
AhR	CYP1A1 (+)[1, 3, 4] (D) (+)[5] CYP1A2 (+)[1, 2, 3, 4, 5] CYP1B1 (+)[1, 4] CYP2S1 (+)[1]	Cyp1a1 (+)[1] Cyp1a2 (+)[1] Cyp1b1 (+)[1] Cyp2s1 (+)[1] Cyp2a5 (+)[1]
PXR	CYP2A6 (+)[1] CYP2B6 (+)[1,5] CYP2C8 (+)[1, 5] CYP2C9 (+)[1, 5] CYP2C19 (+)[1, 5] CYP3A4 (+)[1, 5] CYP3A5 (D) (+)[5] CYP3A7 (D) (+)[5] CYP3A43 (D) (+)[5]	Cyp2a4 (+)[1] Cyp2b10 (+)[1] Cyp2c55 (+)[1] Cyp3a11 (L) (D) (+)[1] Cyp3a13 (+) (D) [1] Cyp3a16 (+) (D) [1] Cyp4a14 (+)[1] Cyp3a44 (+)[1]
CAR	CYP2A6 (+)[1] CYP2B6 (+)[1] CYP2C8 (+)[1] CYP2C9 (+)[1] CYP2C19 (+)[1] CYP3A4 (+)[1]	Cyp2a4 (+)[1] Cyp2a5 (+)[1] Cyp2b10 (+)[1] Cyp2c29 (+)[1] Cyp2c37 (+)[1] Cyp3a11 (+)[1] Cyp3a44 (+)[1] Cyp2a41 (-)[1] Cyp2c40 (-)[1]
PPARa	CYPA (+)[1] CYPF (+)[1] CYP4F11 (+)[1] CYP4A11 (+)[1]	Cyp11a1 (O) (-)[1] Cyp17a1 (O) (+)[1] Cyp19a1 (O) (-)[1] Cyp2a5 (-)[1]

		Cyp2b10 (+)[1] Cyp3a11 (+), (-)[1] Cyp4a10 (+), (-)[1] Cyp4a14 (+)[1], (K) (-)[1] Cyp4f15 (K) (+)[1] Cyp2c29 (-)[1]
PPARy		Cyp3a13 (-)[1]
ER	CYP2A6 (+)[5]	
LXRa		Cyp7a1 (+)[1, 6] Cyp7b1 (-)[1]
FXR	CYP7A1[7]	Cyp7a1 (-)[1] Cyp8b1 (-)[1]
ROR		Cyp2b9 (+)[1] Cyp2b10 (+)[1] Cyp2b13 (+)[1] Cyp2c38 (+)[1] Cyp3a11 (+)[1] Cyp3a25 (+)[1] Cyp3a41 (+)[1] Cyp4a10 (+)[1] Cyp4a14 (+)[1] Cyp7b1 (-)[1] Cyp8b1 (-)[1]

Chapter 1 References

Abraham, K. *et al.* (2002) Severe 2,3,7,8-tetrachlorodibenzo- *p* -dioxin (TCDD) intoxication: Insights into the measurement of hepatic cytochrome P450 1A2 induction*. *Clin. Pharmacol. Ther.*, **72**, 163–174.

Ahlawat, S. *et al.* (2021) Gut–organ axis: a microbial outreach and networking. *Lett. Appl. Microbiol.*, **72**, 636–668.

Arnold, W.A. *et al.* (2023) Quaternary Ammonium Compounds: A Chemical Class of Emerging Concern. *Environ. Sci. Technol.*

Asgharpour, A. *et al.* (2015) Bile acids: emerging role in management of liver diseases. *Hepatol. Int.*, **9**, 527–533.

Barko, P.C. *et al.* (2018) The Gastrointestinal Microbiome: A Review. *J. Vet. Intern. Med.*, **32**, 9–25.

Baudouin, C. *et al.* (1999) Ocular surface inflammatory changes induced by topical antiglaucoma drugs: human and animal studies. *Ophthalmology*, **106**, 556–63.

Bhattacharya, A. *et al.* (2023) In vivo mouse models to study bile acid synthesis and signaling. *Hepatobiliary Pancreat. Dis. Int.*, **22**, 466–473.

Bond, P. (2017) Phosphatidic acid: biosynthesis, pharmacokinetics, mechanisms of action and effect on strength and body composition in resistance-trained individuals. *Nutr. Metab.*, **14**, 12.

Boursier, J. and Diehl, A.M. (2015) Implication of Gut Microbiota in Nonalcoholic Fatty Liver Disease. *PLOS Pathog.*, **11**, e1004559.

Breton, J. *et al.* (2013) Ecotoxicology inside the gut: impact of heavy metals on the mouse microbiome. *BMC Pharmacol. Toxicol.*, **14**, 62.

Caporaso, J.G. *et al.* (2010) QIIME allows analysis of high-throughput community sequencing data. *Nat Methods*, **7**, 335–6.

Chen, M. *et al.* (2021) Enterohepatic circulation of bile acids and their emerging roles on glucolipid metabolism. *Steroids*, **165**, 108757.

Chew, J.L. and Chua, K.Y. (2003) Collection of Mouse Urine for Bioassays. *Lab Anim.*, **32**, 48–50.

Chiang, H.-L. and Lin, C.-H. (2019) Altered Gut Microbiome and Intestinal Pathology in Parkinson's Disease. *J. Mov. Disord.*, **12**, 67–83.

Chiang, J.Y. *et al.* (2000) Farnesoid X receptor responds to bile acids and represses cholesterol 7alpha-hydroxylase gene (CYP7A1) transcription. *J Biol Chem*, **275**, 10918–24.

Chiang, J.Y.L. *et al.* (2001) Regulation of cholesterol 7α-hydroxylase gene (CYP7A1) transcription by the liver orphan receptor (LXRα). *Gene*, **262**, 257–265.

Chiang, J.Y.L. and Ferrell, J.M. (2018) Bile Acid Metabolism in Liver Pathobiology. *Gene Expr.*, **18**, 71–87.

Chiu, K. *et al.* (2020) The Impact of Environmental Chemicals on the Gut Microbiome. *Toxicol. Sci.*, **176**, 253–284.

Chow, M.D. *et al.* (2017) The role of bile acids in nonalcoholic fatty liver disease and nonalcoholic steatohepatitis. *Mol. Aspects Med.*, **56**, 34–44.

Claus, S.P. *et al.* (2016) The gut microbiota: a major player in the toxicity of environmental pollutants? *Npj Biofilms Microbiomes*, **2**, 16003.

Clayton, P.T. (1998) Disorders of cholesterol biosynthesis. *Arch Child*, **78**, 185–9.

Cryle, M.J. and De Voss, J.J. (2004) Carbon–carbon bond cleavage by cytochrome P450 $_{BioI}$ (CYP107H1). *Chem Commun*, 86–87.

Cui, J.Y. and Klaassen, C.D. (2016) RNA-Seq reveals common and unique PXR- and CAR-target gene signatures in the mouse liver transcriptome. *Biochim Biophys Acta*, **1859**, 1198–1217.

Dalhat, M.H. *et al.* (2022) NAT10: An RNA cytidine transferase regulates fatty acid metabolism in cancer cells. *Clin. Transl. Med.*, **12**, e1045.

Deutschle, T. *et al.* (2006) In vitro genotoxicity and cytotoxicity of benzalkonium chloride. *Toxicol. In Vitro*, **20**, 1472–1477.

Di Ciaula, A. *et al.* (2020) Liver Steatosis, Gut-Liver Axis, Microbiome and Environmental Factors. A Never-Ending Bidirectional Cross-Talk. *J. Clin. Med.*, **9**, 2648.

Edson, K. and Rettie, A. (2013) CYP4 Enzymes As Potential Drug Targets: Focus on Enzyme Multiplicity, Inducers and Inhibitors, and Therapeutic Modulation of 20-Hydroxyeicosatetraenoic Acid (20-HETE) Synthase and Fatty Acid ω-Hydroxylase Activities. *Curr. Top. Med. Chem.*, **13**, 1429–1440.

Edson, K. Z. *et al.* (2013) Cytochrome P450-dependent catabolism of vitamin K: omega-hydroxylation catalyzed by human CYP4F2 and CYP4F11. *Biochemistry*, **52**, 8276–85.

Edson, Katheryne Z. *et al.* (2013) Cytochrome P450-Dependent Catabolism of Vitamin K: ω-Hydroxylation Catalyzed by Human CYP4F2 and CYP4F11. *Biochemistry*, **52**, 8276–8285.

Eloe-Fadrosh, E.A. and Rasko, D.A. (2013) The human microbiome: from symbiosis to pathogenesis. *Annu Rev Med*, **64**, 145–63.

Esteves, F. *et al.* (2021) The Central Role of Cytochrome P450 in Xenobiotic Metabolism—A Brief Review on a Fascinating Enzyme Family. *J. Xenobiotics*, **11**, 94–114.

Fan, Y. and Pedersen, O. (2021) Gut microbiota in human metabolic health and disease. *Nat Rev Microbiol*, **19**, 55–71.

Fazeli, M. *et al.* (2011) Cadmium chloride exhibits a profound toxic effect on bacterial microflora of the mice gastrointestinal tract. *Hum. Exp. Toxicol.*, **30**, 152–159.

Feng, D. *et al.* (2020) Bisphenol A exposure induces gut microbiota dysbiosis and consequent activation of gut-liver axis leading to hepatic steatosis in CD-1 mice. *Environ. Pollut.*, **265**, 114880.

Finkelstein, J. *et al.* (2014) Lipids in health and disease. *Nature*, **510**, 47–47.

Fleishman, J.S. and Kumar, S. (2024) Bile acid metabolism and signaling in health and disease: molecular mechanisms and therapeutic targets. *Signal Transduct. Target. Ther.*, **9**, 97.

Fu, Z.D. *et al.* (2017) RNA-Seq Profiling of Intestinal Expression of Xenobiotic Processing Genes in Germ-Free Mice. *Drug Metab Dispos*, **45**, 1225–1238.

Fuchs, C.D. and Trauner, M. (2022) Role of bile acids and their receptors in gastrointestinal and hepatic pathophysiology. *Nat. Rev. Gastroenterol. Hepatol.*, **19**, 432–450.

Ghazalpour, A. *et al.* (2016) Expanding role of gut microbiota in lipid metabolism. *Curr Opin Lipidol*, **27**, 141–7.

Goldstein, J.L. *et al.* (2006) Protein sensors for membrane sterols. *Cell*, **124**, 35–46.

Gonzalez, M. *et al.* (2014) Asthma among workers in healthcare settings: role of disinfection with quaternary ammonium compounds. *Clin. Exp. Allergy*, **44**, 393–406.

Goodwin, B. *et al.* (2000a) A Regulatory Cascade of the Nuclear Receptors FXR, SHP-1, and LRH-1 Represses Bile Acid Biosynthesis. *Mol. Cell*, **6**, 517–526.

Goodwin, B. *et al.* (2000b) A Regulatory Cascade of the Nuclear Receptors FXR, SHP-1, and LRH-1 Represses Bile Acid Biosynthesis. *Mol. Cell*, **6**, 517–526.

Grangeon, A. *et al.* (2021) Determination of CYP450 Expression Levels in the Human Small Intestine by Mass Spectrometry-Based Targeted Proteomics. *Int. J. Mol. Sci.*, **22**, 12791.

Guengerich, F.P. and Yoshimoto, F.K. (2018) Formation and Cleavage of C–C Bonds by Enzymatic Oxidation–Reduction Reactions. *Chem. Rev.*, **118**, 6573–6655.

Hakkola, J. *et al.* (2020) Inhibition and induction of CYP enzymes in humans: an update. *Arch. Toxicol.*, **94**, 3671–3722.

Herron, J. *et al.* (2018) Assessment of Altered Cholesterol Homeostasis by Xenobiotics Using Ultra-High Performance Liquid Chromatography-Tandem Mass Spectrometry. *Curr Protoc Toxicol*, **78**, e65.

Herron, J. *et al.* (2016) Identification of Environmental Quaternary Ammonium Compounds as Direct Inhibitors of Cholesterol Biosynthesis. *Toxicol Sci*, **151**, 261–270.

Herron, J.M. *et al.* (2019) Multiomics investigation reveals benzalkonium chloride disinfectants alter sterol and lipid homeostasis in the mouse neonatal brain. *Toxicol Sci*, **171**, 32–45.

Hild, B. *et al.* (2021) Bile Acids in Control of the Gut-Liver-Axis. *Z. Für Gastroenterol.*, **59**, 63–68.

Hills, R. *et al.* (2019) Gut Microbiome: Profound Implications for Diet and Disease. *Nutrients*, **11**, 1613.

Hines, K. *et al.* (2017) Assessment of Altered Lipid Homeostasis by HILIC-Ion Mobility-Mass Spectrometry-Based Lipidomics. *J Lipid Res*, **58**, 809–819.

Hines, K.M. *et al.* (2016) Evaluation of Collision Cross Section Calibrants for Structural Analysis of Lipids by Traveling Wave Ion Mobility-Mass Spectrometry. *Anal Chem*, **88**, 7329–36.

Hirani, V. *et al.* (2008) Expression of CYP4F2 in human liver and kidney: Assessment using targeted peptide antibodies. *Arch. Biochem. Biophys.*, **478**, 59–68.

Hitosugi, M. *et al.* (1998) A case of fatal benzalkonium chloride poisoning. *Int J Leg. Med*, **111**, 265–6.

Hofmann, A.F. (1999) The Continuing Importance of Bile Acids in Liver and Intestinal Disease. *Arch. Intern. Med.*, **159**, 2647.

Holter, M.M. *et al.* (2020) TGR5 Signaling in Hepatic Metabolic Health. *Nutrients*, **12**, 2598.

Hrubec, T.C. *et al.* (2021a) Altered toxicological endpoints in humans from common quaternary ammonium compound disinfectant exposure. *Toxicol Rep*, **8**, 646–656.

Hrubec, T.C. *et al.* (2021b) Altered toxicological endpoints in humans from common quaternary ammonium compound disinfectant exposure. *Toxicol Rep*, **8**, 646–656.

Hrubec, T.C. *et al.* (2017) Ambient and Dosed Exposure to Quaternary Ammonium Disinfectants Causes Neural Tube Defects in Rodents. *Birth Defects Res*, **109**, 1166–1178.

Hrycay, E. and Bandiera, S. (2009) Expression, Function and Regulation of Mouse Cytochrome P450 Enzymes: Comparison With Human Cytochrome P450 Enzymes. *Curr. Drug Metab.*, **10**, 1151–1183.

Hukkanen, J. *et al.* (2002) Expression and Regulation of Xenobiotic-Metabolizing Cytochrome P450 (CYP) Enzymes in Human Lung. *Crit. Rev. Toxicol.*, **32**, 391–411.

Jaeschke, H. (2015) Toxic Responses of the Liver. In, Klaassen,C.D. and Watkins III,J.B. (eds), *Casarett & Doull's Essentials of Toxicology, 3e*. McGraw-Hill Education, New York, NY.

Jiang, L. *et al.* (2021) Farnesoid X receptor (FXR): Structures and ligands. *Comput. Struct. Biotechnol. J.*, **19**, 2148–2159.

Johnson, A.L. *et al.* (2015) Cytochrome P450 omega-Hydroxylases in Inflammation and Cancer. *Adv Pharmacol*, **74**, 223–62.

Johnson, E.L. *et al.* (2020) Sphingolipids produced by gut bacteria enter host metabolic pathways impacting ceramide levels. *Nat Commun*, **11**, 2471.

Kapelyukh, Y. *et al.* (2019) Defining the Contribution of CYP1A1 and CYP1A2 to Drug Metabolism Using Humanized CYP1A1/1A2 and Cyp1a1/Cyp1a2 Knockout Mice. *Drug Metab. Dispos.*, **47**, 907–918.

Kera, H. *et al.* (2021) Kinetics and distribution of benzalkonium compounds with different alkyl chain length following intravenous administration in rats. *Leg. Med.*, **48**, 101821.

Kim, Y.S. *et al.* (2020) Sex Differences in Gut Microbiota. *World J. Mens Health*, **38**, 48.

Klyushova, L.S. *et al.* (2022) The Role of CYP3A in Health and Disease. *Biomedicines*, **10**, 2686.

Kojima, R. *et al.* (2016) A phospholipid transfer function of ER-mitochondria encounter structure revealed in vitro. *Sci. Rep.*, **6**, 30777.

Koliada, A. *et al.* (2021) Sex differences in the phylum-level human gut microbiota composition. *BMC Microbiol.*, **21**, 131.

Koontz, J.M. *et al.* (2019) The Role of the Human Microbiome in Chemical Toxicity. *Int. J. Toxicol.*, **38**, 251–264.

Kröckel, L. *et al.* (2003) Identification of benzalkonium chloride in food additives and its inefficacy against bacteria in minced meat and raw sausage batters. *Eur. Food Res. Technol.*, **216**, 402–406.

Kuban, W. and Daniel, W.A. (2021) Cytochrome P450 expression and regulation in the brain. *Drug Metab. Rev.*, **53**, 1–29.

Kwon, Y.-J. *et al.* (2021) Biological roles of cytochrome P450 1A1, 1A2, and 1B1 enzymes. *Arch. Pharm. Res.*, **44**, 63–83.

Lee, B.H. and Kim, S.H. (2007) Benzalkonium chloride induced bronchoconstriction in patients with stable bronchial asthma. *Korean J Intern Med*, **22**, 244–8.

Lee, H. and Park, K. (2019) Acute toxicity of benzalkonium chloride in Balb/c mice following intratracheal instillation and oral administration. *Environ. Anal. Health Toxicol.*, **34**, e2019009.

Levy, M. *et al.* (2017) Microbiome, metabolites and host immunity. *Curr. Opin. Microbiol.*, **35**, 8–15.

Li, A. *et al.* (2020) Lipidomics by HILIC-Ion Mobility-Mass Spectrometry. *Methods Mol. Biol.*, **2084**, 119–132.

Li, C. Y. *et al.* (2018) PBDEs Altered Gut Microbiome and Bile Acid Homeostasis in Male C57BL/6 Mice. *Drug Metab Dispos*, **46**, 1226–1240.

Li, Cindy Yanfei *et al.* (2018) PBDEs Altered Gut Microbiome and Bile Acid Homeostasis in Male C57BL/6 Mice. *Drug Metab. Dispos.*, **46**, 1226–1240.

Li, D. *et al.* (2020) Evaluating consumer exposure to disinfecting chemicals against coronavirus disease 2019 (COVID-19) and associated health risks. *Env. Int*, **145**, 106108.

Li, S. *et al.* (2021) Cytochrome P450 Omega-Hydroxylase 4a14 Attenuates Cholestatic Liver Fibrosis. *Front. Physiol.*, **12**, 688259.

Li, T. and Chiang, J.Y.L. (2012) Bile Acid Signaling in Liver Metabolism and Diseases. *J. Lipids*, **2012**, 1–9.

Liao, Y. *et al.* (2014) featureCounts: an efficient general purpose program for assigning sequence reads to genomic features. *Bioinformatics*, **30**, 923–930.

Liu, X. *et al.* (2021) *Blautia* —a new functional genus with potential probiotic properties? *Gut Microbes*, **13**, 1875796.

Liu, Y. *et al.* (2020) The Dysbiosis of Gut Microbiota Caused by Low-Dose Cadmium Aggravate the Injury of Mice Liver through Increasing Intestinal Permeability. *Microorganisms*, **8**, 211.

Lopez, V.A. *et al.* (2024) Oral Exposure to Benzalkonium Chlorides in Male and Female Mice Reveals Sex-Dependent Alteration of the Gut Microbiome and Bile Acid Profile. *bioRxiv*, 2024.05.13.593991.

Love, M.I. *et al.* (2014) Moderated estimation of fold change and dispersion for RNA-seq data with DESeq2. *Genome Biol*, **15**, 550.

Lu, J. *et al.* (2020) New insights of CYP1A in endogenous metabolism: a focus on single nucleotide polymorphisms and diseases. *Acta Pharm. Sin. B*, **10**, 91–104.

Lu, K. *et al.* (2014) Arsenic Exposure Perturbs the Gut Microbiome and Its Metabolic Profile in Mice: An Integrated Metagenomics and Metabolomics Analysis. *Environ. Health Perspect.*, **122**, 284–291.

Luz, A. *et al.* (2020) Human health hazard assessment of quaternary ammonium compounds: Didecyl dimethyl ammonium chloride and alkyl (C12-C16) dimethyl benzyl ammonium chloride. *Regul Toxicol Pharmacol*, **116**, 104717.

Manor, O. *et al.* (2020) Health and disease markers correlate with gut microbiome composition across thousands of people. *Nat. Commun.*, **11**, 5206.

Manos, J. (2022) The human microbiome in disease and pathology. *APMIS*, **130**, 690–705.

Melin, V.E. *et al.* (2014) Exposure to common quaternary ammonium disinfectants decreases fertility in mice. *Reprod Toxicol*, **50**, 163–70.

Melin, V.E. *et al.* (2016) Quaternary ammonium disinfectants cause subfertility in mice by targeting both male and female reproductive processes. *Reprod Toxicol*, **59**, 159–66.

Merchel Piovesan Pereira, B. and Tagkopoulos, I. (2019) Benzalkonium Chlorides: Uses, Regulatory Status, and Microbial Resistance. *Appl. Environ. Microbiol.*, **85**, e00377-19.

Mertens, K.L. *et al.* (2017) Bile Acid Signaling Pathways from the Enterohepatic Circulation to the Central Nervous System. *Front. Neurosci.*, **11**, 617.

Minchin, R.F. *et al.* (2007) Arylamine N-acetyltransferase I. *Int. J. Biochem. Cell Biol.*, **39**, 1999–2005.

Mishima-Kimura, S. *et al.* (2018) Liquid chromatography-tandem mass spectrometry detection of benzalkonium chloride (BZK) in a forensic autopsy case with survival for 18 days post BZK ingestion. *Leg Med Tokyo*, **32**, 48–51.

Mohapatra, S. *et al.* (2023) Quaternary ammonium compounds of emerging concern: Classification, occurrence, fate, toxicity and antimicrobial resistance. *J. Hazard. Mater.*, **445**, 130393.

Molinero, N. *et al.* (2019) Intestinal Bacteria Interplay With Bile and Cholesterol Metabolism: Implications on Host Physiology. *Front Physiol*, **10**, 185.

Monte, M.J. *et al.* (2009) Bile acids: Chemistry, physiology, and pathophysiology. *World J. Gastroenterol.*, **15**, 804.

Naspolini, N.F. *et al.* (2022) Environmental pollutant exposure associated with altered early-life gut microbiome: Results from a birth cohort study. *Environ. Res.*, **205**, 112545.

Nguyen, R. *et al.* (2024) Development and Application of a Multidimensional Database for the Detection of Quaternary Ammonium Compounds and Their Phase I Hepatic Metabolites in Humans. *Environ. Sci. Technol.*, **58**, 6236–6249.

O'Flaherty, S. *et al.* (2018) The *Lactobacillus* Bile Salt Hydrolase Repertoire Reveals Niche-Specific Adaptation. *mSphere*, **3**, e00140-18.

Okita, R.T. *et al.* (1979) Lauric acid hydroxylation in human liver and kidney cortex microsomes. *Biochem. Pharmacol.*, **28**, 3385–3390.

Patterson, A.D. *et al.* (2010) Xenobiotic Metabolism: A View through the Metabolometer. *Chem. Res. Toxicol.*, **23**, 851–860.

Petriello, M.C. *et al.* (2018) Dioxin-like PCB 126 increases intestinal inflammation and disrupts gut microbiota and metabolic homeostasis. *Environ. Pollut.*, **242**, 1022–1032.

Phelps, T. *et al.* (2019) The influence of biological sex and sex hormones on bile acid synthesis and cholesterol homeostasis. *Biol. Sex Differ.*, **10**, 52.

Phillips, I.R. and Shephard, E.A. (2017) Drug metabolism by flavin-containing monooxygenases of human and mouse. *Expert Opin. Drug Metab. Toxicol.*, **13**, 167–181.

Pradista, L.A. *et al.* (2022) Metagenomic analysis of non-pathogenic and pathogenic cecal bacteria profiles in quail supplemented with betaine. *IOP Conf. Ser. Earth Environ. Sci.*, **1114**, 012008.

Prysyazhnyuk, V. *et al.* (2021) Glutathione-S-transferases genes-promising predictors of hepatic dysfunction. *World J. Hepatol.*, **13**, 620–633.

Qin, X. and Wang, X. (2019) Role of vitamin D receptor in the regulation of CYP3A gene expression. *Acta Pharm. Sin. B*, **9**, 1087–1098.

Qiu, X. *et al.* (2016) Disruption of BSEP Function in HepaRG Cells Alters Bile Acid Disposition and Is a Susceptive Factor to Drug-Induced Cholestatic Injury. *Mol. Pharm.*, **13**, 1206–1216.

Rinninella, E. *et al.* (2019) What is the Healthy Gut Microbiota Composition? A Changing Ecosystem across Age, Environment, Diet, and Diseases. *Microorganisms*, **7**, 14.

Robinson, A.J. *et al.* (2017) Granular parakeratosis induced by benzalkonium chloride exposure from laundry rinse aids. *Australas J Dermatol*, **58**, e138–e140.

Röder, A. *et al.* (2023) Spotlight on CYP4B1. *Int. J. Mol. Sci.*, **24**, 2038.

Ross, D.H. *et al.* (2020) LiPydomics: A Python Package for Comprehensive Prediction of Lipid Collision Cross Sections and Retention Times and Analysis of Ion Mobility-Mass Spectrometry-Based Lipidomics Data. *Anal. Chem.*, **92**, 14967–14975.

Sarkar, J. *et al.* (2012) Corneal neurotoxicity due to topical benzalkonium chloride. *Invest Ophthalmol Vis Sci*, **53**, 1792–802.

Saxami, G. *et al.* (2023) The Gut–Organ Axis within the Human Body: Gut Dysbiosis and the Role of Prebiotics. *Life*, **13**, 2023.

Schneider, K.M. *et al.* (2018) Role of bile acids in the gut-liver axis. *J. Hepatol.*, **68**, 1083–1085.

Seebacher, F. *et al.* (2020) Hepatic lipid droplet homeostasis and fatty liver disease. *Semin. Cell Dev. Biol.*, **108**, 72–81.

Seguin, R. P. *et al.* (2019) Metabolism of Benzalkonium Chlorides by Human Hepatic Cytochromes P450. *Chem Res Toxicol*, **32**, 2466–2478.

Seguin, Ryan P. *et al.* (2019) Metabolism of Benzalkonium Chlorides by Human Hepatic Cytochromes P450. *Chem. Res. Toxicol.*, **32**, 2466–2478.

Selwyn, F.P., Cheng, S.L., *et al.* (2015) Developmental Regulation of Drug-Processing Genes in Livers of Germ-Free Mice. *Toxicol Sci*, **147**, 84–103.

Selwyn, F.P. *et al.* (2016) Regulation of Hepatic Drug-Metabolizing Enzymes in Germ-Free Mice by Conventionalization and Probiotics. *Drug Metab Dispos*, **44**, 262–74.

Selwyn, F.P., Cui, J.Y., *et al.* (2015) RNA-Seq Quantification of Hepatic Drug Processing Genes in Germ-Free Mice. *Drug Metab Dispos*, **43**, 1572–80.

Shulpekova, Y. *et al.* (2022) The Role of Bile Acids in the Human Body and in the Development of Diseases. *Molecules*, **27**, 3401.

Siddiqui, R. *et al.* (2022) The Gut Microbiome and Female Health. *Biology*, **11**, 1683.

Sim, E. *et al.* (2014) Arylamine N-acetyltransferases: from drug metabolism and pharmacogenetics to drug discovery. *Br. J. Pharmacol.*, **171**, 2705–2725.

Slimani, K. *et al.* (2017) Liquid chromatography-tandem mass spectrometry multiresidue method for the analysis of quaternary ammonium compounds in cheese and milk products: Development and validation using the total error approach. *J Chromatogr A*, **1517**, 86–96.

Sreevidya, V.S. *et al.* (2018) Benzalkonium chloride, benzethonium chloride, and chloroxylenol - Three replacement antimicrobials are more toxic than triclosan and triclocarban in two model organisms. *Environ. Pollut.*, **235**, 814–824.

Stellaard, F. and Lütjohann, D. (2021) Dynamics of the enterohepatic circulation of bile acids in healthy humans. *Am. J. Physiol.-Gastrointest. Liver Physiol.*, **321**, G55–G66.

Stok, J.E. and De Voss, J.J. (2000) Expression, Purification, and Characterization of BioI: A Carbon–Carbon Bond Cleaving Cytochrome P450 Involved in Biotin Biosynthesis in Bacillus subtilis. *Arch. Biochem. Biophys.*, **384**, 351–360.

Takahashi, S. *et al.* (2016) Cyp2c70 is responsible for the species difference in bile acid metabolism between mice and humans. *J. Lipid Res.*, **57**, 2130–2137.

Takeoka, G.R. *et al.* (2005) Identification of benzalkonium chloride in commercial grapefruit seed extracts. *J Agric Food Chem*, **53**, 7630–6.

Taylor, C. *et al.* (2020) A Review of the Important Role of CYP2D6 in Pharmacogenomics. *Genes*, **11**, 1295.

Ten Hove, M. *et al.* (2020) The hepatic lipidome: From basic science to clinical translation. *Adv. Drug Deliv. Rev.*, **159**, 180–197.

The Federal Institute for Risk Assessment (BfR) of Germany (2012) Health assessment of benzalkonium chloride residues in food. *BfR Opin. No 0322012*.

Thursby, E. and Juge, N. (2017) Introduction to the human gut microbiota. *Biochem. J.*, **474**, 1823–1836.

Tian, S. *et al.* (2022) FXR: structures, biology, and drug development for NASH and fibrosis diseases. *Acta Pharmacol. Sin.*, **43**, 1120–1132.

Trapani, L. (2012) Regulation and deregulation of cholesterol homeostasis: The liver as a metabolic "power station". *World J. Hepatol.*, **4**, 184.

Tripathi, A. *et al.* (2018) The gut-liver axis and the intersection with the microbiome. *Nat Rev Gastroenterol Hepatol*, **15**, 397–411.

Tripathi, Anupriya *et al.* (2018) The gut–liver axis and the intersection with the microbiome. *Nat. Rev. Gastroenterol. Hepatol.*, **15**, 397–411.

Tu, P. *et al.* (2020) Gut Microbiome Toxicity: Connecting the Environment and Gut Microbiome-Associated Diseases. *Toxics*, **8**, 19.

Turesky, R.J. and Lu, K. (2020) Biomarkers of Environmental Toxicants: Exposure and Biological Effects. *Toxics*, **8**, 37.

Umehara, K., Kudo, S., Hirao, Y., Morita, S., Ohtani, T., *et al.* (2000) In vitro characterization of the oxidative cleavage of the octyl side chain of olanexidine, a novel antimicrobial agent, in dog liver microsomes. *Drug Metab. Dispos. Biol. Fate Chem.*, **28**, 1417–1424.

Umehara, K., Kudo, S., Hirao, Y., Morita, S., Uchida, M., *et al.* (2000) Oxidative cleavage of the octyl side chain of 1-(3,4-dichlorobenzyl)-5-octylbiguanide (OPB-2045) in rat and dog liver preparations. *Drug Metab. Dispos. Biol. Fate Chem.*, **28**, 887–894.

Umehara, K. *et al.* (2004) Oxidative one-carbon cleavage of the octyl side chain of olanexidine, a novel antimicrobial agent, in dog liver microsomes. *Xenobiotica*, **34**, 61–71.

US EPA (2006) Reregistration Eligibility Decision for Alkyl Dimethyl Benzyl Ammonium Chloride (ADBAC). *EPA-HQ-OPP-2006-0339*, Office of Prevention, Pesticides and Toxic Substances, Antimicrobials Division, U.S. Environmental Protection Agency. Signed on August 3, 2006.

US FDA (2016a) Quaternary ammonium chloride combination. *Code Fed. Regul. 21CFR172165*, Food and Drug Administration, U.S. Department of Health&Human Services. Revised as of April 1, 2016.

US FDA (2016b) Safety and Effectiveness of Consumer Antiseptics; Topical Antimicrobial Drug Products for Over-the-Counter Human Use; Proposed Amendment of the Tentative Final Monograph; Reopening of Administrative Record. *Fed. Regist.*, **21 CFR Part 310, 81**, 42911–42937.

US FDA (2015) Safety and Effectiveness of Health Care Antiseptics; Topical Antimicrobial Drug Products for Over-the-Counter Human Use; Proposed Amendment of the Tentative

Final Monograph; Reopening of Administrative Record. *Fed. Regist.*, **21 CFR Part 310, 80**, 25165–25205.

Vassileva, G. *et al.* (2010) Gender-dependent effect of Gpbar1 genetic deletion on the metabolic profiles of diet-induced obese mice. *J. Endocrinol.*, **205**, 225–232.

Vázquez-Baeza, Y. *et al.* (2013) EMPeror: a tool for visualizing high-throughput microbial community data. *GigaScience*, **2**, 16.

Veiga-da-Cunha, M. *et al.* (2010) Molecular Identification of NAT8 as the Enzyme That Acetylates Cysteine S-Conjugates to Mercapturic Acids. *J. Biol. Chem.*, **285**, 18888–18898.

Vieira, L.S. *et al.* (2024) Interaction and Transport of Benzalkonium Chlorides by the Organic Cation and Multidrug and Toxin Extrusion Transporters. *Drug Metab. Dispos.*, **52**, 312–321.

Wang, B. and Tontonoz, P. (2018) Liver X receptors in lipid signalling and membrane homeostasis. *Nat. Rev. Endocrinol.*, **14**, 452–463.

Wang, R. *et al.* (2021) Gut microbiome, liver immunology, and liver diseases. *Cell. Mol. Immunol.*, **18**, 4–17.

Weakly, H.M.J. *et al.* (2024) Several common methods of making vesicles (except an emulsion method) capture intended lipid ratios. *bioRxiv*, 2024.02.21.581444.

Wu, G.D. and Lewis, J.D. (2013) Analysis of the Human Gut Microbiome and Association With Disease. *Clin. Gastroenterol. Hepatol.*, **11**, 774–777.

Xiong, Z.E. *et al.* (2020) Exposure to dibutyl phthalate impairs lipid metabolism and causes inflammation via disturbing microbiota-related gut–liver axis. *Acta Biochim. Biophys. Sin.*, **52**, 1382–1393.

Xue, Y. *et al.* (2004) Distribution and disposition of benzalkonium chloride following various routes of administration in rats. *Toxicol Lett*, **148**, 113–23.

Xue, Y. *et al.* (2002) Sensitive determination of benzalkonium chloride in blood and tissues using high-performance liquid chromatography with solid-phase extraction. *Leg Med Tokyo*, **4**, 232–8.

Yamashita, T. (2011) Glycosphingolipid Modification: Structural Diversity, Functional and Mechanistic Integration of Diabetes. *Diabetes Metab. J.*, **35**, 309.

Yoon, H. *et al.* (2021) Lipid metabolism in sickness and in health: Emerging regulators of lipotoxicity. *Mol. Cell*, **81**, 3708–3730.

Yoshimoto, F.K. *et al.* (2016) Isotope-Labeling Studies Support the Electrophilic Compound I Iron Active Species, FeO^{3+}, for the Carbon–Carbon Bond Cleavage Reaction of the Cholesterol Side-Chain Cleavage Enzyme, Cytochrome P450 11A1. *J. Am. Chem. Soc.*, **138**, 12124–12141.

Zhang, L. *et al.* (2015) Persistent Organic Pollutants Modify Gut Microbiota–Host Metabolic Homeostasis in Mice Through Aryl Hydrocarbon Receptor Activation. *Environ. Health Perspect.*, **123**, 679–688.

Zhang, R. *et al.* (2020) Dose-dependent benzalkonium chloride toxicity imparts ocular surface epithelial changes with features of dry eye disease. *Ocul. Surf.*, **18**, 158–169.

Zhang, S. *et al.* (2015) Subchronic Exposure of Mice to Cadmium Perturbs Their Hepatic Energy Metabolism and Gut Microbiome. *Chem. Res. Toxicol.*, **28**, 2000–2009.

Zhang, Y. and Klaassen, C.D. (2010) Effects of feeding bile acids and a bile acid sequestrant on hepatic bile acid composition in mice. *J Lipid Res*, **51**, 3230–42.

Zhao, Yueming *et al.* (2022) Alleviating effects of gut micro-ecologically regulatory treatments on mice with constipation. *Front. Microbiol.*, **13**, 956438.

Zheng, G. *et al.* (2020) Increased Indoor Exposure to Commonly Used Disinfectants during the COVID-19 Pandemic. *Environ. Sci. Technol. Lett.*, **7**, 760–765.

Zheng, G. *et al.* (2021a) Quaternary Ammonium Compounds: Bioaccumulation Potentials in Humans and Levels in Blood before and during the Covid-19 Pandemic. *Environ. Sci. Technol.*, **55**, 14689–14698.

Zheng, G. *et al.* (2021b) Quaternary Ammonium Compounds: Bioaccumulation Potentials in Humans and Levels in Blood before and during the Covid-19 Pandemic. *Environ. Sci. Technol.*, **55**, 14689–14698.

Zheng, G. *et al.* (2022) The first detection of quaternary ammonium compounds in breast milk: Implications for early-life exposure. *J. Expo. Sci. Environ. Epidemiol.*, **32**, 682–688.

Zhong, C.Y. *et al.* (2015) Microbiota prevents cholesterol loss from the body by regulating host gene expression in mice. *Sci Rep*, **5**, 10512.

Zhou, M. *et al.* (2023) Exploring human CYP4 enzymes: Physiological roles, function in diseases and focus on inhibitors. *Drug Discov. Today*, **28**, 103560.

Chapter 2. Oral Exposure to Benzalkonium Chlorides in Male and Female Mice Reveals Alteration of the Gut Microbiome and Bile Acid Profile

Portions of this chapter have been deposited as a preprint in BioRxiv

Lopez, V.A. *et al.* (2024) Oral Exposure to Benzalkonium Chlorides in Male and Female Mice Reveals Sex-Dependent Alteration of the Gut Microbiome and Bile Acid Profile. *bioRxiv*, 2024.05.13.593991.

2.1 Introduction

A comprehensive overview of BACs, the gut microbiome, and the gut-liver axis are described in **Chapter 1**. The ubiquitous usage of BACs throughout a wide range of applications in residential, agricultural, industrial (food processing equipment and milking equipment), and clinical (hand sanitizers, eye, and nasal drops) settings (Merchel Piovesan Pereira and Tagkopoulos, 2019), humans may be chronically and systemically exposed by several routes: direct dermal/eye contact, inhalation, and ingestion (US EPA, 2006) **(Figure 1.4)**.We reported BAC detection in the blood of 80% of human participants—half of whom had BAC concentrations in the 10-150 nM range (Hrubec *et al.*, 2021), and the COVID-19 pandemic led to increased BAC concentrations in human blood samples (Zheng *et al.*, 2021)

The prevalent use of BACs as antimicrobials raises the concern of potential disruption to gut microbiota homeostasis. Previous studies in rat models have shown fecal excretion as a major route of elimination of the BACs even when administered through IV injection (Luz *et al.*, 2020). More recently, we detected BACs and BAC metabolites in five human fecal samples, reaching over 1 μM for total BAC concentrations (Nguyen *et al.*, 2024). Thus, the interaction of BACs with gut microbiota is highly likely regardless of the exposure route.

The gastrointestinal microbiome has become increasingly recognized as an invaluable contributor to human (host) health. The symbiotic relationship between the host and the gut microbiome has been linked with beneficial contributions to overall host health, like immunity, nutrition, and human development (Eloe-Fadrosh and Rasko, 2013), while gut microbiome dysbiosis was found to contribute to many human diseases, such as obesity, asthma, some cancers, heart disease, and autism (Barko *et al.*, 2018).

Crosstalk between the gut and liver has become increasingly recognized by parallel rises in occurrences of liver diseases and GI and immune disorders (Anupriya Tripathi *et al.*, 2018). The gut and liver communicate via tight bidirectional links through the biliary tract, portal vein, and systemic circulation **(Figure 1.7, Figure 2.1)**. BAs are a group of steroidal acids derived from cholesterol in hepatocytes and are imperative signaling molecules for intermediary metabolism within the gut-liver axis (A. Tripathi *et al.*, 2018). Dysbiosis in the gut microbiome shifts the balance between primary and secondary BAs and their subsequent enterohepatic recycling.

An imbalance in BAs and gut bacteria can elicit a cascade of host immune responses relevant to the progression of liver diseases (Anupriya Tripathi *et al.*, 2018). Previous work (L. Zhang *et al.*, 2015; S. Zhang *et al.*, 2015; Fazeli *et al.*, 2011; Lu *et al.*, 2014; Breton *et al.*, 2013; Claus *et al.*, 2016; Naspolini *et al.*, 2022) has elucidated the potential of environmental toxicant exposure on microbiome composition. The objective of this study was to assess the hypothesis that BAC exposure could alter gut microbiome composition and diversity and subsequently affect bile acid homeostasis between the gut and liver.

To achieve this objective, we started with an in vivo oral BAC-exposure paradigm, dosing two chain length BACs (d_7-C12-BAC and d_7-C16-BAC) through Nutra-gel diet in male and female

C57BL/6 mice at ½ of the lowest observed adverse effective level (LOAEL) dosage for one week. Parent BAC and BAC metabolites were measured in biological extracts of control and BAC-exposed mice, including feces, liver and blood. 16S rRNA sequencing was performed on isolated DNA from cecum of control and BAC-exposed mice, and data was processed using the bioinformatic platform QIIME2.2 for microbiome diversity and composition analysis. Finally, a BA quantitation assay was developed using UHPLC-MS/MS, to quantify levels of unconjugated primary and secondary BAs in feces and liver of control and BAC-exposed mice.

2.2 Results and Discussion

The gut microbiome has become increasingly recognized as an essential marker for numerous disease pathologies (Chiang and Lin, 2019; Manos, 2022; Wu and Lewis, 2013; Wang *et al.*, 2021; Boursier and Diehl, 2015). Various groups have studied the potential of environmental toxicant exposure on microbiome composition. For example, cadmium exposure altered energy metabolism and gut microbiota composition in male C57BL/6J mice (S. Zhang *et al.*, 2015). Li et al. found that environmental contaminants, polybrominated diphenyl ethers, altered gut microbiome composition and bile acid homeostasis in male C57BL/6J mice (Cindy Yanfei Li *et al.*, 2018). *Understanding the mechanisms by which environmental agents can induce changes in the gut-liver axis is important in elucidating the association between environmental exposure and human health.*

To assess the consequences of oral BAC exposure on the gut microbiome, C57BL/6J male and female mice were exposed to either control Nutra-Gel diet or Nutra-Gel diet with added d_7-C12- BAC or d_7-C16- BAC at a dosage of 120 µg/g/day for a duration of 1-week. This dosage

paradigm (**Figure 2.2**) was adapted from Melin et al., who had previously revealed that 120 μg/g/day was half of the lowest observable adverse effect limit (LOAEL) (Melin *et al.*, 2014).

2.2.1 BAC and BAC metabolite distribution

BACs were quantified in male and female liver, feces, and blood (**Figure 2.3**). Neither d_7-C12-BAC nor d_7-C16-BAC was detected in mice fed the control diet. The highest levels of BACs were observed in the fecal samples, reaching 100s of μM to low mM concentrations, while their levels were in a few to 100s nM range in the liver and blood. Comparing the two sexes, higher average levels of parent C12- and C16-BACs were generally observed in female samples, particularly in blood and feces. However, there is no statistical difference in the level of parent C12- or C16-BAC between male and female groups (**Figure 2.9**). Our study also describes the metabolic route of BAC structures in an orally exposed mouse model. Our previous work elucidated the cytochrome P450-mediated oxidation of BACs, which occurs on the alkyl chain region (R. P. Seguin *et al.*, 2019), forming primary ω- and (ω-1)-hydroxy-BAC metabolites and secondary ω-COOH-BAC metabolite (**Figure 1.9**). Quantifiable levels of ω- and (ω-1)-hydroxy (OH) metabolites of both d_7-C12- and d_7-C16-BAC structures were observed in the respective exposed group (**Figure 2.3**). The levels of (ω and ω-1)-OH metabolites in the liver, blood, and feces between male and female groups show no statistical difference, either (**Figure 2.9**).

. Most CYP oxidation of BACs occurs on the even-numbered alkyl chain, such as those of the d_7-C12- or d_7-C16-BAC structures, to produce even-numbered alkyl chain COOH metabolites. However, if CYP oxidation catalyzes a carbon-carbon cleavage, the resulting removal of the ω-carbon leaves β-oxidation to occur on an odd-numbered alkyl chain (Umehara, Kudo, Hirao, Morita, Uchida, *et al.*, 2000; Umehara, Kudo, Hirao, Morita, Ohtani, *et al.*, 2000; Umehara *et al.*,

2004) , and subsequent chain-shortened COOH BAC products will contain an odd-numbered carbon alkyl chain length. Products from β-oxidation of the carboxylic acid (COOH) metabolites were observed in male and female blood, liver, and feces. Even numbered chain-shortened carboxylic acid BACs (C6, C8, C10, C12, C14, and C16) were all quantified in the blood, liver, and feces of both d_7-C12- and d_7-C16-BAC exposed groups (**Figure 2.4**), with the feces containing the highest levels of individual COOH BACs (up to mM), followed by livers (up to 1000s nM) and blood (generally < 100 nM). Again, female samples appear to contain higher average levels of COOH BACs than male samples, particularly in the feces; however, a majority of the COOH metabolites were not significantly different between male and female groups (**Figure 2.10 and Figure 2.11**). Carboxylic acid metabolites, d_7-COOH C14-BAC and d_7-COOH C16-BAC, products of d_7-C16-BAC, were only seen in d_7-C16-BAC-treated mice. We also observed a series of odd-chain carboxylic acids but at much lower levels (**Figure 2.8, Figure 2.12 and Figure 2.13**). The initial odd-chain carboxylic acid could be formed from terminal C-C cleavage mediated by cytochromes P450. Such reactions are known in other CYP-mediated metabolisms (Guengerich and Yoshimoto, 2018; Yoshimoto *et al.*, 2016; Stok and De Voss, 2000; Cryle and De Voss, 2004; Umehara, *et al.*, 2000a; Umehara, *et al.*, 2000b; Umehara *et al.*, 2004), but the specific CYP isoform responsible for the C-C cleavage of BACs remains to be elucidated. The levels of odd-numbered β-oxidation products of d_7-C12- and d_7-C16-BAC in male and female blood, liver, and feces were much lower than that of the even-numbered β-oxidation products, indicating that P450 oxidation occurring with a carbon-carbon cleavage is a minor pathway.

2.2.2 Effects of BACs on gut microbiome using 16S rRNA gene sequencing

To evaluate the effects of BAC exposure on the gut microbiome, 16S rRNA sequencing targeting the V4 region was performed in the cecum of male and female C57BL/6J mice exposed to either control, d_7-C12-BAC (120 µg/g/day), or d_7-C16-BAC (120 µg/g/day). Alpha diversity, a description of species richness, has been studied extensively and is decreased in subjects in various metabolic disease states (Carroll *et al.*, 2012; Shen *et al.*, 2017; Palmas *et al.*, 2021). Alpha diversity analysis by the Rarefaction Plot on QIIME2, demonstrates that exposure to either d_7-C12-BAC or d_7-C16-BAC led to decreased microbial richness in both male and female cohorts (**Figure 2.5**). Beta diversity, a measurement of species differences amongst samples, was determined and visualized by principal coordinates analysis (PCoA) using Emperor (Vázquez-Baeza *et al.*, 2013). This analysis shows that the microbial communities differ between the BAC-treated and control mice in male and female cohorts (**Figure 2.5**). The female cohort had a clear separation of treatment groups, indicating distinct microbial communities amongst the controls, d_7-C12-, and d_7-C16-BAC female mice. In the male cohort, while the separation was apparent between the BAC-treated mice and controls, large variability in the d_7-C16-BAC group led to overlaps with the d_7-C12-BAC group (**Figure 2.5**).

Our results are the first to show BAC exposure can alter the gut microbiota composition. Taxa analysis by QIIME2 revealed the composition of the gut microbiome in different groups: control, d_7-C12-BAC, and d_7-C16-BAC exposed mice (**Figure 2.5**). We observed that gram-negative phyla (*Proteobacteria* and *Verrucomicrobia*) were significantly increased in BAC-treated mice relative to controls (**Figure 2.5**). In contrast, the gram-positive phylum (*Firmicutes* and *Actinobacteria*) was significantly decreased relative to controls. In human populations, the

predominant phyla are *Firmicutes*, *Bacteroidetes*, *Actinobacteria*, and *Proteobacteria* (Rizzatti *et al.*, 2017). The majority of operational taxonomic units were assigned to phyla *Firmicutes* (41.8% in females; 40.8% in males), *Verrucomicrobia* (38.0% in females, 28.4% in males), *Bacteroides* (6.1% in females, 21.1% in males), *Proteobacteria* (10.4% in females; 6.7% in males), and *Actinobacteria* (1.8% in females; 1.9% in males). Of all defined taxonomical units, 1.8% in the female cohort and 0.05% in the male cohort were not assigned to any bacteria phylum. *Actinobacteria* phyla were greatly decreased by both d_7-C12-BAC and d_7-C16-BAC treatments in the female cohort. Both *Proteobacteria* and *Verrucomicrobia* were significantly increased in d_7-C12-BAC- and d_7-C16-BAC-treated mice in both male and female cohorts, relative to controls. *Firmicutes* was significantly lower in both BAC-exposed groups in the female cohort but only in the d_7-C12-BAC group of the male cohort. *Bacteroides* was not significantly changed following BAC exposure in either male or female cohorts (**Figure 2.5**).

The *Firmicutes* phylum has essential roles in the fermentation of dietary fibers, producing metabolites like vitamins and short-chain fatty acids. Because BAC-treated mice have lowered *Firmicutes* relative to controls, a consequence could be less short-chain fatty acid formation. Less short-chain fatty acid formation can result in effects like inflammation or deprived gut lining cells. In male and female cohorts, the *Proteobacteria* phylum was significantly increased in both d_7-C12-BAC and d_7-C16-BAC treated mice relative to controls. *Proteobacteria* is often increased in disease and has been noted as a potential marker of microbiota instability and predisposition of inflammatory-sustained disease onset (Rizzatti *et al.*, 2017). The consistent increases in *Proteobacteria* in BAC-exposed mice could foreshadow subsequent proinflammatory diseases.

Notably, the *Actinobacteria* phylum was significantly decreased in BAC-treated female mice relative to controls. *Actinobacteria* are recognized contributors to maintaining gut barrier

homeostasis and are also involved in the transformation of linoleic acid into conjugated linoleic acids, which have health-promoting effects like anti-obesity and anti-diabetes (Binda *et al.*, 2018). The *Coriobacteriia* class was the predominant bacteria belonging to the *Actinobacteria* phylum in both cohorts. While the effects of BAC exposure on *Actinobacteria* phylum are notable in the female cohort, the male cohort did not show significant changes relative to their controls. This difference in the microbiome changes between the male and female cohort could result from the variability in the male d_7-C16-BAC group, and such variability could also explain the nuances in secondary bile acid formation.

Analysis at the family level revealed identifications of taxa belonging to the *Firmicutes*, *Verrucomicrobia*, *Proteobacteria*, *Bacteroides*, and *Actinobacteria* phyla (**Figure 2.6**). The composition of family microbial taxa was changed in BAC-treated mice compared to controls. The sums of individual counts of family taxa were plotted and not found to be significantly different between treatment groups, indicating that shifts in family microbial taxa were not the result of lowered or higher counts of family microbial taxa (**Figure 2.6**). The top 10 abundant families of bacteria are plotted via heat maps. *Akkermansiaceae*, of the *Verrucomicrobia* phylum, was the most abundant family in both male and female cohorts (28.2 and 38.0%). Additionally, BAC exposure led to increased *Akkermansiaceae* in both male and female cohorts. *Lachnospiraceae* and *Ruminococcaceae* were also notable contributors to the family microbial composition, and both families were significantly lower in the composition of the BAC-exposed male and female mice. *Burkholderiaceae* (of the *Proteobacteria* phylum) and *Muribaculaceae* (of the *Bacteroides* phylum) were both significantly different in abundance in BAC-exposed mice relative to controls (**Figure 2.6**). Absolute total microbial counts within each treatment group were not significantly different, indicating that the differences in the abundance of bacteria are results of compositional

shifts. In both d_7-C12-BAC and d_7-C16-BAC male mice and d_7-C16-BAC female mice, *Akkermansiaceae* and *Akkermansia* of the *Verrucomicrobia* phyla were significantly increased. *Akkermansia* is currently the only defined genus within the *Akkermansiaceae* family and is known to specialize in mucin degradation. *Akkermansia* is consistently recognized for its beneficial role in maintaining a healthy mucosal layer and gut barrier integrity (González *et al.*, 2023). Interestingly, *Akkermansia* decreases in various disease states and metabolic disorders like inflammatory bowel disease, obesity, and diabetes (González *et al.*, 2023).

Lachnospiraceae and *Ruminococcaceae* of the *Firmicutes* phylum decreased in d_7-C12- and d_7-C16-BAC treated mice relative to controls. *Lachnospiraceae* and *Ruminococcaceae* have roles in secondary bile acid formation. Thus, their decreases could be correlated to the lowered secondary bile acid quantitation in male and female feces. *Atopobiaceae*, a part of the *Actinobacteria* phylum, was significantly decreased in female d_7-C12- and d_7-C16-BAC treated mice. *Atopobiaceae* is lactate-producing and, when isolated from mouse intestines, showed high resistance to mammalian bile extracts due to their significant bile salt hydrolase activity. This finding is interesting considering the sex differences we observe in secondary BA (Morinaga *et al.*, 2022). Female BAC-exposed mice revealed more significant decreases in secondary BA formation, as well as significant decreases in bacteria known to play roles within secondary BA formation.

Our study also identifies specific genera that were impacted by oral BAC exposure in male and female cohorts (**Figure 2.6**). *Parasutterella* was significantly higher in both male d_7-C12-BAC and d_7-C16-BAC-treated mice and female d_7-C16-BAC-treated mice. *Parasutterella* is supportive of bile acid maintenance and cholesterol metabolism. *Parasutterella* isolates are asaccharolytic and succinate producers (Ju *et al.*, 2019). BAC exposure leading to *Parasutterella* increases could

be evidence of the microbiota trying to mediate the decreases of other important bacteria in bile acid maintenance, like *Lachnospiraceae*, *Lactobacilliceae*, and *Ruminococcaceae*. Analysis at the genus level revealed the identification of taxa primarily in Firmicutes phyla (**Figure 2.6**). In the female cohort, six of the top ten most abundantly identified genera belong to the *Firmicutes* phyla, including *Ruminococcaceae UCG-013*, *Lachnoclostridium*, *Oscillibacter*, *Lactobacillus*, *Ruminiclostridium 9*, and *Blautia*. *Blautia* and *Ruminococcaceae UCG-013* were significantly decreased in d_7-C12-BAC and d_7-C16-BAC exposed mice, while *Lactobacillus* was significantly increased. Additionally, chain length-specific alterations occurred; *Oscillibacter* was only significantly increased in d_7-C12-BAC-exposed female mice, and *Ruminiclostridium 9* was only significantly decreased in d_7-C16-BAC-exposed female mice. In the male cohort, six of the top ten most abundantly identified genera belong to the *Firmicutes* phyla as well: *Lachnoclostridium*, *Ruminococcaceae UCG-013*, *Oscillibacter*, *Ruminiclostridium 9*, *Blautia* and *Roseburia*. *Oscillibacter*, *Parasutterella*, and *Akkermansia* were significantly increased in d_7-BAC-exposed male mice relative to controls. *Blautia* and *Ruminococcaceae UCG-013* were significantly lowered in d_7-BAC-exposed male mice relative to controls. *Akkermansia* genera described the most significant proportion of the identified genera in the microbiomes of both the male and female cohorts. Additionally, *Coriobacteriaceae UCG-002*, part of *Actinobacteria* phyla, was identified within the top 10 most abundant genera in the female cohort and was significantly lower in BAC-treated female mice relative to controls. Total individual genera count within the treatment groups showed no significant difference in male and female cohorts, indicating that changes noted in the composition are not due to a loss or gain of microbiota within a treatment group (**Figure 2.6**).

Blautia was significantly decreased in both d_7-C12- and d_7-C16-BAC-treated mice relative to controls. *Blautia* has become extensively recognized as a genus capable of using glucose for

carbohydrate utilization. Different strains demonstrate varying capacities to use sucrose, fructose, lactose, and more. *Blautia* can ferment glucose and produce final products, acetic acid, succinic acid, lactic acid, and ethanol. Notably, certain *Blautia* species can perform 7α-dehydroxylation of primary BAs and convert them to secondary BAs like lithocholic and deoxycholic acid (Liu *et al.*, 2021). *Lactobacillus* was increased in both d_7-C12- and d_7-C16-BAC female groups. Various *Lactobacillus* species have been recognized for their ability to deconjugate BAs in the GI tract through BSH proteins (O'Flaherty *et al.*, 2018). *Ruminiclostridium 9*, of the *Firmicutes* phyla was significantly decreased in the d_7-C16-BAC group relative to female controls and has been reported to be a short-chain fatty acid (SCFA) producer in the gut (Zhao *et al.*, 2022)

Lastly, in the female cohort only, both d_7-C12-BAC and d_7-C16-BAC led to *Coriobacteriaceae UCG-002* of the *Actinobacteria* phyla being significantly decreased. *Coriobacteriaceae UCG-002* has been reported to be positively correlated with serum triglycerides, total cholesterol, and LDL cholesterol levels, as well as serum TNF-a, IL-6, and LPS levels, suggesting a significant role in the female inflammatory response. Other work has shown the correlation between *Coriobacteriaceae UCG-002* and SCFAs (Pradista *et al.*, 2022). Furthermore, we found that there are baseline differences in bacteria composition at the phylum, family, and genus levels and the levels of primary and secondary BAs between control male and female groups (**Figures 2.14, Figure 2.15 and Figure 2.16**). Therefore, the baseline differences could also contribute to the different responses to BAC treatments between male and female cohorts.

2.2.3 BAs in feces and liver

To understand how oral BAC exposure impacts BA homeostasis, a targeted BA quantitation assay was developed and performed on the blood, liver, and feces of male and female C57BL/6J mice exposed to either control, d_7-C12-BAC, or d_7-C16-BAC (120 μg/g/day) (n = 4-6 per group). Primary BAs, including cholic acid (CA), chenodeoxycholic acid (CDCA), α-muricholic acid (α-MCA), and β-muricholic acid (β-MCA), were quantified in the male and female liver and fecal extracts (**Figure 2.7**). In the female and male liver extracts, primary BAs, CA, CDCA, α-MCA, and β-MCA amounts were not significantly altered in d_7-C12- or d_7-C16-BAC treated mice relative to controls. In both the female and male fecal extracts, the d_7-C16-BAC treated mice had a significantly higher level of CA, a product of cholesterol, than controls.

Secondary BAs, DCA, LCA, and ω-MCA, were also quantified in liver and fecal extracts (**Figure 2.7**). In the female liver, both DCA and ω-MCA were significantly lower in d_7-C16-BAC treated mice relative to controls. ω-MCA was also significantly lower in the d_7-C12-BAC female liver. There were no significant differences in DCA or ω-MCA amounts in the three treatment groups in the male liver. LCA was not detected in either male or female liver. Significantly, d_7-C12-BAC and d_7-C16-BAC led to greatly decreased amounts of secondary BAs, DCA, LCA, and ω-MCA in female feces. In the male cohort, only d_7-C12-BAC treated mice had statistically lower amounts of LCA and ω-MCA in feces.

Regulation of the unconjugated BA pool was further analyzed by summing the total BAs (either primary or secondary) per sample in the liver and feces (**Figure 2.7**). Total primary unconjugated BA content was not significantly different between d_7-BAC exposed mice and controls in feces or liver in male and female cohorts. However, total secondary unconjugated BA

content was significantly lower in the d_7-C16-BAC exposed female livers, but not male livers, relative to controls. In the feces of both male and female d_7-C12-BAC exposed mice, total secondary unconjugated BA content was significantly lower. d_7-C16-BAC treated mice also had significantly lowered total secondary unconjugated BA content in the feces of the female cohort, but not the male cohort, relative to controls.

2.3 Experimental Procedure

Animals. Seven to eight-week-old C57BL/6J male and female mice were purchased from Jackson Laboratories (Bar Harbor, Maine). Experiments were staggered, with male mice undergoing the exposure protocol first. The University of Washington Institutional Animal Care and Use Committee approved all animal protocols. All experiments followed the Guiding Principles in the Use of Animals in Toxicology. Mice were acclimated to the animal facility for 2 weeks. Mice were then acclimated to an untreated Nutra-Gel diet (Product F5769-KIT, Bio-Serv, Frenchtown, New Jersey) for 2 weeks before BAC exposure. Deuterated BACs were used to ensure accurate quantitation, as described in Herron et al., 2018. Mice were randomly assigned to exposure groups (n = 6): control Nutra-Gel diet, or treatment with d_7-C12- BAC (120 µg/g/day) or d_7-C16- BAC (120 µg/g/day) for 1 week. To ensure mice were not subject to isolation and had enough enrichment throughout the experiment, mice were housed at two per cage. For each sex, there were nine cages, with each treatment group having three cages. Because of a cage-fighting incident, Controls 3 and 4 were individually housed in the male cohort. At the end of the first week, mice were sacrificed, and the following tissues and fluids were collected, flash-frozen in 2-methylbutane on dry ice and stored at -80 °C until subsequent analyses: liver, ileum, jejunum, duodenum, including intestinal content in all three intestinal tissue section, and large intestine (colon and cecum), and blood via

cardiac puncture. Feces were collected throughout the Nutra-gel acclimation period, as well as the treatment period (days 1, 6, 15, 18, and 21). Feces were kept at -80°C until subsequent analysis.

Chemicals. Optima LC/MS solvents (acetonitrile, chloroform, methanol, and water), 2-methylbutane, and formic acid were purchased from Thermo Fisher Scientific (Grand Island, New York). d_7-C12-BAC and d_7-C16-BAC were prepared as described previously (Herron et al., 2016). The deuterated (d_4-) bile acid standards, including tauro-α-muricholic acid-d_4 (sodium salt) (T-α-MCA), α-muricholic acid-d_4 (α-MCA), and ω-muricholic acid-d_4 (ω-MCA), were purchased from Cayman Chemical (Ann Arbor, Michigan). BAs, including cholic acid (CA), chenodeoxycholic acid (CDCA), deoxycholic acid (DCA), lithocholic acid (LCA), α-muricholic acid (α-MCA), β-muricholic acid (β-MCA), and ω-muricholic acid (ω-MCA), were purchased from Cayman Chemical (Ann Arbor, Michigan).

Bacterial DNA Isolation and 16S rRNA Sequencing. Total DNA was extracted from the cecum of untreated and treated mice using E.Z.N.A. DNA Stool Kit (Omega Bio-tek, Inc., Norcross, GA) according to the manufacturer's protocol. The concentration of DNA was determined via Qubit 2.0 Fluorometer (Life Technologies/Thermo Fisher Scientific, Grand Island, NY). The integrity and quality of DNA samples were confirmed by the Agilent 2100 Bioanalyzer (Agilent Technologies Inc., Santa Clara, CA). The V4 region of the 16S rRNA gene was amplified and sequenced using HiSeq. 2500 platform (250-bp paired-end) (Novogene, Beijing, China) (n = 4). The paired-end sequence reads were merged, demultiplexed, and filtered using QIIME2 version 2020. 2 (Caporaso *et al.*, 2010). Alpha diversity was assessed by QIIME2-2020.2. at the p-max depth of 10,000. The input table was acquired from qiime dada2 denoise paired steps. Input phylogeny came from the acquisition of a rooted phylogenetic tree using QIIME2-2020.2. Beta diversity was examined by a weighted unifrac distance matrix from core metric results acquired.

Taxa composition (bacterial phyla to species level) was defined by Silva132. Taxa data acquired by QIIME2-2020.2 were used for analysis at different levels (phylum, family, and genera). The raw data of the 16S sequencing are available at Dryad (https://doi.org/10.5061/dryad.9zw3r22ph).

Bile Acid and BAC Extractions. A standard stock solution of each BA and deuterated IS was prepared at a concentration of 1 mg/ml in methanol. A 5% NH_4OH in Acetonitrile solution containing each d_4-BA at a concentration of 0.175 µg/mL was spiked into each sample for LC/MS-MS analysis.

For fecal BA extraction, feces were accurately weighed and stored at -80 °C until the time of BA extraction. 2.5 µL of MilliQ water was added for every mg of feces. Feces-water mixtures were sonicated in ice water for 30 minutes to produce feces-water homogenates. 10 µL of ice-cold alkaline acetonitrile (ACN) (5% ammonia in ACN) with IS mixture (d_0-C12 and C16 BACs, ω-OH C12- and C16-BAC, COOH metabolites 1µM each; d_4-BAs 0.175 µg/mL) for every mg of feces was added to the homogenate, and vortexed vigorously for 5-8 seconds and left to equilibrate on ice for 10 minutes. Samples were sonicated for 1 hour and then centrifuged at 12, 000 x g for 15 min at 4 °C. Supernatants were collected in new tubes, and pellets were resuspended in 750 µL of 100% methanol. Samples were sonicated for 20 minutes and then centrifuged at 12,000 x g for 20 minutes to isolate a second supernatant. Two supernatants were combined and evaporated by SpeedVac Vacuum (30 °C) for 3-5 hours. Samples were reconstituted in 100 µL of 1:1 methanol:water mix. The suspension was transferred into 0.2 µm costar Spin-X HPLC microcentrifuge filter tubes and centrifuged at 12, 000 x g for 10 minutes. Filtrate (70 µL) was transferred to LC–MS vials and stored for analysis in -80°C.

For liver BA extraction, 60-70 mg of liver were accurately weighed. Frozen liver tissues were homogenized in 5 volumes of MilliQ water by Bead Homogenizer. Homogenates were transferred from homogenization tubes to clean tubes. 10 µl of cold alkaline Acetonitrile (ACN) (5% ammonia in ACN) with IS mixture (d_0-C12- and C16-BACs, ω-OH C12- and C16-BAC, COOH metabolites 1µM each; d_4 BAs 0.175 µg/mL) for every mg of liver tissue weight was added. This extraction process extracted BAs, as well as BAC and BAC metabolites. Tubes were vortexed and then sonicated for 1 hour at room temperature. Samples were centrifuged at 12,000 g for 15 minutes at 4°C. Supernatants were transferred to clean tubes, and 750 µL MeOH was added to the pellets. The mixture was sonicated for 30 minutes and then centrifuged at 15,000 g for 20 minutes. Supernatants were combined and dried under SpeedVac. The residue was reconstituted in 100 µL of 50% MeOH, and samples were vortexed and transferred into a 0.2 µm Costar Spin-X centrifuge tube filter. Samples were centrifuged at 12,000g for 10 minutes. Filtrate (70 µL) was transferred to LC-MS vials and stored for analysis.

For male and female blood BAC extractions, 10 µL of thawed whole blood was added to 20 µL of water and sonicated for 15-20 minutes. 10 µL of ACN spiked with d_0-BAC Internal Standard series (C6, C8, C10, C12, C14 and C16 d_0-BACs; C8, C10, C12, C14 and C16 d_0-COOH-BACs; d_0-ω-OH-C12 and d_0-ω-OH-C16 at 40 nM each). Samples were vortexed and left to sit on ice for 5-10 minutes. 100 µL of ACN: MeOH (1:1) was added to each sample. Samples were vortexed and left to rest on ice for 5-10 minutes. Samples were centrifuged at 4°C for 15 minutes, and sample supernatants were transferred to LC-MS vials and stored for analysis.

Targeted Analysis of BAs, BAC, and BAC metabolites. BAs were analyzed by ultra-high-performance liquid chromatography-tandem mass spectrometry (UHPLC-MS/MS) using a triple-

quadrupole mass spectrometer (Triple-Quad 6500+; SCIEX, Vaughan, Ontario, Canada) equipped with electrospray ionization (ESI) by modifying previous methods (Zhang and Klaassen, 2010; Qiu *et al.*, 2016). 5 µl of each prepared sample was injected into the system. Reverse chromatographic separation was achieved on a Thermo Hypersil GOLD C18 column (100 x 2.1 mm, 1.9 µm particle size) under the following conditions; flow rate, 0.400 ml/min, and gradient elution method with solvent A (20% acetonitrile/80% H_2O with 0.1% formic acid) and solvent B (20% H_2O/80% acetonitrile with 0.1% formic acid), 0 min, 5% B; 2 min, 5% B; 4 min, 8% B; 8 min, 30% B; 12 min, 80% B; 13.5 min, 90% B; 15 min, 80% B; 16 min, 5% B; 19 min, 5% B. (**Table 2.1**).

Selective reaction monitoring (SRM) was used to monitor mass-to-charge ratios (m/z) of the parent ion (Q1) for each respective bile acid and their respective characteristic fragment (Q3). Mass transitions are shown in **Table 2.2**. Utilization of both positive and negative modes was performed for this assay. Analyst software was used to integrate extracted BA peaks. Calibration curves were constructed for each BA internal standard, and BA concentrations were calculated based on the ratio of the analyte peak area to the internal standard peak area. β-MCA was ratioed to the average of d_4-α-MCA and d_4-ω-MCA; d_0-CDCA was ratioed to d_4-CA. All data are presented as the median. Statistical analyses were performed on GraphPad Prism 10.3.0 (GraphPad Software, La Jolla, CA) using Welch's one-way ANOVA analysis followed by Dunnett's multiple comparison tests relative to the Control.

BAC and BAC metabolites were analyzed by ultra-high-performance liquid chromatography-tandem mass spectrometry (UHPLC-MS/MS) using a Synapt G2-XS ion mobility Q-TOF mass spectrometer equipped with electrospray ionization (ESI) in the positive mode (Waters Corporation, Milford, MA). 5-10 µl of each prepared sample was injected into the system. Reverse

chromatographic separation was achieved on a Thermo Hypersil GOLD C18 column (100 x 2.1 mm, 1.9 µm particle size) at ambient temperature, with a flow rate of 0.4 ml/min. ACUITY UPLC system and autosampler (Waters Corporation, Wilford, MA) were used for mobile phase delivery and sample injection. The solvent gradient comprised of mobile phase A: 0.1% formic acid, 2mM ammonium formate in water, and solvent B: Acetonitrile: 0 min: 15% B, 14 min: 85%, 15-17 min: 100% B, 18.5-20 min: 15%B. ESI conditions were as described in (Vieira *et al.*, 2024). **Table 2.3** describes all Analyte retention times and precursor to product ion *m/z* transitions. Because the C57BL/6J mice were dosed with a deuterated BAC structure (d_7), use of the following d_0-BACs were utilized as internal standards (COOH C_8-BAC, COOH C_{10}-BAC, COOH C_{12}-BAC, COOH C_{16}-BAC, C_{12}-BAC and C_{16}-BAC). The Target Lynx application in Mass Lynx (Waters Corporation) was utilized for peak integrations and analysis.

Analyte peak areas were normalized to the appropriate internal standard peak area; d_0-ω-OH internal standards were used to quantify any oxidized d_7-C12- or d_7-C16- BAC metabolite that is not a COOH product; d_0-COOH BACs were used to quantify d_7-COOH BAC products; and d_0-BACs were used to quantify the d_7-BAC parent levels. All data are presented as the median. Statistical analyses were performed on GraphPad Prism 10.3.0 (GraphPad Software, La Jolla, CA) using Welch's one-way ANOVA analysis, followed by Dunnett's multiple comparison tests relative to the Control.

2.4 Conclusions

In conclusion, our study provides novel insights into benzalkonium chloride toxicity and metabolism following an oral dose model. We showed that BACs decreased microbial richness and elicited a microbial community different from control mice, which is more prominent in the

female cohort. However, due to the large variability in the C16-BAC-treated group of the male cohort, whether there is a true sex difference warrants further investigation. The changes in the microbial community include bacteria related to BAs, gut barrier homeostasis, short-chain fatty acids, and pro-inflammatory biomarkers. We observed decreased levels of secondary bile acid-forming bacteria, which may be responsible for the lowered levels of secondary BAs in the feces of both sexes and in the female liver. Remarkably, we observed different microbial communities between male and female cohorts. We believe these differences discussed may be responsible for secondary BAs decreasing much more in female fecal extracts than the males. Additionally, quantitative analysis of BAC metabolites in the liver, blood, and feces provided evidence of β-oxidation as a major metabolic route following CYP-mediated oxidation. This present study is the first to elucidate the capacity of ubiquitously used BACs to alter an emerging health biomarker, the gut microbiome, and the gut-liver axis. Future work should consider other gut microbiome axes and clinically relevant lifetime exposure to either occupational exposure or demographic exposure to BACs. Future work should incorporate primary and secondary conjugated BAs to understand the full scope of BAC-induced impact on BA pool.

Chapter 2 Figures

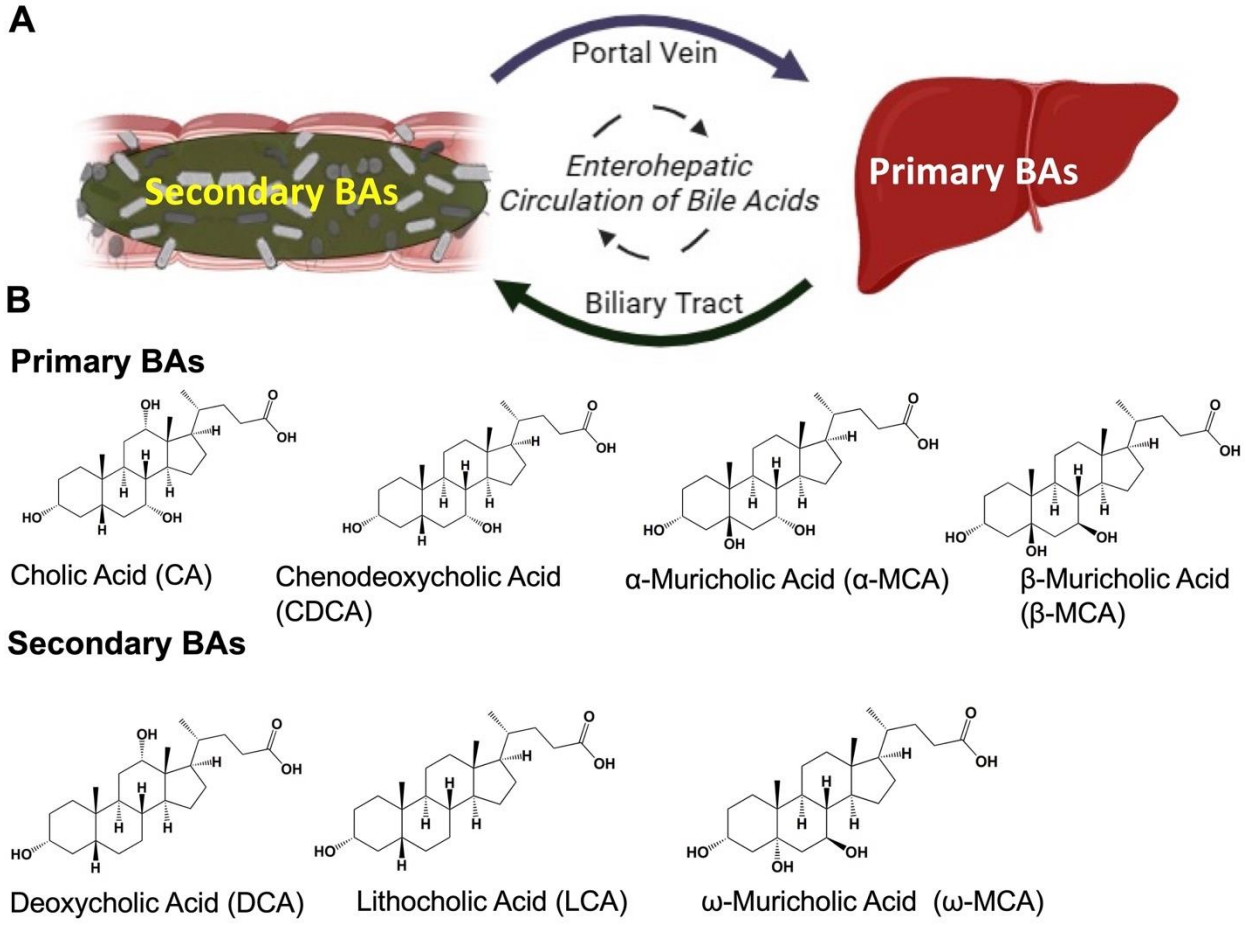

Figure 2.1 Schematic of Enterohepatic Circulation of BAs.

A. Primary BAs, cholic acid (CA) and chenodeoxycholic acid (CDCA) are formed from cholesterol in hepatocytes (Hofmann, 1984). The muricholic acid (MCA) family belongs to rodents (Hofmann, 2009,) of which α- and β-MCA are primary BAs. The primary BAs become conjugated to taurine or glycine to increase their hydrophilicity and enter the biliary tract (Staels and Fonseca, 2009). After brief storage in the gallbladder, the conjugated primary BAs travel through the biliary tract to the small intestine and eventually reach the distal ileum. Conjugated BAs can get absorbed by the portal vein and travel back to the liver for secretion to the bile (Stellaard and Lütjohann, 2021). The unabsorbed BAs will undergo modification by bacteria, such as a) deconjugation; b) dehydrogenation and c) dehydroxylation (Hofmann, 2009), forming "secondary" BAs. The following secondary BAs, lithocholic acid (LCA), deoxycholic acid (DCA) and ω-muricholic acid (ω-MCA), are formed from the respective primary BAs. BAs enter the portal vein by either passive diffusion in the small intestine and colon or active transport in the distal ileum (Winston and Theriot, 2020), followed by uptake by hepatocytes.

B. Chemical structures of BAs quantified in this study; from left to right; first panel CA, CDCA, α-MCA, β-MCA; second panel DCA, LCA, ω-MCA.

A. Made with BioRender.

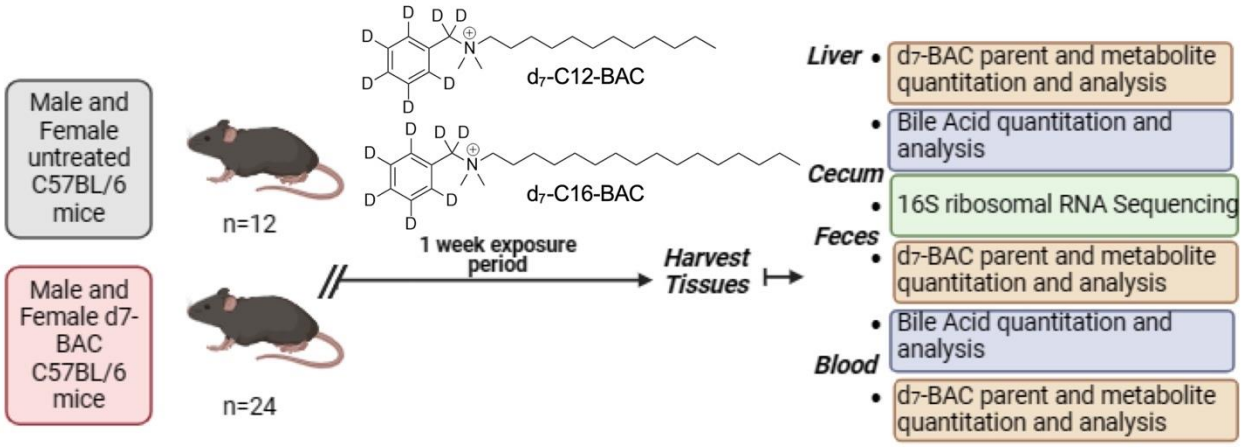

Figure 2.2 Schematic Overview of the Experimental Design.

Male and female C57BL/6 mice were randomly assigned to either the control group, or d_7-C12- or d_7-C16-BAC exposed group; each had N=6. Mice were exposed via a gel diet for one week. Harvested tissues were utilized for either d_7-BAC parent and metabolite analysis, bile acid analysis, or 16S ribosomal RNA sequencing.

Made with BioRender.

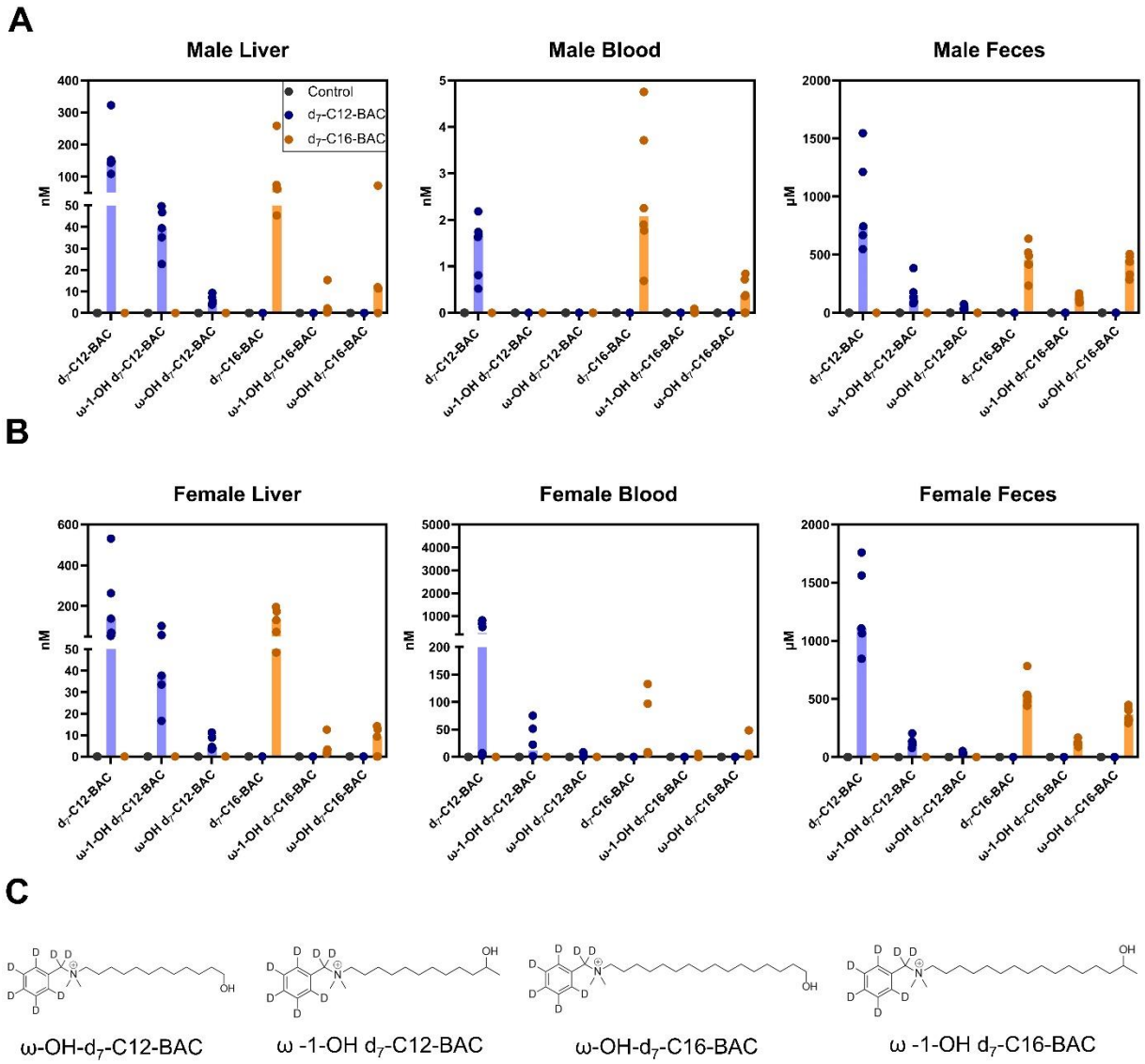

Figure 2.3 Quantified Levels of Parent BACs and their Hydroxy Metabolites.

Quantified levels of parent BACs and their hydroxy metabolites in Male **(A)** and Female **(B)** liver, blood, and feces. Male and female C57BL/6 mice were randomly assigned to either the control group, (120 µg/g/day) d_7-C12-BAC group, or (120 µg/g/day) d_7-C16-BAC group; each group had N = 4-6. Mice were exposed via a gel diet for one week. **(C)**. Chemical structures of (ω-OH)-d_7-C12-BAC, (ω-1)-OH d_7-C12-BAC, (ω-OH)-d_7-C16-BAC and (ω-1)-OH-d_7-C16-BAC.

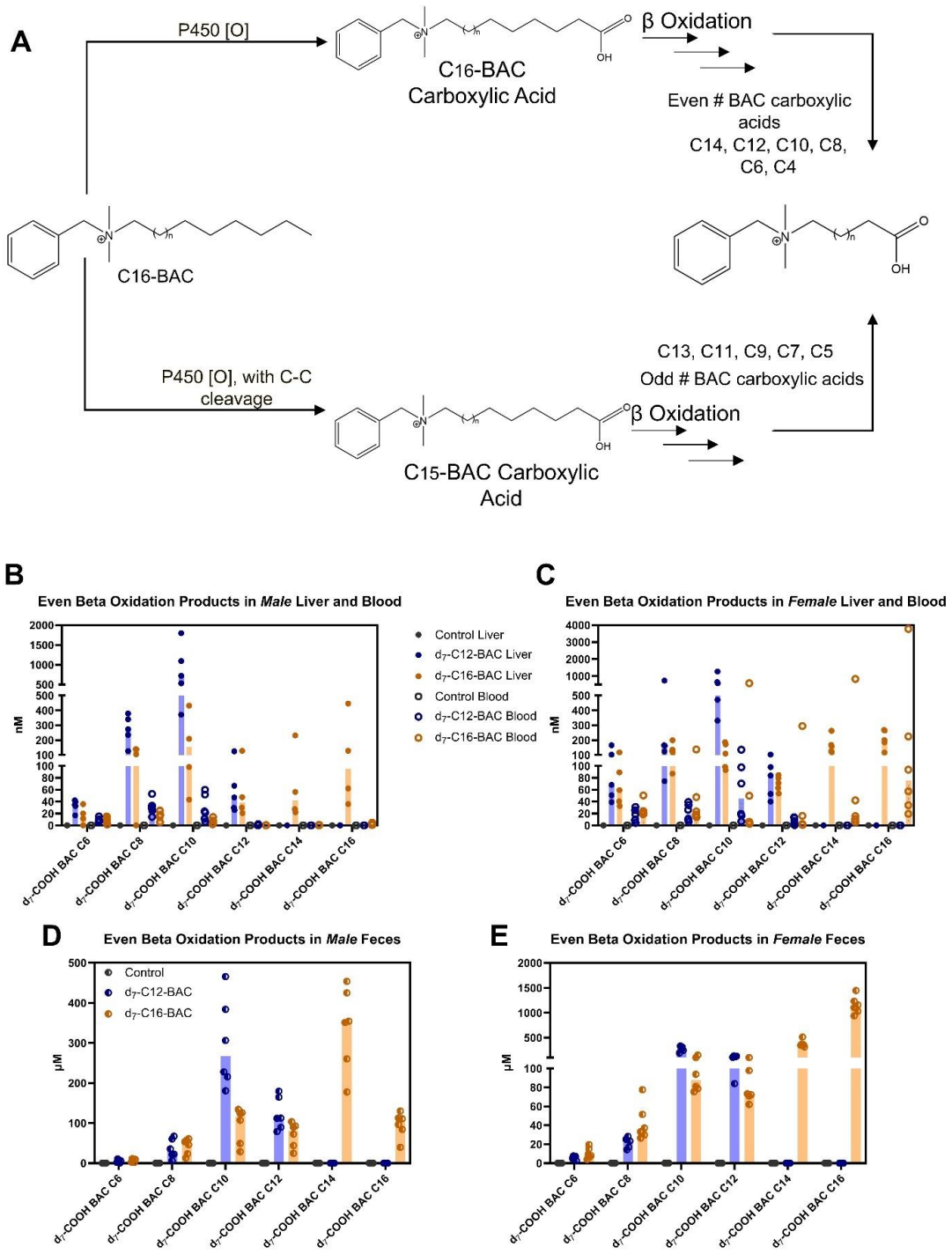

Figure 2.4 Formation and Detection of Beta Oxidation Products from BACs.

A. Schematic overview of proposed pathways of the formation of beta-oxidation products. B-E. Even beta-oxidation products were quantified in Male (B and C) and Female (D and E) liver, blood, and feces using targeted mass spectrometry. N=4-6 per group.

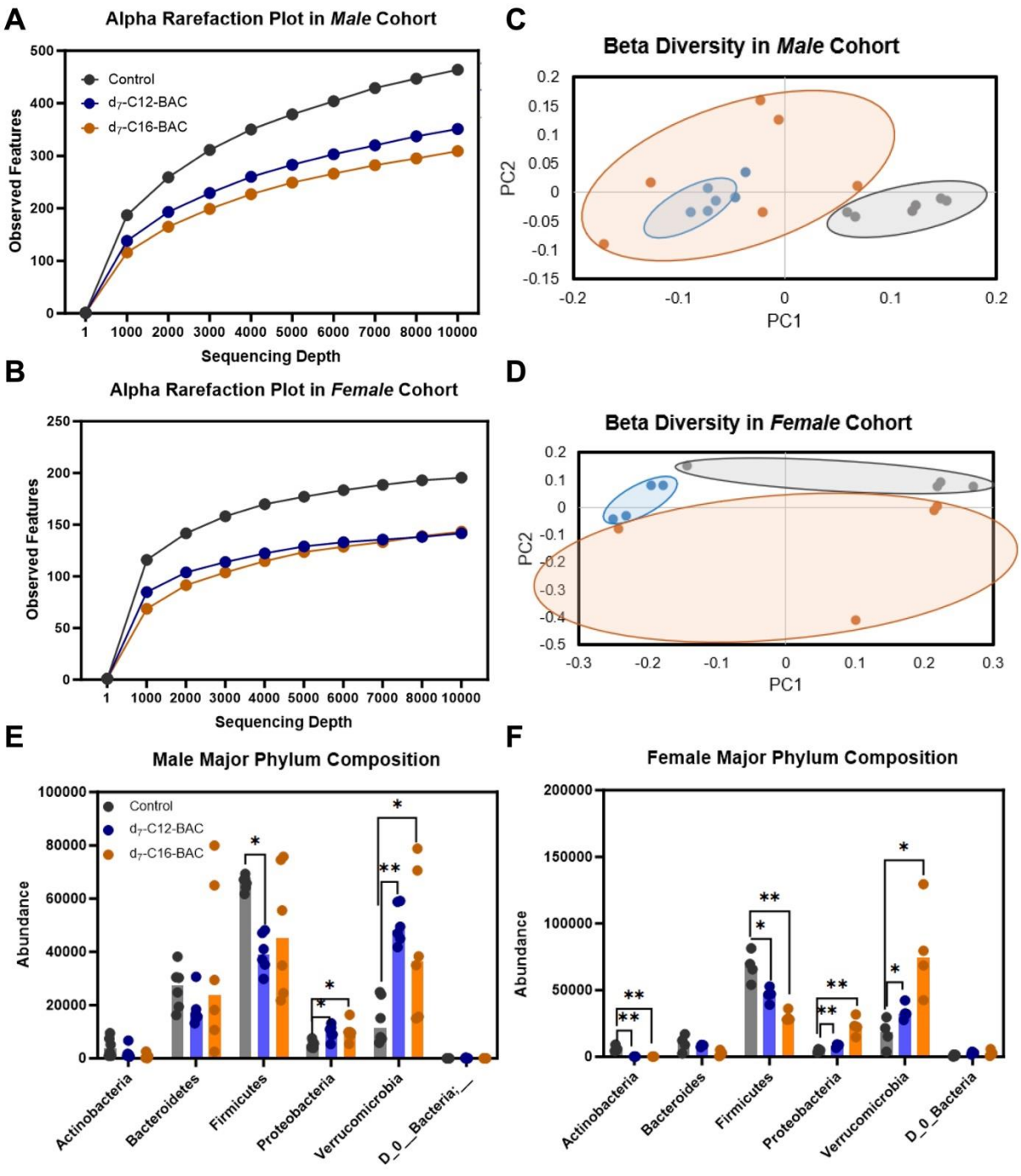

Figure 2.5 Diversity and Phyla Taxonomic Analysis.

A, B. Rarefaction plots demonstrating Alpha Diversity in Male (A) and Female (B) cohorts. **C, D.** Beta diversity PCoA plots were plotted via weighted unifrac distance matrix on qiime2. PC1 and PC2 are plotted for both Male and Female cohorts (*Materials and Methods*). **E, F.** Major Phylum compositions of Male (E) and Female (F) cohorts. Data are presented as median; asterisks signify statistical significance by one-way ANOVA using Welch's test. Comparisons are relative to

control. Male (N = 6 per group), Female (N = 4 per group). * $P \leq 0.05$; ** $P \leq 0.01$; *** $P \leq 0.001$; **** $P \leq 0.0001$.

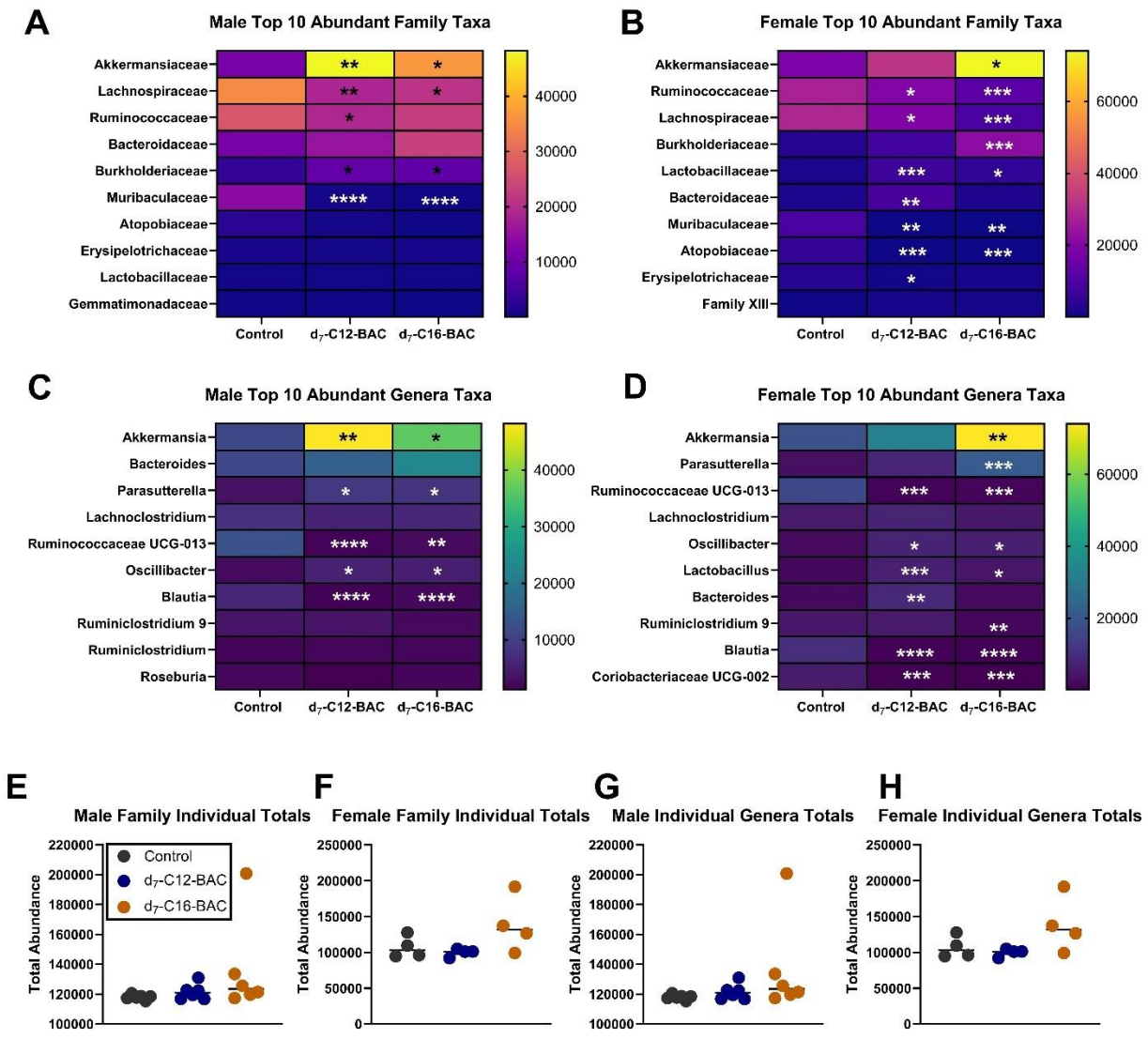

Figure 2.6 Taxonomic Analysis at the Family and Genera Levels.

A, B. Heatmaps demonstrating the top 10 abundant families of bacteria in Male (A) and Female (B) cohorts. **C, D.** Heatmaps demonstrating the top 10 abundant genera of bacteria detected in Male (C) and Female (D) cohorts. Each column in heatmaps (A-D) showcases the median of the respective group: control, d_7-C12-BAC, and d_7-C16-BAC. Taxonomic analysis was completed as described in materials and methods by Qiime2. **E-H**, Sums of either family or genera totals per sample were plotted and assessed for statistical significance in Male (E, G) and Female (F, H) cohorts. All data are presented as medians; asterisks signify statistical significance by one-way ANOVA using Welch's test. Comparisons are relative to control. Male (N=6 per group), Female (N=4 per group). * $P \leq 0.05$; ** $P \leq 0.01$; *** $P \leq 0.001$; **** $P \leq 0.0001$.

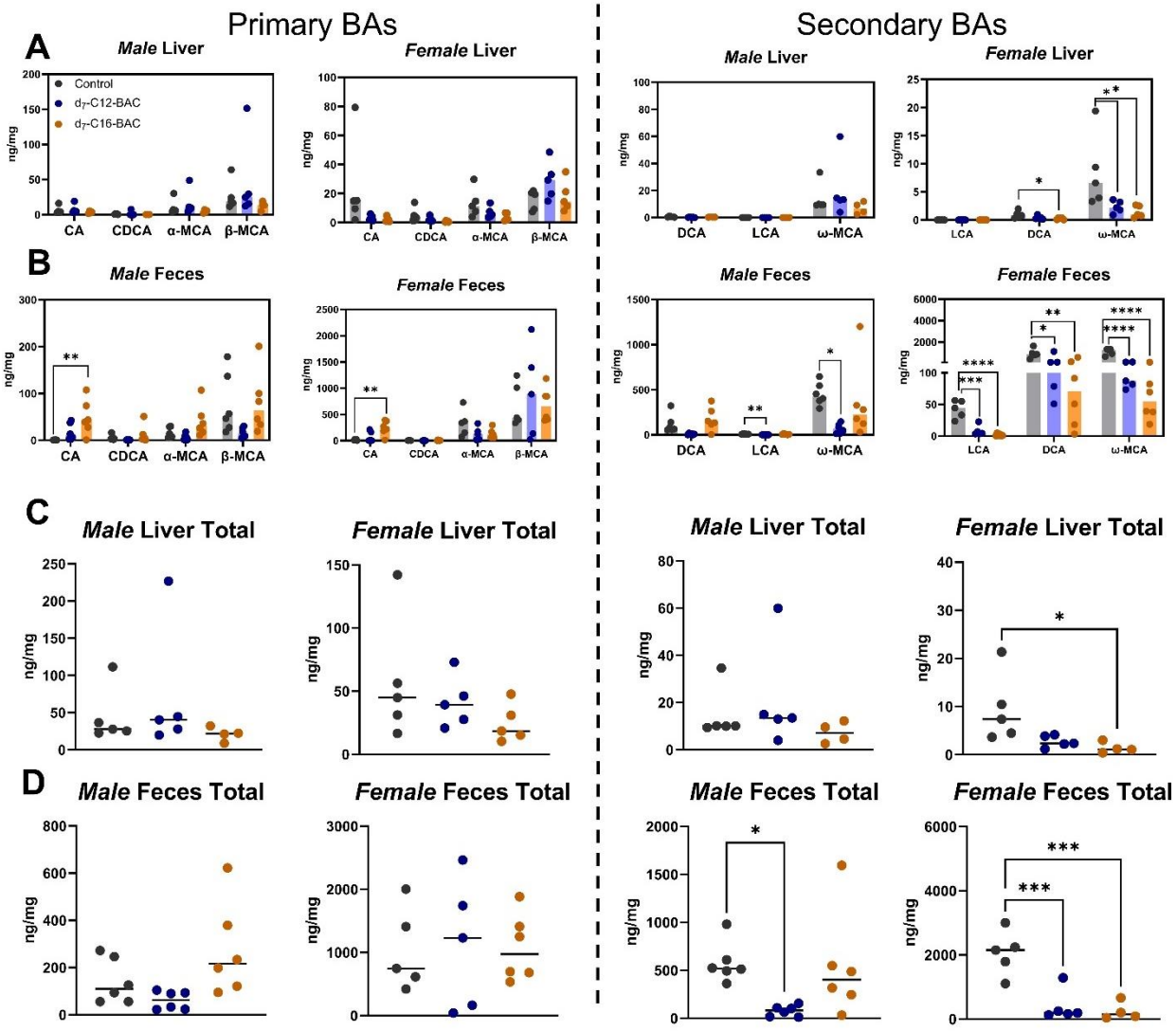

Figure 2.7 Quantified Primary and Secondary BAs in Male and Female mice.

A. Primary (CA, CDCA, α-MCA, and β-MCA) and secondary (DCA, LCA, ω-MCA) BAs, quantified in liver extracts of control, d_7-C12- and d_7-C16-BAC (120 µg/g/day) male and female mice. N=4-6. B. Primary and Secondary BAs quantified in feces of control, d_7-C12-BAC, and d_7-C16-BAC (120 µg/g/day) male and female mice. N=5-6. **C-D.** Sums of either primary or secondary BAs in male and female liver (C) and feces (D). All data are presented as medians; asterisks signify statistical significance by one-way ANOVA using Welch's test. * $P \leq 0.05$; ** $P \leq 0.01$; *** $P \leq 0.001$; **** $P \leq 0.0001$.

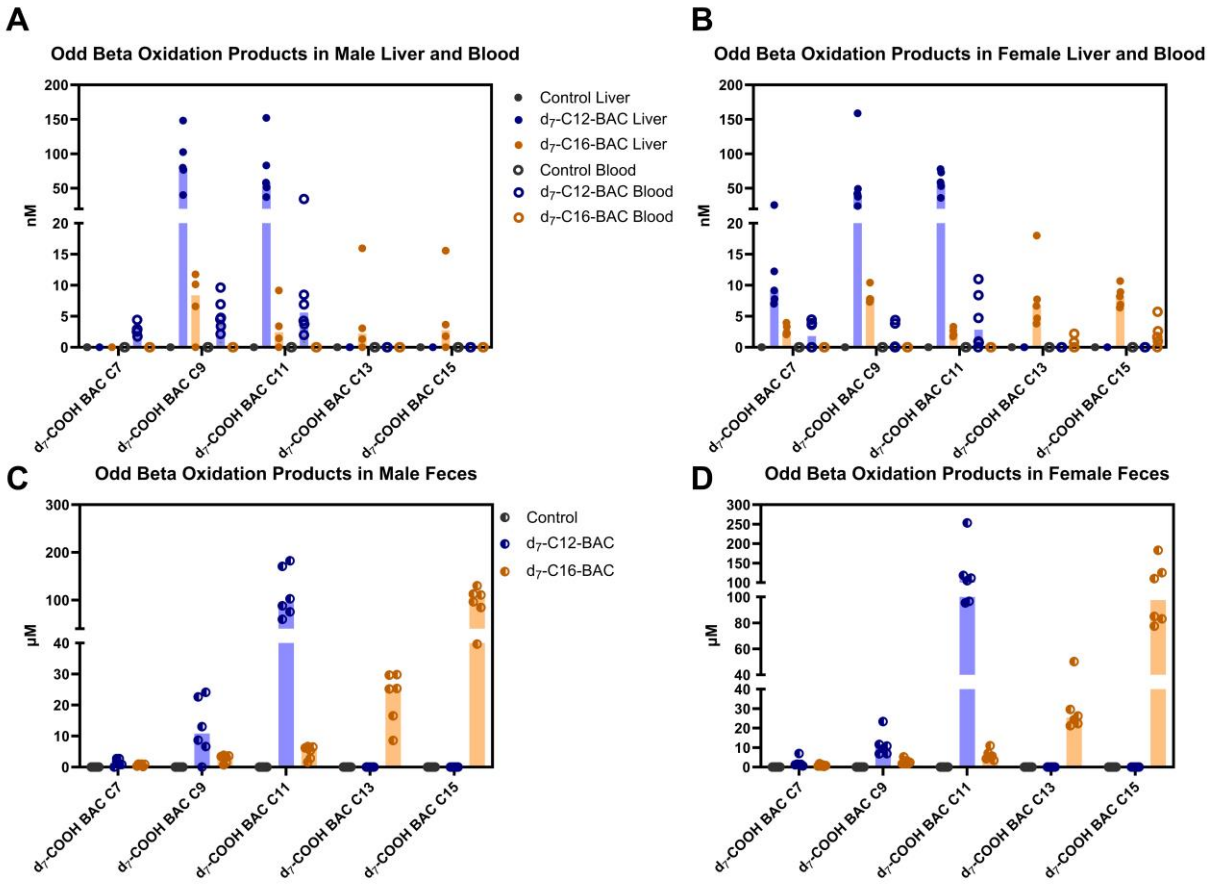

Figure 2.8 Odd Beta Oxidation Products in Male and Female Blood, Liver and Feces.

Odd Beta Oxidation products were quantified in Male (A and C) and Female (B and D) liver, blood, and feces using targeted mass spectrometry. N=4-6 per group.

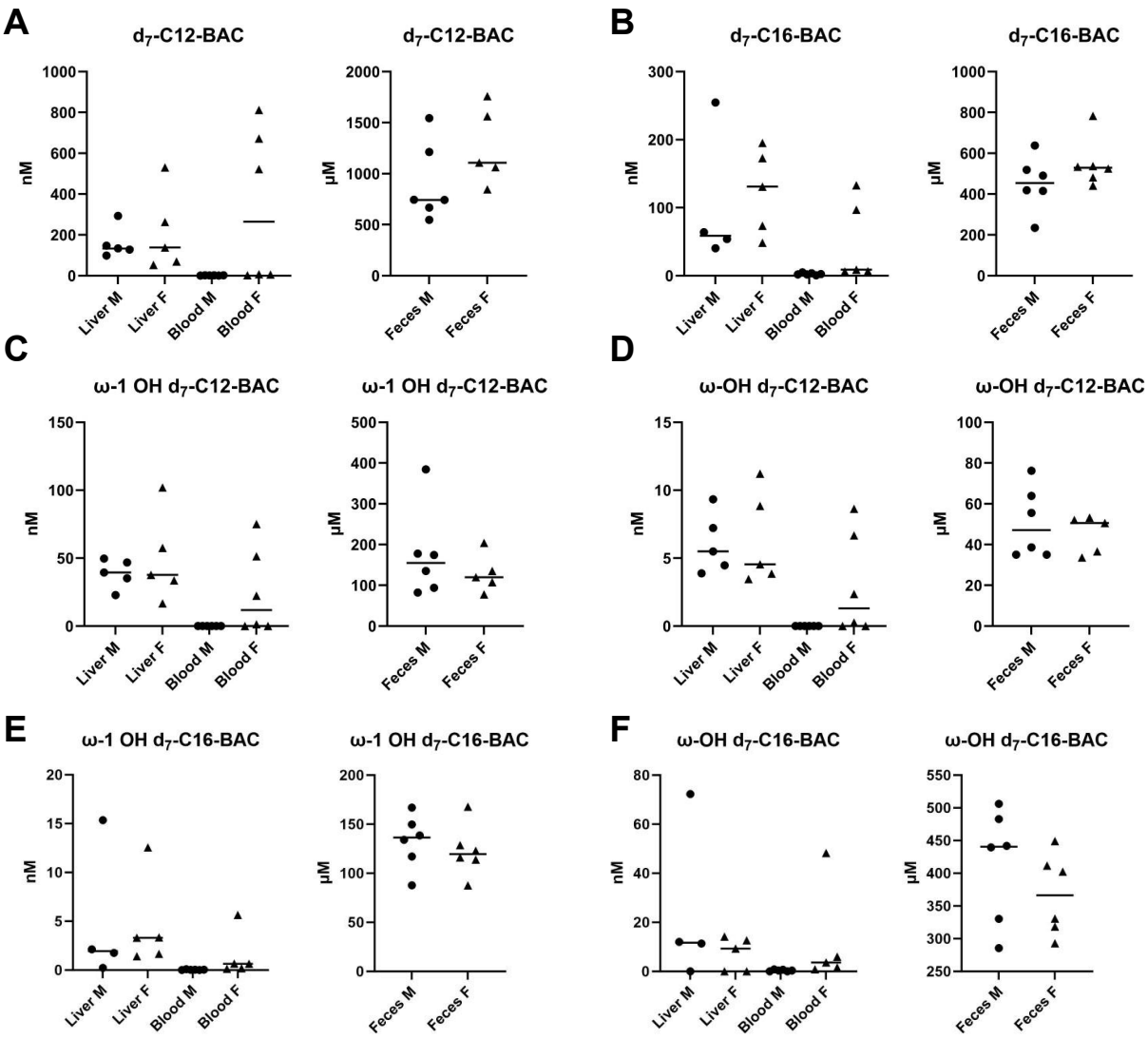

Figure 2.9 BAC Parent and (ω- and ω-1 OH) Metabolites between Male and Female Cohorts.

Statistical analyses were carried out using unpaired *t*-tests with Welch's correction to compare male and female groups for each measurement. No statistical difference was observed between any pairs.

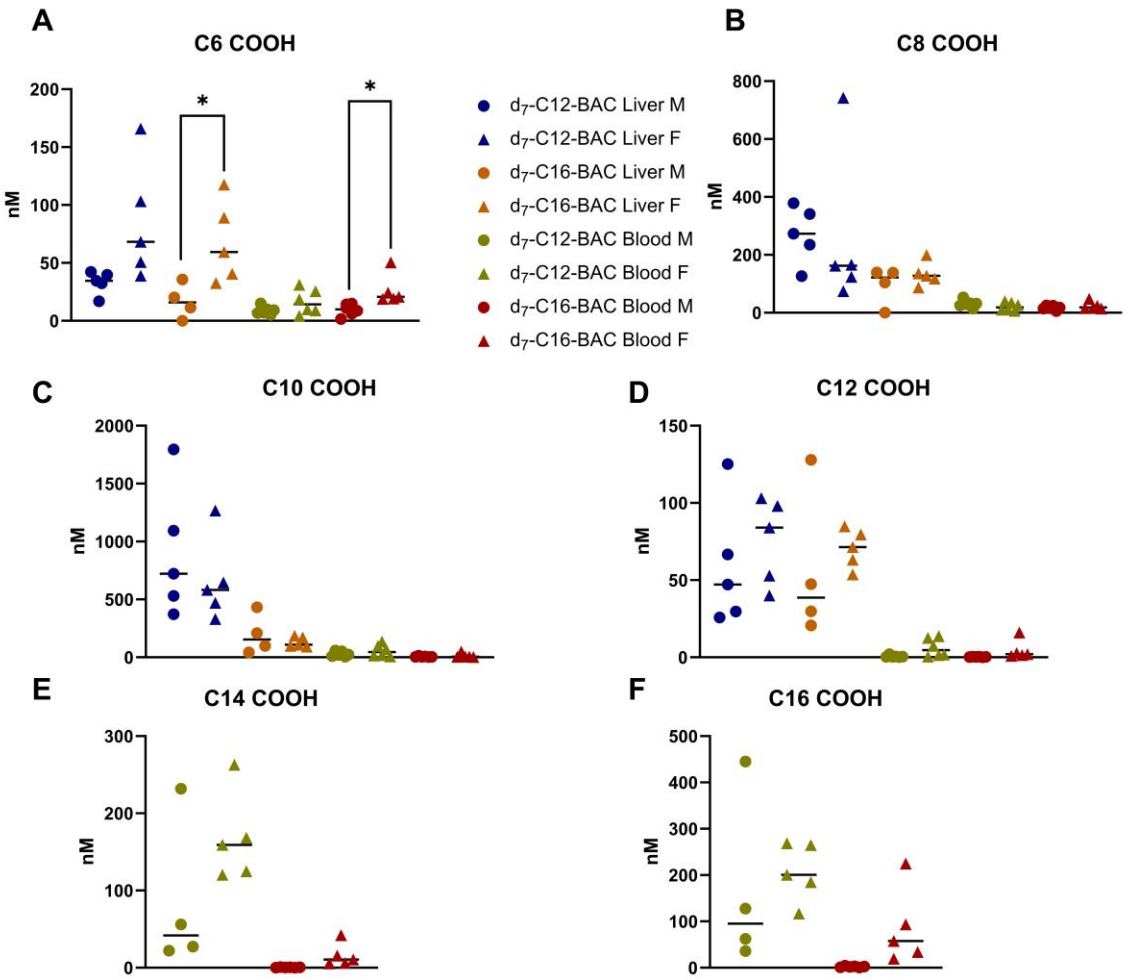

Figure 2.10 Even-Chained COOH Products in Liver and Blood between Male and Female Cohorts.

Statistical analyses were carried out using unpaired *t*-tests with Welch's correction to compare male and female groups for each measurement. *, $P < 0.05$; **** $P \leq 0.0001$.

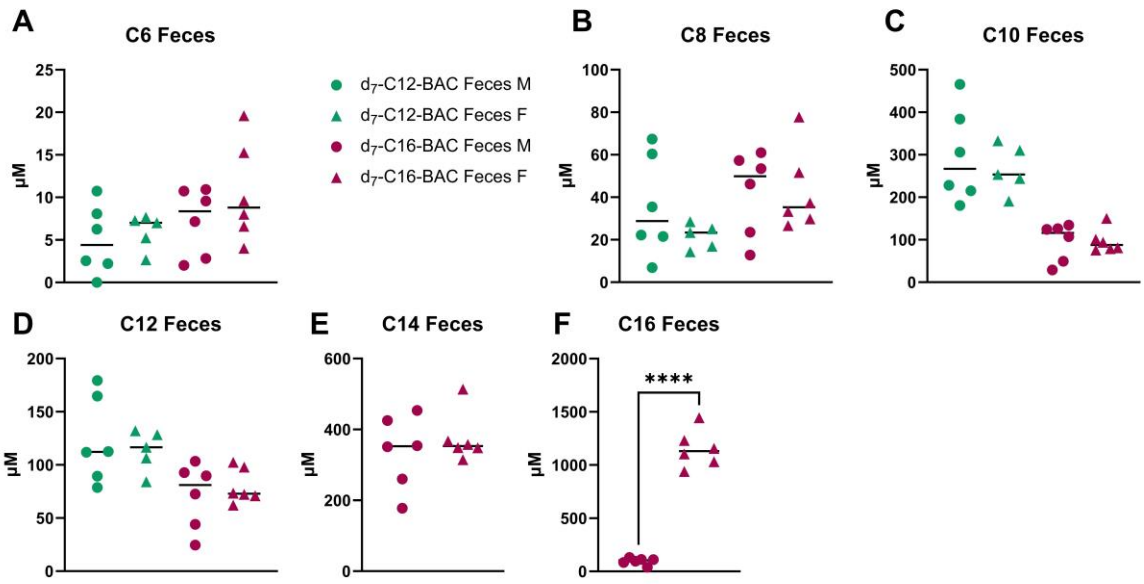

Figure 2.11 Even-Chained COOH Products in Feces between Male and Female Cohorts.

Statistical analyses were carried out using unpaired *t*-tests with Welch's correction to compare male and female groups for each measurement. *, $P < 0.05$; **** $P \leq 0.0001$.

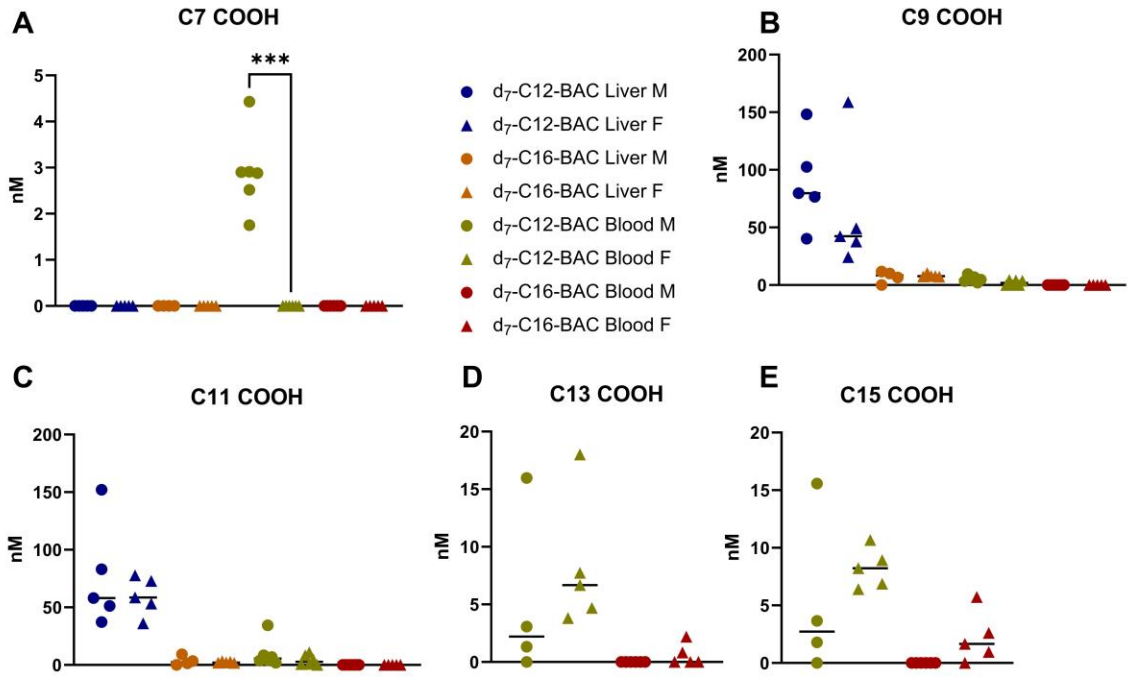

Figure 2.12 Odd-Chained COOH Products in Liver and Blood between Male and Female Cohorts.

Statistical analyses were carried out using unpaired *t*-tests with Welch's correction to compare male and female groups for each measurement. *, $P < 0.05$; **** $P \leq 0.0001$.

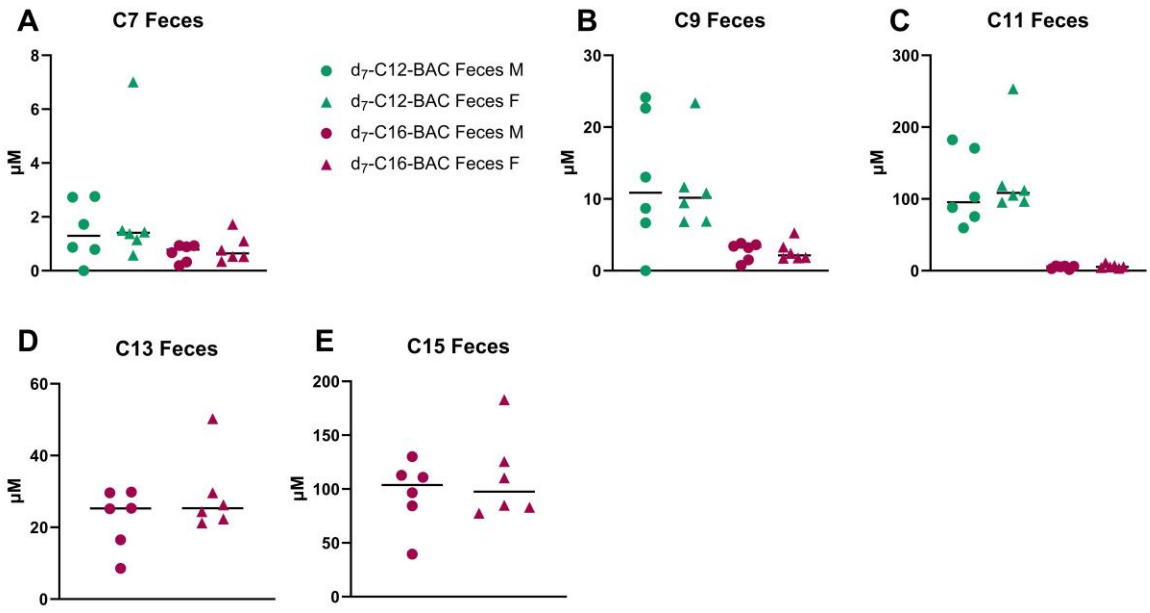

Figure 2.13 Odd-Chained COOH Products in Feces between Male and Female Cohorts.

Statistical analyses were carried out using unpaired *t*-tests with Welch's correction to compare male and female groups for each measurement. *, $P < 0.05$; **** $P \leq 0.0001$.

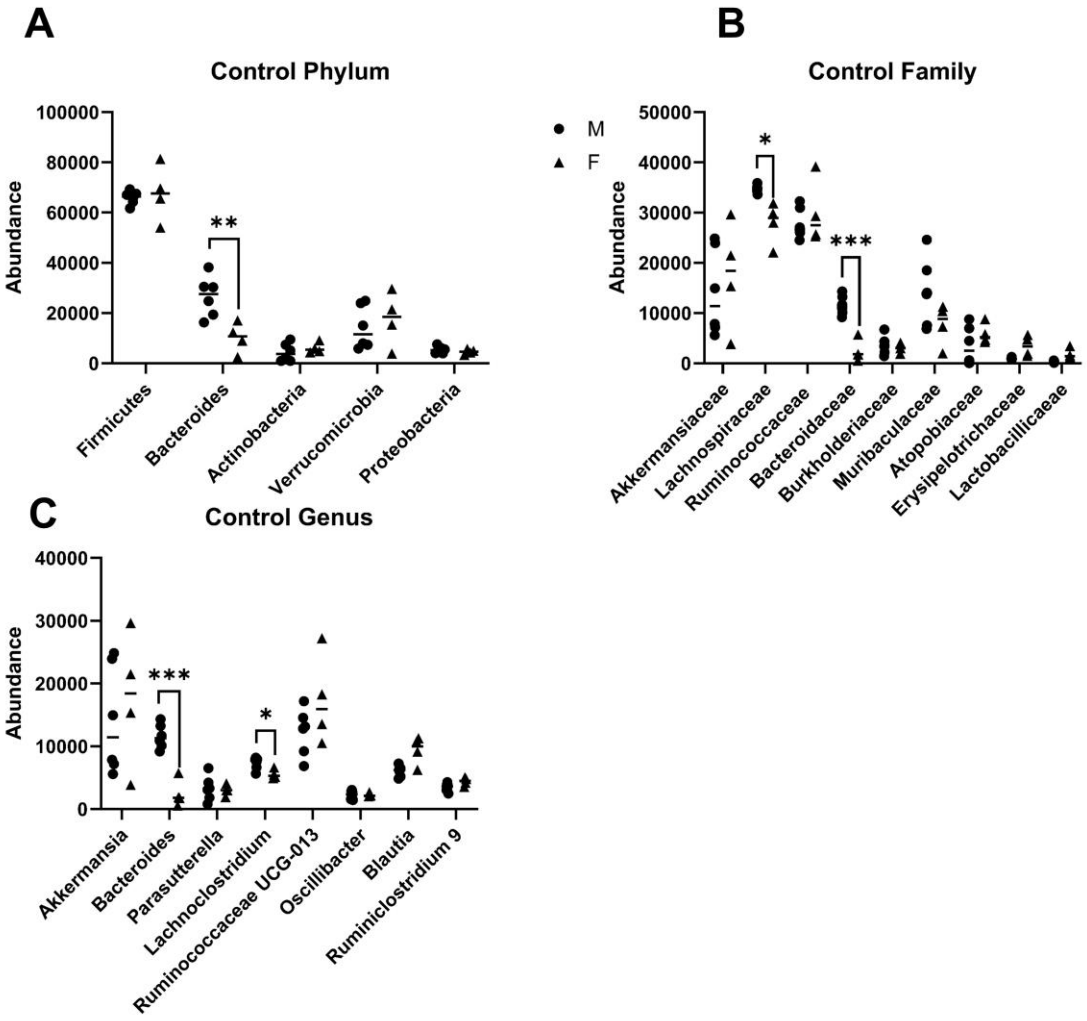

Figure 2.14 Comparisons of Shared Bacteria Taxa Totals between Control Male and Female Cohorts.

Statistical analyses were carried out using unpaired *t*-tests with Welch's correction to compare male and female groups for each measurement. * $P \leq 0.05$; ** $P \leq 0.01$; *** $P \leq 0.001$.

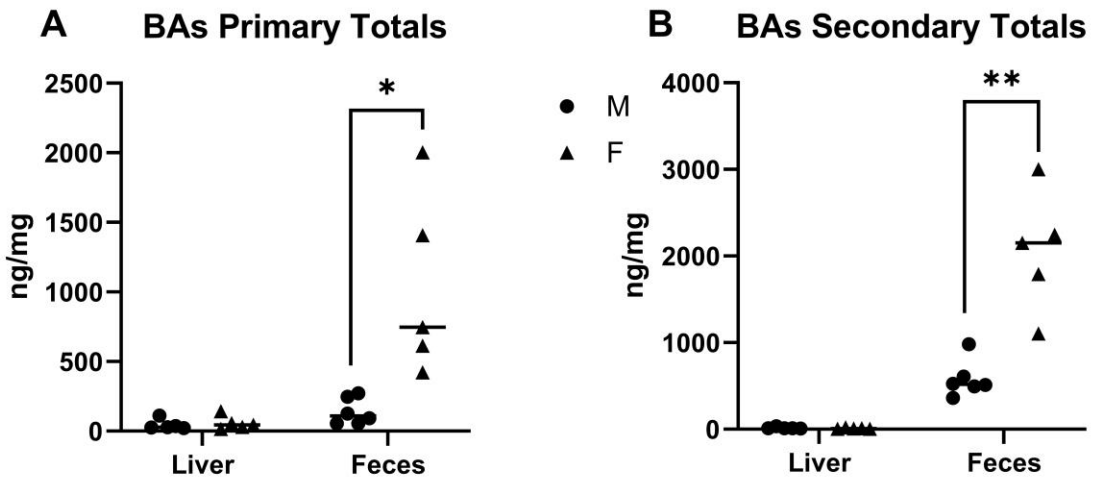

Figure 2.15 Comparisons of Primary and Secondary BA Totals between Male and Female Controls.

Statistical analyses were carried out using unpaired *t*-tests with Welch's correction to compare male and female groups for each measurement. * $P \leq 0.05$; ** $P \leq 0.01$.

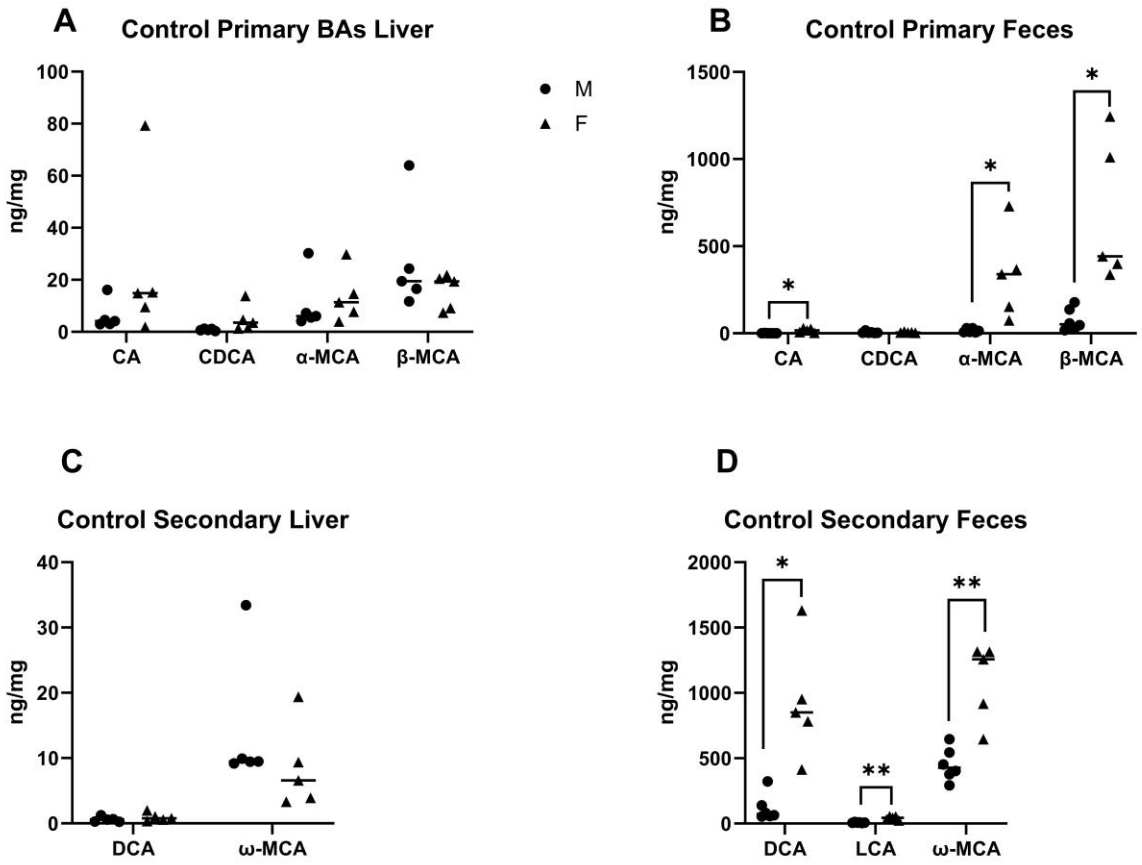

Figure 2.16 Comparisons of Primary and Secondary BAs between Male and Female Cohorts.

Statistical analyses were carried out using unpaired *t*-tests with Welch's correction to compare male and female groups for each measurement. * $P \leq 0.05$; ** $P \leq 0.01$; *** $P \leq 0.001$.

Chapter 2 Tables

Table 2.1. Sciex 6500 Conditions for BA Analysis.

Source/Gas	
Ion Source	Turbo Spray Ion Drive
Curtain Gas (CUR)	40
Collision Gas (CAD)	12
Ion Spray Voltage (IS)	-4500
Temperature (TEM)	450
Ion Source Gas 1 (GS1)	50
Ion Source Gas 2 (GS2)	70
UPLC Sample Manager	
Column Temperature	45°C
Sample Temperature	5°C

Table 2.2. Multiple Reaction Monitoring (MRM) Transition Conditions in both Positive and Negative Mode.

Abbreviations: DP = Declustering Potential; EP = Entrance Potential; CE = Collision Energy; CXP = Collision Cell Exit Potential; Q = Quadrupole Mass Filter

Table 2. MRM Transition Conditions for BA Analysis						
Negative Mode						
Bile Acid	Q1	Q3	DP (volts)	EP (volts)	CE (volts)	CXP (volts)
d0-α-MCA	407.2	387.2	-200	-10	-48	-19
d0-β-MCA	407.2	371.3	-210	-10	-44	-19
d0-ω-MCA	407.2	387.1	-195	-10	-46	-23
d0-CA	407.2	343.1	-210	-10	-44	-23
d0-CDCA	391.2	373.2	-185	-10	-44	-19
d0-DCA	391.2	345.2	-180	-10	-46	-23
d4-α-MCA	411.2	390.1	-200	-10	-48	-21
d4-ω-MCA	411.2	390	-200	-10	-48	-23
d4-CA	411.2	347.2	-150	-10	-46	-21
d4-DCA	395.2	349.2	-175	-10	-46	-21
Positive Mode						
d0-CA	359.2	135.1	130	10	35	10
d4-LCA	363.2	135.1	130	10	35	10

Table 2.3 Precursor and Product Ion Transitions for BAC Quantitation.

Analyte	Retention Time (min)	Pre-cursor Ion m/z	Product Ion m/z
d_7-COOH C6 BAC	1.5750	257.228	158.119/98.099
d_7-COOH C7 BAC	2.0950	271.16	172.133/98.099
d_7-COOH C8 BAC	2.6950	285.258	186.151/98.099
d_7-COOH C9 BAC	3.4950	299.275	200.17/98.099
d_7-COOH C10 BAC	4.2500	313.291	214.182/98.099
d_7-COOH C11 BAC	5.0050	327.31	228.201/98.099
d_7-COOH C12 BAC	5.6900	341.215	242.215/98.096
(ω-1 OH)-d_7-C12-BAC	5.7250	327.31	228.201/98.099
(ω-OH)-d_7-C12-BAC	5.9600	327.31	228.201/98.099
d_7-COOH C13 BAC	6.4450	355.34	256.23/98.099
d_7-COOH C14 BAC	7.1150	369.354	270.251/98.099
d_7-COOH C15 BAC	7.7800	383.37	284.261/98.099
d_7-COOH C16 BAC	8.4600	397.388	298.277/98.099
(ω-1 OH)-d_7-C16-BAC	8.7250	383.404	284.296/98.096
(ω-OH)-d_7-C16-BAC	9.0050	383.404	284.296/98.096
d_7-C12-BAC	10.1500	311.345	212.236/98.099
d_7-C16-BAC	13.4800	367.316	268.306/98.099

COOH C8	2.7400	278.22	186.151/91.053
COOH C10	4.2900	306.252	214.182/91.053
COOH C12	5.7200	334.277	242.215/91.053
16 Da C12	5.8350	320.303	288.233/91.053
COOH C14	7.1100	362.31	270.246/91.053
COOH C16	8.4950	390.344	298.277/91.053
16 Da C16	8.8450	376.363	284.296/91.053
C12 BAC	10.1400	304.304	212.241/91.053
C16 BAC	13.5600	360.366	268.301/91.054

Table 2.4 Average (Avg.) and Standard Deviations (Stdev.) of Parent BACs, Hydroxylated Metabolites, and Even-Chained Beta-Oxidation products in Male and Female Liver and Blood (N=4-6).

Male Liver (nM)						
Analyte	*Control Average*	*Control Stdev*	*d_7-C12-BAC Average*	*d_7-C12-BAC Stdev*	*d_7-C16-BAC Average*	*d_7-C16-BAC Stdev*
d_7-C12-BAC	0.0	0.0	174.6	84.4	0.0	0.0
d_7-C16-BAC	0.0	0.0	0.0	0.0	109.9	99.8
ω-1 OH-d_7-C12-BAC	0.0	0.0	38.8	10.6	0.0	0.0
ω-OH-d_7-C12-BAC	0.0	0.0	6.1	2.2	0.0	0.0
ω-1 OH-d_7-C16-BAC	0.0	0.0	0.0	0.0	4.9	7.1
ω-OH-d_7-C16-BAC	0.0	0.0	0.0	0.0	24.0	32.7
d_7-COOH BAC C6	0.0	0.0	33.2	10.0	16.9	15.1
d_7-COOH BAC C8	0.0	0.0	270.7	98.4	95.5	65.7
d_7-COOH BAC C10	0.0	0.0	903.2	567.5	195.6	172.0
d_7-COOH BAC C12	0.0	0.0	59.0	40.4	56.5	48.9
d_7-COOH BAC C14	0.0	0.0	0.0	0.0	84.4	99.4
d_7-COOH BAC C16	0.0	0.0	0.0	0.0	167.9	189.0
Male Blood (nM)						
Analyte	*Control Average*	*Control Stdev*	*d_7-C12-BAC Average*	*d_7-C12-BAC Stdev*	*d_7-C16-BAC Average*	*d_7-C16-BAC Stdev*
d_7-C12-BAC	0.0	0.0	1.4	0.6	0.0	0.0
d_7-C16-BAC	0.0	0.0	0.0	0.0	1.9	1.6
ω-1-OH-d_7-C12-BAC	0.0	0.0	0.0	0.0	0.0	0.0

ω-OH-d_7-C12-BAC	0.0	0.0	0.0	0.0	0.0	0.0
ω-1-OH-d_7-C16-BAC	0.0	0.0	0.0	0.0	0.0	0.0
ω-OH-d_7-C16-BAC	0.0	0.0	0.0	0.0	0.4	0.4
d_7-COOH BAC C6	0.0	0.0	8.9	3.5	9.5	5.1
d_7-COOH BAC C8	0.0	0.0	31.0	12.7	17.3	7.3
d_7-COOH BAC C10	0.0	0.0	29.1	21.9	5.9	4.6
d_7-COOH BAC C12	0.0	0.0	0.6	0.7	0.3	0.1
d_7-COOH BAC C14	0.0	0.0	0.0	0.0	0.5	0.3
d_7-COOH BAC C16	0.0	0.0	0.0	0.0	2.4	1.4
Female Liver (nM)						
Analyte	*Control Average*	*Control Stdev*	*d_7-C12-BAC Average*	*d_7-C12-BAC Stdev*	*d_7-C16-BAC Average*	*d_7-C16-BAC Stdev*
d_7-C12-BAC	0.0	0.0	210.7	197.1	0.0	0.0
d_7-C16-BAC	0.0	0.0	0.0	0.0	124.1	62.7
ω-1-OH-d_7-C12-BAC	0.0	0.0	49.5	32.7	0.0	0.0
ω-OH-d_7-C12-BAC	0.0	0.0	6.4	3.5	0.0	0.0
ω-1-OH-d_7-C16-BAC	0.0	0.0	0.0	0.0	4.5	4.6
ω-OH-d_7-C16-BAC	0.0	0.0	0.0	0.0	7.2	6.8
d_7-COOH BAC C6	0.0	0.0	85.4	51.1	67.8	35.3
d_7-COOH BAC C8	0.0	0.0	253.8	275.7	133.4	41.1
d_7-COOH BAC C10	0.0	0.0	660.0	360.1	131.9	43.8

d_7-COOH BAC C12	0.0	0.0	75.7	27.9	70.5	12.5
d_7-COOH BAC C14	0.0	0.0	0.0	0.0	167.1	57.5
d_7-COOH BAC C16	0.0	0.0	0.0	0.0	207.2	62.7
Female Blood (nM)						
Analyte	*Control Average*	*Control Stdev*	*d_7-C12-BAC Average*	*d_7-C12-BAC Stdev*	*d_7-C16-BAC Average*	*d_7-C16-BAC Stdev*
d_7-C12-BAC	0.0	0.0	336.6	375.0	0.0	0.0
d_7-C16-BAC	0.0	0.0	0.0	0.0	50.3	60.3
ω-1-OH-d_7-C12-BAC	0.0	0.0	25.0	31.7	0.0	0.0
ω-OH-d_7-C12-BAC	0.0	0.0	3.0	3.8	0.0	0.0
ω-1-OH-d_7-C16-BAC	0.0	0.0	0.0	0.0	1.5	2.4
ω-OH-d_7-C16-BAC	0.0	0.0	0.0	0.0	12.1	20.4
d_7-COOH BAC C6	0.0	0.0	16.4	10.5	26.7	13.4
d_7-COOH BAC C8	0.0	0.0	21.2	14.0	23.9	13.8
d_7-COOH BAC C10	0.0	0.0	57.8	52.1	13.8	20.3
d_7-COOH BAC C12	0.0	0.0	6.2	5.9	4.6	6.4
d_7-COOH BAC C14	0.0	0.0	0.0	0.0	16.1	15.2
d_7-COOH BAC C16	0.0	0.0	0.0	0.0	85.9	82.5

Table 2.5 Avg and Stdev. of Parent BACs, Hydroxylated Metabolites, and Even-Chained Beta-Oxidation Products in Male and Female Feces (N=5-6).

Male Feces (μM)						
Analyte	*Control Average*	*Control Stdev*	*d_7-C12-BAC Average*	*d_7-C12-BAC Stdev*	*d_7-C16-BAC Average*	*d_7-C16-BAC Stdev*
d_7-C12-BAC	0.0	0.0	909.6	384.9	0.0	0.0
d_7-C16-BAC	0.0	0.0	0.0	0.0	452.4	134.3
ω-1-OH-d_7-C12-BAC	0.0	0.0	174.7	110.0	0.0	0.0
ω-OH-d_7-C12-BAC	0.0	0.0	50.7	17.2	0.0	0.0
ω-1-OH-d_7-C16-BAC	0.0	0.0	0.0	0.0	132.4	27.4
ω-OH-d_7-C16-BAC	0.0	0.0	0.0	0.0	414.4	87.4
d_7-COOH BAC C6	0.0	0.0	5.0	4.1	7.2	4.0
d_7-COOH BAC C8	0.0	0.0	35.6	23.8	42.4	19.7
d_7-COOH BAC C10	0.0	0.0	296.6	110.6	95.0	44.6
d_7-COOH BAC C12	0.0	0.0	122.8	40.6	71.2	30.8
d_7-COOH BAC C14	0.0	0.0	0.0	0.0	337.0	103.1
d_7-COOH BAC C16	0.0	0.0	0.0	0.0	95.7	31.5
Female Feces (μM)						
Analyte	*Control Average*	*Control Stdev*	*d_7-C12-BAC Average*	*d_7-C12-BAC Stdev*	*d_7-C16-BAC Average*	*d_7-C16-BAC Stdev*
d_7-C12-BAC	0.0	0.0	1267.5	378.8	0.0	0.0
d_7-C16-BAC	0.0	0.0	0.0	0.0	550.1	119.7
ω-1-OH-d_7-C12-BAC	0.0	0.0	128.8	46.9	0.0	0.0

ω-OH-d_7-C12-BAC	0.0	0.0	45.2	9.3	0.0	0.0
ω-1-OH-d_7-C16-BAC	0.0	0.0	0.0	0.0	122.8	26.2
ω-OH-d_7-C16-BAC	0.0	0.0	0.0	0.0	367.5	61.9
d_7-COOH BAC C6	0.0	0.0	6.0	2.1	10.5	5.8
d_7-COOH BAC C8	0.0	0.0	21.6	5.9	42.7	19.2
d_7-COOH BAC C10	0.0	0.0	266.3	56.4	96.8	28.0
d_7-COOH BAC C12	0.0	0.0	113.5	19.3	79.8	16.3
d_7-COOH BAC C14	0.0	0.0	0.0	0.0	375.0	70.2
d_7-COOH BAC C16	0.0	0.0	0.0	0.0	1151.0	175.7

Table 2.6 Avg. and Stdev. of Odd-Chained Beta-Oxidation Products in Male and Female Liver and Blood (N=4-6).

Male Liver (nM)						
Analyte	*Control Average*	*Control Stdev*	*d_7-C12-BAC Average*	*d_7-C12-BAC Stdev*	*d_7-C16-BAC Average*	*d_7-C16-BAC Stdev*
d_7-COOH BAC C7	0.0	0.0	0.0	0.0	0.0	0.0
d_7-COOH BAC C9	0.0	0.0	89.5	39.7	7.1	5.2
d_7-COOH BAC C11	0.0	0.0	76.4	45.5	3.5	4.0
d_7-COOH BAC C13	0.0	0.0	0.0	0.0	5.1	7.4
d_7-COOH BAC C15	0.0	0.0	0.0	0.0	5.3	7.0
Male Blood (nM)						
Analyte	*Control Average*	*Control Stdev*	*d_7-C12-BAC Average*	*d_7-C12-BAC Stdev*	*d_7-C16-BAC Average*	*d_7-C16-BAC Stdev*
d_7-COOH BAC C7	0.0	0.0	2.9	0.9	0.0	0.0
d_7-COOH BAC C9	0.0	0.0	5.2	2.7	0.0	0.0
d_7-COOH BAC C11	0.0	0.0	10.0	12.2	0.0	0.0
d_7-COOH BAC C13	0.0	0.0	0.0	0.0	0.0	0.0
d_7-COOH BAC C15	0.0	0.0	0.0	0.0	0.0	0.0
Female Liver (nM)						
Analyte	*Control Average*	*Control Stdev*	*d_7-C12-BAC Average*	*d_7-C12-BAC Stdev*	*d_7-C16-BAC Average*	*d_7-C16-BAC Stdev*
d_7-COOH BAC C7	0.0	0.0	12.4	7.6	2.8	0.8
d_7-COOH BAC C9	0.0	0.0	62.5	54.6	8.2	1.3
d_7-COOH BAC C11	0.0	0.0	59.7	16.7	2.3	0.7

d_7-COOH BAC C13	0.0	0.0	0.0	0.0	8.2	5.7
d_7-COOH BAC C15	0.0	0.0	0.0	0.0	8.2	1.7
Female Blood (nM)						
Analyte	*Control Average*	*Control Stdev*	*d_7-C12-BAC Average*	*d_7-C12-BAC Stdev*	*d_7-C16-BAC Average*	*d_7-C16-BAC Stdev*
d_7-COOH BAC C7	0.0	0.0	0.0	0.0	0.0	0.0
d_7-COOH BAC C9	0.0	0.0	2.3	2.1	0.0	0.0
d_7-COOH BAC C11	0.0	0.0	4.3	4.6	0.0	0.0
d_7-COOH BAC C13	0.0	0.0	0.0	0.0	0.6	1.0
d_7-COOH BAC C15	0.0	0.0	0.0	0.0	2.2	2.2

Table 2.7 Avg. and Stdev. of Odd-Chained Beta-Oxidation Products in Male and Female Feces (N=5-6).

Male Feces (μM)						
Analyte	*Control Average*	*Control Stdev*	*d_7-C12-BAC Average*	*d_7-C12-BAC Stdev*	*d_7-C16-BAC Average*	*d_7-C16-BAC Stdev*
d_7-COOH BAC C7	0.0	0.0	1.5	1.1	0.7	0.3
d_7-COOH BAC C9	0.0	0.0	12.5	9.4	2.7	1.3
d_7-COOH BAC C11	0.0	0.0	113.2	51.2	4.8	2.1
d_7-COOH BAC C13	0.0	0.0	0.0	0.0	22.5	8.4
d_7-COOH BAC C15	0.0	0.0	0.0	0.0	95.7	31.5
Female Feces (μM)						
Analyte	*Control Average*	*Control Stdev*	*d_7-C12-BAC Average*	*d_7-C12-BAC Stdev*	*d_7-C16-BAC Average*	*d_7-C16-BAC Stdev*
d_7-COOH BAC C7	0.0	0.0	1.2	0.4	0.8	0.5
d_7-COOH BAC C9	0.0	0.0	9.1	2.2	2.7	1.4
d_7-COOH BAC C11	0.0	0.0	105.5	9.8	6.1	2.7
d_7-COOH BAC C13	0.0	0.0	0.0	0.0	29.0	10.8
d_7-COOH BAC C15	0.0	0.0	0.0	0.0	110.8	39.9

Table 2.8 Quantified Primary and Secondary BAs in Chapter 2; Humans vs Murine Expression.

(Takahashi *et al.*, 2016)

		Human	Murine
CA	Primary BA	X	X
CDCA	Primary BA	X	X
α-MCA	Primary BA		X
β-MCA	Primary BA		X
LCA	Secondary BA	X	X
DCA	Secondary BA	X	X
ω-MCA	Secondary BA		X

Chapter 2 References

Abraham, K. *et al.* (2002) Severe 2,3,7,8-tetrachlorodibenzo- *p* -dioxin (TCDD) intoxication: Insights into the measurement of hepatic cytochrome P450 1A2 induction*. *Clin. Pharmacol. Ther.*, **72**, 163–174.

Ahlawat, S. *et al.* (2021) Gut–organ axis: a microbial outreach and networking. *Lett. Appl. Microbiol.*, **72**, 636–668.

Arnold, W.A. *et al.* (2023) Quaternary Ammonium Compounds: A Chemical Class of Emerging Concern. *Environ. Sci. Technol.*

Asgharpour, A. *et al.* (2015) Bile acids: emerging role in management of liver diseases. *Hepatol. Int.*, **9**, 527–533.

Barko, P.C. *et al.* (2018) The Gastrointestinal Microbiome: A Review. *J. Vet. Intern. Med.*, **32**, 9–25.

Baudouin, C. *et al.* (1999) Ocular surface inflammatory changes induced by topical antiglaucoma drugs: human and animal studies. *Ophthalmology*, **106**, 556–63.

Bhattacharya, A. *et al.* (2023) In vivo mouse models to study bile acid synthesis and signaling. *Hepatobiliary Pancreat. Dis. Int.*, **22**, 466–473.

Bond, P. (2017) Phosphatidic acid: biosynthesis, pharmacokinetics, mechanisms of action and effect on strength and body composition in resistance-trained individuals. *Nutr. Metab.*, **14**, 12.

Boursier, J. and Diehl, A.M. (2015) Implication of Gut Microbiota in Nonalcoholic Fatty Liver Disease. *PLOS Pathog.*, **11**, e1004559.

Breton, J. *et al.* (2013) Ecotoxicology inside the gut: impact of heavy metals on the mouse microbiome. *BMC Pharmacol. Toxicol.*, **14**, 62.

Caporaso, J.G. *et al.* (2010) QIIME allows analysis of high-throughput community sequencing data. *Nat Methods*, **7**, 335–6.

Chen, M. *et al.* (2021) Enterohepatic circulation of bile acids and their emerging roles on glucolipid metabolism. *Steroids*, **165**, 108757.

Chew, J.L. and Chua, K.Y. (2003) Collection of Mouse Urine for Bioassays. *Lab Anim.*, **32**, 48–50.

Chiang, H.-L. and Lin, C.-H. (2019) Altered Gut Microbiome and Intestinal Pathology in Parkinson's Disease. *J. Mov. Disord.*, **12**, 67–83.

Chiang, J.Y. *et al.* (2000) Farnesoid X receptor responds to bile acids and represses cholesterol 7alpha-hydroxylase gene (CYP7A1) transcription. *J Biol Chem*, **275**, 10918–24.

Chiang, J.Y.L. *et al.* (2001) Regulation of cholesterol 7α-hydroxylase gene (CYP7A1) transcription by the liver orphan receptor (LXRα). *Gene*, **262**, 257–265.

Chiang, J.Y.L. and Ferrell, J.M. (2018) Bile Acid Metabolism in Liver Pathobiology. *Gene Expr.*, **18**, 71–87.

Chiu, K. *et al.* (2020) The Impact of Environmental Chemicals on the Gut Microbiome. *Toxicol. Sci.*, **176**, 253–284.

Chow, M.D. *et al.* (2017) The role of bile acids in nonalcoholic fatty liver disease and nonalcoholic steatohepatitis. *Mol. Aspects Med.*, **56**, 34–44.

Claus, S.P. *et al.* (2016) The gut microbiota: a major player in the toxicity of environmental pollutants? *Npj Biofilms Microbiomes*, **2**, 16003.

Clayton, P.T. (1998) Disorders of cholesterol biosynthesis. *Arch Child*, **78**, 185–9.

Cryle, M.J. and De Voss, J.J. (2004) Carbon–carbon bond cleavage by cytochrome P450 $_{BioI}$ (CYP107H1). *Chem Commun*, 86–87.

Cui, J.Y. and Klaassen, C.D. (2016) RNA-Seq reveals common and unique PXR- and CAR-target gene signatures in the mouse liver transcriptome. *Biochim Biophys Acta*, **1859**, 1198–1217.

Dalhat, M.H. *et al.* (2022) NAT10: An RNA cytidine transferase regulates fatty acid metabolism in cancer cells. *Clin. Transl. Med.*, **12**, e1045.

Deutschle, T. *et al.* (2006) In vitro genotoxicity and cytotoxicity of benzalkonium chloride. *Toxicol. In Vitro*, **20**, 1472–1477.

Di Ciaula, A. *et al.* (2020) Liver Steatosis, Gut-Liver Axis, Microbiome and Environmental Factors. A Never-Ending Bidirectional Cross-Talk. *J. Clin. Med.*, **9**, 2648.

Edson, K. and Rettie, A. (2013) CYP4 Enzymes As Potential Drug Targets: Focus on Enzyme Multiplicity, Inducers and Inhibitors, and Therapeutic Modulation of 20-Hydroxyeicosatetraenoic Acid (20-HETE) Synthase and Fatty Acid ω-Hydroxylase Activities. *Curr. Top. Med. Chem.*, **13**, 1429–1440.

Edson, K. Z. *et al.* (2013) Cytochrome P450-dependent catabolism of vitamin K: omega-hydroxylation catalyzed by human CYP4F2 and CYP4F11. *Biochemistry*, **52**, 8276–85.

Edson, Katheryne Z. *et al.* (2013) Cytochrome P450-Dependent Catabolism of Vitamin K: ω-Hydroxylation Catalyzed by Human CYP4F2 and CYP4F11. *Biochemistry*, **52**, 8276–8285.

Eloe-Fadrosh, E.A. and Rasko, D.A. (2013) The human microbiome: from symbiosis to pathogenesis. *Annu Rev Med*, **64**, 145–63.

Esteves, F. *et al.* (2021) The Central Role of Cytochrome P450 in Xenobiotic Metabolism—A Brief Review on a Fascinating Enzyme Family. *J. Xenobiotics*, **11**, 94–114.

Fan, Y. and Pedersen, O. (2021) Gut microbiota in human metabolic health and disease. *Nat Rev Microbiol*, **19**, 55–71.

Fazeli, M. *et al.* (2011) Cadmium chloride exhibits a profound toxic effect on bacterial microflora of the mice gastrointestinal tract. *Hum. Exp. Toxicol.*, **30**, 152–159.

Feng, D. *et al.* (2020) Bisphenol A exposure induces gut microbiota dysbiosis and consequent activation of gut-liver axis leading to hepatic steatosis in CD-1 mice. *Environ. Pollut.*, **265**, 114880.

Finkelstein, J. *et al.* (2014) Lipids in health and disease. *Nature*, **510**, 47–47.

Fleishman, J.S. and Kumar, S. (2024) Bile acid metabolism and signaling in health and disease: molecular mechanisms and therapeutic targets. *Signal Transduct. Target. Ther.*, **9**, 97.

Fu, Z.D. *et al.* (2017) RNA-Seq Profiling of Intestinal Expression of Xenobiotic Processing Genes in Germ-Free Mice. *Drug Metab Dispos*, **45**, 1225–1238.

Fuchs, C.D. and Trauner, M. (2022) Role of bile acids and their receptors in gastrointestinal and hepatic pathophysiology. *Nat. Rev. Gastroenterol. Hepatol.*, **19**, 432–450.

Ghazalpour, A. *et al.* (2016) Expanding role of gut microbiota in lipid metabolism. *Curr Opin Lipidol*, **27**, 141–7.

Goldstein, J.L. *et al.* (2006) Protein sensors for membrane sterols. *Cell*, **124**, 35–46.

Gonzalez, M. *et al.* (2014) Asthma among workers in healthcare settings: role of disinfection with quaternary ammonium compounds. *Clin. Exp. Allergy*, **44**, 393–406.

Goodwin, B. *et al.* (2000a) A Regulatory Cascade of the Nuclear Receptors FXR, SHP-1, and LRH-1 Represses Bile Acid Biosynthesis. *Mol. Cell*, **6**, 517–526.

Goodwin, B. *et al.* (2000b) A Regulatory Cascade of the Nuclear Receptors FXR, SHP-1, and LRH-1 Represses Bile Acid Biosynthesis. *Mol. Cell*, **6**, 517–526.

Grangeon, A. *et al.* (2021) Determination of CYP450 Expression Levels in the Human Small Intestine by Mass Spectrometry-Based Targeted Proteomics. *Int. J. Mol. Sci.*, **22**, 12791.

Guengerich, F.P. and Yoshimoto, F.K. (2018) Formation and Cleavage of C–C Bonds by Enzymatic Oxidation–Reduction Reactions. *Chem. Rev.*, **118**, 6573–6655.

Hakkola, J. *et al.* (2020) Inhibition and induction of CYP enzymes in humans: an update. *Arch. Toxicol.*, **94**, 3671–3722.

Herron, J. *et al.* (2018) Assessment of Altered Cholesterol Homeostasis by Xenobiotics Using Ultra-High Performance Liquid Chromatography-Tandem Mass Spectrometry. *Curr Protoc Toxicol*, **78**, e65.

Herron, J. *et al.* (2016) Identification of Environmental Quaternary Ammonium Compounds as Direct Inhibitors of Cholesterol Biosynthesis. *Toxicol Sci*, **151**, 261–270.

Herron, J.M. *et al.* (2019) Multiomics investigation reveals benzalkonium chloride disinfectants alter sterol and lipid homeostasis in the mouse neonatal brain. *Toxicol Sci*, **171**, 32–45.

Hild, B. *et al.* (2021) Bile Acids in Control of the Gut-Liver-Axis. *Z. Für Gastroenterol.*, **59**, 63–68.

Hills, R. *et al.* (2019) Gut Microbiome: Profound Implications for Diet and Disease. *Nutrients*, **11**, 1613.

Hines, K. *et al.* (2017) Assessment of Altered Lipid Homeostasis by HILIC-Ion Mobility-Mass Spectrometry-Based Lipidomics. *J Lipid Res*, **58**, 809–819.

Hines, K.M. *et al.* (2016) Evaluation of Collision Cross Section Calibrants for Structural Analysis of Lipids by Traveling Wave Ion Mobility-Mass Spectrometry. *Anal Chem*, **88**, 7329–36.

Hirani, V. *et al.* (2008) Expression of CYP4F2 in human liver and kidney: Assessment using targeted peptide antibodies. *Arch. Biochem. Biophys.*, **478**, 59–68.

Hitosugi, M. *et al.* (1998) A case of fatal benzalkonium chloride poisoning. *Int J Leg. Med*, **111**, 265–6.

Hofmann, A.F. (1999) The Continuing Importance of Bile Acids in Liver and Intestinal Disease. *Arch. Intern. Med.*, **159**, 2647.

Holter, M.M. *et al.* (2020) TGR5 Signaling in Hepatic Metabolic Health. *Nutrients*, **12**, 2598.

Hrubec, T.C. *et al.* (2021a) Altered toxicological endpoints in humans from common quaternary ammonium compound disinfectant exposure. *Toxicol Rep*, **8**, 646–656.

Hrubec, T.C. *et al.* (2021b) Altered toxicological endpoints in humans from common quaternary ammonium compound disinfectant exposure. *Toxicol Rep*, **8**, 646–656.

Hrubec, T.C. *et al.* (2017) Ambient and Dosed Exposure to Quaternary Ammonium Disinfectants Causes Neural Tube Defects in Rodents. *Birth Defects Res*, **109**, 1166–1178.

Hrycay, E. and Bandiera, S. (2009) Expression, Function and Regulation of Mouse Cytochrome P450 Enzymes: Comparison With Human Cytochrome P450 Enzymes. *Curr. Drug Metab.*, **10**, 1151–1183.

Hukkanen, J. *et al.* (2002) Expression and Regulation of Xenobiotic-Metabolizing Cytochrome P450 (CYP) Enzymes in Human Lung. *Crit. Rev. Toxicol.*, **32**, 391–411.

Jaeschke, H. (2015) Toxic Responses of the Liver. In, Klaassen,C.D. and Watkins III,J.B. (eds), *Casarett & Doull's Essentials of Toxicology, 3e*. McGraw-Hill Education, New York, NY.

Jiang, L. *et al.* (2021) Farnesoid X receptor (FXR): Structures and ligands. *Comput. Struct. Biotechnol. J.*, **19**, 2148–2159.

Johnson, A.L. *et al.* (2015) Cytochrome P450 omega-Hydroxylases in Inflammation and Cancer. *Adv Pharmacol*, **74**, 223–62.

Johnson, E.L. *et al.* (2020) Sphingolipids produced by gut bacteria enter host metabolic pathways impacting ceramide levels. *Nat Commun*, **11**, 2471.

Kapelyukh, Y. *et al.* (2019) Defining the Contribution of CYP1A1 and CYP1A2 to Drug Metabolism Using Humanized CYP1A1/1A2 and Cyp1a1/Cyp1a2 Knockout Mice. *Drug Metab. Dispos.*, **47**, 907–918.

Kera, H. *et al.* (2021) Kinetics and distribution of benzalkonium compounds with different alkyl chain length following intravenous administration in rats. *Leg. Med.*, **48**, 101821.

Kim, Y.S. *et al.* (2020) Sex Differences in Gut Microbiota. *World J. Mens Health*, **38**, 48.

Klyushova, L.S. *et al.* (2022) The Role of CYP3A in Health and Disease. *Biomedicines*, **10**, 2686.

Kojima, R. *et al.* (2016) A phospholipid transfer function of ER-mitochondria encounter structure revealed in vitro. *Sci. Rep.*, **6**, 30777.

Koliada, A. *et al.* (2021) Sex differences in the phylum-level human gut microbiota composition. *BMC Microbiol.*, **21**, 131.

Koontz, J.M. *et al.* (2019) The Role of the Human Microbiome in Chemical Toxicity. *Int. J. Toxicol.*, **38**, 251–264.

Kröckel, L. *et al.* (2003) Identification of benzalkonium chloride in food additives and its inefficacy against bacteria in minced meat and raw sausage batters. *Eur. Food Res. Technol.*, **216**, 402–406.

Kuban, W. and Daniel, W.A. (2021) Cytochrome P450 expression and regulation in the brain. *Drug Metab. Rev.*, **53**, 1–29.

Kwon, Y.-J. *et al.* (2021) Biological roles of cytochrome P450 1A1, 1A2, and 1B1 enzymes. *Arch. Pharm. Res.*, **44**, 63–83.

Lee, B.H. and Kim, S.H. (2007) Benzalkonium chloride induced bronchoconstriction in patients with stable bronchial asthma. *Korean J Intern Med*, **22**, 244–8.

Lee, H. and Park, K. (2019) Acute toxicity of benzalkonium chloride in Balb/c mice following intratracheal instillation and oral administration. *Environ. Anal. Health Toxicol.*, **34**, e2019009.

Levy, M. *et al.* (2017) Microbiome, metabolites and host immunity. *Curr. Opin. Microbiol.*, **35**, 8–15.

Li, A. *et al.* (2020) Lipidomics by HILIC-Ion Mobility-Mass Spectrometry. *Methods Mol. Biol.*, **2084**, 119–132.

Li, C. Y. *et al.* (2018) PBDEs Altered Gut Microbiome and Bile Acid Homeostasis in Male C57BL/6 Mice. *Drug Metab Dispos*, **46**, 1226–1240.

Li, Cindy Yanfei *et al.* (2018) PBDEs Altered Gut Microbiome and Bile Acid Homeostasis in Male C57BL/6 Mice. *Drug Metab. Dispos.*, **46**, 1226–1240.

Li, D. *et al.* (2020) Evaluating consumer exposure to disinfecting chemicals against coronavirus disease 2019 (COVID-19) and associated health risks. *Env. Int*, **145**, 106108.

Li, S. *et al.* (2021) Cytochrome P450 Omega-Hydroxylase 4a14 Attenuates Cholestatic Liver Fibrosis. *Front. Physiol.*, **12**, 688259.

Li, T. and Chiang, J.Y.L. (2012) Bile Acid Signaling in Liver Metabolism and Diseases. *J. Lipids*, **2012**, 1–9.

Liao, Y. *et al.* (2014) featureCounts: an efficient general purpose program for assigning sequence reads to genomic features. *Bioinformatics*, **30**, 923–930.

Liu, X. *et al.* (2021) *Blautia* —a new functional genus with potential probiotic properties? *Gut Microbes*, **13**, 1875796.

Liu, Y. *et al.* (2020) The Dysbiosis of Gut Microbiota Caused by Low-Dose Cadmium Aggravate the Injury of Mice Liver through Increasing Intestinal Permeability. *Microorganisms*, **8**, 211.

Lopez, V.A. *et al.* (2024) Oral Exposure to Benzalkonium Chlorides in Male and Female Mice Reveals Sex-Dependent Alteration of the Gut Microbiome and Bile Acid Profile. *bioRxiv*, 2024.05.13.593991.

Love, M.I. *et al.* (2014) Moderated estimation of fold change and dispersion for RNA-seq data with DESeq2. *Genome Biol*, **15**, 550.

Lu, J. *et al.* (2020) New insights of CYP1A in endogenous metabolism: a focus on single nucleotide polymorphisms and diseases. *Acta Pharm. Sin. B*, **10**, 91–104.

Lu, K. *et al.* (2014) Arsenic Exposure Perturbs the Gut Microbiome and Its Metabolic Profile in Mice: An Integrated Metagenomics and Metabolomics Analysis. *Environ. Health Perspect.*, **122**, 284–291.

Luz, A. *et al.* (2020) Human health hazard assessment of quaternary ammonium compounds: Didecyl dimethyl ammonium chloride and alkyl (C12-C16) dimethyl benzyl ammonium chloride. *Regul Toxicol Pharmacol*, **116**, 104717.

Manor, O. *et al.* (2020) Health and disease markers correlate with gut microbiome composition across thousands of people. *Nat. Commun.*, **11**, 5206.

Manos, J. (2022) The human microbiome in disease and pathology. *APMIS*, **130**, 690–705.

Melin, V.E. *et al.* (2014) Exposure to common quaternary ammonium disinfectants decreases fertility in mice. *Reprod Toxicol*, **50**, 163–70.

Melin, V.E. *et al.* (2016) Quaternary ammonium disinfectants cause subfertility in mice by targeting both male and female reproductive processes. *Reprod Toxicol*, **59**, 159–66.

Merchel Piovesan Pereira, B. and Tagkopoulos, I. (2019) Benzalkonium Chlorides: Uses, Regulatory Status, and Microbial Resistance. *Appl. Environ. Microbiol.*, **85**, e00377-19.

Mertens, K.L. *et al.* (2017) Bile Acid Signaling Pathways from the Enterohepatic Circulation to the Central Nervous System. *Front. Neurosci.*, **11**, 617.

Minchin, R.F. *et al.* (2007) Arylamine N-acetyltransferase I. *Int. J. Biochem. Cell Biol.*, **39**, 1999–2005.

Mishima-Kimura, S. *et al.* (2018) Liquid chromatography-tandem mass spectrometry detection of benzalkonium chloride (BZK) in a forensic autopsy case with survival for 18 days post BZK ingestion. *Leg Med Tokyo*, **32**, 48–51.

Mohapatra, S. *et al.* (2023) Quaternary ammonium compounds of emerging concern: Classification, occurrence, fate, toxicity and antimicrobial resistance. *J. Hazard. Mater.*, **445**, 130393.

Molinero, N. *et al.* (2019) Intestinal Bacteria Interplay With Bile and Cholesterol Metabolism: Implications on Host Physiology. *Front Physiol*, **10**, 185.

Monte, M.J. *et al.* (2009) Bile acids: Chemistry, physiology, and pathophysiology. *World J. Gastroenterol.*, **15**, 804.

Naspolini, N.F. *et al.* (2022) Environmental pollutant exposure associated with altered early-life gut microbiome: Results from a birth cohort study. *Environ. Res.*, **205**, 112545.

Nguyen, R. *et al.* (2024) Development and Application of a Multidimensional Database for the Detection of Quaternary Ammonium Compounds and Their Phase I Hepatic Metabolites in Humans. *Environ. Sci. Technol.*, **58**, 6236–6249.

O'Flaherty, S. *et al.* (2018) The *Lactobacillus* Bile Salt Hydrolase Repertoire Reveals Niche-Specific Adaptation. *mSphere*, **3**, e00140-18.

Okita, R.T. *et al.* (1979) Lauric acid hydroxylation in human liver and kidney cortex microsomes. *Biochem. Pharmacol.*, **28**, 3385–3390.

Patterson, A.D. *et al.* (2010) Xenobiotic Metabolism: A View through the Metabolometer. *Chem. Res. Toxicol.*, **23**, 851–860.

Petriello, M.C. *et al.* (2018) Dioxin-like PCB 126 increases intestinal inflammation and disrupts gut microbiota and metabolic homeostasis. *Environ. Pollut.*, **242**, 1022–1032.

Phelps, T. *et al.* (2019) The influence of biological sex and sex hormones on bile acid synthesis and cholesterol homeostasis. *Biol. Sex Differ.*, **10**, 52.

Phillips, I.R. and Shephard, E.A. (2017) Drug metabolism by flavin-containing monooxygenases of human and mouse. *Expert Opin. Drug Metab. Toxicol.*, **13**, 167–181.

Pradista, L.A. *et al.* (2022) Metagenomic analysis of non-pathogenic and pathogenic cecal bacteria profiles in quail supplemented with betaine. *IOP Conf. Ser. Earth Environ. Sci.*, **1114**, 012008.

Prysyazhnyuk, V. *et al.* (2021) Glutathione-S-transferases genes-promising predictors of hepatic dysfunction. *World J. Hepatol.*, **13**, 620–633.

Qin, X. and Wang, X. (2019) Role of vitamin D receptor in the regulation of CYP3A gene expression. *Acta Pharm. Sin. B*, **9**, 1087–1098.

Qiu, X. *et al.* (2016) Disruption of BSEP Function in HepaRG Cells Alters Bile Acid Disposition and Is a Susceptive Factor to Drug-Induced Cholestatic Injury. *Mol. Pharm.*, **13**, 1206–1216.

Rinninella, E. *et al.* (2019) What is the Healthy Gut Microbiota Composition? A Changing Ecosystem across Age, Environment, Diet, and Diseases. *Microorganisms*, **7**, 14.

Robinson, A.J. *et al.* (2017) Granular parakeratosis induced by benzalkonium chloride exposure from laundry rinse aids. *Australas J Dermatol*, **58**, e138–e140.

Röder, A. *et al.* (2023) Spotlight on CYP4B1. *Int. J. Mol. Sci.*, **24**, 2038.

Ross, D.H. *et al.* (2020) LiPydomics: A Python Package for Comprehensive Prediction of Lipid Collision Cross Sections and Retention Times and Analysis of Ion Mobility-Mass Spectrometry-Based Lipidomics Data. *Anal. Chem.*, **92**, 14967–14975.

Sarkar, J. *et al.* (2012) Corneal neurotoxicity due to topical benzalkonium chloride. *Invest Ophthalmol Vis Sci*, **53**, 1792–802.

Saxami, G. *et al.* (2023) The Gut–Organ Axis within the Human Body: Gut Dysbiosis and the Role of Prebiotics. *Life*, **13**, 2023.

Schneider, K.M. *et al.* (2018) Role of bile acids in the gut-liver axis. *J. Hepatol.*, **68**, 1083–1085.

Seebacher, F. *et al.* (2020) Hepatic lipid droplet homeostasis and fatty liver disease. *Semin. Cell Dev. Biol.*, **108**, 72–81.

Seguin, R. P. *et al.* (2019) Metabolism of Benzalkonium Chlorides by Human Hepatic Cytochromes P450. *Chem Res Toxicol*, **32**, 2466–2478.

Seguin, Ryan P. *et al.* (2019) Metabolism of Benzalkonium Chlorides by Human Hepatic Cytochromes P450. *Chem. Res. Toxicol.*, **32**, 2466–2478.

Selwyn, F.P., Cheng, S.L., *et al.* (2015) Developmental Regulation of Drug-Processing Genes in Livers of Germ-Free Mice. *Toxicol Sci*, **147**, 84–103.

Selwyn, F.P. *et al.* (2016) Regulation of Hepatic Drug-Metabolizing Enzymes in Germ-Free Mice by Conventionalization and Probiotics. *Drug Metab Dispos*, **44**, 262–74.

Selwyn, F.P., Cui, J.Y., *et al.* (2015) RNA-Seq Quantification of Hepatic Drug Processing Genes in Germ-Free Mice. *Drug Metab Dispos*, **43**, 1572–80.

Shulpekova, Y. *et al.* (2022) The Role of Bile Acids in the Human Body and in the Development of Diseases. *Molecules*, **27**, 3401.

Siddiqui, R. *et al.* (2022) The Gut Microbiome and Female Health. *Biology*, **11**, 1683.

Sim, E. *et al.* (2014) Arylamine N-acetyltransferases: from drug metabolism and pharmacogenetics to drug discovery. *Br. J. Pharmacol.*, **171**, 2705–2725.

Slimani, K. *et al.* (2017) Liquid chromatography-tandem mass spectrometry multiresidue method for the analysis of quaternary ammonium compounds in cheese and milk products: Development and validation using the total error approach. *J Chromatogr A*, **1517**, 86–96.

Sreevidya, V.S. *et al.* (2018) Benzalkonium chloride, benzethonium chloride, and chloroxylenol - Three replacement antimicrobials are more toxic than triclosan and triclocarban in two model organisms. *Environ. Pollut.*, **235**, 814–824.

Stellaard, F. and Lütjohann, D. (2021) Dynamics of the enterohepatic circulation of bile acids in healthy humans. *Am. J. Physiol.-Gastrointest. Liver Physiol.*, **321**, G55–G66.

Stok, J.E. and De Voss, J.J. (2000) Expression, Purification, and Characterization of BioI: A Carbon–Carbon Bond Cleaving Cytochrome P450 Involved in Biotin Biosynthesis in Bacillus subtilis. *Arch. Biochem. Biophys.*, **384**, 351–360.

Takahashi, S. *et al.* (2016) Cyp2c70 is responsible for the species difference in bile acid metabolism between mice and humans. *J. Lipid Res.*, **57**, 2130–2137.

Takeoka, G.R. *et al.* (2005) Identification of benzalkonium chloride in commercial grapefruit seed extracts. *J Agric Food Chem*, **53**, 7630–6.

Taylor, C. *et al.* (2020) A Review of the Important Role of CYP2D6 in Pharmacogenomics. *Genes*, **11**, 1295.

Ten Hove, M. *et al.* (2020) The hepatic lipidome: From basic science to clinical translation. *Adv. Drug Deliv. Rev.*, **159**, 180–197.

The Federal Institute for Risk Assessment (BfR) of Germany (2012) Health assessment of benzalkonium chloride residues in food. *BfR Opin. No 0322012*.

Thursby, E. and Juge, N. (2017) Introduction to the human gut microbiota. *Biochem. J.*, **474**, 1823–1836.

Tian, S. *et al.* (2022) FXR: structures, biology, and drug development for NASH and fibrosis diseases. *Acta Pharmacol. Sin.*, **43**, 1120–1132.

Trapani, L. (2012) Regulation and deregulation of cholesterol homeostasis: The liver as a metabolic "power station". *World J. Hepatol.*, **4**, 184.

Tripathi, A. *et al.* (2018) The gut-liver axis and the intersection with the microbiome. *Nat Rev Gastroenterol Hepatol*, **15**, 397–411.

Tripathi, Anupriya *et al.* (2018) The gut–liver axis and the intersection with the microbiome. *Nat. Rev. Gastroenterol. Hepatol.*, **15**, 397–411.

Tu, P. *et al.* (2020) Gut Microbiome Toxicity: Connecting the Environment and Gut Microbiome-Associated Diseases. *Toxics*, **8**, 19.

Turesky, R.J. and Lu, K. (2020) Biomarkers of Environmental Toxicants: Exposure and Biological Effects. *Toxics*, **8**, 37.

Umehara, K., Kudo, S., Hirao, Y., Morita, S., Ohtani, T., *et al.* (2000) In vitro characterization of the oxidative cleavage of the octyl side chain of olanexidine, a novel antimicrobial agent, in dog liver microsomes. *Drug Metab. Dispos. Biol. Fate Chem.*, **28**, 1417–1424.

Umehara, K., Kudo, S., Hirao, Y., Morita, S., Uchida, M., *et al.* (2000) Oxidative cleavage of the octyl side chain of 1-(3,4-dichlorobenzyl)-5-octylbiguanide (OPB-2045) in rat and dog liver preparations. *Drug Metab. Dispos. Biol. Fate Chem.*, **28**, 887–894.

Umehara, K. *et al.* (2004) Oxidative one-carbon cleavage of the octyl side chain of olanexidine, a novel antimicrobial agent, in dog liver microsomes. *Xenobiotica*, **34**, 61–71.

US EPA (2006) Reregistration Eligibility Decision for Alkyl Dimethyl Benzyl Ammonium Chloride (ADBAC). *EPA-HQ-OPP-2006-0339*, Office of Prevention, Pesticides and Toxic Substances, Antimicrobials Division, U.S. Environmental Protection Agency. Signed on August 3, 2006.

US FDA (2016a) Quaternary ammonium chloride combination. *Code Fed. Regul. 21CFR172165*, Food and Drug Administration, U.S. Department of Health&Human Services. Revised as of April 1, 2016.

US FDA (2016b) Safety and Effectiveness of Consumer Antiseptics; Topical Antimicrobial Drug Products for Over-the-Counter Human Use; Proposed Amendment of the Tentative Final Monograph; Reopening of Administrative Record. *Fed. Regist.*, **21 CFR Part 310, 81**, 42911–42937.

US FDA (2015) Safety and Effectiveness of Health Care Antiseptics; Topical Antimicrobial Drug Products for Over-the-Counter Human Use; Proposed Amendment of the Tentative

Final Monograph; Reopening of Administrative Record. *Fed. Regist.*, **21 CFR Part 310, 80**, 25165–25205.

Vassileva, G. *et al.* (2010) Gender-dependent effect of Gpbar1 genetic deletion on the metabolic profiles of diet-induced obese mice. *J. Endocrinol.*, **205**, 225–232.

Vázquez-Baeza, Y. *et al.* (2013) EMPeror: a tool for visualizing high-throughput microbial community data. *GigaScience*, **2**, 16.

Veiga-da-Cunha, M. *et al.* (2010) Molecular Identification of NAT8 as the Enzyme That Acetylates Cysteine S-Conjugates to Mercapturic Acids. *J. Biol. Chem.*, **285**, 18888–18898.

Vieira, L.S. *et al.* (2024) Interaction and Transport of Benzalkonium Chlorides by the Organic Cation and Multidrug and Toxin Extrusion Transporters. *Drug Metab. Dispos.*, **52**, 312–321.

Wang, B. and Tontonoz, P. (2018) Liver X receptors in lipid signalling and membrane homeostasis. *Nat. Rev. Endocrinol.*, **14**, 452–463.

Wang, R. *et al.* (2021) Gut microbiome, liver immunology, and liver diseases. *Cell. Mol. Immunol.*, **18**, 4–17.

Weakly, H.M.J. *et al.* (2024) Several common methods of making vesicles (except an emulsion method) capture intended lipid ratios. *bioRxiv*, 2024.02.21.581444.

Wu, G.D. and Lewis, J.D. (2013) Analysis of the Human Gut Microbiome and Association With Disease. *Clin. Gastroenterol. Hepatol.*, **11**, 774–777.

Xiong, Z.E. *et al.* (2020) Exposure to dibutyl phthalate impairs lipid metabolism and causes inflammation via disturbing microbiota-related gut–liver axis. *Acta Biochim. Biophys. Sin.*, **52**, 1382–1393.

Xue, Y. *et al.* (2004) Distribution and disposition of benzalkonium chloride following various routes of administration in rats. *Toxicol Lett*, **148**, 113–23.

Xue, Y. *et al.* (2002) Sensitive determination of benzalkonium chloride in blood and tissues using high-performance liquid chromatography with solid-phase extraction. *Leg Med Tokyo*, **4**, 232–8.

Yamashita, T. (2011) Glycosphingolipid Modification: Structural Diversity, Functional and Mechanistic Integration of Diabetes. *Diabetes Metab. J.*, **35**, 309.

Yoon, H. *et al.* (2021) Lipid metabolism in sickness and in health: Emerging regulators of lipotoxicity. *Mol. Cell*, **81**, 3708–3730.

Yoshimoto, F.K. *et al.* (2016) Isotope-Labeling Studies Support the Electrophilic Compound I Iron Active Species, FeO^{3+}, for the Carbon–Carbon Bond Cleavage Reaction of the Cholesterol Side-Chain Cleavage Enzyme, Cytochrome P450 11A1. *J. Am. Chem. Soc.*, **138**, 12124–12141.

Zhang, L. *et al.* (2015) Persistent Organic Pollutants Modify Gut Microbiota–Host Metabolic Homeostasis in Mice Through Aryl Hydrocarbon Receptor Activation. *Environ. Health Perspect.*, **123**, 679–688.

Zhang, R. *et al.* (2020) Dose-dependent benzalkonium chloride toxicity imparts ocular surface epithelial changes with features of dry eye disease. *Ocul. Surf.*, **18**, 158–169.

Zhang, S. *et al.* (2015) Subchronic Exposure of Mice to Cadmium Perturbs Their Hepatic Energy Metabolism and Gut Microbiome. *Chem. Res. Toxicol.*, **28**, 2000–2009.

Zhang, Y. and Klaassen, C.D. (2010) Effects of feeding bile acids and a bile acid sequestrant on hepatic bile acid composition in mice. *J Lipid Res*, **51**, 3230–42.

Zhao, Yueming *et al.* (2022) Alleviating effects of gut micro-ecologically regulatory treatments on mice with constipation. *Front. Microbiol.*, **13**, 956438.

Zheng, G. *et al.* (2020) Increased Indoor Exposure to Commonly Used Disinfectants during the COVID-19 Pandemic. *Environ. Sci. Technol. Lett.*, **7**, 760–765.

Zheng, G. *et al.* (2021a) Quaternary Ammonium Compounds: Bioaccumulation Potentials in Humans and Levels in Blood before and during the Covid-19 Pandemic. *Environ. Sci. Technol.*, **55**, 14689–14698.

Zheng, G. *et al.* (2021b) Quaternary Ammonium Compounds: Bioaccumulation Potentials in Humans and Levels in Blood before and during the Covid-19 Pandemic. *Environ. Sci. Technol.*, **55**, 14689–14698.

Zheng, G. *et al.* (2022) The first detection of quaternary ammonium compounds in breast milk: Implications for early-life exposure. *J. Expo. Sci. Environ. Epidemiol.*, **32**, 682–688.

Zhong, C.Y. *et al.* (2015) Microbiota prevents cholesterol loss from the body by regulating host gene expression in mice. *Sci Rep*, **5**, 10512.

Zhou, M. *et al.* (2023) Exploring human CYP4 enzymes: Physiological roles, function in diseases and focus on inhibitors. *Drug Discov. Today*, **28**, 103560.

Chapter 3 Distribution and Disposition of BACs

3.1 Introduction

The literature demonstrates that exposure within human populations is significant, and the FDA recently called for additional safety data on their usage in healthcare and consumer antiseptic products (US FDA, 2015, 2016b, 2016a). In **Chapter 2**, we demonstrated that oral BAC exposure to male and female mice results in altered gut microbiome composition, lowered microbial diversity, and significant decreases in secondary BA formation (Lopez *et al.*, 2024). Notably, recent recommendations by the Toxics Use Reduction Institute at the University of Massachusetts implicate certain BACs be added to the Toxic Use Reduction Act List of Hazardous Substances because of the associations with health effects (download (mass.gov))

Despite widespread exposure to BACs and increasing concern about BAC safety usage, few studies have evaluated BAC distribution and disposition in vivo. We have previously elucidated the metabolic pathway of BACs by cytochrome p450 enzymes within the cyp4 (CYP4F2, CYP4F11 and CYP4F12) and cyp2 (CYP2D6) family (Ryan P. Seguin *et al.*, 2019) (**Chapter 1**, **Figure 1.9**). We have also recently reported beta-oxidation as a prominent biotransformation pathway in BAC-exposed mice (**Chapter 2**) (Lopez *et al.*, 2024). Recent work by Kera et al. examined levels of BACs in the lung, liver, spleen, fat, brain, and blood of rats exposed to varying chain length BACs by Intravenous (IV) and Drip-Intravenous (DIV) administrations (Kera *et al.*, 2021).After oral administration (250 mg/kg) by gavage, BAC levels reached their highest concentrations after 24 hours: kidney (5.25 ug/g), lung (2.75 ug/g), liver (after 2 hours: 0.78 ug/g) and blood (0.34 ug/g) (Xue *et al.*, 2004). Oral dosage of radiolabeled BACs led to 87-99% of BACs being excreted through the feces, a third of which were metabolites (Luz *et al.*, 2020). In accidental ingestion of a 10% BAC solution, samples of serum, urine, and

stomach contents were harvested at the autopsy, and quantitative assay of BACs revealed a concentration of 1.15 mg/ml in serum and no detection in the urine nor stomach contents (Hitosugi *et al.*, 1998).

To evaluate BAC and BAC metabolite distribution following an oral dosage paradigm, C57BL/6 male and female mice were exposed to either control Nutra-Gel diet or Nutra-Gel diet with added d_7-C12- BAC or d_7-C16- BAC at a dosage of 120 µg/g/day for a duration of one week (**Figure 3.1**). This dosage paradigm was adapted from Melin et al., who had previously revealed that 120 µg/g/day was half the lowest observable adverse effect limit (LOAEL) (Melin *et al.*, 2014). Brain, spleen, lung, liver, kidney, duodenum, jejunum, ileum, large intestine, feces, and urine samples were collected and processed for BAC and BAC metabolite quantitation by UPLC/MS-MS.

3.2 Results and Discussion

3.2.1 Parent BAC Distribution

BACs were quantified in the male and female brain, lung, kidney, spleen, liver, duodenum, jejunum, ileum, large intestine, blood, urine, feces at day four, and feces at day 7 (**Figure 3.2**). Female heart samples were also harvested and underwent BAC and BAC metabolite quantification (**Figure 3.20**). Neither d_7-C12-BAC nor d_7-C16-BAC were detected in mice fed the control diet. The lowest levels of parent BACs were quantified in the brain, with levels in the low nM range. Of the six brain samples processed in the male d_7-C12-BAC exposed group, only two reached levels in the low nM range, and only one in the female d_7-C12-BAC exposed group. d_7-C16-BAC was detected in all male and female brain samples. Low nM concentrations of d_7-C12- and d_7-C16-BAC were also quantified in male and female blood extracts. Lung, kidney, spleen, and liver

all had levels of parent BACs in the median range compared to brain and intestinal sections, with levels reaching up to a couple of 100s nM range. The intestinal tissues, duodenum, jejunum, ileum, and large intestine contained the highest levels of parent BACs in tissue, reaching low micromolar ranges. Feces samples had the highest levels of BACs, with levels reaching low millimolar concentrations. A comparison of parent BAC levels in feces at the day 4 (middle) timepoint compared to the day 7 (end) timepoint revealed no statistical difference in concentration in both male and female cohorts (**Figure 3.2C**).

UPLC/MS-MS of isolated biological extracts, we accurately quantified d_7-C12- and d_7-C16-BAC structures in BAC exposed groups. We demonstrate following an oral BAC exposure paradigm via gel diet for one week led to parent BACs being detectable in all isolated samples: brain, blood, lung, kidney, urine, spleen, liver, duodenum, jejunum, ileum, large intestine and feces (**Figure 3.2**). In the brain, of the six samples processed per sex per treatment group, only two reached detectable levels and only one in the female d_7-C12-BAC exposed group. d_7-C16-BAC was detected in all male and female brain samples. In the kidney samples, though all processed samples demonstrated detectable levels, there were higher levels of d_7-C16-BAC compared to d_7-C12-BAC. This demonstrates insightful information about longer chained length BACs accumulating in organs like the brain and kidney. Furthermore, no d_7-C16-BAC was detected in female urine samples. Moreover, both parent BACs were quantified in the low nM range in isolated whole blood samples. (**Figure 3.3**) Based on averages taken from each sample group in the male d_7-C12-BAC distribution is from highest to lowest accumulation of Feces (Mid-timepoint) > Feces (Endpoint) > Large Intestine > Jejunum > Duodenum > Ileum > Liver > Spleen > Lung > Kidney > Urine and Blood > Brain (**Figure 3.3**). In the Female d_7-C12-BAC exposed group, Feces (End-timepoint) > Feces (Mid-timepoint) > Large Intestine > Ileum > Duodenum > Jejunum > Lung >

Spleen > Liver > Kidney > Urine and Blood > Brain (**Figure 3.3**). In the Male d_7-C16-BAC exposed group, Feces (Mid-timepoint) > Feces (End-timepoint) > Jejunum > Duodenum > Large Intestine > Ileum > Spleen > Kidney > Lung > Liver > Brain > Urine and Blood (**Figure 3.3**). In the Female d_7-C16-BAC exposed group, Feces (End-timepoint) > Feces (Mid-timepoint) > Jejunum > Large Intestine > Duodenum > Ileum > Kidney > Spleen > Lung > Liver > Urine and Blood > Brain (**Figure 3.3**).

3.2.2 Hydroxylation Metabolite Distribution

Previous work has elucidated cytochrome P450 oxidation as a metabolic route of BAC parent structures (R. P. Seguin *et al.*, 2019). Specifically, recombinant CYP2D6, CYP4F2, and CYP4F12 produced major microsomal metabolites, notably CYP4-mediated ω-hydroxylation and CYP2D6/CYP4-mediated (ω-1)-hydroxylation. ω- and ω-1 hydroxy metabolites were quantified in the male and female blood, lung, kidney, liver, duodenum, jejunum, ileum, large intestine, feces (mid-time point), and feces (end timepoint) (**Figure 3.4 and Figure 3.5**). In samples like male and female liver and large intestine, we report the longer chain length d_7-C16-BAC had higher levels of the ω-OH metabolite relative to the ω-1 OH metabolite. In contrast, the shorter chain length BAC d_7-C12-BAC had higher levels of the ω-1 OH metabolite than the ω-OH metabolite (**Figure 3.4 and Figure 3.5**). Male d_7-C16-BAC groups, including lung, kidney, spleen, feces (mid-time point), and feces (end time point) samples, had higher levels of the ω-OH metabolite.

Our results are the first to show a cohesive description of BAC metabolite distribution in vivo. Our previous work elucidated the metabolic route of BAC structures by cytochrome p450-mediated oxidation (**Figure 1.9**). On the alkyl chain region, cytochrome p450-mediated oxidation leads to the formation of the primary ω- and (ω-1)-hydroxy-BAC metabolites and the secondary ω-COOH-BAC metabolite. We were able to quantify levels of the ω and ω-1 oxidized metabolites

of the parent deuterated d_7-C12- and d_7-C16-BAC structures in most of the isolated biological samples. We have previously elucidated that CYP4-mediated oxidation results in ω-hydroxylation while CYP2D6/CYP4-mediated oxidation results in w-1 hydroxylation. Shorter chain length BAC (C12) had higher concentrations of the ω-1 metabolite in both male and female livers.

In contrast, the longer chained parent, C16, had substantially higher concentrations of the ω-OH metabolite. Significantly, the cytochrome P450 4 family prefers oxidation on ω-hydroxylation (Zhou *et al.*, 2023). Higher levels of ω-1-OH metabolite were seen in d_7-C12-BAC male jejunum, ileum, and large intestine, as well as female duodenum, ileum, large intestine, and both feces time points. Higher levels of the ω-OH metabolite were seen in the d_7-C16-BAC male lung, kidney, spleen, jejunum, large intestine, and both feces timepoints. Higher averages of d_7-C16-BAC were observed within the male lung, kidney, spleen, and large intestine compared to levels of d_7-C12-BAC in those same tissues.

In human liver microsomes (HLM), with an approximate total CYP content of 380 pmol/mg, CYP2D6 is found at about 12 pmol/mg, and total CYP4F ranges from 18-128 pmol/mg with an average of 40 pmol/mg (Okita *et al.*, 1979; Edson and Rettie, 2013; K. Z. Edson *et al.*, 2013; Katheryne Z. Edson *et al.*, 2013; Johnson *et al.*, 2015). Thus, detecting levels of both the ω and ω-1 OH metabolite are likely due to cytochrome p450s previously determined as being responsible for p450-mediated oxidation. The liver has estimated amounts of both CYP4F2 and 4F11, as described in **Table 3.1**. The kidney, has little to no CYP2D6 expression and unknown amounts of 4F11/12. However, CYP4F2 has been determined in human kidney microsomes by Hirani et al. Thus, the increased levels of theω-OH metabolite in the male cohort of the d_7-C16-BAC group could be a result of increased accumulation of the longer chained length BAC and suspected CYP4F oxidation.

Interestingly, overall CYP levels in the lung range from 2-10 pmol/mg; however, while there is no current evidence for CYP4F expression, there are conflicting results on CYP2D6 determination (Hukkanen *et al.*, 2002). In the spleen, there are no current protein content levels reported. Next-generation sequencing techniques are utilized in pig spleen that support the conclusion that the spleen contains levels of cytochrome p450. Within our study, we observed that an overwhelming ratio of observed analytes in the spleen belong to parent structures. Lastly, despite higher levels of CYP4F2 being reported throughout the intestinal sections relative to expression levels of CYP2D6, there were still statistically significant increases in the w-1 OH metabolite in the male jejunum, ileum and female ileum.

3.2.3 Even and Odd Beta Oxidation Product Distribution

Additionally, we report that BAC COOH metabolites formed by CYP-mediated metabolism undergo further metabolism by β-oxidation, as previously reported (Lopez *et al.*, 2024). We report that CYP-mediated oxidation of BAC structures occurs on d_7-C12- and d_7-C16-BAC structures to produce even-numbered alkyl chain COOH metabolites. However, β-oxidation can occur on odd-numbered alkyl-chained BACs due to CYP oxidation catalyzing a carbon-carbon cleavage. This p450 reaction results in the removal of the ω-carbon, thus leaving β-oxidation to appear on an odd-numbered alkyl chain and therefore produce odd-numbered alkyl chain COOH BAC metabolites (Umehara, Kudo, Hirao, Morita, Uchida, et al., 2000; Umehara, Kudo, Hirao, Morita, Ohtani, et al., 2000; Umehara et al., 2004). Our study demonstrates that even and odd beta oxidation are important routes of BAC metabolism (**Figures 3.6-3.11**). Shorter chained length COOH BAC metabolites were quantifiable in extracts like urine and feces at comparable levels. Longer chained-length BACs were primarily seen in intestinal sections and feces time points. While odd-chained-length beta-oxidation products were observed, levels of these metabolites

throughout the samples indicate this pathway is minor compared to even-chained length β oxidation.

We have previously reported beta-oxidation as a significant route of metabolism in the liver, blood, and feces in male and female mice following the BAC-exposure paradigm (**Chapter 2**). In this study, we observed levels of short to long-chain d_7-COOH BAC structures, including even (C6, C8, C10, C12, C14, and C16) and odd (C7, C9, C11, C13, C15) beta-oxidation products (**Table 3.5 and 3.6**). Short-chained beta-oxidation products (d_7-COOH BAC C6, C8, C7, and C9) had the highest quantifiable levels in urine and feces extracts. d_7-COOH BAC C10 and C11 metabolites levels were higher in d_7-C12-BAC exposed groups compared to d_7-C16-BAC exposed groups in tissue samples in both male and female cohorts. Importantly, longer chained beta-oxidation products d_7-COOH BAC C14 and C16, d_7-COOH C13, and C15 are only seen in d_7-C16 BAC exposed groups, specifically within intestinal sections and feces. Even-chained beta-oxidation products have higher concentration levels than odd-chained beta-oxidation products.

3.2.4 Parent to Metabolite Profiles

The distribution of parent BACs and BAC metabolites was studied to understand BAC disposition. Sums of all analytes were categorized into parent or metabolite and then divided by the sum of all analytes quantified in the sample (**Figure 3.12 and Figure 3.13**). The brain only consisted of quantifiable levels of the parent BACs. Conversely, biological extracts like urine and blood were mostly comprised of metabolite. The liver samples consist of up to 90% of all quantified analytes being metabolites in both d_7-C12- and d_7-C16-BAC exposed groups in male and female samples. Interestingly, tissue sections like the lung, kidney, and ileum contained up to 50% metabolite detection. Tissues like the duodenum and jejunum had lower percentages of

metabolite detection relative to the lung, kidney, and ileum. Additionally, we observed in the feces, both at mid- and end-time points, higher levels of parent in the d_7-C12-BAC groups compared to parents detected in levels of the d_7-C16-BAC group. Furthermore, metabolite distribution was evaluated in each biological sample (**Figures 3.14-3.17, 3.21**), and revealed overwhelmingly that even-chained BAC-COOH products were the predominant metabolic route.

3.3 Experimental Procedure

Animals. Seven to eight-week-old C57BL/6J male and female mice were purchased from Jackson Laboratories (Bar Harbor, Maine). All animal protocols were approved by The University of Washington Institutional Animal Care and Use Committee, and all experiments agreed with the Guiding Principles in the Use of Animals in Toxicology. After acclimation to the animal facility, mice were acclimated to the Nutra-Gel diet (Product F5769-KIT, Bio-Serv, Frenchtown, New Jersey) for two weeks before BAC exposure. Deuterated BACs were used to ensure accurate quantitation, as Herron et al., 2018 described. Mice were randomly assigned to exposure groups (n = 6) and housed into pairs of two per cage: control Nutra-Gel diet, d_7-C12 BAC (120 µg/g/day) or d_7-C16 BAC (120 µg/g/day) for one week. Mice were sacrificed, and the following tissues were collected, flash-frozen in 2-methybutane on dry ice, and stored at -80 °C until subsequent analyses: brain, lung, kidney, spleen, liver, duodenum, jejunum, ileum, large intestine, and blood via cardiac puncture. Intestinal tissues were flushed with PBS and cut into the duodenum, jejunum, ileum, and large intestine. Feces were collected throughout the Nutra-gel acclimation time and the treatment period. Feces samples were kept in -80 until subsequent analysis. Urine samples were collected on the first day of treatment and the day of sacrifice (Chew and Chua, 2003). Nutra-gel acclimation and treatment period occurred first with the male cohort, and then the female cohort commenced Nutra-gel acclimation directly after.

Chemicals. Optima LC/MS solvents (acetonitrile, chloroform, methanol, and water), 2-methylbutane, and formic acid were purchased from Thermo Fisher Scientific (Grand Island, New York. d_7-C12 BAC and d_7-C16 BAC were prepared as described previously (Herron *et al.*, 2016).

BAC Extraction. A standard stock solution of d0-BAC Internal Standard series (C6, C8, C10, C12, C14, and C16 d_0-BACs; C8, C10, C12, C14, and C16 d0-COOH-BACs; d_0-ω-OH-C12 and d_0-ω-OH-C16; 400 nM each) was prepared in Acetonitrile (ACN) for BAC extractions of brain, blood, lung, spleen, liver, kidney, duodenum, jejunum, ileum, large intestine, feces and urine.

For male and female blood BAC extractions, 10 µL of thawed whole blood was added to 20 µL of H_2O and sonicated for 15-20 minutes. 10 µL of ACN spiked with 40 nM d_0-BAC Internal Standard series (C6, C8, C10, C12, C14 and C16 d_0-BACs; C8, C10, C12, C14 and C16 d0-COOH-BACs; d_0-ω-OH-C12 and d_0-ω-OH-C16). Samples were vortexed and left on ice for 5-10 minutes. 100 µL of ACN: MeOH (1:1) was added to each sample. Samples were vortexed and left on ice for 5-10 minutes. Samples were centrifuged at 4°C for 15 minutes, transferred to UHPLC-MS vials, and stored for analysis.

For BAC extractions from the male and female brain, half of each brain was cut along the longitudinal fissure into the right and left hemispheres. A hemisphere was weighed for each sample and placed in a homogenization tube. Two volumes of water were added to each tube, and samples were homogenized by Precellys bead homogenizer. 150 µL of homogenate was portioned, and 400 µL of 50 nM d0-BAC Internal Standard series was added to each sample. Samples were centrifuged for 15 minutes. 200 µL of supernatant was isolated and centrifuged for 15 minutes.

Before undergoing mass spectrometry, 100 µL of supernatant was added to 100 µL 2:1 H2O: MeOH in a 96-well plate.

For BAC extractions from male and female lungs, approximately 45 mgs of tissue were weighed and homogenized with two volumes of water by Precellys bead homogenizer. For each 150 µL of homogenate, 400 µL of 100 nM d0-BAC Internal Standard series was added to the sample. Samples were centrifuged for 15 minutes. 200 µL of supernatant was isolated and centrifuged for 15 minutes. 100 µL of supernatant was added to 100 µL 2:1 H2O: MeOH in a 96 well plate.

For BAC extractions from male and female spleen, the whole spleen was weighed and homogenized with two volumes of water using Precellys bead homogenizer. For each 150 µL of homogenate, 400 µL of 100 nM d0-BAC Internal Standard series was added to the sample. Samples were centrifuged for 15 minutes. 200 µL of supernatant was isolated and centrifuged for 15 minutes. 100 µL of supernatant was added to 100 µL 2:1 H2O: MeOH in a 96 well plate.

For BAC extractions from the male and female liver, approximately 50 mgs of tissue were weighed and homogenized with two volumes of water by Precellys bead homogenizer. For each 150 µL of homogenate, 400 µL of 100 nM d0-BAC Internal Standard series was added to the sample. Samples were centrifuged for 15 minutes. 200 µL of supernatant was isolated and centrifuged for 15 minutes. 100 µL of supernatant was added to 100 µL 2:1 H2O: MeOH in a 96 well plate.

For male and female kidney BAC extraction, approximately half of the tissue was cut on the sagittal plane to account for all the regions of the kidney (pelvis, medulla, and cortex). Tissues were weighed and homogenized with two volumes of water using a Precellys bead homogenizer. For each 150 µL of homogenate, 400 µL of 100 nM d0-BAC Internal Standard series was added to the sample. Samples were centrifuged for 15 minutes. 200 µL of supernatant was isolated and

centrifuged for 15 minutes. 100 µL of supernatant was added to 100 µL 2:1 H2O: MeOH in a 96 well plate.

For male and female duodenum tissue, approximately 60 mgs of tissue was homogenized with two volumes of water by Precellys bead homogenizer. For each 150 µL of homogenate, 400 µL of 100 nM d0-BAC Internal Standard series was added to the sample. Samples were centrifuged for 15 minutes. 200 µL of supernatant was isolated and centrifuged for 15 minutes. 100 µL of supernatant was added to 100 µL 2:1 H2O: MeOH in a 96 well plate.

For male and female jejunum tissue, approximately 70 mgs of tissues were homogenized with two volumes of water by Precellys bead homogenizer. For each 150 µL of homogenate, 400 µL of 100 nM d0-BAC Internal Standard series was added to the sample. Samples were centrifuged for 15 minutes. 200 µL of supernatant was isolated and centrifuged for 15 minutes. 100 µL of supernatant was added to 100 µL 2:1 H2O: MeOH in a 96 well plate.

For male and female ileum, approximately 60 mgs of ileum were homogenized with two volumes of water by Precellys bead homogenizer. For each 150 µL of homogenate, 400 µL of 200 nM d0-BAC Internal Standard series was added to the sample. Samples were centrifuged for 15 minutes. 133 µL of supernatant was isolated and centrifuged for 15 minutes. 66.5 µL of supernatant was added to 100 µL 2:1 H2O: MeOH in a 96 well plate.

For male and female large intestines, approximately 90 mgs of large intestine were homogenized with two volumes of water by Precellys bead homogenizer. For each 150 µL of homogenate, 400 µL of 200 nM d0-BAC Internal Standard series was added to the sample. Samples were centrifuged for 15 minutes. 200 µL of supernatant was isolated and centrifuged for 15 minutes. 100 µL of supernatant was added to 100 µL 2:1 H2O: MeOH in a 96 well plate.

For male and female fecal samples, approximately 2.5 mgs were accurately measured. 2.5 µL of water was added for every mg of feces. Feces were sonicated in ice water for 30 minutes and left to equilibrate on ice for 10 minutes. 10 µL of d0-BAC Internal Standard series for every mg of feces was added to the homogenate and vortexed vigorously for 5-8 seconds. Samples were sonicated for 1 hour and then centrifuged at 12 000 x g for 15 min at 4°C. Supernatants were collected in new tubes, and pellets were resuspended in 50 µL of 100% methanol. Samples were sonicated for 20 minutes and then centrifuged at 12,000 x g for 20 minutes. Two supernatants were combined and evaporated by SpeedVac Vacuum (30 °C) for 30 minutes. Samples were reconstituted in 100 µL of 1:1 MeOH: H2O. The suspension was transferred into 0.2 um costar Spin-X HPLC microcentrifuge filter tubes and centrifuged at 12 000 x g for 10 minutes. 100 µL was transferred onto UHPLC – MS vials and stored for analysis.

For male and female urine, 20 µL of urine was measured and dispersed in 96 well plates. 20 µL of 40 nM d0-BAC, Internal Standard series, was added to each sample. Samples were vortexed, and then the plate was centrifuged (4000 rpm, 10 min, 4°C) before diluting the supernatant into pre-labeled LC vials containing 20 µL pure H_2O.

Targeted Analysis of BAC and BAC metabolites. BAC and BAC metabolites were detected by ultra-high-performance liquid chromatography-tandem mass spectrometry (UHPLC-MS/MS) using a Synapt G2-XS ion mobility Q-TOF mass spectrometer equipped with electrospray ionization in the positive mode, as described in (VL) (ESI- (+)) mode. 5-10 µl of each prepared sample was injected into the system. Reverse chromatographic separation was achieved on a Thermo Hypersil GOLD C18 column (100 x 2.1 mm, 1.9 µm particle size) at ambient temperature, with a 0.4 ml/min flow rate.

ACUITY UPLC system and autosampler (Waters Corporation, Wilford, MA) were used for mobile phase delivery and sample injection. The solvent gradient was defined as follows: mobile phase A: 0.1% formic acid, 2mM ammonium formate in water and solvent B: Acetonitrile: 0 min: 15% B, 14 min: 85%, 15-17 min: 100% B, 18.5-20 min: 15%B. ESI parameters were described in (Vieira *et al.*, 2024). The system was calibrated with Na formate. Source temperature was set to 100°C, Desolvation temperature was set to 50 °C, Cone gas (L/h): 50, Desolvation gas (L/h): 800, Nebulizer (Bar): 6.5 and the capillary voltage (kV) was set to 2.5.

Analyte retention times and precursor to product ion transitions monitored are described in Table 1. Analyte peak areas were normalized to the appropriate internal standard peak area; d0-ω-OH internal standards were used to quantify oxidized d_7-C12- or d_7-C16- BAC metabolite that is not a COOH product; d0-COOH BACs were used to quantify d_7-COOH BAC products; and d0-BACs were used to quantify the d_7-BAC parent levels. All data are presented as the median. Statistical analyses were performed on GraphPad Prism 10.3.0. (GraphPad Software, La Jolla, CA) using an unpaired t-test, followed by Welch's correction.

3.4 Conclusions

In conclusion, this study provides the first insight into BAC Disposition and Distribution following an oral BAC exposure paradigm. We demonstrate that BACs are readily distributed and quantifiable in all harvested tissue: brain, spleen, lung, liver, kidney, duodenum, jejunum, ileum, BI, and feces. We demonstrate BACs are metabolized by cyps to form w and w-1 hydroxylation metabolites. Of which, samples that came from mice that were dosed with d_7-C12-BAC had higher levels of the ω-1 metabolite, while samples that came from mice that were dosed with d_7-C16-BAC had higher levels of the ω metabolite. This signifies unique metabolite distribution in BAC exposed tissues dependent on what the subject is exposed to. We elucidate CYP-mediated oxidation followed by Beta Oxidation is a substantial route of metabolism of BACs. In all biological samples that had metabolites, we observe the highest concentrations of analytes belonging to even-chained COOH products. Additionally, we report novel insight into parent: metabolite distribution within each of the biological samples, highlighting the need of future work being the elucidation of the metabolizing capability of the tissues.

Chapter 3 Figures

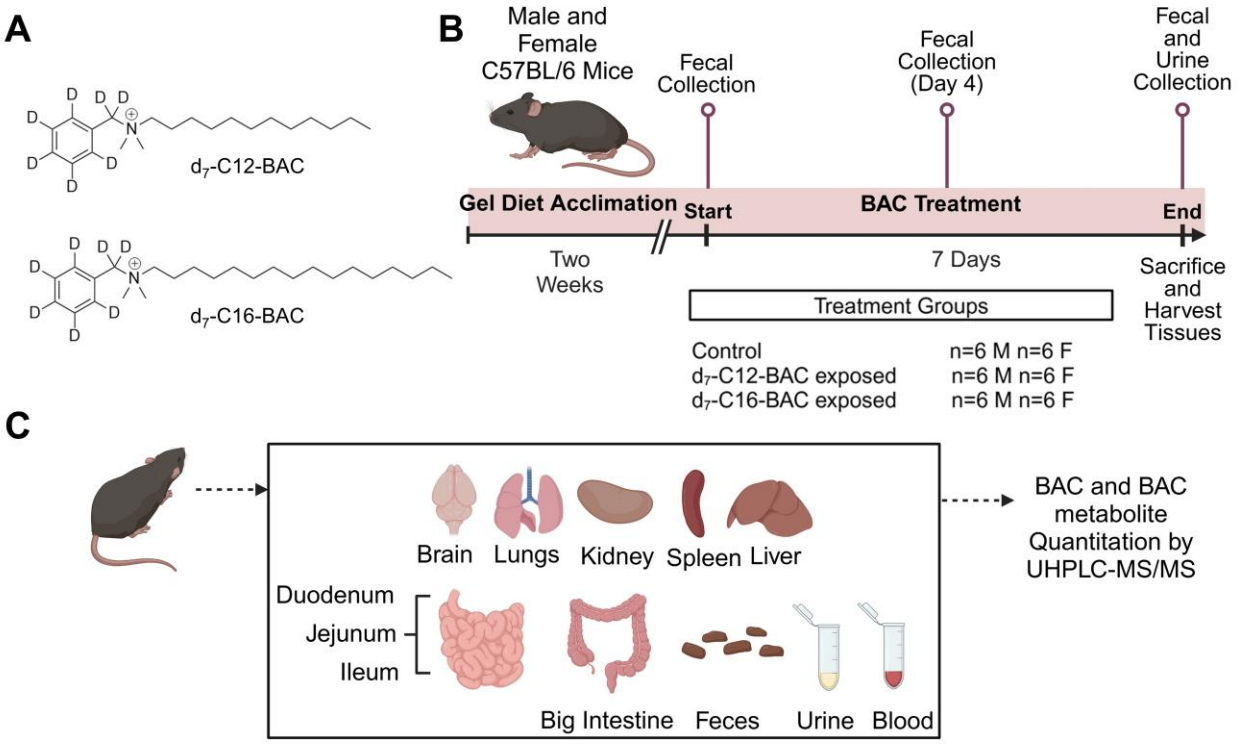

Figure 3.1 Animal Exposure Paradigm.

Figure 1. Animal Exposure Paradigm. A) Chemical structures of d_7-C12-BAC and d_7-C16-BAC. B) Exposure schematic detailing Male and Female C57BL/6 mice were acclimated to gel food diet for two weeks before being randomly exposed to either control, d_7-C12-BAC or d_7-C16-BAC treatment group. Mice underwent treatment for one week before sacrifice. C) On day of sacrifice, brain, lung, kidney, spleen, liver, duodenum, jejunum, ileum, large intestine tissues as well as; feces, urine and blood extracts were collected and processed for BAC and BAC metabolite quantitation.

Made with BioRender.

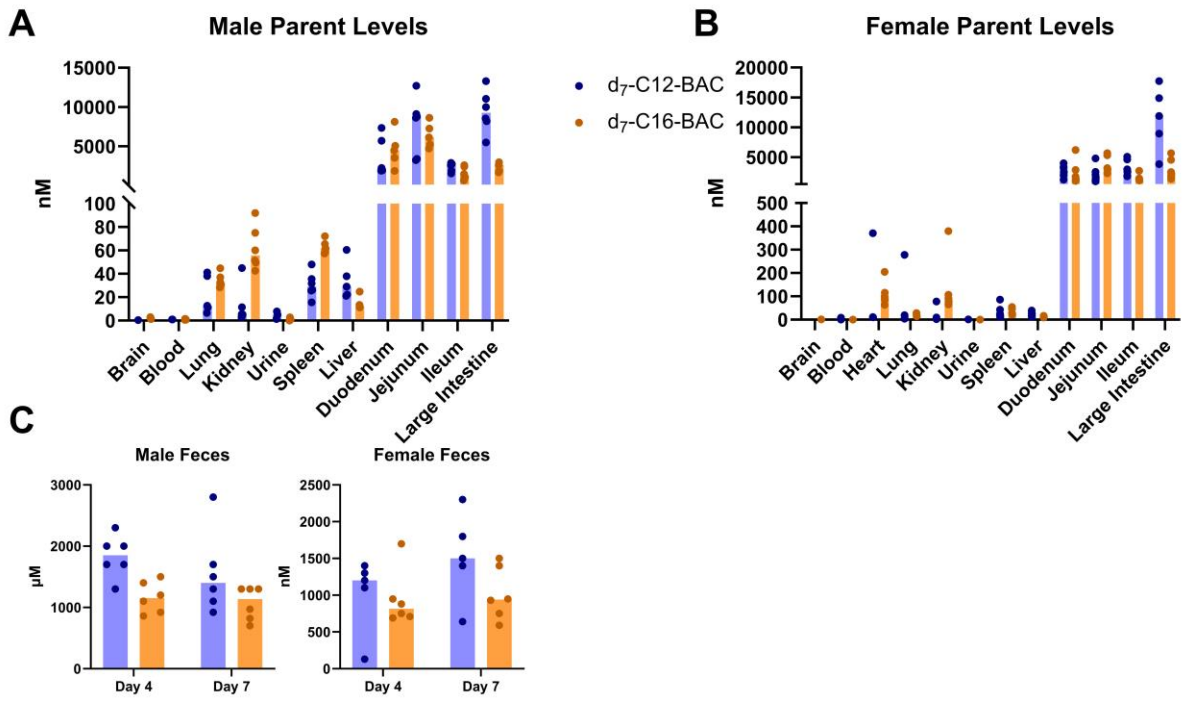

Figure 3.2 Quantified Parent BAC Levels in Harvested Tissues.

Quantified parent (A) d_7-C12-BAC and (B) d_7-C16-BAC levels in brain, blood, lung, kidney, urine, spleen, liver, duodenum, jejunum, ileum and large intestine of male and female C57BL/6 mice. Note that female samples include heart samples C) Quantified levels of d_7-C12-BAC and d_7-C16-BAC in day 4 and day 7 fecal extracts. Male and female C57BL/6 mice were randomly assigned to either the control, d_7-C12-BAC or d_7-C16-BAC group. Mice were exposed to BAC via gel diet for one week (120 μg/g/day). N=4-6.

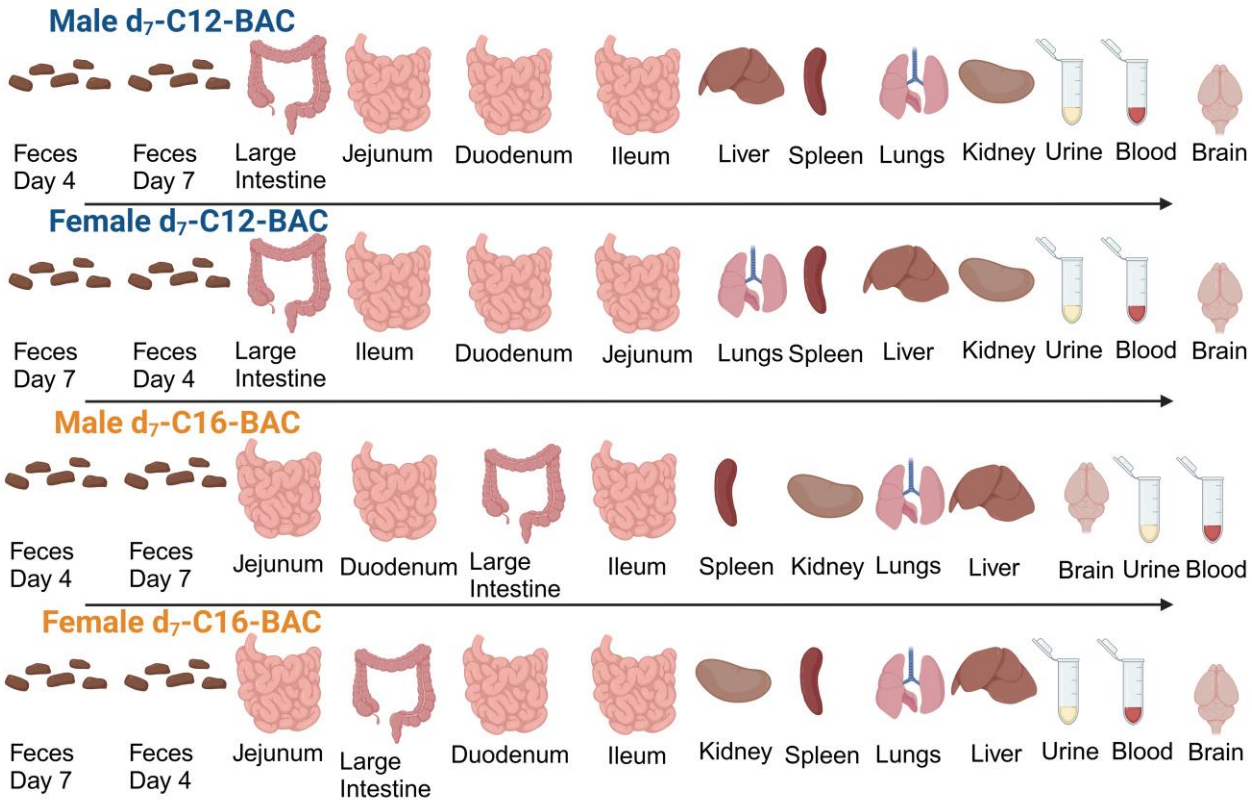

Figure 3.3 Ordering of Parent BAC Levels in Male and Female Biological Samples. N=4-6

Depiction of biological samples in order of highest to lowest levels (averages) of parent BACs quantified in each of the biological sample sets.

Made with BioRender.

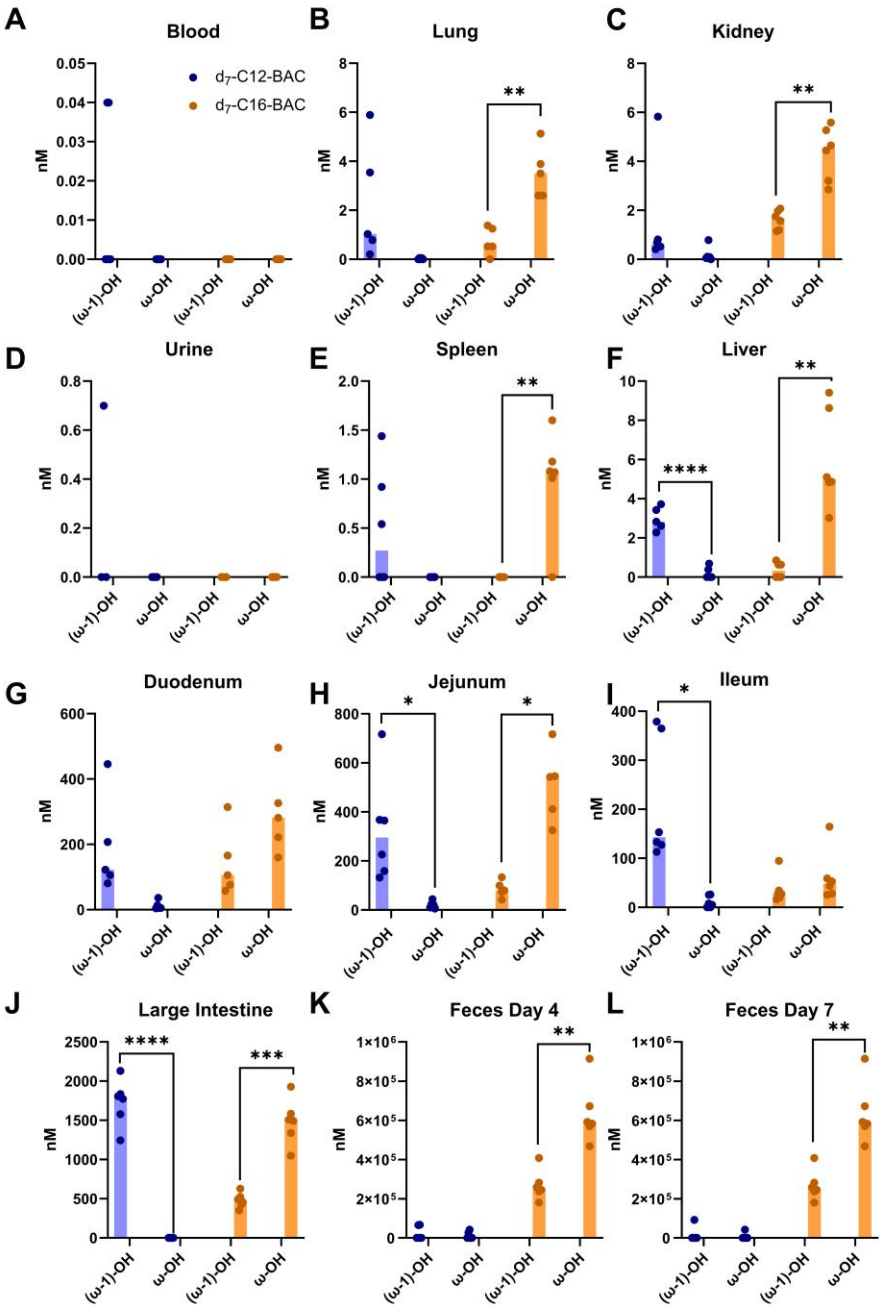

Figure 3.4 Concentrations of ω and ω-1 Hydroxy Metabolites in Male Biological Samples. N=4-6

Statistical analyses were carried out using unpaired *t*-tests with Welch's correction to compare male and female groups for each measurement. * $P \leq 0.05$; ** $P \leq 0.01$; *** $P \leq 0.001$; **** $P \leq 0.0001$.

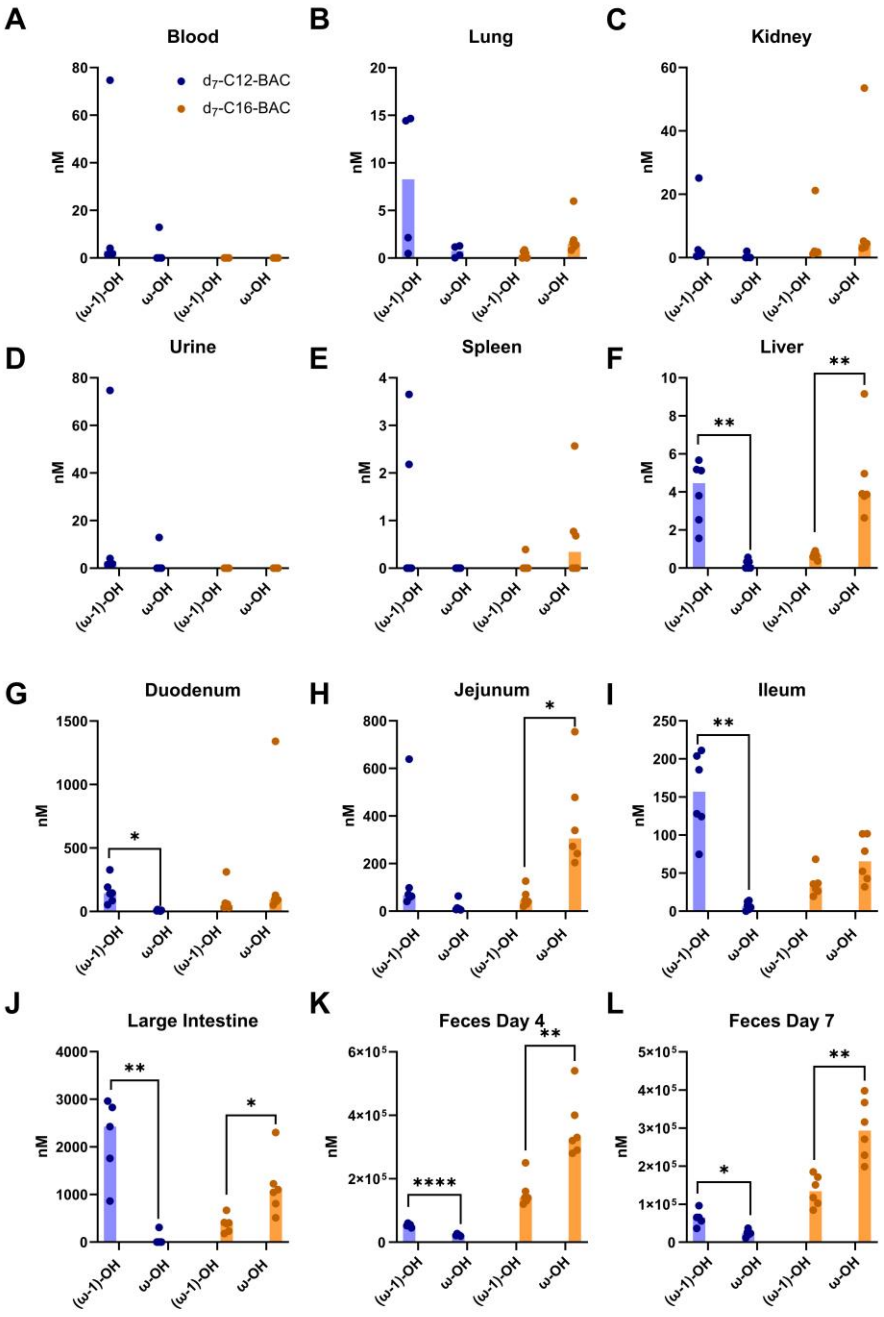

Figure 3.5 Concentrations of ω and ω-1 Hydroxy Metabolites in Female Biological Samples. N=4-6

Statistical analyses were carried out using unpaired *t*-tests with Welch's correction to compare male and female groups for each measurement. * $P \leq 0.05$; ** $P \leq 0.01$; *** $P \leq 0.001$; **** $P \leq 0.0001$.

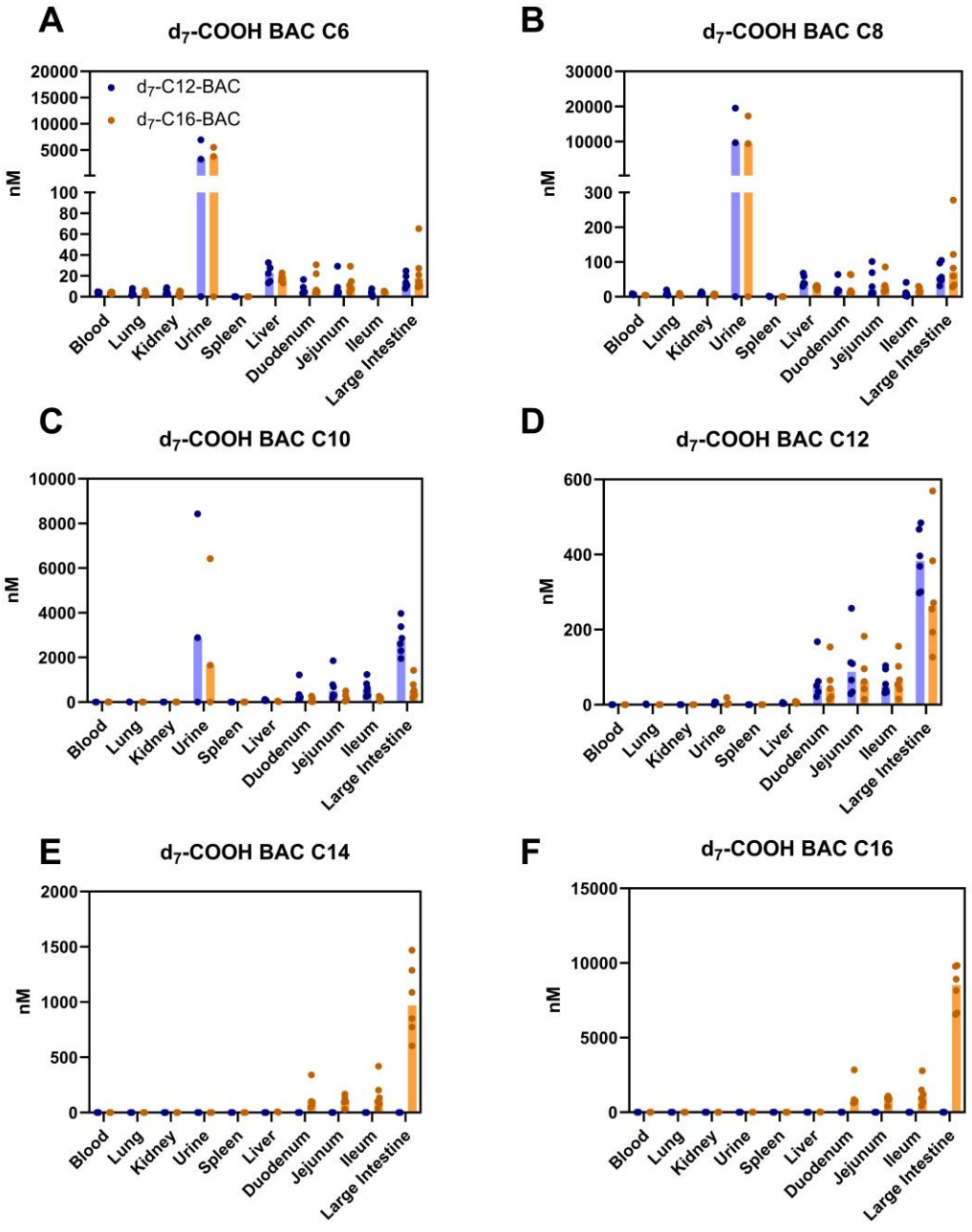

Figure 3.6 Even-Chained BAC-COOH Products in Male Biological Samples.

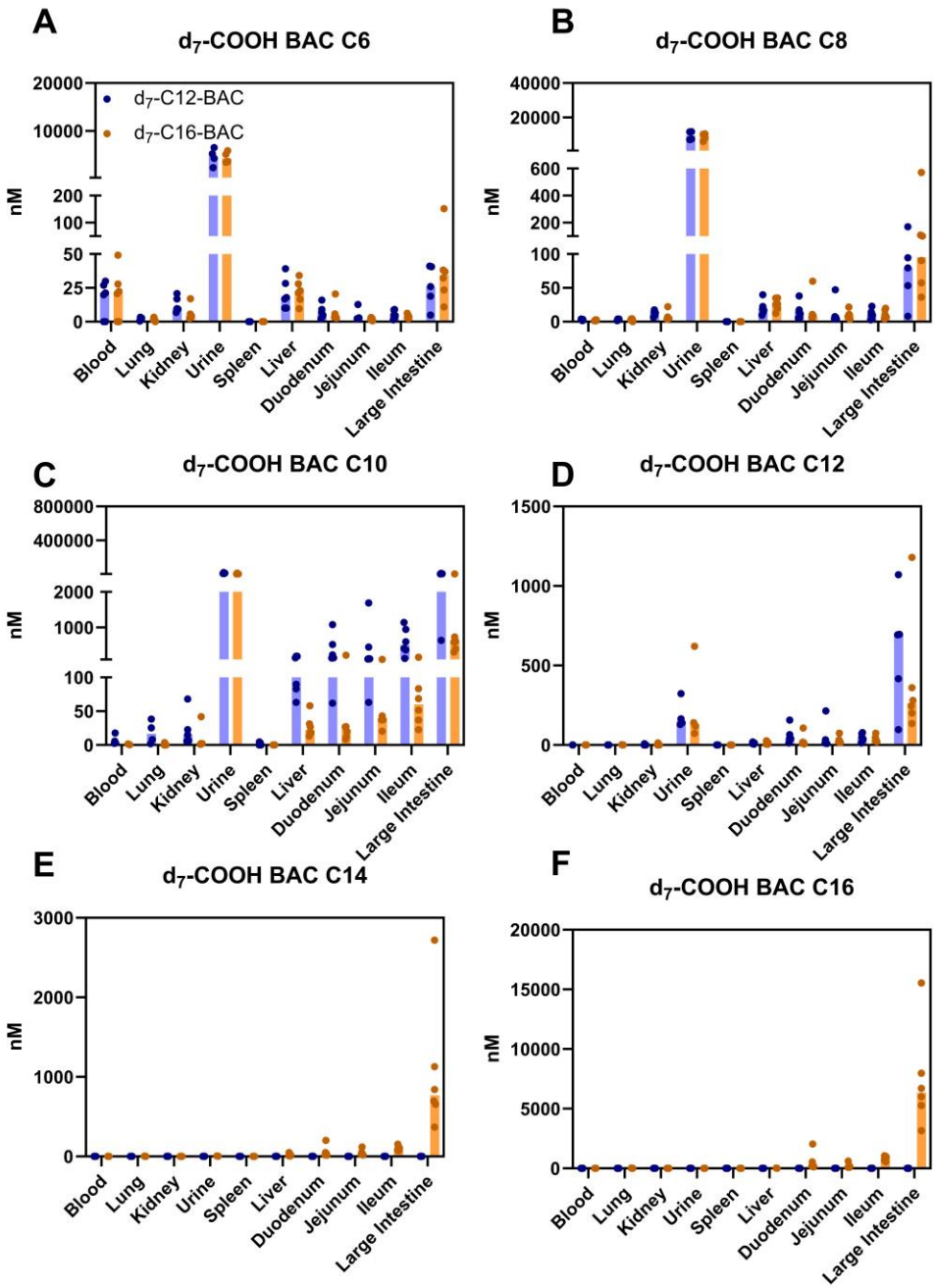

Figure 3.7 Even-Chained BAC-COOH Products in Female Biological Samples.

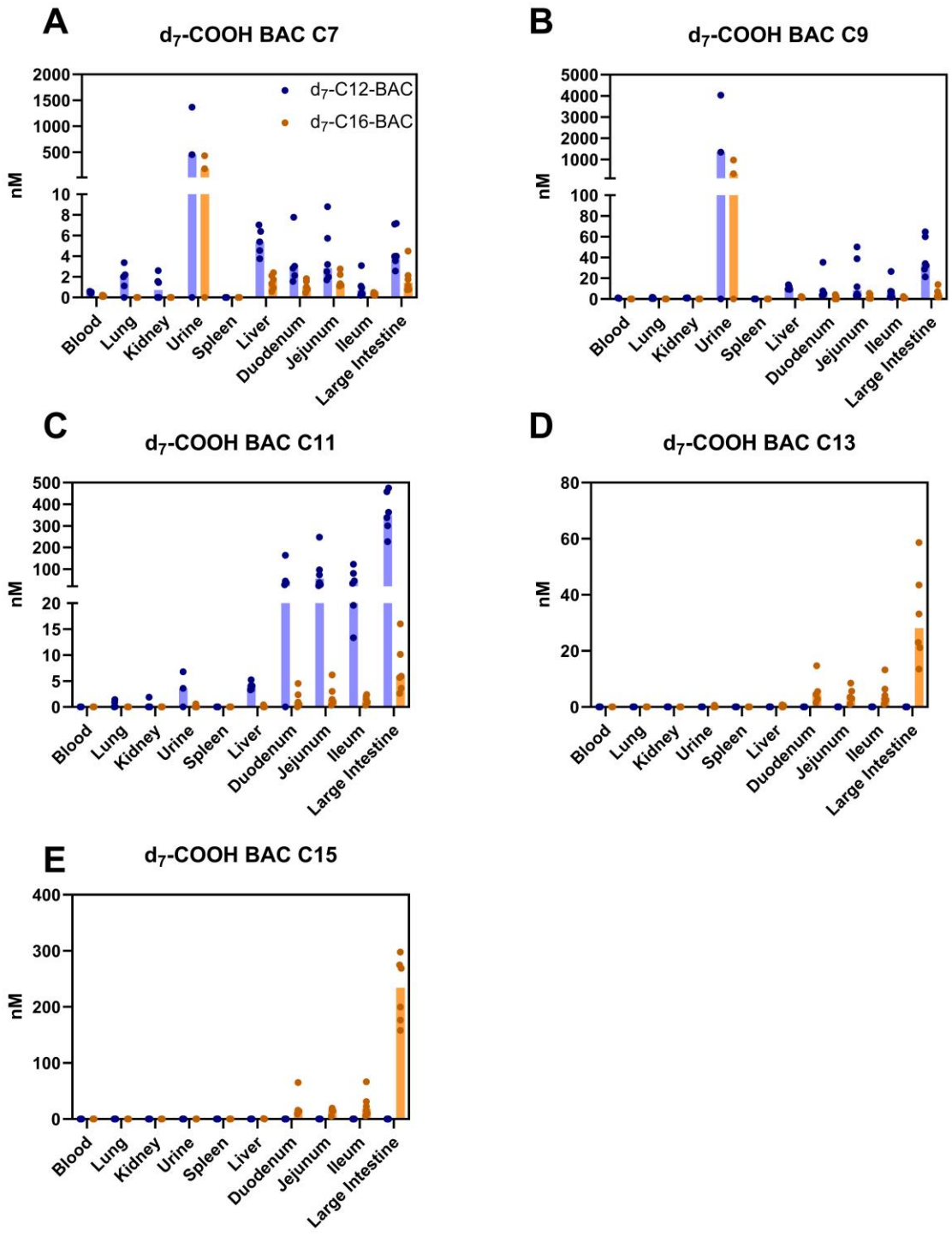

Figure 3.8 Odd-Chained BAC-COOH Products in Male Biological Samples.

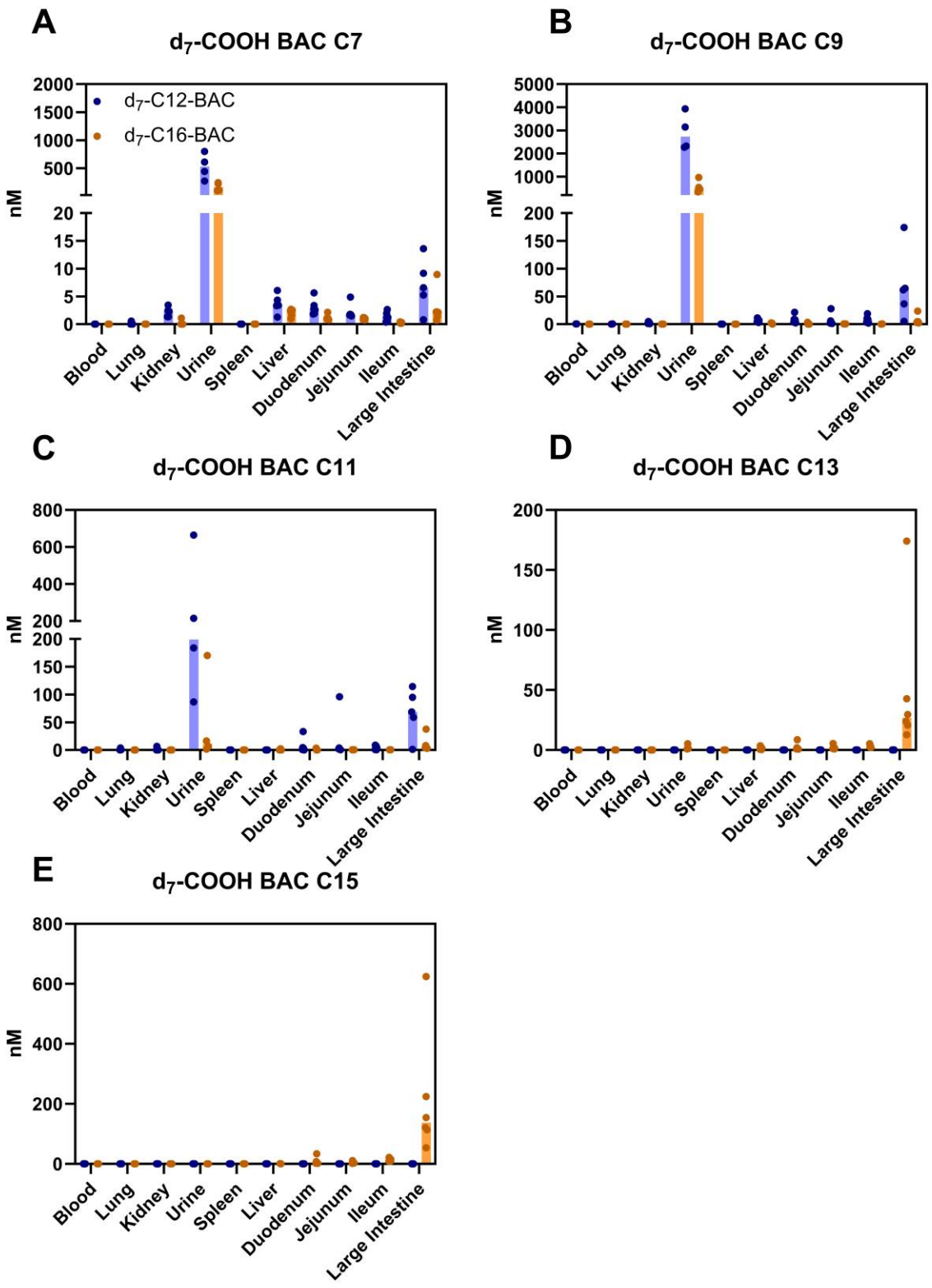

Figure 3.9 Odd-Chained BAC-COOH Products in Female Biological Samples.

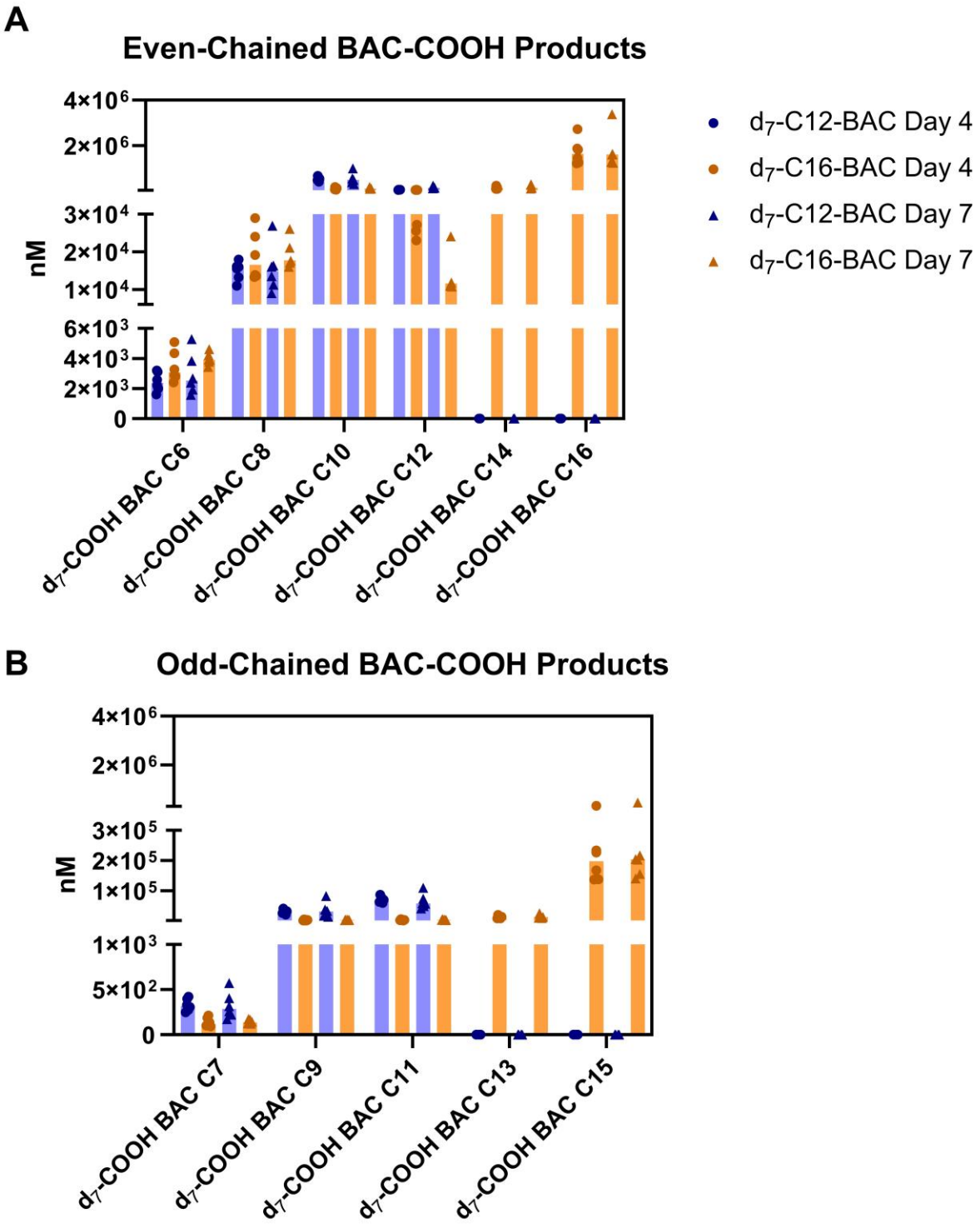

Figure 3.10 Even and Odd-Chained BAC-COOH Products in Male Feces.

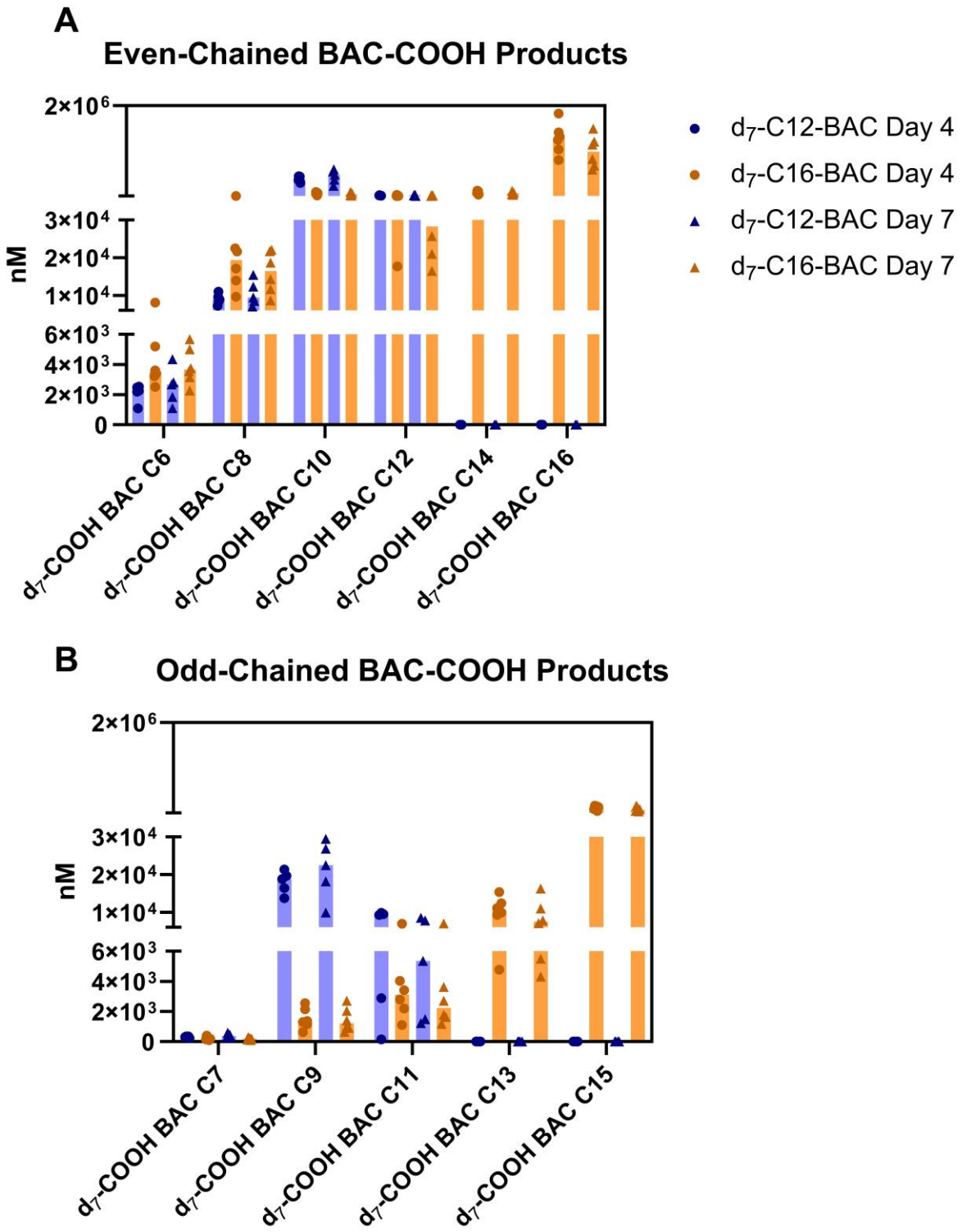

Figure 3.11 Even and Odd-Chained BAC-COOH Products in Female Feces.

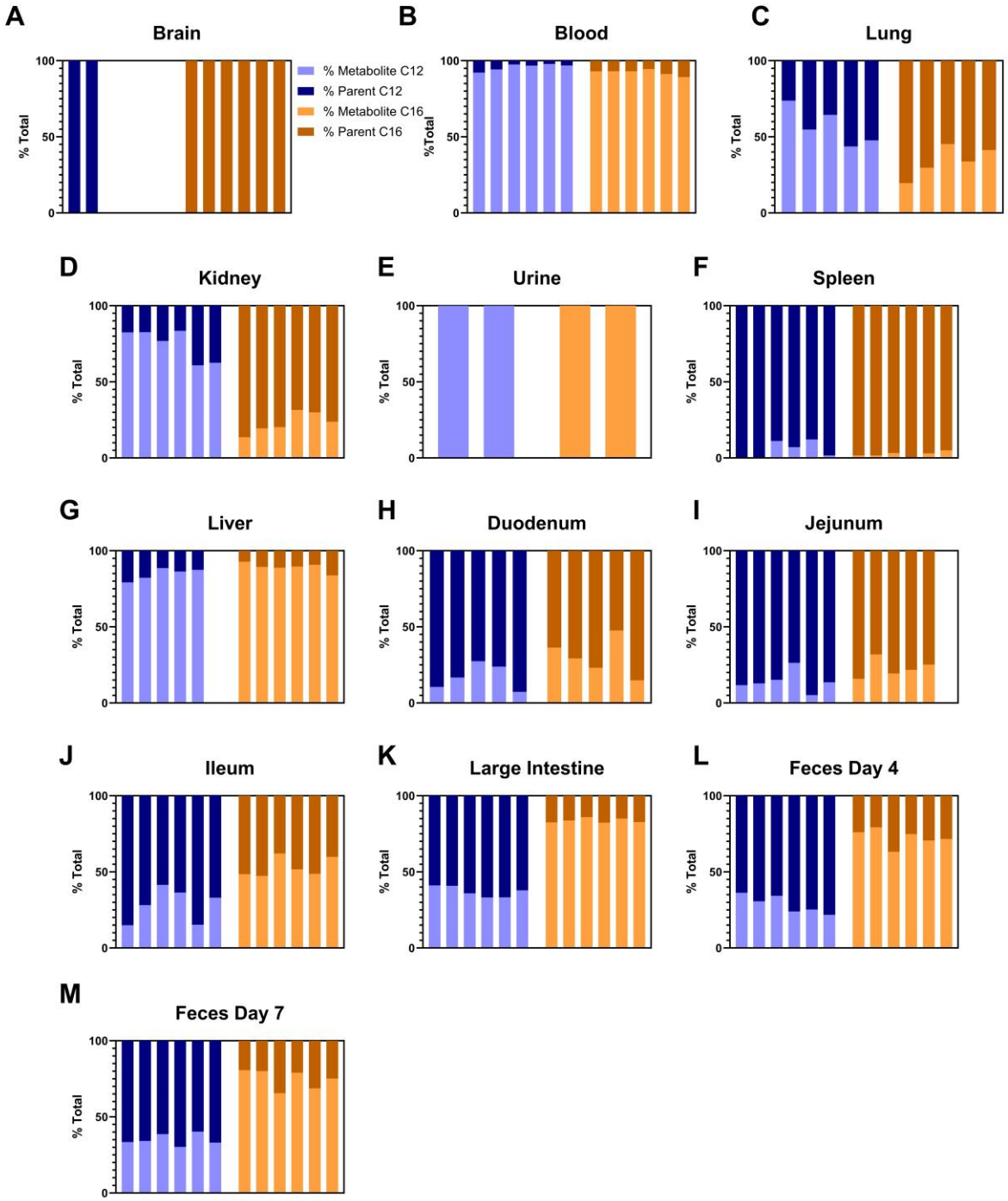

Figure 3.12 Parent to Metabolite Profiles in Male Biological Samples.
Sums of metabolites include even and odd COOH products, and ω and ω-1 hydroxylation products.

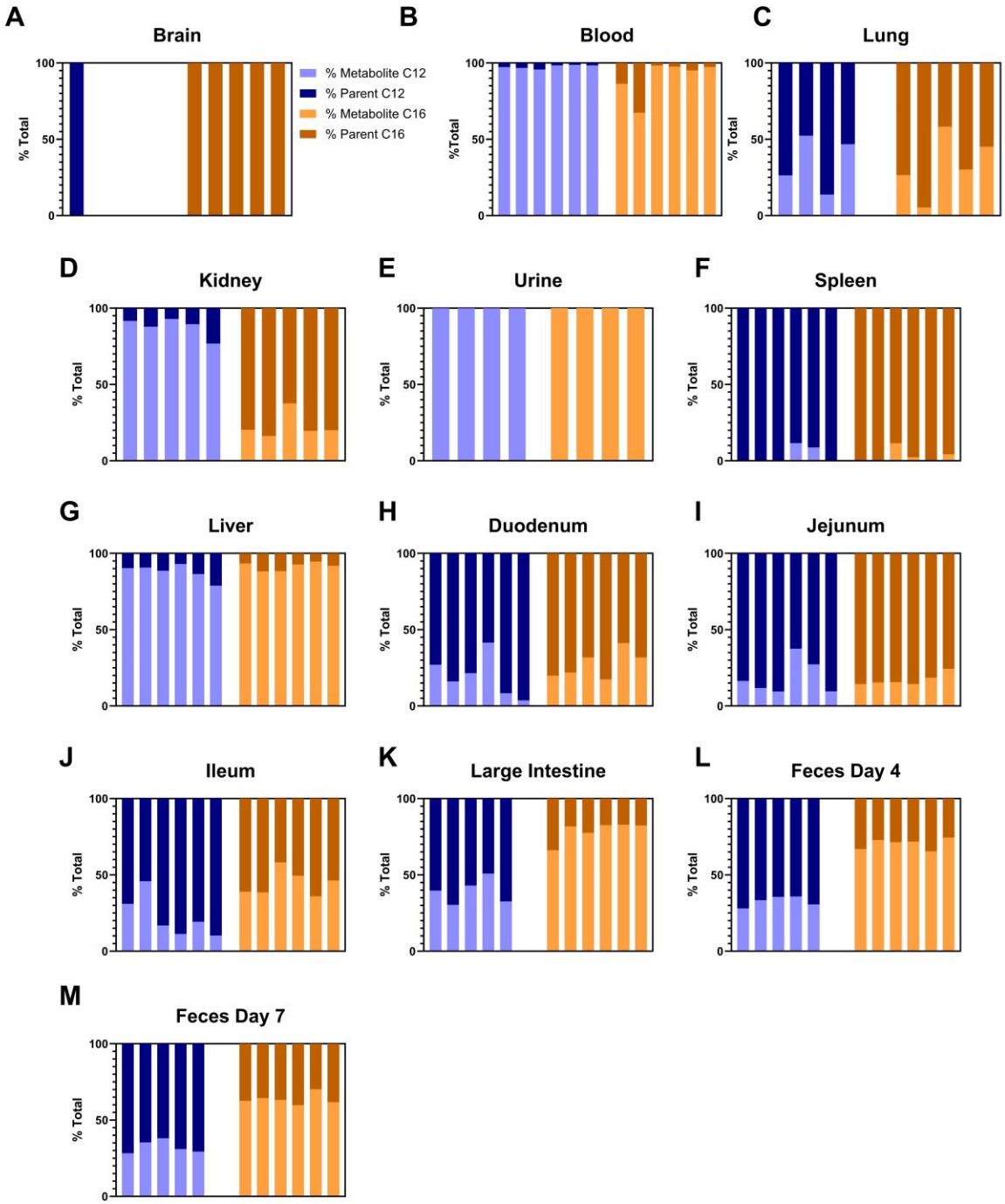

Figure 3.13 Parent to Metabolite Profiles in Female Biological Samples.

Sums of metabolites include even and odd COOH products, and ω and ω-1 hydroxylation products.

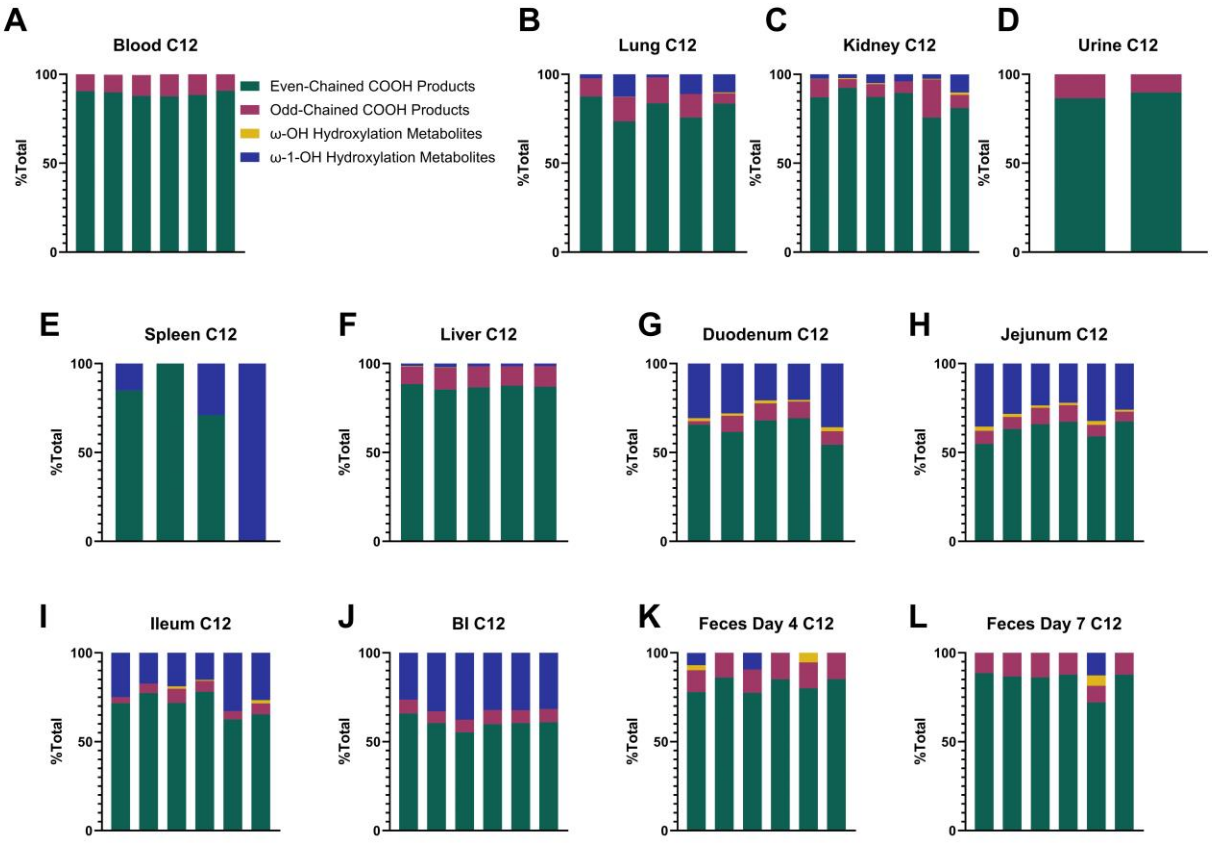

Figure 3.14 Metabolite Distribution Profiles in Male d_7-C12-BAC Exposed Biological Samples.

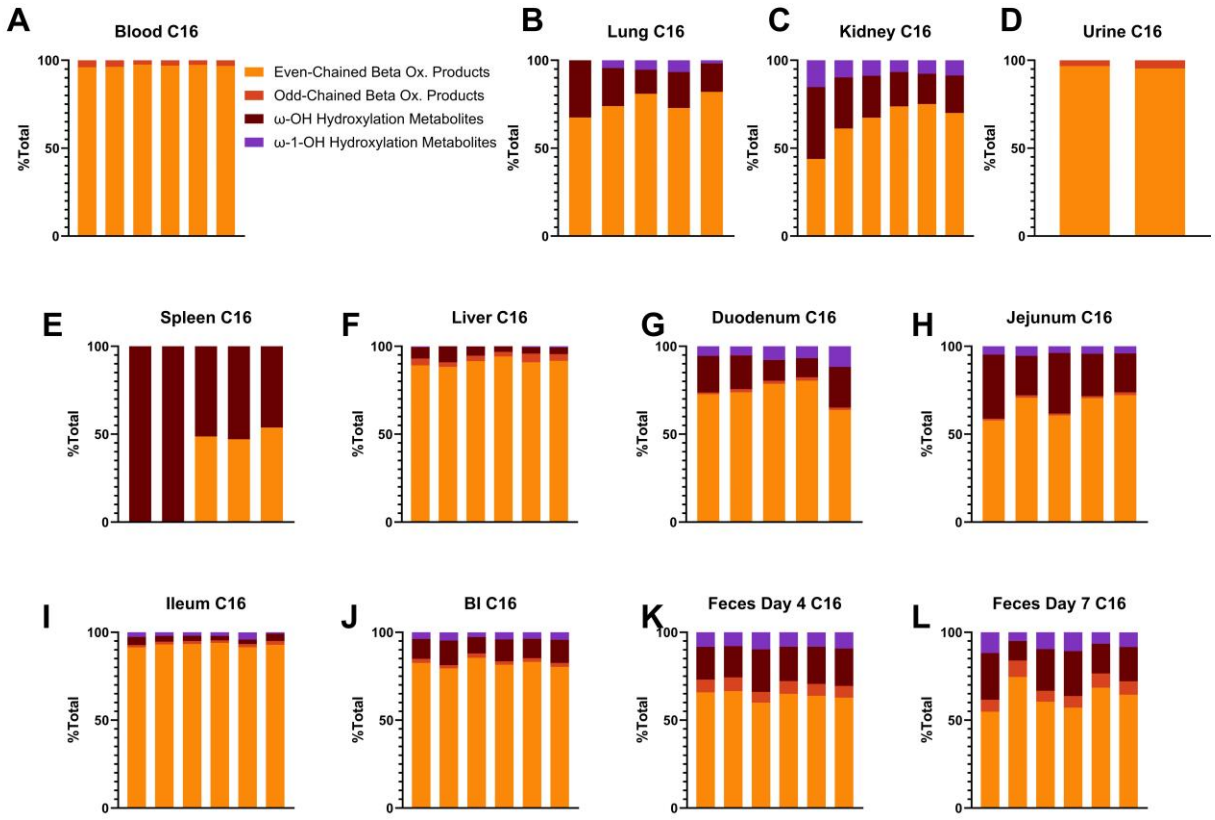

Figure 3.15 Metabolite Distribution Profiles in Male d_7-C16-BAC Exposed Biological Samples.

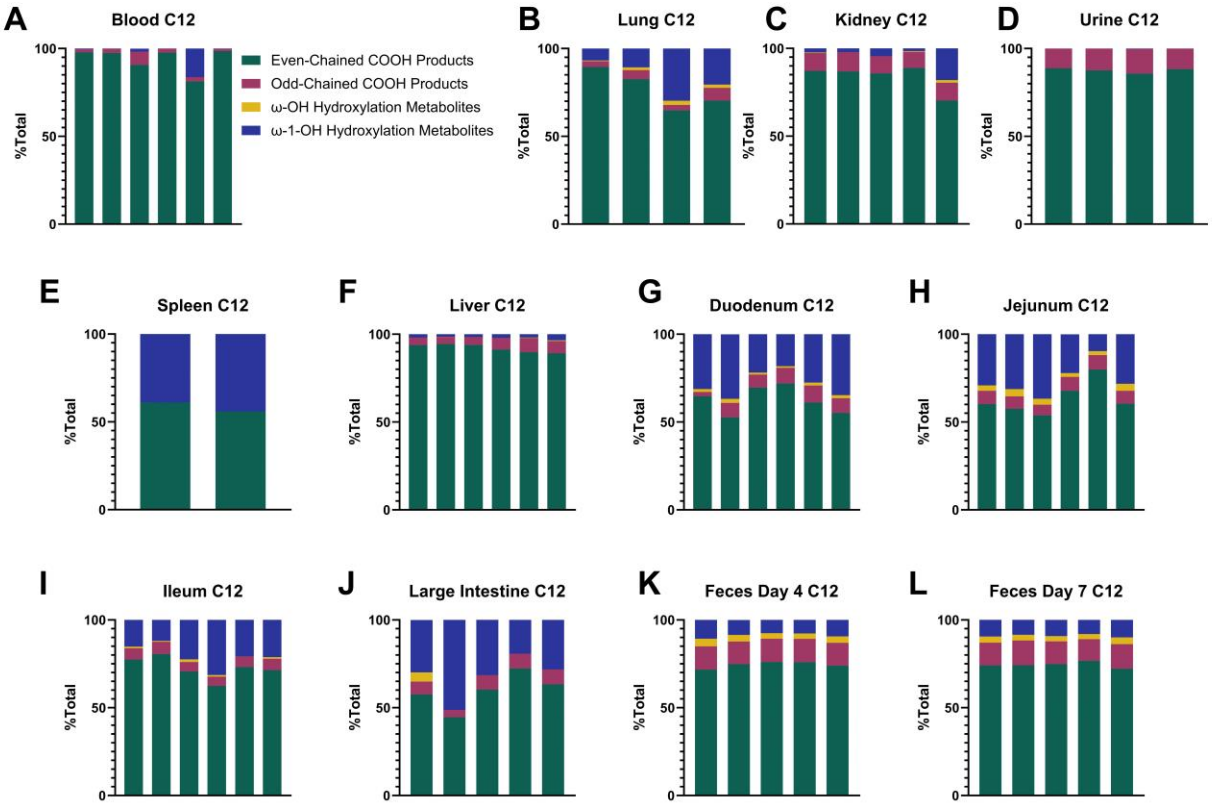

Figure 3.16 Metabolite Distribution Profiles in Female d_7-C12-BAC Exposed Biological Samples.

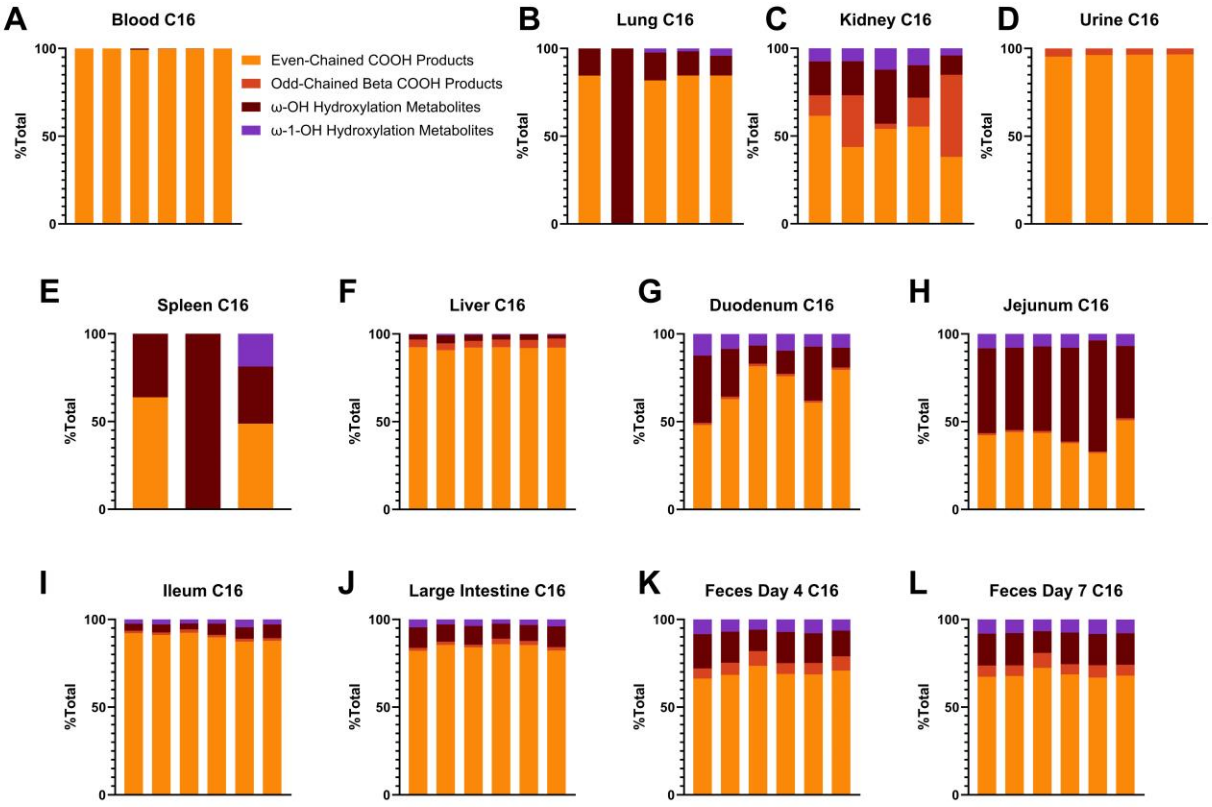

Figure 3.17 Metabolite Distribution Profiles in Female d_7-C16-BAC Exposed Biological Samples.

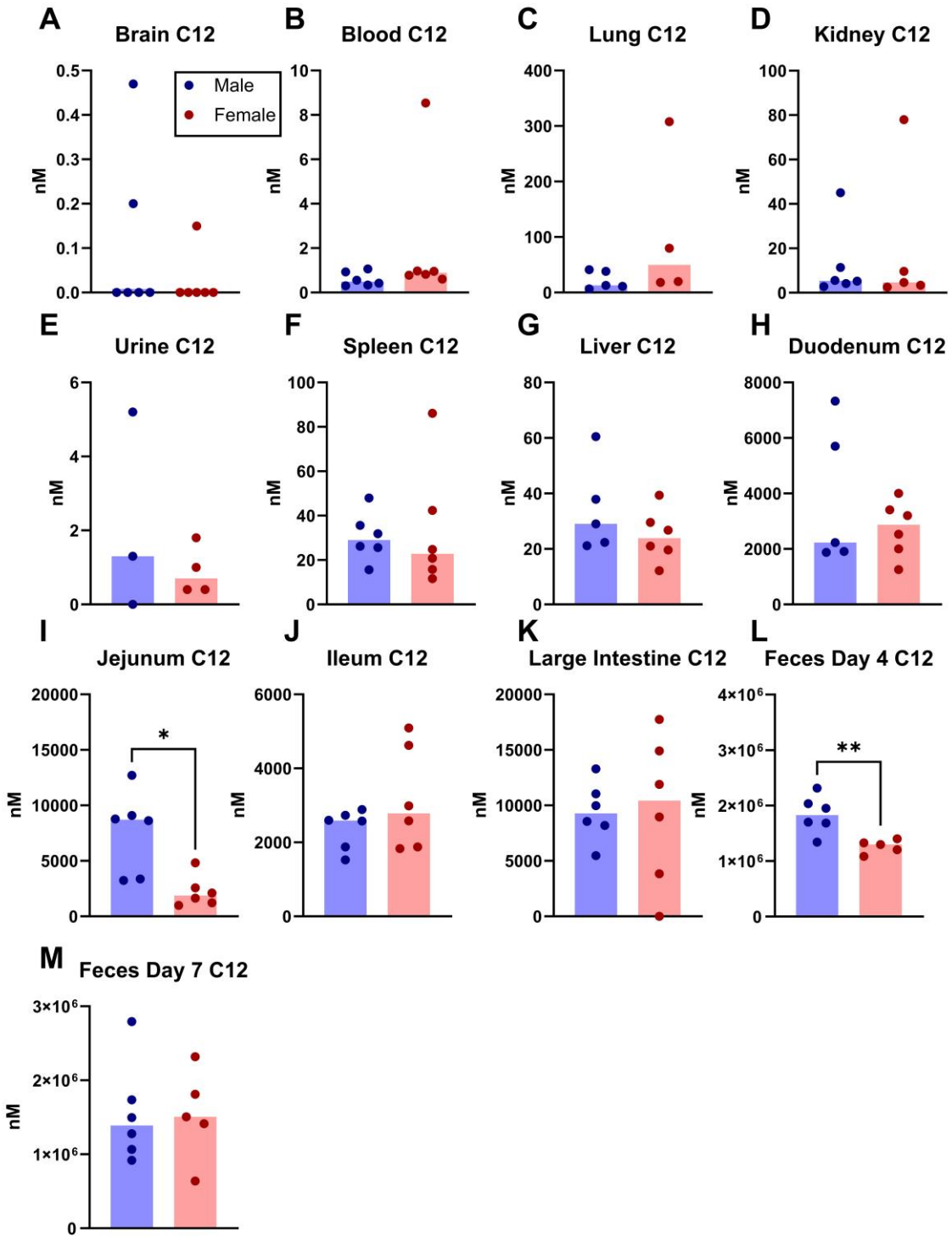

Figure 3.18 Parent C12 BAC levels in Male and Female Samples.

Statistical analyses were carried out using unpaired *t*-tests with Welch's correction to compare male and female groups for each measurement. * $P \leq 0.05$; ** $P \leq 0.01$; *** $P \leq 0.001$; **** $P \leq 0.0001$.

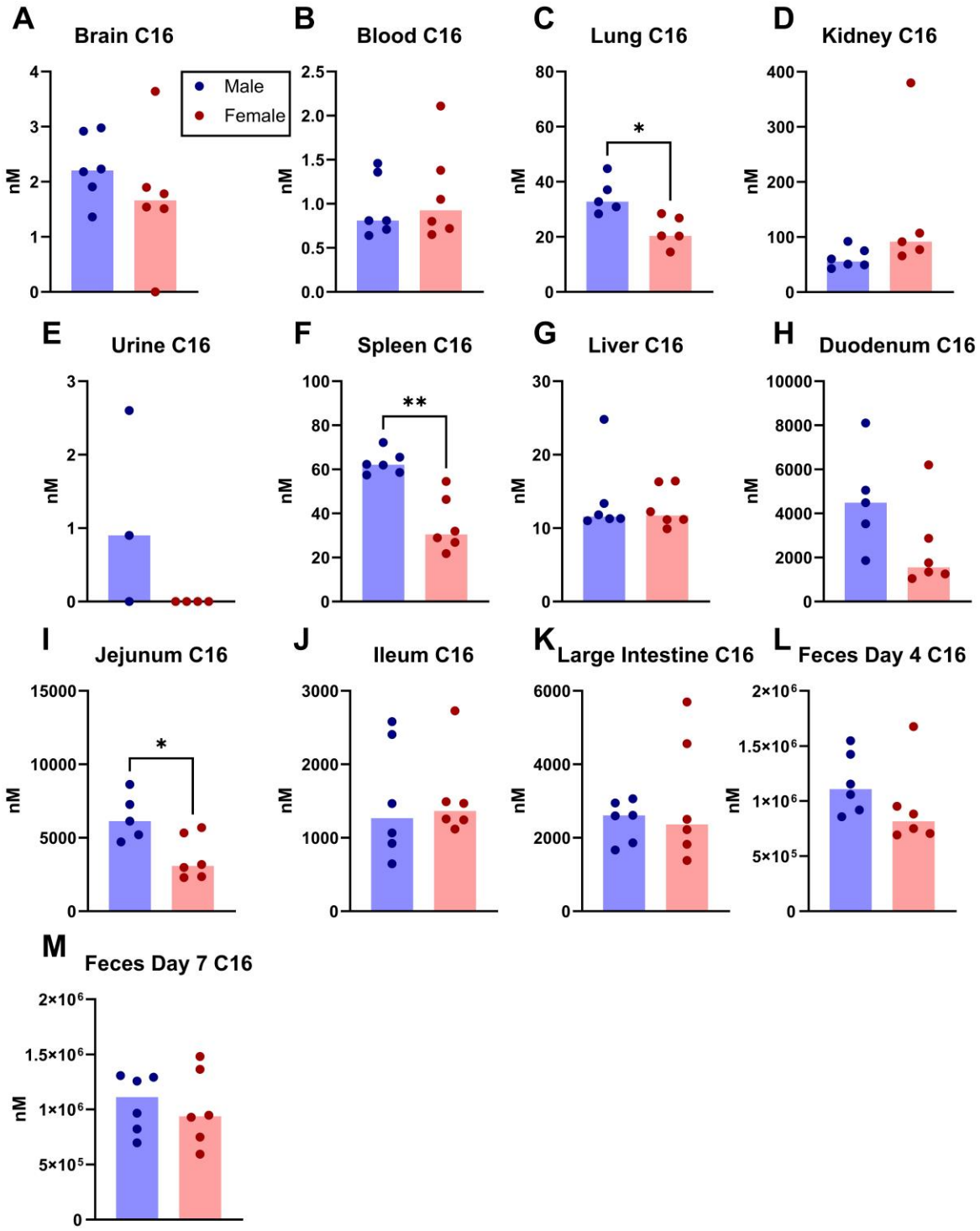

Figure 3.19 Parent C16 BAC levels in Male and Female Samples.

Statistical analyses were carried out using unpaired *t*-tests with Welch's correction to compare male and female groups for each measurement. * $P \leq 0.05$; ** $P \leq 0.01$; *** $P \leq 0.001$; **** $P \leq 0.0001$.

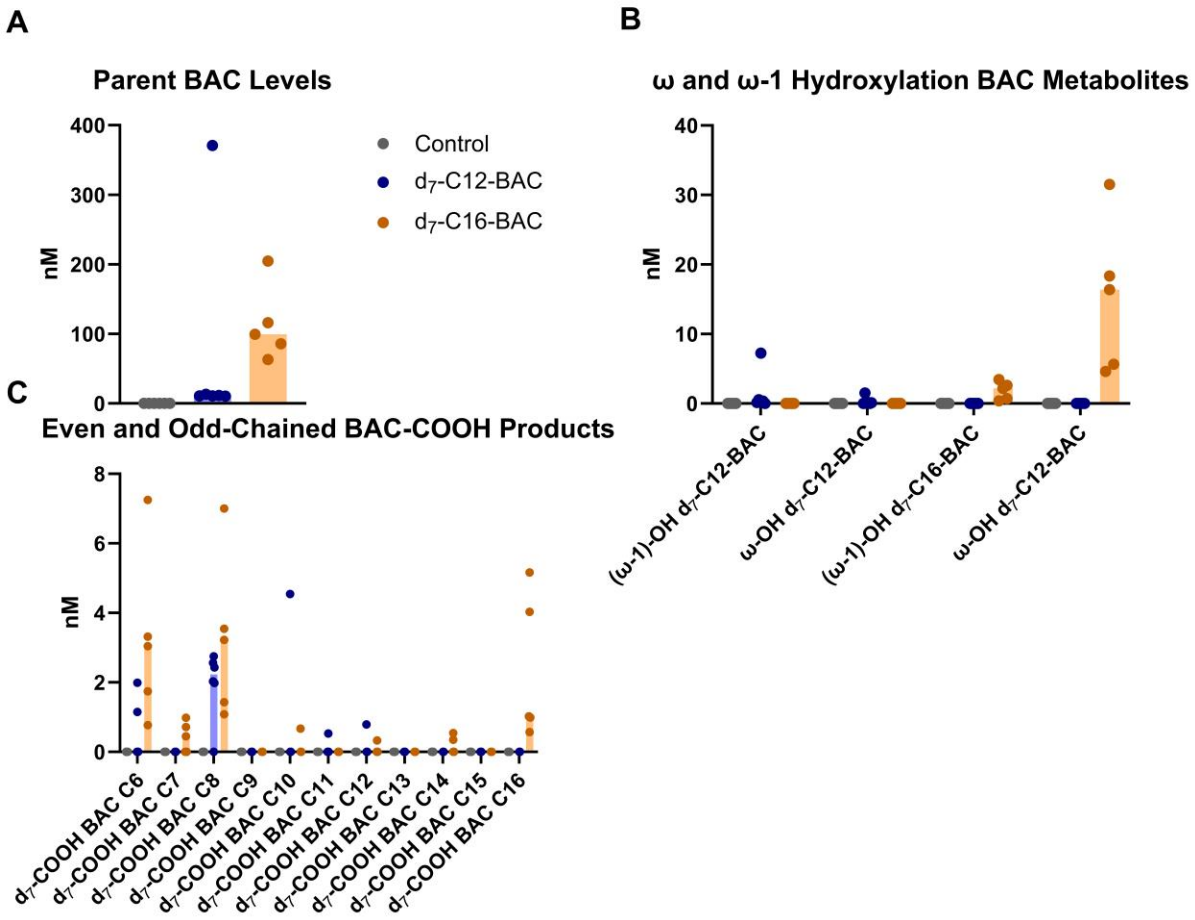

Figure 3.20 Parent and Metabolites Quantified in Female Hearts.

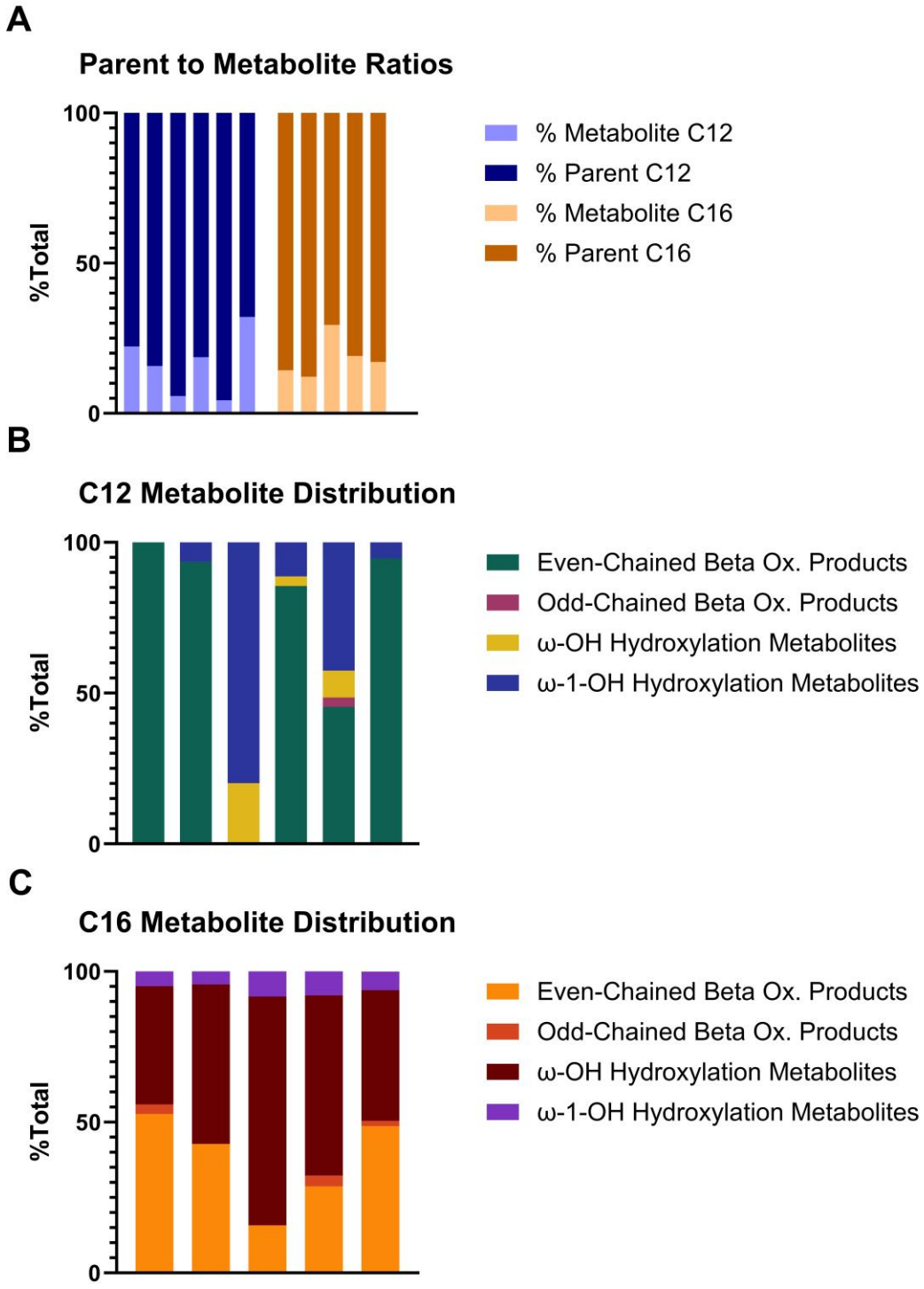

Figure 3.21 Parent and Metabolite Distributions in Female Hearts.

Chapter 3 Tables

Table 3.1 Analyte Retention Times and Precursor to Product Ions.

Table 3.1 Analyte Retention Times and Precursor to Product Ions

Analyte	Precursor to Product Ions (m/z)	Product Ions (m/z)	Retention Times (min)
d_7-COOH C6 BAC	257.228	158.119+98.099	1.5750
d_7-COOH C7 BAC	271.16	172.133+98.099	2.0950
d_7-COOH C8 BAC	285.258	186.151+98.099	2.6950
COOH C8	278.22	186.151+91.053	2.7400
d_7-COOH C9 BAC	299.275	200.17+98.099	3.4950
d_7-COOH C10 BAC	313.291	214.182+98.099	4.2500
COOH C10	306.252	214.182+91.053	4.2900
d_7-COOH C11 BAC	327.31	228.201+98.099	5.0050
d_7-COOH C12 BAC	341.215	242.215+98.096	5.6900
COOH C12	334.277	242.215+91.053	5.7200
ω-1 OH d_7-C12-BAC	327.31	228.201+98.099	5.7250
16 Da C12 BAC	320.303	288.233+91.053	5.8350
ω-OH d_7-C12-BAC	327.31	228.201+98.099	5.9600
d_7-COOH C13 BAC	355.34	256.23+98.099	6.4450
COOH C14	362.31	270.246+91.053	7.1100
d_7-COOH C14 BAC	369.354	270.251+98.099	7.1150
d_7-COOH C15 BAC	383.37	284.261+98.099	7.7800
d_7-COOH C16 BAC	397.388	298.277+98.099	8.4600
COOH C16	390.344	298.277+91.053	8.4950
ω-1 OH d_7-C16-BAC	383.404	284.296+98.096	8.7250
16 Da C16	376.363	284.296+91.053	8.8450
ω-OH d_7-C16-BAC	383.404	284.296+98.096	9.0050

C12 BAC	304.304	212.241+91.053	10.1400
d_7-C12-BAC	311.345	212.236+98.099	10.1500
d_7-C16-BAC	367.316	268.306+98.099	13.4800
C16 BAC	360.366	268.301+91.054	13.5600

Table 3.2 CYP4 and CYP2D6 Expression.

Table 3.2 CYP4 and CYP2D6 Expression			
Brain[1]	Tissue cDNA clones	CYP2D6 CYP4F	Yes Yes
Kidney[2,3]	HKM	CYP2D6 CYP4F2 CYP4F11/12	Little to None 4+- pmol/mg unknown
Liver[2,3,4,5]	HLM	CYP2D6 CYP4F2 CYP4F11 CYP4F12	12 pmol/mg 18 +- 20 pmol/mg 8.4 pmol/mg Unknown
Intestine[6]			
Duodenum	Tissue	CYP2D6 CYP4F2 CYP4F11 CYP4F12	0.38 +- 0.41 pmol/mg 3.6 +- 2.9 pmol/mg Unknown Unknown
Jejunum	Tissue	CYP2D6 CYP4F2 CYP4F11 CYP4F12	0.54 +- 0.41 pmol/mg 6.1 +- 3.6 pmol/mg Unknown Unknown
Ileum	Tissue	CYP2D6 CYP4F2 CYP4F11 CYP4F12	0.64 +- 0.61 pmol/mg 5.4 +- 3.5 pmol/mg Unknown Unknown
Large Intestine		CYP2D6 CYP4F	2.4% Unknown

1. (Kuban and Daniel, 2021)
2. (Okita *et al.*, 1979)
3. (Hirani *et al.*, 2008)
4. (Edson and Rettie, 2013)
5. (Katheryne Z. Edson *et al.*, 2013)
6. (Grangeon *et al.*, 2021)

Table 3.3 Parent BAC Levels in Isolated Biological Samples from BAC-Exposed Male and Female C57BL/6 mice.

d_7-C12-BAC				
	Male		Female	
	Avg.	Stdev.	Avg.	Stdev.
Brain (nM)	0.1	0.2	0.3	0.6
Blood (nM)	0.6	0.3	2.1	3.2
Lung (nM)	22.0	16.4	106.4	137.3
Kidney (nM)	12.4	16.3	19.6	32.7
Urine (nM)	0.6	0.3	2.1	3.2
Spleen (nM)	30.5	10.9	33.6	27.9
Liver (nM)	34.2	16.2	24.7	9.4
Duodenum (nM)	3810.6	2541.0	2734.2	1006.4
Jejunum (nM)	7638.5	3677.1	2223.2	1394.6
Ileum (nM)	2366.4	537.6	3165.3	1389.3
Large Intestine (nM)	9420.6	2674.7	7921.2	6020.2
Feces Day 4 (μM)	1838.8	336.9	1263.3	122.9
Feces Day 7 (μM)	1548.3	676.8	1537.5	614.1
d_7-C16-BAC				
	Male		Female	
	Avg.	Stdev.	Avg.	Stdev.
Brain (nM)	2.3	0.6	1.7	1.2
Blood (nM)	1.0	0.4	1.1	0.6
Lung (nM)	34.8	6.4	22.1	5.6
Kidney (nM)	61.7	18.6	144.3	132.7
Urine (nM)	1.0	0.4	1.1	0.6
Spleen (nM)	63.0	5.4	35.1	12.6
Liver (nM)	13.9	5.4	12.9	2.8
Duodenum (nM)	4607.8	2297.7	2414.1	1969.2
Jejunum (nM)	6392.5	1586.1	3639.7	1496.7

Ileum (nM)	1515.4	805.3	1551.1	593.7
Large Intestine (nM)	2458.9	571.6	3193.2	1855.7
Feces Day 4 (μM)	1160.6	275.7	981.7	403.3
Feces Day 7 (μM)	1057.6	265.2	1027.1	384.0

Table 3.4 ω-hydroxylation Product Levels in Isolated Biological Samples from BAC-exposed Male and Female C57BL/6 mice.

ω-OH d_7-C12-BAC (nM)				
	Male		Female	
	Avg.	Stdev.	Avg.	Stdev.
Brain (nM)	0.0	0.0	0.0	0.0
Blood (nM)	0.0	0.0	0.0	0.0
Lung (nM)	0.0	0.0	0.7	0.6
Kidney (nM)	0.2	0.3	0.4	0.9
Urine (nM)	0.0	0.0	3.2	6.5
Spleen (nM)	0.0	0.0	0.0	0.0
Liver (nM)	0.2	0.3	0.2	0.2
Duodenum (nM)	12.9	13.6	8.3	4.5
Jejunum (nM)	19.7	13.6	18.1	22.6
Ileum (nM)	9.5	12.9	7.0	5.6
Large Intestine (nM)	0.0	0.0	61.4	137.3
Feces Day 4 (μM)	633.3	152.4	22.2	2.9
Feces Day 7 (μM)	7.0	17.1	23.6	9.0
ω-1-OH d_7-C12-BAC				
	Male		Female	
	Avg.	Stdev.	Avg.	Stdev.
Brain (nM)	0.0	0.0	0.0	0.0
Blood (nM)	0.0	0.0	0.8	1.8
Lung (nM)	2.3	2.4	7.9	7.7
Kidney (nM)	1.5	2.1	6.0	10.7
Urine (nM)	2.6	4.5	20.5	36.1
Spleen (nM)	0.5	0.6	1.0	1.6
Liver (nM)	3.0	0.6	4.0	1.7
Duodenum (nM)	192.3	149.5	157.6	96.6
Jejunum (nM)	328.0	215.2	161.8	234.5
Ileum (nM)	211.8	124.7	154.7	54.0

Large Intestine (nM)	1728.5	1707.3	1682.7	1271.3
Feces Day 4 (μM)	268.7	76.1	53.2	5.4
Feces Day 7 (μM)	15.3	37.5	63.8	21.5
ω-OH d_7-C16-BAC				
	Male		Female	
	Avg.	Stdev.	Avg.	Stdev.
Brain (nM)	0.0	0.0	0.0	0.0
Blood (nM)	0.0	0.0	0.1	0.1
Lung (nM)	3.5	1.1	2.3	2.1
Kidney (nM)	4.3	1.1	13.9	22.2
Urine (nM)	0.0	0.0	0.0	0.0
Spleen (nM)	1.0	0.5	0.7	1.0
Liver (nM)	6.0	2.5	4.7	2.3
Duodenum (nM)	296.9	127.5	297.9	511.6
Jejunum (nM)	508.6	149.0	381.9	206.4
Ileum (nM)	62.3	51.7	68.2	30.2
Large Intestine (nM)	1483.4	289.4	1166.2	611.6
Feces Day 4 (μM)	1160.6	275.7	981.7	403.3
Feces Day 7 (μM)	633.3	152.4	296.3	78.1
ω-1-OH d_7-C16-BAC				
	Male		Female	
	Avg.	Stdev.	Avg.	Stdev.
Brain (nM)	0.0	0.0	0.0	0.0
Blood (nM)	0.0	0.0	0.0	0.0
Lung (nM)	0.7	0.6	0.3	0.4
Kidney (nM)	1.6	0.4	5.5	8.8
Urine (nM)	0.0	0.0	0.0	0.0
Spleen (nM)	0.0	0.0	0.1	0.2
Liver (nM)	0.4	0.4	0.7	0.2
Duodenum (nM)	144.1	103.5	89.7	109.6
Jejunum (nM)	85.7	33.8	55.7	38.5

Ileum (nM)	36.7	29.1	36.0	17.1
Large Intestine (nM)	479.8	94.5	380.5	172.4
Feces Day 4 (μM)	1838.8	336.9	156.7	47.6
Feces Day 7 (μM)	268.7	76.1	135.1	40.0

Table 3.5 Even-Numbered Beta-Oxidation Product Levels in Isolated Biological Samples from BAC-exposed Male and Female C57BL/6 mice.

d_7-COOH BAC C6								
	Male				Female			
	d_7-C12-BAC		d_7-C16-BAC		d_7-C12-BAC		d_7-C16-BAC	
	Avg.	Stdev.	Avg.	Stdev.	Avg.	Stdev.	Avg.	Stdev.
Brain (nM)	0.0	0.0	0.0	0.0	0.0	0.0	0.0	0.0
Blood (nM)	3.9	0.9	4.0	0.7	16.4	13.2	20.0	18.5
Lung (nM)	3.6	2.8	2.9	2.1	2.1	1.2	1.7	1.2
Kidney (nM)	4.8	2.5	3.6	2.3	12.7	5.9	6.6	5.9
Urine (nM)	3390.1	3460.6	3088.5	2806.4	4567.5	1774.9	4473.9	1179.5
Spleen (nM)	0.0	0.0	0.0	0.0	0.0	0.0	0.0	0.0
Liver (nM)	22.2	8.3	17.9	3.3	20.4	11.4	22.1	8.6
Duodenum (nM)	7.7	5.3	13.6	12.1	7.1	5.0	6.7	6.9
Jejunum (nM)	9.0	10.2	13.3	9.7	3.0	4.9	1.8	1.2
Ileum (nM)	2.9	2.7	4.7	0.4	5.3	3.1	4.0	1.4
Large Intestine (nM)	14.7	6.4	24.7	21.0	21.9	17.4	49.0	51.5

Feces Day 4 (nM)	2453.5	627.3	3469.9	1036.5	2110.4	588.5	4338.9	2050.5
Feces Day 7 (nM)	2952.6	1379.8	3980.6	401.7	2554.8	1214.0	3900.2	1241.1
d_7-COOH BAC C8								
	Male				Female			
	d_7-C12-BAC		d_7-C16-BAC		d_7-C12-BAC		d_7-C16-BAC	
	Avg.	Stdev.	Avg.	Stdev.	Avg.	Stdev.	Avg.	Stdev.
Brain (nM)	0.0	0.0	0.0	0.0	0.0	0.0	0.0	0.0
Blood (nM)	6.6	1.4	5.0	0.9	3.0	0.8	2.3	0.9
Lung (nM)	10.0	6.2	5.8	2.9	3.1	1.1	3.0	1.8
Kidney (nM)	10.5	3.8	6.3	2.8	12.2	4.4	8.6	7.8
Urine (nM)	9730.8	9759.1	8900.6	8647.0	9395.5	2529.3	8624.1	2055.1
Spleen (nM)	0.3	0.7	0.0	0.0	0.0	0.0	0.0	0.0
Liver (nM)	46.9	15.9	29.3	5.2	20.4	10.5	25.6	8.8
Duodenum (nM)	26.3	21.3	34.0	27.5	15.6	12.0	16.5	21.3
Jejunum (nM)	38.4	38.4	47.9	35.6	12.5	17.1	10.9	6.0
Ileum (nM)	11.9	14.8	19.1	7.7	10.7	7.4	10.8	6.4
Large Intestine (nM)	64.9	29.1	100.9	93.3	67.6	62.7	160.7	203.1

Feces Day 4 (nM)	14976.0	2478.9	18825.3	6518.6	9025.8	1381.1	19701.4	8239.4
Feces Day 7 (nM)	15520.7	6274.7	19296.0	3729.1	10536.4	3337.6	16177.2	5505.3
d_7-COOH BAC C10								
	Male				Female			
	d_7-C12-BAC		d_7-C16-BAC		d_7-C12-BAC		d_7-C16-BAC	
	Avg.	Stdev.	Avg.	Stdev.	Avg.	Stdev.	Avg.	Stdev.
Brain (nM)	0.0	0.0	0.0	0.0	0.0	0.0	0.0	0.0
Blood (nM)	2.3	0.7	1.4	0.6	5.6	6.1	0.6	0.6
Lung (nM)	7.2	6.2	1.3	0.6	18.4	16.6	1.0	1.5
Kidney (nM)	5.7	6.9	1.4	0.6	23.7	25.7	9.9	17.9
Urine (nM)	3772.0	4282.2	2693.0	3335.7	12266.3	5443.9	6088.0	4763.1
Spleen (nM)	1.5	1.7	0.0	0.0	1.3	2.1	0.0	0.0
Liver (nM)	88.4	20.2	33.4	9.3	128.1	57.2	27.7	16.3
Duodenum (nM)	418.8	454.6	112.4	113.8	365.6	386.3	52.1	81.4
Jejunum (nM)	690.2	612.8	208.0	188.1	426.2	633.4	46.3	27.9
Ileum (nM)	623.9	367.7	158.5	76.5	598.9	379.6	71.6	51.3
Large Intestine (nM)	2843.9	734.9	624.6	438.2	3779.18	3569.06	962.2	1071.0

Feces Day 4 (μM)	526.0	91.7	106.4	45.7	403.9	61.6	85.7	31.1
Feces Day 7 (μM)	535.2	242.2	111.2	31.7	462.7	143.6	72.4	30.7
d_7-COOH BAC C12								
	Male				Female			
	d_7-C12-BAC		d_7-C16-BAC		d_7-C12-BAC		d_7-C16-BAC	
	Avg.	Stdev.	Avg.	Stdev.	Avg.	Stdev.	Avg.	Stdev.
Brain (nM)	0.0	0.0	0.0	0.0	0.0	0.0	0.0	0.0
Blood (nM)	0.0	0.0	0.0	0.0	0.5	0.8	0.2	0.3
Lung (nM)	0.8	0.9	0.0	0.0	2.4	2.1	0.5	0.8
Kidney (nM)	0.5	0.9	0.2	0.1	2.99	3.1	3.1	5.5
Urine (nM)	4.7	4.1	7.6	10.3	189.1	90.6	238.0	256.3
Spleen (nM)	0.0	0.0	0.0	0.0	0.0	0.0	0.0	0.0
Liver (nM)	4.1	1.2	5.6	2.0	12.3	5.5	12.7	8.0
Duodenum (nM)	67.5	58.1	59.7	56.3	58.9	50.8	28.3	38.6
Jejunum (nM)	101.3	84.1	79.3	64.7	50.4	80.9	30.4	22.4
Ileum (nM)	59.9	31.8	72.6	50.0	46.8	24.9	38.2	20.1
Large Intestine (nM)	385.8	79.7	299.8	157.3	495.8	405.1	400.70	389.12

Feces Day 4 (nM)	53162.0	7043.3	38184.6	15479.5	43589.6	4857.3	37501.2	13492.6
Feces Day 7 (nM)	146344.4	49520.6	13497.0	5221.8	50029.5	14417.4	31055.3	13247.2
d_7-COOH BAC C14								
	Male				Female			
	d_7-C12-BAC		d_7-C16-BAC		d_7-C12-BAC		d_7-C16-BAC	
	Avg.	Stdev.	Avg.	Stdev.	Avg.	Stdev.	Avg.	Stdev.
Brain (nM)	0.0	0.0	0.0	0.0	0.0	0.0	0.0	0.0
Blood (nM)	0.0	0.0	0.0	0.0	0.0	0.0	0.4	0.8
Lung (nM)	0.0	0.0	0.4	0.4	0.0	0.0	0.7	1.1
Kidney (nM)	0.0	0.0	0.2	0.1	0.0	0.0	3.0	5.5
Urine (nM)	0.0	0.0	1.6	1.7	0.0	0.0	3.8	1.5
Spleen (nM)	0.0	0.0	0.0	0.0	0.0	0.0	0.0	0.0
Liver (nM)	0.0	0.0	5.3	2.1	0.0	0.0	21.2	15.8
Duodenum (nM)	0.0	0.0	130.5	119.4	0.0	0.0	57.8	71.2
Jejunum (nM)	0.0	0.0	105.7	51.3	0.0	0.0	45.4	37.2
Ileum (nM)	0.0	0.0	162.1	137.8	0.0	0.0	106.8	30.3
Large Intestine (nM)	0.0	0.0	1012.2	328.3	0.0	0.0	1068.2	846.5

Feces Day 4 (μM)	0.0	0.0	144.1	54.1	0.0	0.00	113.9	29.0
Feces Day 7 (μM)	0.00	0.0	154.9	70.8	0.0	0.0	95.5	32.2
d_7-COOH BAC C16								
	Male				Female			
	d_7-C12-BAC		d_7-C16-BAC		d_7-C12-BAC		d_7-C16-BAC	
	Avg.	Stdev.	Avg.	Stdev.	Avg.	Stdev.	Avg.	Stdev.
Brain (nM)	0.0	0.0	0.0	0.0	0.0	0.0	0.00	0.00
Blood (nM)	0.0	0.0	0.8	0.2	0.0	0.0	2.7	4.7
Lung (nM)	0.0	0.0	4.5	3.4	0.0	0.0	5.2	7.4
Kidney (nM)	0.0	0.0	1.1	0.4	0.0	0.0	11.2	20.5
Urine (nM)	0.0	0.0	0.5	0.5	0.0	0.0	3.4	2.6
Spleen (nM)	0.0	0.0	0.7	0.8	0.0	0.0	0.9	1.8
Liver (nM)	0.0	0.0	12.9	5.4	0.0	0.0	36.4	19.9
Duodenum (nM)	0.0	0.0	1154.0	950.1	0.0	0.0	594.6	722.4
Jejunum (nM)	0.0	0.0	840.9	261.6	0.0	0.0	214.3	201.5
Ileum (nM)	0.0	0.0	1252.6	835.7	0.0	0.0	866.7	206.4
Large Intestine (nM)	0.0	0.0	8314.6	1463.8	0.0	0.0	7444.3	4282.0

Feces Day 4 (μM)	0.0	0.0	1721.7	562.2	0.0	0.0	1280.4	344881.41
Feces Day 7 (μM)	0.0	0.0	1791.5	794.3	0.0	0.0	1000.9	344.4

Table 3.6 Odd-Numbered Beta-Oxidation Product Levels in Isolated Biological Samples from BAC-exposed Male and Female C57BL/6 mice.

d_7-COOH BAC C7								
	Male				Female			
	d_7-C12-BAC		d_7-C16-BAC		d_7-C12-BAC		d_7-C16-BAC	
	Avg.	Stdev.	Avg.	Stdev.	Avg.	Stdev.	Avg.	Stdev.
Brain (nM)	0.0	0.0	0.0	0.0	0.0	0.0	0.0	0.0
Blood (nM)	0.5	0.1	0.2	0.1	0.0	0.0	0.0	0.0
Lung (nM)	1.7	1.3	0.0	0.0	0.1	0.3	0.0	0.0
Kidney (nM)	0.9	1.1	0.0	0.0	2.2	0.9	0.2	0.5
Urine (nM)	607.0	695.9	203.9	217.2	531.0	226.6	167.9	75.0
Spleen (nM)	0.0	0.0	0.0	0.0	0.0	0.0	0.0	0.0
Liver (nM)	5.4	1.3	1.5	0.7	3.7	1.6	2.1	0.6
Duodenum (nM)	3.5	2.5	1.1	0.6	3.0	1.4	1.2	0.5
Jejunum (nM)	4.0	2.8	1.7	0.7	2.2	1.3	1.0	0.2
Ileum (nM)	1.0	1.1	0.4	0.1	1.3	0.9	0.3	0.1
Large Intestine (nM)	4.7	1.9	1.8	1.4	5.9	5.1	2.9	3.0

Feces Day 4 (nM)	330.1	68.5	138.8	51.0	312.6	46.8	198.9	98.6
Feces Day 7 (nM)	323.6	145.2	144.4	22.1	392.6	135.3	186.5	68.9
d_7-COOH BAC C9								
	Male				Female			
	d_7-C12-BAC		d_7-C16-BAC		d_7-C12-BAC		d_7-C16-BAC	
	Avg.	Stdev.	Avg.	Stdev.	Avg.	Stdev.	Avg.	Stdev.
Brain (nM)	0.0	0.0	0.0	0.0	0.0	0.0	0.0	0.0
Blood (nM)	1.0	0.2	0.2	0.1	0.6	0.1	0.0	0.0
Lung (nM)	1.0	0.6	0.0	0.0	0.4	0.2	0.0	0.0
Kidney (nM)	1.2	0.3	0.0	0.0	2.6	1.6	0.3	0.6
Urine (nM)	1791.4	2054.7	431.5	495.3	2917.0	787.0	575.4	271.8
Spleen (nM)	0.0	0.0	0.0	0.0	0.0	0.0	0.0	0.0
Liver (nM)	11.1	1.9	1.8	0.4	6.6	2.9	1.2	0.8
Duodenum (nM)	11.3	13.5	1.6	1.8	8.3	6.9	0.8	1.4
Jejunum (nM)	18.8	20.5	2.6	2.3	7.2	10.3	0.6	0.4
Ileum (nM)	8.3	9.3	1.2	0.6	8.6	6.0	0.7	0.6
Large Intestine (nM)	40.2	17.8	5.6	4.5	57.1	63.5	7.0	8.2

Feces Day 4 (μM)	30.4	7.3	2.8	1.6	18.0	3.0	1.5	0.7
Feces Day 7 (μM)	35.7	24.6	3.1	0.7	21.4	7.7	1.5	0.8
d_7-COOH BAC C11								
	Male				Female			
	d_7-C12-BAC		d_7-C16-BAC		d_7-C12-BAC		d_7-C16-BAC	
	Avg.	Stdev.	Avg.	Stdev.	Avg.	Stdev.	Avg.	Stdev.
Brain (nM)	0.0	0.0	0.0	0.0	0.0	0.0	0.0	0.0
Blood (nM)	0.0	0.0	0.0	0.0	0.0	0.0	0.0	0.0
Lung (nM)	0.5	0.6	0.0	0.0	1.4	1.7	0.0	0.0
Kidney (nM)	0.3	0.8	0.0	0.0	1.8	2.8	0.1	0.3
Urine (nM)	3.5	3.4	0.2	0.4	287.2	257.2	48.7	81.2
Spleen (nM)	0.0	0.0	0.0	0.0	0.0	0.0	0.0	0.0
Liver (nM)	4.0	0.8	0.1	0.2	0.6	0.9	1.0	1.6
Duodenum (nM)	54.5	63.3	1.7	1.8	40.5	49.0	0.9	1.3
Jejunum (nM)	84.5	85.1	2.4	2.3	47.3	74.0	0.7	0.6
Ileum (nM)	52.5	41.7	1.4	0.8	45.6	29.3	0.7	0.4
Large Intestine (nM)	360.3	94.2	7.3	5.0	483.1	420.2	10.8	13.2

Feces Day 4 (μM)	70.2	9.9	3.1	1.5	62.3	7189.46	3421.83	2015.63
Feces Day 7 (μM)	65.0	24.4	3.6	1.2	72.9	24.3	3.0	2.2
d_7-COOH BAC C13								
	Male				Female			
	d_7-C12-BAC		d_7-C16-BAC		d_7-C12-BAC		d_7-C16-BAC	
	Avg.	Stdev.	Avg.	Stdev.	Avg.	Stdev.	Avg.	Stdev.
Brain (nM)	0.0	0.0	0.0	0.0	0.0	0.0	0.0	0.0
Blood (nM)	0.0	0.0	0.0	0.0	0.0	0.0	0.0	0.0
Lung (nM)	0.0	0.0	0.0	0.0	0.0	0.0	0.0	0.0
Kidney (nM)	0.0	0.0	0.0	0.0	0.0	0.0	0.2	0.4
Urine (nM)	0.0	0.0	0.2	0.4	0.0	0.0	2.2	2.0
Spleen (nM)	0.0	0.0	0.0	0.0	0.0	0.0	0.0	0.0
Liver (nM)	0.0	0.0	0.3	0.4	0.0	0.0	1.5	1.2
Duodenum (nM)	0.0	0.0	5.8	5.2	0.0	0.0	2.5	3.1
Jejunum (nM)	0.0	0.0	4.3	2.8	0.0	0.0	2.1	1.6
Ileum (nM)	0.0	0.0	5.0	4.4	0.0	0.0	3.0	1.2
Large Intestine (nM)	0.0	0.0	32.2	16.6	0.0	0.0	50.7	61.3

Feces Day 4 (nM)	0.0	0.0	12482.8	4633.3	0.0	0.0	10479.9	3516.4
Feces Day 7 (nM)	0.0	0.0	14016.9	5754.7	0.0	0.0	8657.1	4355.3
d_7-COOH BAC C15								
	Male				Female			
	d_7-C12-BAC		d_7-C16-BAC		d_7-C12-BAC		d_7-C16-BAC	
	Avg.	Stdev.	Avg.	Stdev.	Avg.	Stdev.	Avg.	Stdev.
Brain (nM)	0.0	0.0	0.0	0.0	0.0	0.0	0.0	0.0
Blood (nM)	0.0	0.0	0.0	0.0	0.0	0.0	0.0	0.0
Lung (nM)	0.0	0.0	0.0	0.0	0.0	0.0	0.0	0.0
Kidney (nM)	0.0	0.0	0.0	0.0	0.0	0.0	0.2	0.5
Urine (nM)	0.0	0.0	0.0	0.0	0.0	0.0	0.0	0.0
Spleen (nM)	0.0	0.0	0.0	0.0	0.0	0.0	0.0	0.0
Liver (nM)	0.0	0.0	0.4	0.4	0.0	0.0	1.3	0.9
Duodenum (nM)	0.0	0.0	23.6	23.3	0.0	0.0	9.1	12.3
Jejunum (nM)	0.0	0.0	14.2	5.3	0.0	0.0	34.0	3.6
Ileum (nM)	0.0	0.0	25.1	22.3	0.0	0.0	14.4	5.1
Large Intestine (nM)	0.0	0.0	229.3	58.5	0.0	0.0	215.2	208.0

Feces Day 4 (μM)	0.0	0.0	205.1	73.5	0.0	0.0	140.0	42.6
Feces Day 7 (μM)	0.00	0.00	229.1	114.4	0.0	0.0	108.0	49.0

Table 3.2 Parent BAC and Metabolite Avg. and Stdev. in Female Heart.

Table 3.2 Parent BAC and Metabolite Avg. and Stdev. (nM)						
d_7-C12-BAC	Control		d_7-C12-BAC		d_7-C16-BAC	
	0.00	0.00	71.32	146.78	0.00	0.00
d_7-C16-BAC	0.00	0.00	0.00	0.00	113.83	54.32
ω-1 OH C12	0.00	0.00	1.42	2.86	0.00	0.00
ω -OH C12	0.00	0.00	0.29	0.60	0.00	0.00
ω -1 OH C16	0.00	0.00	0.00	0.00	1.86	1.30
ω -OH C16	0.00	0.00	0.00	0.00	15.31	10.95
d_7-COOH BAC C6	0.00	0.00	0.52	0.85	3.22	2.48
d_7-COOH BAC C7	0.00	0.00	0.00	0.00	0.43	0.44
d_7-COOH BAC C8	0.00	0.00	1.96	1.00	3.25	2.36
d_7-COOH BAC C9	0.00	0.00	0.00	0.00	0.00	0.00
d_7-COOH BAC C10	0.00	0.00	0.76	1.85	0.13	0.30
d_7-COOH BAC C11	0.00	0.00	0.09	0.22	0.00	0.00
d_7-COOH BAC C12	0.00	0.00	0.13	0.32	0.13	0.18
d_7-COOH BAC C13	0.00	0.00	0.00	0.00	0.00	0.00
d_7-COOH BAC C14	0.00	0.00	0.00	0.00	0.18	0.25
d_7-COOH BAC C15	0.00	0.00	0.00	0.00	0.00	0.00
d_7-COOH BAC C16	0.00	0.00	0.00	0.00	2.36	2.09

Chapter 3 References

Abraham, K. *et al.* (2002) Severe 2,3,7,8-tetrachlorodibenzo- *p* -dioxin (TCDD) intoxication: Insights into the measurement of hepatic cytochrome P450 1A2 induction*. *Clin. Pharmacol. Ther.*, **72**, 163–174.

Ahlawat, S. *et al.* (2021) Gut–organ axis: a microbial outreach and networking. *Lett. Appl. Microbiol.*, **72**, 636–668.

Arnold, W.A. *et al.* (2023) Quaternary Ammonium Compounds: A Chemical Class of Emerging Concern. *Environ. Sci. Technol.*

Asgharpour, A. *et al.* (2015) Bile acids: emerging role in management of liver diseases. *Hepatol. Int.*, **9**, 527–533.

Barko, P.C. *et al.* (2018) The Gastrointestinal Microbiome: A Review. *J. Vet. Intern. Med.*, **32**, 9–25.

Baudouin, C. *et al.* (1999) Ocular surface inflammatory changes induced by topical antiglaucoma drugs: human and animal studies. *Ophthalmology*, **106**, 556–63.

Bhattacharya, A. *et al.* (2023) In vivo mouse models to study bile acid synthesis and signaling. *Hepatobiliary Pancreat. Dis. Int.*, **22**, 466–473.

Bond, P. (2017) Phosphatidic acid: biosynthesis, pharmacokinetics, mechanisms of action and effect on strength and body composition in resistance-trained individuals. *Nutr. Metab.*, **14**, 12.

Boursier, J. and Diehl, A.M. (2015) Implication of Gut Microbiota in Nonalcoholic Fatty Liver Disease. *PLOS Pathog.*, **11**, e1004559.

Breton, J. *et al.* (2013) Ecotoxicology inside the gut: impact of heavy metals on the mouse microbiome. *BMC Pharmacol. Toxicol.*, **14**, 62.

Caporaso, J.G. *et al.* (2010) QIIME allows analysis of high-throughput community sequencing data. *Nat Methods*, **7**, 335–6.

Chen, M. *et al.* (2021) Enterohepatic circulation of bile acids and their emerging roles on glucolipid metabolism. *Steroids*, **165**, 108757.

Chew, J.L. and Chua, K.Y. (2003) Collection of Mouse Urine for Bioassays. *Lab Anim.*, **32**, 48–50.

Chiang, H.-L. and Lin, C.-H. (2019) Altered Gut Microbiome and Intestinal Pathology in Parkinson's Disease. *J. Mov. Disord.*, **12**, 67–83.

Chiang, J.Y. *et al.* (2000) Farnesoid X receptor responds to bile acids and represses cholesterol 7alpha-hydroxylase gene (CYP7A1) transcription. *J Biol Chem*, **275**, 10918–24.

Chiang, J.Y.L. *et al.* (2001) Regulation of cholesterol 7α-hydroxylase gene (CYP7A1) transcription by the liver orphan receptor (LXRα). *Gene*, **262**, 257–265.

Chiang, J.Y.L. and Ferrell, J.M. (2018) Bile Acid Metabolism in Liver Pathobiology. *Gene Expr.*, **18**, 71–87.

Chiu, K. *et al.* (2020) The Impact of Environmental Chemicals on the Gut Microbiome. *Toxicol. Sci.*, **176**, 253–284.

Chow, M.D. *et al.* (2017) The role of bile acids in nonalcoholic fatty liver disease and nonalcoholic steatohepatitis. *Mol. Aspects Med.*, **56**, 34–44.

Claus, S.P. *et al.* (2016) The gut microbiota: a major player in the toxicity of environmental pollutants? *Npj Biofilms Microbiomes*, **2**, 16003.

Clayton, P.T. (1998) Disorders of cholesterol biosynthesis. *Arch Child*, **78**, 185–9.

Cryle, M.J. and De Voss, J.J. (2004) Carbon–carbon bond cleavage by cytochrome P450 $_{BioI}$ (CYP107H1). *Chem Commun*, 86–87.

Cui, J.Y. and Klaassen, C.D. (2016) RNA-Seq reveals common and unique PXR- and CAR-target gene signatures in the mouse liver transcriptome. *Biochim Biophys Acta*, **1859**, 1198–1217.

Dalhat, M.H. *et al.* (2022) NAT10: An RNA cytidine transferase regulates fatty acid metabolism in cancer cells. *Clin. Transl. Med.*, **12**, e1045.

Deutschle, T. *et al.* (2006) In vitro genotoxicity and cytotoxicity of benzalkonium chloride. *Toxicol. In Vitro*, **20**, 1472–1477.

Di Ciaula, A. *et al.* (2020) Liver Steatosis, Gut-Liver Axis, Microbiome and Environmental Factors. A Never-Ending Bidirectional Cross-Talk. *J. Clin. Med.*, **9**, 2648.

Edson, K. and Rettie, A. (2013) CYP4 Enzymes As Potential Drug Targets: Focus on Enzyme Multiplicity, Inducers and Inhibitors, and Therapeutic Modulation of 20-Hydroxyeicosatetraenoic Acid (20-HETE) Synthase and Fatty Acid ω-Hydroxylase Activities. *Curr. Top. Med. Chem.*, **13**, 1429–1440.

Edson, K. Z. *et al.* (2013) Cytochrome P450-dependent catabolism of vitamin K: omega-hydroxylation catalyzed by human CYP4F2 and CYP4F11. *Biochemistry*, **52**, 8276–85.

Edson, Katheryne Z. *et al.* (2013) Cytochrome P450-Dependent Catabolism of Vitamin K: ω-Hydroxylation Catalyzed by Human CYP4F2 and CYP4F11. *Biochemistry*, **52**, 8276–8285.

Eloe-Fadrosh, E.A. and Rasko, D.A. (2013) The human microbiome: from symbiosis to pathogenesis. *Annu Rev Med*, **64**, 145–63.

Esteves, F. *et al.* (2021) The Central Role of Cytochrome P450 in Xenobiotic Metabolism—A Brief Review on a Fascinating Enzyme Family. *J. Xenobiotics*, **11**, 94–114.

Fan, Y. and Pedersen, O. (2021) Gut microbiota in human metabolic health and disease. *Nat Rev Microbiol*, **19**, 55–71.

Fazeli, M. *et al.* (2011) Cadmium chloride exhibits a profound toxic effect on bacterial microflora of the mice gastrointestinal tract. *Hum. Exp. Toxicol.*, **30**, 152–159.

Feng, D. *et al.* (2020) Bisphenol A exposure induces gut microbiota dysbiosis and consequent activation of gut-liver axis leading to hepatic steatosis in CD-1 mice. *Environ. Pollut.*, **265**, 114880.

Finkelstein, J. *et al.* (2014) Lipids in health and disease. *Nature*, **510**, 47–47.

Fleishman, J.S. and Kumar, S. (2024) Bile acid metabolism and signaling in health and disease: molecular mechanisms and therapeutic targets. *Signal Transduct. Target. Ther.*, **9**, 97.

Fu, Z.D. *et al.* (2017) RNA-Seq Profiling of Intestinal Expression of Xenobiotic Processing Genes in Germ-Free Mice. *Drug Metab Dispos*, **45**, 1225–1238.

Fuchs, C.D. and Trauner, M. (2022) Role of bile acids and their receptors in gastrointestinal and hepatic pathophysiology. *Nat. Rev. Gastroenterol. Hepatol.*, **19**, 432–450.

Ghazalpour, A. *et al.* (2016) Expanding role of gut microbiota in lipid metabolism. *Curr Opin Lipidol*, **27**, 141–7.

Goldstein, J.L. *et al.* (2006) Protein sensors for membrane sterols. *Cell*, **124**, 35–46.

Gonzalez, M. *et al.* (2014) Asthma among workers in healthcare settings: role of disinfection with quaternary ammonium compounds. *Clin. Exp. Allergy*, **44**, 393–406.

Goodwin, B. *et al.* (2000a) A Regulatory Cascade of the Nuclear Receptors FXR, SHP-1, and LRH-1 Represses Bile Acid Biosynthesis. *Mol. Cell*, **6**, 517–526.

Goodwin, B. *et al.* (2000b) A Regulatory Cascade of the Nuclear Receptors FXR, SHP-1, and LRH-1 Represses Bile Acid Biosynthesis. *Mol. Cell*, **6**, 517–526.

Grangeon, A. *et al.* (2021) Determination of CYP450 Expression Levels in the Human Small Intestine by Mass Spectrometry-Based Targeted Proteomics. *Int. J. Mol. Sci.*, **22**, 12791.

Guengerich, F.P. and Yoshimoto, F.K. (2018) Formation and Cleavage of C–C Bonds by Enzymatic Oxidation–Reduction Reactions. *Chem. Rev.*, **118**, 6573–6655.

Hakkola, J. *et al.* (2020) Inhibition and induction of CYP enzymes in humans: an update. *Arch. Toxicol.*, **94**, 3671–3722.

Herron, J. *et al.* (2018) Assessment of Altered Cholesterol Homeostasis by Xenobiotics Using Ultra-High Performance Liquid Chromatography-Tandem Mass Spectrometry. *Curr Protoc Toxicol*, **78**, e65.

Herron, J. *et al.* (2016) Identification of Environmental Quaternary Ammonium Compounds as Direct Inhibitors of Cholesterol Biosynthesis. *Toxicol Sci*, **151**, 261–270.

Herron, J.M. *et al.* (2019) Multiomics investigation reveals benzalkonium chloride disinfectants alter sterol and lipid homeostasis in the mouse neonatal brain. *Toxicol Sci*, **171**, 32–45.

Hild, B. *et al.* (2021) Bile Acids in Control of the Gut-Liver-Axis. *Z. Für Gastroenterol.*, **59**, 63–68.

Hills, R. *et al.* (2019) Gut Microbiome: Profound Implications for Diet and Disease. *Nutrients*, **11**, 1613.

Hines, K. *et al.* (2017) Assessment of Altered Lipid Homeostasis by HILIC-Ion Mobility-Mass Spectrometry-Based Lipidomics. *J Lipid Res*, **58**, 809–819.

Hines, K.M. *et al.* (2016) Evaluation of Collision Cross Section Calibrants for Structural Analysis of Lipids by Traveling Wave Ion Mobility-Mass Spectrometry. *Anal Chem*, **88**, 7329–36.

Hirani, V. *et al.* (2008) Expression of CYP4F2 in human liver and kidney: Assessment using targeted peptide antibodies. *Arch. Biochem. Biophys.*, **478**, 59–68.

Hitosugi, M. *et al.* (1998) A case of fatal benzalkonium chloride poisoning. *Int J Leg. Med*, **111**, 265–6.

Hofmann, A.F. (1999) The Continuing Importance of Bile Acids in Liver and Intestinal Disease. *Arch. Intern. Med.*, **159**, 2647.

Holter, M.M. *et al.* (2020) TGR5 Signaling in Hepatic Metabolic Health. *Nutrients*, **12**, 2598.

Hrubec, T.C. *et al.* (2021a) Altered toxicological endpoints in humans from common quaternary ammonium compound disinfectant exposure. *Toxicol Rep*, **8**, 646–656.

Hrubec, T.C. *et al.* (2021b) Altered toxicological endpoints in humans from common quaternary ammonium compound disinfectant exposure. *Toxicol Rep*, **8**, 646–656.

Hrubec, T.C. *et al.* (2017) Ambient and Dosed Exposure to Quaternary Ammonium Disinfectants Causes Neural Tube Defects in Rodents. *Birth Defects Res*, **109**, 1166–1178.

Hrycay, E. and Bandiera, S. (2009) Expression, Function and Regulation of Mouse Cytochrome P450 Enzymes: Comparison With Human Cytochrome P450 Enzymes. *Curr. Drug Metab.*, **10**, 1151–1183.

Hukkanen, J. *et al.* (2002) Expression and Regulation of Xenobiotic-Metabolizing Cytochrome P450 (CYP) Enzymes in Human Lung. *Crit. Rev. Toxicol.*, **32**, 391–411.

Jaeschke, H. (2015) Toxic Responses of the Liver. In, Klaassen,C.D. and Watkins III,J.B. (eds), *Casarett & Doull's Essentials of Toxicology, 3e*. McGraw-Hill Education, New York, NY.

Jiang, L. *et al.* (2021) Farnesoid X receptor (FXR): Structures and ligands. *Comput. Struct. Biotechnol. J.*, **19**, 2148–2159.

Johnson, A.L. *et al.* (2015) Cytochrome P450 omega-Hydroxylases in Inflammation and Cancer. *Adv Pharmacol*, **74**, 223–62.

Johnson, E.L. *et al.* (2020) Sphingolipids produced by gut bacteria enter host metabolic pathways impacting ceramide levels. *Nat Commun*, **11**, 2471.

Kapelyukh, Y. *et al.* (2019) Defining the Contribution of CYP1A1 and CYP1A2 to Drug Metabolism Using Humanized CYP1A1/1A2 and Cyp1a1/Cyp1a2 Knockout Mice. *Drug Metab. Dispos.*, **47**, 907–918.

Kera, H. *et al.* (2021) Kinetics and distribution of benzalkonium compounds with different alkyl chain length following intravenous administration in rats. *Leg. Med.*, **48**, 101821.

Kim, Y.S. *et al.* (2020) Sex Differences in Gut Microbiota. *World J. Mens Health*, **38**, 48.

Klyushova, L.S. *et al.* (2022) The Role of CYP3A in Health and Disease. *Biomedicines*, **10**, 2686.

Kojima, R. *et al.* (2016) A phospholipid transfer function of ER-mitochondria encounter structure revealed in vitro. *Sci. Rep.*, **6**, 30777.

Koliada, A. *et al.* (2021) Sex differences in the phylum-level human gut microbiota composition. *BMC Microbiol.*, **21**, 131.

Koontz, J.M. *et al.* (2019) The Role of the Human Microbiome in Chemical Toxicity. *Int. J. Toxicol.*, **38**, 251–264.

Kröckel, L. *et al.* (2003) Identification of benzalkonium chloride in food additives and its inefficacy against bacteria in minced meat and raw sausage batters. *Eur. Food Res. Technol.*, **216**, 402–406.

Kuban, W. and Daniel, W.A. (2021) Cytochrome P450 expression and regulation in the brain. *Drug Metab. Rev.*, **53**, 1–29.

Kwon, Y.-J. *et al.* (2021) Biological roles of cytochrome P450 1A1, 1A2, and 1B1 enzymes. *Arch. Pharm. Res.*, **44**, 63–83.

Lee, B.H. and Kim, S.H. (2007) Benzalkonium chloride induced bronchoconstriction in patients with stable bronchial asthma. *Korean J Intern Med*, **22**, 244–8.

Lee, H. and Park, K. (2019) Acute toxicity of benzalkonium chloride in Balb/c mice following intratracheal instillation and oral administration. *Environ. Anal. Health Toxicol.*, **34**, e2019009.

Levy, M. *et al.* (2017) Microbiome, metabolites and host immunity. *Curr. Opin. Microbiol.*, **35**, 8–15.

Li, A. *et al.* (2020) Lipidomics by HILIC-Ion Mobility-Mass Spectrometry. *Methods Mol. Biol.*, **2084**, 119–132.

Li, C. Y. *et al.* (2018) PBDEs Altered Gut Microbiome and Bile Acid Homeostasis in Male C57BL/6 Mice. *Drug Metab Dispos*, **46**, 1226–1240.

Li, Cindy Yanfei *et al.* (2018) PBDEs Altered Gut Microbiome and Bile Acid Homeostasis in Male C57BL/6 Mice. *Drug Metab. Dispos.*, **46**, 1226–1240.

Li, D. *et al.* (2020) Evaluating consumer exposure to disinfecting chemicals against coronavirus disease 2019 (COVID-19) and associated health risks. *Env. Int*, **145**, 106108.

Li, S. *et al.* (2021) Cytochrome P450 Omega-Hydroxylase 4a14 Attenuates Cholestatic Liver Fibrosis. *Front. Physiol.*, **12**, 688259.

Li, T. and Chiang, J.Y.L. (2012) Bile Acid Signaling in Liver Metabolism and Diseases. *J. Lipids*, **2012**, 1–9.

Liao, Y. *et al.* (2014) featureCounts: an efficient general purpose program for assigning sequence reads to genomic features. *Bioinformatics*, **30**, 923–930.

Liu, X. *et al.* (2021) *Blautia* —a new functional genus with potential probiotic properties? *Gut Microbes*, **13**, 1875796.

Liu, Y. *et al.* (2020) The Dysbiosis of Gut Microbiota Caused by Low-Dose Cadmium Aggravate the Injury of Mice Liver through Increasing Intestinal Permeability. *Microorganisms*, **8**, 211.

Lopez, V.A. *et al.* (2024) Oral Exposure to Benzalkonium Chlorides in Male and Female Mice Reveals Sex-Dependent Alteration of the Gut Microbiome and Bile Acid Profile. *bioRxiv*, 2024.05.13.593991.

Love, M.I. *et al.* (2014) Moderated estimation of fold change and dispersion for RNA-seq data with DESeq2. *Genome Biol*, **15**, 550.

Lu, J. *et al.* (2020) New insights of CYP1A in endogenous metabolism: a focus on single nucleotide polymorphisms and diseases. *Acta Pharm. Sin. B*, **10**, 91–104.

Lu, K. *et al.* (2014) Arsenic Exposure Perturbs the Gut Microbiome and Its Metabolic Profile in Mice: An Integrated Metagenomics and Metabolomics Analysis. *Environ. Health Perspect.*, **122**, 284–291.

Luz, A. *et al.* (2020) Human health hazard assessment of quaternary ammonium compounds: Didecyl dimethyl ammonium chloride and alkyl (C12-C16) dimethyl benzyl ammonium chloride. *Regul Toxicol Pharmacol*, **116**, 104717.

Manor, O. *et al.* (2020) Health and disease markers correlate with gut microbiome composition across thousands of people. *Nat. Commun.*, **11**, 5206.

Manos, J. (2022) The human microbiome in disease and pathology. *APMIS*, **130**, 690–705.

Melin, V.E. *et al.* (2014) Exposure to common quaternary ammonium disinfectants decreases fertility in mice. *Reprod Toxicol*, **50**, 163–70.

Melin, V.E. *et al.* (2016) Quaternary ammonium disinfectants cause subfertility in mice by targeting both male and female reproductive processes. *Reprod Toxicol*, **59**, 159–66.

Merchel Piovesan Pereira, B. and Tagkopoulos, I. (2019) Benzalkonium Chlorides: Uses, Regulatory Status, and Microbial Resistance. *Appl. Environ. Microbiol.*, **85**, e00377-19.

Mertens, K.L. *et al.* (2017) Bile Acid Signaling Pathways from the Enterohepatic Circulation to the Central Nervous System. *Front. Neurosci.*, **11**, 617.

Minchin, R.F. *et al.* (2007) Arylamine N-acetyltransferase I. *Int. J. Biochem. Cell Biol.*, **39**, 1999–2005.

Mishima-Kimura, S. *et al.* (2018) Liquid chromatography-tandem mass spectrometry detection of benzalkonium chloride (BZK) in a forensic autopsy case with survival for 18 days post BZK ingestion. *Leg Med Tokyo*, **32**, 48–51.

Mohapatra, S. *et al.* (2023) Quaternary ammonium compounds of emerging concern: Classification, occurrence, fate, toxicity and antimicrobial resistance. *J. Hazard. Mater.*, **445**, 130393.

Molinero, N. *et al.* (2019) Intestinal Bacteria Interplay With Bile and Cholesterol Metabolism: Implications on Host Physiology. *Front Physiol*, **10**, 185.

Monte, M.J. *et al.* (2009) Bile acids: Chemistry, physiology, and pathophysiology. *World J. Gastroenterol.*, **15**, 804.

Naspolini, N.F. *et al.* (2022) Environmental pollutant exposure associated with altered early-life gut microbiome: Results from a birth cohort study. *Environ. Res.*, **205**, 112545.

Nguyen, R. *et al.* (2024) Development and Application of a Multidimensional Database for the Detection of Quaternary Ammonium Compounds and Their Phase I Hepatic Metabolites in Humans. *Environ. Sci. Technol.*, **58**, 6236–6249.

O'Flaherty, S. *et al.* (2018) The *Lactobacillus* Bile Salt Hydrolase Repertoire Reveals Niche-Specific Adaptation. *mSphere*, **3**, e00140-18.

Okita, R.T. *et al.* (1979) Lauric acid hydroxylation in human liver and kidney cortex microsomes. *Biochem. Pharmacol.*, **28**, 3385–3390.

Patterson, A.D. *et al.* (2010) Xenobiotic Metabolism: A View through the Metabolometer. *Chem. Res. Toxicol.*, **23**, 851–860.

Petriello, M.C. *et al.* (2018) Dioxin-like PCB 126 increases intestinal inflammation and disrupts gut microbiota and metabolic homeostasis. *Environ. Pollut.*, **242**, 1022–1032.

Phelps, T. *et al.* (2019) The influence of biological sex and sex hormones on bile acid synthesis and cholesterol homeostasis. *Biol. Sex Differ.*, **10**, 52.

Phillips, I.R. and Shephard, E.A. (2017) Drug metabolism by flavin-containing monooxygenases of human and mouse. *Expert Opin. Drug Metab. Toxicol.*, **13**, 167–181.

Pradista, L.A. *et al.* (2022) Metagenomic analysis of non-pathogenic and pathogenic cecal bacteria profiles in quail supplemented with betaine. *IOP Conf. Ser. Earth Environ. Sci.*, **1114**, 012008.

Prysyazhnyuk, V. *et al.* (2021) Glutathione-S-transferases genes-promising predictors of hepatic dysfunction. *World J. Hepatol.*, **13**, 620–633.

Qin, X. and Wang, X. (2019) Role of vitamin D receptor in the regulation of CYP3A gene expression. *Acta Pharm. Sin. B*, **9**, 1087–1098.

Qiu, X. *et al.* (2016) Disruption of BSEP Function in HepaRG Cells Alters Bile Acid Disposition and Is a Susceptive Factor to Drug-Induced Cholestatic Injury. *Mol. Pharm.*, **13**, 1206–1216.

Rinninella, E. *et al.* (2019) What is the Healthy Gut Microbiota Composition? A Changing Ecosystem across Age, Environment, Diet, and Diseases. *Microorganisms*, **7**, 14.

Robinson, A.J. *et al.* (2017) Granular parakeratosis induced by benzalkonium chloride exposure from laundry rinse aids. *Australas J Dermatol*, **58**, e138–e140.

Röder, A. *et al.* (2023) Spotlight on CYP4B1. *Int. J. Mol. Sci.*, **24**, 2038.

Ross, D.H. *et al.* (2020) LiPydomics: A Python Package for Comprehensive Prediction of Lipid Collision Cross Sections and Retention Times and Analysis of Ion Mobility-Mass Spectrometry-Based Lipidomics Data. *Anal. Chem.*, **92**, 14967–14975.

Sarkar, J. *et al.* (2012) Corneal neurotoxicity due to topical benzalkonium chloride. *Invest Ophthalmol Vis Sci*, **53**, 1792–802.

Saxami, G. *et al.* (2023) The Gut–Organ Axis within the Human Body: Gut Dysbiosis and the Role of Prebiotics. *Life*, **13**, 2023.

Schneider, K.M. *et al.* (2018) Role of bile acids in the gut-liver axis. *J. Hepatol.*, **68**, 1083–1085.

Seebacher, F. *et al.* (2020) Hepatic lipid droplet homeostasis and fatty liver disease. *Semin. Cell Dev. Biol.*, **108**, 72–81.

Seguin, R. P. *et al.* (2019) Metabolism of Benzalkonium Chlorides by Human Hepatic Cytochromes P450. *Chem Res Toxicol*, **32**, 2466–2478.

Seguin, Ryan P. *et al.* (2019) Metabolism of Benzalkonium Chlorides by Human Hepatic Cytochromes P450. *Chem. Res. Toxicol.*, **32**, 2466–2478.

Selwyn, F.P., Cheng, S.L., *et al.* (2015) Developmental Regulation of Drug-Processing Genes in Livers of Germ-Free Mice. *Toxicol Sci*, **147**, 84–103.

Selwyn, F.P. *et al.* (2016) Regulation of Hepatic Drug-Metabolizing Enzymes in Germ-Free Mice by Conventionalization and Probiotics. *Drug Metab Dispos*, **44**, 262–74.

Selwyn, F.P., Cui, J.Y., *et al.* (2015) RNA-Seq Quantification of Hepatic Drug Processing Genes in Germ-Free Mice. *Drug Metab Dispos*, **43**, 1572–80.

Shulpekova, Y. *et al.* (2022) The Role of Bile Acids in the Human Body and in the Development of Diseases. *Molecules*, **27**, 3401.

Siddiqui, R. *et al.* (2022) The Gut Microbiome and Female Health. *Biology*, **11**, 1683.

Sim, E. *et al.* (2014) Arylamine N-acetyltransferases: from drug metabolism and pharmacogenetics to drug discovery. *Br. J. Pharmacol.*, **171**, 2705–2725.

Slimani, K. *et al.* (2017) Liquid chromatography-tandem mass spectrometry multiresidue method for the analysis of quaternary ammonium compounds in cheese and milk products: Development and validation using the total error approach. *J Chromatogr A*, **1517**, 86–96.

Sreevidya, V.S. *et al.* (2018) Benzalkonium chloride, benzethonium chloride, and chloroxylenol - Three replacement antimicrobials are more toxic than triclosan and triclocarban in two model organisms. *Environ. Pollut.*, **235**, 814–824.

Stellaard, F. and Lütjohann, D. (2021) Dynamics of the enterohepatic circulation of bile acids in healthy humans. *Am. J. Physiol.-Gastrointest. Liver Physiol.*, **321**, G55–G66.

Stok, J.E. and De Voss, J.J. (2000) Expression, Purification, and Characterization of BioI: A Carbon–Carbon Bond Cleaving Cytochrome P450 Involved in Biotin Biosynthesis in Bacillus subtilis. *Arch. Biochem. Biophys.*, **384**, 351–360.

Takahashi, S. *et al.* (2016) Cyp2c70 is responsible for the species difference in bile acid metabolism between mice and humans. *J. Lipid Res.*, **57**, 2130–2137.

Takeoka, G.R. *et al.* (2005) Identification of benzalkonium chloride in commercial grapefruit seed extracts. *J Agric Food Chem*, **53**, 7630–6.

Taylor, C. *et al.* (2020) A Review of the Important Role of CYP2D6 in Pharmacogenomics. *Genes*, **11**, 1295.

Ten Hove, M. *et al.* (2020) The hepatic lipidome: From basic science to clinical translation. *Adv. Drug Deliv. Rev.*, **159**, 180–197.

The Federal Institute for Risk Assessment (BfR) of Germany (2012) Health assessment of benzalkonium chloride residues in food. *BfR Opin. No 0322012*.

Thursby, E. and Juge, N. (2017) Introduction to the human gut microbiota. *Biochem. J.*, **474**, 1823–1836.

Tian, S. *et al.* (2022) FXR: structures, biology, and drug development for NASH and fibrosis diseases. *Acta Pharmacol. Sin.*, **43**, 1120–1132.

Trapani, L. (2012) Regulation and deregulation of cholesterol homeostasis: The liver as a metabolic "power station". *World J. Hepatol.*, **4**, 184.

Tripathi, A. *et al.* (2018) The gut-liver axis and the intersection with the microbiome. *Nat Rev Gastroenterol Hepatol*, **15**, 397–411.

Tripathi, Anupriya *et al.* (2018) The gut–liver axis and the intersection with the microbiome. *Nat. Rev. Gastroenterol. Hepatol.*, **15**, 397–411.

Tu, P. *et al.* (2020) Gut Microbiome Toxicity: Connecting the Environment and Gut Microbiome-Associated Diseases. *Toxics*, **8**, 19.

Turesky, R.J. and Lu, K. (2020) Biomarkers of Environmental Toxicants: Exposure and Biological Effects. *Toxics*, **8**, 37.

Umehara, K., Kudo, S., Hirao, Y., Morita, S., Ohtani, T., *et al.* (2000) In vitro characterization of the oxidative cleavage of the octyl side chain of olanexidine, a novel antimicrobial agent, in dog liver microsomes. *Drug Metab. Dispos. Biol. Fate Chem.*, **28**, 1417–1424.

Umehara, K., Kudo, S., Hirao, Y., Morita, S., Uchida, M., *et al.* (2000) Oxidative cleavage of the octyl side chain of 1-(3,4-dichlorobenzyl)-5-octylbiguanide (OPB-2045) in rat and dog liver preparations. *Drug Metab. Dispos. Biol. Fate Chem.*, **28**, 887–894.

Umehara, K. *et al.* (2004) Oxidative one-carbon cleavage of the octyl side chain of olanexidine, a novel antimicrobial agent, in dog liver microsomes. *Xenobiotica*, **34**, 61–71.

US EPA (2006) Reregistration Eligibility Decision for Alkyl Dimethyl Benzyl Ammonium Chloride (ADBAC). *EPA-HQ-OPP-2006-0339*, Office of Prevention, Pesticides and Toxic Substances, Antimicrobials Division, U.S. Environmental Protection Agency. Signed on August 3, 2006.

US FDA (2016a) Quaternary ammonium chloride combination. *Code Fed. Regul. 21CFR172165*, Food and Drug Administration, U.S. Department of Health&Human Services. Revised as of April 1, 2016.

US FDA (2016b) Safety and Effectiveness of Consumer Antiseptics; Topical Antimicrobial Drug Products for Over-the-Counter Human Use; Proposed Amendment of the Tentative Final Monograph; Reopening of Administrative Record. *Fed. Regist.*, **21 CFR Part 310, 81**, 42911–42937.

US FDA (2015) Safety and Effectiveness of Health Care Antiseptics; Topical Antimicrobial Drug Products for Over-the-Counter Human Use; Proposed Amendment of the Tentative

Final Monograph; Reopening of Administrative Record. *Fed. Regist.*, **21 CFR Part 310, 80**, 25165–25205.

Vassileva, G. *et al.* (2010) Gender-dependent effect of Gpbar1 genetic deletion on the metabolic profiles of diet-induced obese mice. *J. Endocrinol.*, **205**, 225–232.

Vázquez-Baeza, Y. *et al.* (2013) EMPeror: a tool for visualizing high-throughput microbial community data. *GigaScience*, **2**, 16.

Veiga-da-Cunha, M. *et al.* (2010) Molecular Identification of NAT8 as the Enzyme That Acetylates Cysteine S-Conjugates to Mercapturic Acids. *J. Biol. Chem.*, **285**, 18888–18898.

Vieira, L.S. *et al.* (2024) Interaction and Transport of Benzalkonium Chlorides by the Organic Cation and Multidrug and Toxin Extrusion Transporters. *Drug Metab. Dispos.*, **52**, 312–321.

Wang, B. and Tontonoz, P. (2018) Liver X receptors in lipid signalling and membrane homeostasis. *Nat. Rev. Endocrinol.*, **14**, 452–463.

Wang, R. *et al.* (2021) Gut microbiome, liver immunology, and liver diseases. *Cell. Mol. Immunol.*, **18**, 4–17.

Weakly, H.M.J. *et al.* (2024) Several common methods of making vesicles (except an emulsion method) capture intended lipid ratios. *bioRxiv*, 2024.02.21.581444.

Wu, G.D. and Lewis, J.D. (2013) Analysis of the Human Gut Microbiome and Association With Disease. *Clin. Gastroenterol. Hepatol.*, **11**, 774–777.

Xiong, Z.E. *et al.* (2020) Exposure to dibutyl phthalate impairs lipid metabolism and causes inflammation via disturbing microbiota-related gut–liver axis. *Acta Biochim. Biophys. Sin.*, **52**, 1382–1393.

Xue, Y. *et al.* (2004) Distribution and disposition of benzalkonium chloride following various routes of administration in rats. *Toxicol Lett*, **148**, 113–23.

Xue, Y. *et al.* (2002) Sensitive determination of benzalkonium chloride in blood and tissues using high-performance liquid chromatography with solid-phase extraction. *Leg Med Tokyo*, **4**, 232–8.

Yamashita, T. (2011) Glycosphingolipid Modification: Structural Diversity, Functional and Mechanistic Integration of Diabetes. *Diabetes Metab. J.*, **35**, 309.

Yoon, H. *et al.* (2021) Lipid metabolism in sickness and in health: Emerging regulators of lipotoxicity. *Mol. Cell*, **81**, 3708–3730.

Yoshimoto, F.K. *et al.* (2016) Isotope-Labeling Studies Support the Electrophilic Compound I Iron Active Species, FeO^{3+}, for the Carbon–Carbon Bond Cleavage Reaction of the Cholesterol Side-Chain Cleavage Enzyme, Cytochrome P450 11A1. *J. Am. Chem. Soc.*, **138**, 12124–12141.

Zhang, L. *et al.* (2015) Persistent Organic Pollutants Modify Gut Microbiota–Host Metabolic Homeostasis in Mice Through Aryl Hydrocarbon Receptor Activation. *Environ. Health Perspect.*, **123**, 679–688.

Zhang, R. *et al.* (2020) Dose-dependent benzalkonium chloride toxicity imparts ocular surface epithelial changes with features of dry eye disease. *Ocul. Surf.*, **18**, 158–169.

Zhang, S. *et al.* (2015) Subchronic Exposure of Mice to Cadmium Perturbs Their Hepatic Energy Metabolism and Gut Microbiome. *Chem. Res. Toxicol.*, **28**, 2000–2009.

Zhang, Y. and Klaassen, C.D. (2010) Effects of feeding bile acids and a bile acid sequestrant on hepatic bile acid composition in mice. *J Lipid Res*, **51**, 3230–42.

Zhao, Yueming *et al.* (2022) Alleviating effects of gut micro-ecologically regulatory treatments on mice with constipation. *Front. Microbiol.*, **13**, 956438.

Zheng, G. *et al.* (2020) Increased Indoor Exposure to Commonly Used Disinfectants during the COVID-19 Pandemic. *Environ. Sci. Technol. Lett.*, **7**, 760–765.

Zheng, G. *et al.* (2021a) Quaternary Ammonium Compounds: Bioaccumulation Potentials in Humans and Levels in Blood before and during the Covid-19 Pandemic. *Environ. Sci. Technol.*, **55**, 14689–14698.

Zheng, G. *et al.* (2021b) Quaternary Ammonium Compounds: Bioaccumulation Potentials in Humans and Levels in Blood before and during the Covid-19 Pandemic. *Environ. Sci. Technol.*, **55**, 14689–14698.

Zheng, G. *et al.* (2022) The first detection of quaternary ammonium compounds in breast milk: Implications for early-life exposure. *J. Expo. Sci. Environ. Epidemiol.*, **32**, 682–688.

Zhong, C.Y. *et al.* (2015) Microbiota prevents cholesterol loss from the body by regulating host gene expression in mice. *Sci Rep*, **5**, 10512.

Zhou, M. *et al.* (2023) Exploring human CYP4 enzymes: Physiological roles, function in diseases and focus on inhibitors. *Drug Discov. Today*, **28**, 103560.

Chapter 4 Multiomics Analysis of BAC Exposed Livers

4.1 Introduction

In **Chapter 2**, we depict oral BAC exposure at the same dosage (120 mg/kg/day for 1 week) led to decreased microbial diversity, altered microbiome composition, and decreased secondary BA formation. However, this work depicts the first multi-omics approach to understanding BAC toxicity in the liver following an oral BAC exposure paradigm. It is imperative to consider the liver as the major detoxifying organ, and the significant metabolite formation we observe in the liver (**Chapter 3**). Thus, we are motivated to study the impact of oral BAC exposure on endogenous and exogenous metabolism in the liver.

4.1.2 Cholesterol Biosynthesis: Importance in the Liver

The liver is the principal site for cholesterol homeostasis (Trapani, 2012). Cholesterol is imperative to human biology because of its role in various structural and metabolic responsibilities (Trapani, 2012). This is exemplified by increasing evidence that abnormal cholesterol metabolism is closely related to systemic diseases like cardiovascular disease, neurological conditions, immune system disorders, tumors, and eye diseases (Guo *et al.*, 2024).

Cholesterol biosynthesis starts with the conversion of acetyl-CoA to acetoacetyl-CoA, then to 3-hydroxy-3-methylglutaryl-CoA. Significantly, the reduction of 3-hydroxy-3-methylglutaru1-CoA to mevalonate by 3-hydroxy-3-methylglutaryl coenzyme reductase (HMGCR) represents the rate-limiting step within the cholesterol biosynthetic pathway (Trapani, 2012; Guo *et al.*, 2024; Duan *et al.*, 2022). Following the conversion of mevalonate to squalene, and then lanosterol, cholesterol biosynthesis is further divided into the Block and Kandutsh-Russell pathways, where enzymes 24-dehydrocholesterol reductase (DHCR24) and 7-dehydrocholesterol reductase (DHCR7) catalyze the last step of each respective pathway to produce cholesterol (Guo *et al.*,

2024). The cholesterol biosynthetic pathway is a highly energy-consuming process that is tightly regulated (Guo *et al.*, 2024; Duan *et al.*, 2022).

Proteins involved in cholesterol metabolism regulation, like HMGCR, are regulated by a group of transcription factors called sterol regulatory element binding proteins (SREBPs) (Trapani, 2012). SREBP cleavage activating protein (SCAP) is understood as the sterol sensor and interaction with the SREBP C-terminus in the ER. Thus, in cells with deprived sterol levels, SCAP binds SREBPs and escorts them from the ER to the Golgi apparatus, where part of SREBP is cleaved and translocated to the nucleus to induce the expression of target genes like HMCGR (Trapani, 2012). If intracellular sterol content is too high, cholesterol-bound SCAP will also bind to the insulin-induced gene protein (Insig), keeping the Insig/SCAP/SREBP complex in the ER and thus, blocking the upregulation of cholesterol biosynthesis-related genes (Trapani, 2012; Goldstein *et al.*, 2006). While almost all cells in the human body can produce cholesterol, only a few types cells are capable of metabolizing it (Guo *et al.*, 2024). Thus, maintenance of cholesterol homeostasis in cells is performed by exporting excess cholesterol transporting it to the liver, where it is metabolized, and then excreted (Guo *et al.*, 2024).

Various studies have highlighted BAC accumulation in the liver is possible following various BAC exposure methods (Xue *et al.*, 2002, 2004) (**Chapters 2 and 3**). Additionally, our lab has previously found BACs inhibit cholesterol biosynthesis in vitro and in neonatal mouse brains (Herron *et al.*, 2016, 2018, 2019). Thus, it is important to examine whether BACs are capable of disrupting the cholesterol biosynthetic pathway in the liver and thus affecting liver and systemic .

4.1.3 Lipid Synthesis in the Liver and Implications for Health

The lipidome is composed of a diverse consortium of individual molecular components that result in thousands of lipid species (Yoon *et al.*, 2021). Lipids are defined as complex molecules generated from simpler constituents through enzymatic reactions (Yoon *et al.*, 2021). T*he liver is a key site for lipid metabolism and plays a major role in the regulation of lipid distribution throughout the body* (Schwabe and Maher, 2012; Seebacher *et al.*, 2020; Ten Hove *et al.*, 2020). Every lipid consists of a head group with a unique chemical composition and fatty acids are esterified to glycerol backbone (giving glycerolipids and glycerophospholipids) or sphingoid bases (giving sphingolipids) (Yoon *et al.*, 2021). Lipid classes are defined by their lipid head groups, which contribute their unique biological functions (Yoon *et al.*, 2021). Lipids are recognized for their roles as building blocks of cellular membranes, energy storage, cellular signaling, and pre-cursors for hormones (Seebacher *et al.*, 2020).

Lipids are broadly categorized into fatty acids (FAs), phospholipids, sphingolipids or neutral lipids (triglycerides and cholesteryl esters) (Yoon *et al.*, 2021). FAs are defined as the building blocks of all lipids and are primers for the synthesis of glycerolipids, glycerophospholipids, and sphingolipids. Dysregulation of fatty acid metabolism has been observed in various disease states. Cellular and systemic lipid levels and their maintenance are imperative for physiological homeostasis (Wang and Tontonoz, 2018). Perturbations of lipid metabolism have been associated with various disease states like diabetes, cancer, steatosis, cirrhosis, hepatocellular carcinoma, atherosclerosis, and neurodegenerative diseases (Wang and Tontonoz, 2018; Ten Hove *et al.*, 2020). The accumulation of lipids in tissues has become increasingly recognized as a contributor to cellular dysfunction as excess lipids which causes lipotoxicity (Yoon *et al.*, 2021).Previous work has reported that BACs are capable of altering lipid

metabolism in neonatal mouse brains exposed in utero (Herron *et al.*, 2019). Thus, we aim to examine the potential of BACs in disrupting the liver lipidome, metabolism, and homeostasis.

4.1.4 The Liver and Drug Metabolizing Enzymes

Cytochrome (CYP) P450 enzymes are membrane-bound hemeproteins that play a significant role in the metabolism of foreign compounds (Esteves *et al.*, 2021). Within a human lifetime, we are exposed to 1-3 million various foreign compounds (Esteves *et al.*, 2021; Patterson *et al.*, 2010), and thus, effective detoxification and subsequent elimination of foreign compounds is critical in reducing toxic compound accumulation a process that interferes with cellular homeostasis and causes cellular and tissue damage (Esteves *et al.*, 2021). *Significantly, the liver is contains the highest concentrations of CYP enzymes, signifying its critical role in the detoxification of foreign compounds* (Esteves *et al.*, 2021).

The typical CYP-mediated monooxygenation reaction is defined by the incorporation of one oxygen atom into the substrate as defined ($RH + O_2 + 2e^- + 2H^+ \rightarrow ROH + H_2O$) (Esteves *et al.*, 2021), and thus CYPs can catalyze biotransformation reactions like aliphatic, aromatic, and N-hydroxylation, epoxidation, oxygenation, dehydrogenation, dehalogenation, and N-, O- and S-dealkylation (Esteves *et al.*, 2021)).

CYPs are involved in most of enzymatic reactions within the metabolism of xenobiotics (Esteves *et al.*, 2021). Up to 80% of all Phase I metabolism of clinically used drugs is carried out by 15 CYP isoforms in the CYP 1,2 or 3 families (Esteves *et al.*, 2021). Among the 15 isoforms, CYP1A2, CYP2C9, CYP2D6, and CYP3A4/5 account for 72% of all CYP-mediated metabolism of clinically marketed drugs. Importantly, members of the CYP4 family are recognized for their roles in ω-oxidation of endogenous fatty acids.

The metabolism of xenobiotics is dependent on Phase I and Phase II drug-metabolizing enzymes. While Phase I enzymes are substantially composed of the CYP superfamily, flavin-containing monooxygenases (FMOs), NAD(P)H: quinone oxidoreductases (NQOs), amine oxidases, alcohol dehydrogenases, esterases, peroxidases are all capable of catalyzing Phase I reactions- including oxidation, reduction and hydrolyses of lipophilic compounds (Esteves *et al.*, 2021). Phase I reactions result in increased polarity of the primarily lipophilic xenobiotics, and thus provide Phase II enzymes the opportunity to perform conjugation reactions.

Previous work in the lab has elucidated in HLMs, that BACs are metabolized by CYPs 2D6, 4F2, 4F11, and 4F12 (Seguin *et al.*, 2019). In Chapter 3, we observe up to 90% of analytes quantified in the livers of male and female BAC-exposed mice were metabolites. Thus, it is important to elucidate whether oral BAC exposure has any impact on the DME activities in the livers of BAC-exposed mice.

4.2 Results and Discussion

4.2.1 RNA Sequencing Analysis on BAC-Exposed Livers Relative to Controls

To evaluate whether the transcriptome was altered in the livers of mice exposed to BACs compared to controls, RNA sequencing was performed on isolated RNA from the livers of male and female control, d_7-C12-BAC, and d_7-C16-BAC exposed mice. Overall, exposure to d_7-C12-BAC or d_7-C16-BAC led to differential gene expression patterns that are characteristic to each treatment. **Figure 4.1** depicts numbers of up-and down-regulated genes in d_7-C12- and d_7-C16-BAC treated mice relative to controls in both male and female cohorts. Of the 198 upregulated differentially expressed genes (DEGs) in the male d_7-C12-BAC group, and 91 in the d_7-C16-BAC group, there were only 33 genes that were coregulated by d_7-C12- and d_7-C16-BAC groups,

signifying unique transcriptomic changes caused by each treatment. Of the genes upregulated in the female cohort, more genes were upregulated in the d_7-C16-BAC (641) group compared to the d_7-C12-BAC (346) exposed group with 175 coregulated DEGs. Conversely, in the male cohort, much more DEGs were observed in the d_7-C12-BAC (143) group relative to the d_7-C16-BAC (198) group. In the female cohort, similar number of downregulated genes were uniquely identified in the d_7-C12- (545) and d_7-C16-BAC (553) groups, and there were 123 genes coregulated in both groups.

iPathwayGuide was used to provide a functional representation of the previously identified DEGs. Gene Ontology (GO) analysis of biological processes revealed sterol metabolic processes were significantly affected in both male and female cohorts, particularly in the d_7-C16-BAC treated groups. Shared genes involved in cholesterol and sterol biological processes defined by GO Terms in the male cohort are depicted in **Figure 4.2**. Importantly, the *Hmgcr* gene was found to be significantly upregulated in the d_7-C12-BAC male, d_7-C16-BAC male, and d_7-C16-BAC female cohorts (**Figure 4.3**). *Hmgcr* encodes the enzyme 3-hydroxy-3-methylglutaryl-CoA reductase, the rate-limiting enzyme within the cholesterol biosynthetic pathway (Guo *et al.*, 2024).

GO term analysis also found lipid catabolic and metabolic processes being impacted in BAC-exposed mice. Significantly, gene *Rorc* was upregulated in both the d_7-C12- and d_7-C16-BAC male groups relative to the control, as well as the female d_7-C16-BAC group. Rorc encodes for retinoic acid-related orphan receptor (ROR) gamma (Rorγ). Various RORs have extensive roles in physiological functions and metabolism (Cook *et al.*, 2015). Rorγ is implicated in the regulation of several lipid and glucose metabolic genes (Cook *et al.*, 2015). Another important gene in lipid biological processes that was identified as differentially expressed in the d_7-C12- male and d_7-C16-

BAC male and female groups was the Trib3 gene. This downregulated gene in BAC samples is a valuable oncogene that functions as a central regulator of lipid metabolism (Li *et al.*, 2024).

Nr1d1, a gene that encodes for the nuclear receptor subfamily 1, group D, member 1 protein (Zhang-sun *et al.*, 2023), and has been identified as a crucial physiological regulator of lipid metabolism (Zhang-sun *et al.*, 2023), was downregulated in the d_7-C12- male and d_7-C16-BAC male and female d_7-C16-BAC groups. Lastly, the fibroblast growth factor 1 gene (*Fgf1*) was identified as differentially upregulated in the d_7-C12- male, and d_7-C16-BAC male and female groups relative to controls. Various members of the FGF family have been identified as regulators of metabolic processes (Struik *et al.*, 2019). Recent studies have demonstrated that Fgf1 is a regulator of bile acid, lipid, and carbohydrate metabolism. However, among all GO terms involved in lipid biological processes, no significant processes was identified in the female d_7-C12-BAC group.

Lastly, RNA sequencing analysis revealed that BAC exposure led to significant involved in xenobiotic metabolism. This is seen substantially in the female cohort (**Figure 4.4**). For example, CYP genes *Cyp4b1*, *Cyp2d10*, *Cyp4a14*, and *Cyp2a12* were all lower in the d_7-C12-BAC female cohort relative to controls. cyp4b1 encodes for the mammalian cytochrome P450 monooxygenase Cyp4B1, an enzyme that catalyzed the hydroxylation of fatty acids and fatty alcohols (Röder *et al.*, 2023). CYP4B1 can act at the interface of endogenous and xenobiotic metabolism, because it can hydroxylate fatty acids as described earlier, but can also metabolize xenobiotics like valproic acid (Röder *et al.*, 2023). cyp2d10 in mice is the ortholog for CYP2D6 in humans. CYP2D6 is defined as a critical pharmacogene because of its involvement in the metabolism of up to 20% of commonly used xenobiotics (Taylor *et al.*, 2020). Cyp4a14 encodes for the Cyp4a14 enzyme, which was found to play an important role in the pathogenesis of non-

alcoholic fatty liver disease (NAFLD)- related fibrosis(Li *et al.*, 2021). It participates in ω-hydroxylation reactions (Li *et al.*, 2021). Humans do not have Cyp2a12 however, in mouse models, CYP2a12 plays critical roles in bile acid synthesis, whereby it converts secondary bile acid, deoxycholic acid (DCA) to primary bile acid (cholic acid), by 7α-rehydroxylation (Bhattacharya *et al.*, 2023). Conversely, Cyp3a59 and Cyp3a25 were significantly upregulated in the d_7-C16-BAC group relative to controls. Cyp3a59 in mice is the ortholog of CYP3A43 in humans. CYP3A43 is the most recent CYP3A isoform to be identified. Within the liver, mRNA expression levels can vary up to 1000-fold in white populations (Klyushova *et al.*, 2022; Qin and Wang, 2019). Notably, Cyp3a25 is orthologous to human CYP3A4, 3A43, and 3A5.

Additionally, genes encoding glutathione-S-transferases (GSTs) were significantly decreased in both male and female d_7-C12- and d_7-C16-BAC treated groups, including *Gstm4* (male d_7-C12-BAC and female d_7-C16-BAC), *Gstm2* (female d_7-C12-BAC), *Gstm2-ps1* (male d_7-C12-BAC and d_7-C16-BAC, and female d_7-C16-BAC groups), *Gstm1* (male d_7-C12-BAC and female d_7-C16-BAC), and *Gstm7* (female d_7-C16-BAC). GSTs are phase II detoxification enzymes that catalyze the conjugation of glutathione (GSH) with electrophilic substrates to form highly hydrophilic and less chemically active compounds, thus facilitating the excretion of compounds through bile or urine (Prysyazhnyuk *et al.*, 2021).

Genes encoding the Phase II enzyme N-acetyltransferases (Nat), *Nat1*, *Nat10*, *Natd1*, *Nat8f1*, and *Nat8f2* were significantly differentially regulated in BAC-exposed groups. Arylamine NATs are polymorphic DMEs that participate in various acetylation reactions (Sim *et al.*, 2014). NAT1 acetylates arylamine and hydrazine substrates (Minchin *et al.*, 2007), and *Nat1* gene was significantly increased in the d_7-C12-BAC male group relative to controls. However, the gene encoding N-acetyltransferase domain containing 1 (Natd1) was significantly downregulated in the

female d_7-C16-BAC treated group. Additionally, *Nat10* gene has been described as regulating fatty acid metabolism and its depletion has been shown to reduce levels of overall lipid content and total cholesterol (Dalhat *et al.*, 2022). In female d_7-C16-BAC exposed mice, *Nat10* was significantly upregulated. NAT8, has been recently indicated to have direct roles in mercapturic acid formation (Veiga-da-Cunha *et al.*, 2010), and the *Nat8* gene was significantly increased in the d_7-C16-BAC male cohort relative to control. In conjunction, the gene encoding N-acetyltransferase 8 family member 2 (Nat8f2) was significantly upregulated in the male d_7-C12-BAC group and the Nat8f1 gene was significantly downregulated in the female d_7-C12-BAC group.

Lastly, genes encoding flavin monooxygenases, Fmo5 and Fmo3 were significantly upregulated in the d_7-C16-BAC group relative to controls (**Figure 4.3**), and Fmo2 gene was significantly upregulated in the d_7-C16-BAC male cohort. Flavin-containing monooxygenases (FMOs) play imperative roles in drug metabolism. For example, FMO2 and FMO3 have various genetic variants that directly affect the metabolism of their substates, and FMO5 has significant roles in endogenous metabolism (Phillips and Shephard, 2017).

4.2.2 Sterolomic Analysis on BAC-Exposed Livers Relative to Controls

To understand how an oral BAC exposure paradigm could influence the sterol homeostasis in livers of male and female mice, an established targeted mass spectrometry method was performed on lipid extracts (Herron *et al.*, 2018). Cholesterol biosynthesis begins with the conversion of acetyl-CoA to HMG-CoA. *Importantly, the conversion of HMG-CoA to mevalonate is dependent on the enzyme HMG-CoA reductase, the rate limiting step in the cholesterol biosynthetic pathway process* (Clayton, 1998). Significantly, the gene that encodes for the HMG-CoA reductase enzyme was decreased in the male d_7-C12-, male d_7-C16- and female d_7-C16-BAC treatment groups relative to their respective controls (**Figure 4.3**). Following the conversion of

mevalonate to squalene and subsequent cyclization, begins the "Post-Squalene Cholesterol Biosynthetic Pathway"(Herron *et al.*, 2018). Our lab has an established targeted mass spectrometry-based quantitation assay for various sterols involved in the post squalene cholesterol biosynthetic pathway (**Schematic 4.2**), including lanosterol, 7-DHD, 7-DHC, 8-DHC, desmosterol and cholesterol.

Levels of cholesterol were considerably lower in both d_7-C12- and d_7-C16-BAC treated female mice relative to controls (**Figure 4.5**). This decrease contributed greatly to the decreases in total sterols in female BAC-exposed samples relative to controls. However, in the male cohort, no significant changes in cholesterol or total sterols were observed (**Figure 4.6**). Although the levels of lanosterol were significantly decreased in d_7-C16-BAC treated mice, the levels (< 0.01 μg/mg) were much lower than the levels of cholesterol (~ 4 μg/mg).This work signifies that cholesterol biosynthesis was affected differently by BACs in male and female mice. Similarly, in **Chapter 2**, we observed female BAC-exposed mice had more dramatic decreases in secondary BAs compared to the males. This work signifies BACs capability of lowering cholesterol in the livers, after an oral exposure paradigm in the female mice, which has not been elucidated prior.

4.2.3 Lipidomic Analysis on BAC-Exposed Livers Relative to Controls

RNA sequencing analysis, as described in **Section 4.2.1** revealed that lipid metabolic, catabolic and biosynthetic processes were significantly affected by BAC treatment. To evaluate this finding, we carried out lipidomic analysis on the livers of male and female mice exposed to either control, d_7-C12-BAC or d_7-C16-BAC (120 μg/g/day). The data presented was completed by negative mode ionization on the mass spectrometer. The following lipid classes were identified and relatively quantified: Ceramides (Cer), Glucosylceramide (GlcCer), Lysophosphatidylcholine (LPC), Phosphatic Acid (PA), Phosphatidylcholine (PC), Phosphatidylethanolamine (PE),

Phosphatidylglycerol (PG), Phosphatidylinositol (PI), Phosphatidylserine (PS) and Sphingomyelin (SM). Sums of each lipid class reveal substantial differences in intensity between BAC treated samples and controls (**Figure 4.9 and Figure 4.10**). In male samples, every single lipid class had a significant change between d_7-C12-BAC and d_7-C16-BAC treated groups compared to the controls, expect for LPC in the d_7-C16-BAC group. In the female group, not all lipid classes identified were significantly different in intensities between BAC treated groups and controls. The relative abundance of the individual lipid species within each class in all samples are presented as heatmaps (**Figure 4.7 and Figure 4.8**).

Regulation of lipid processes and the effects of BACs was illustrated in the phospholipid metabolic pathway (**Figure 4.9**). Phosphatidic acid (PA) was significantly increased in both male and female d_7-C12- and d_7-C16-BAC groups relative to controls. PA is recognized as an important regulator in the synthesis of other lipids like glycerophospholipids and triacylglycerol (Bond, 2017). PA can be activated by cytidine diphosphate (CDP) to form CDP-DAG (diacylglycerol), which serves as the precursor to other phospholipids, such as PG, PI, PS, and PC (Bond, 2017). In male d_7-C12-, male d_7-C16-, and female d_7-C16-BAC groups, sum of all lipids in the PG, PS, or PC classes were significantly decreased relative to controls. Conversely, within the PI lipid class totals, while both male BAC-treated groups had lower levels of PI relative to controls, the female d_7-C16-BAC group had higher levels relative to controls. Synthesis of PE starts from PS, and male d_7-C12-BAC, and d_7-C16-BAC-treated groups as well as female d_7-C16-BAC treated groups had significantly lower levels relative to controls. Levels of sphingolipids, such as Cer, GlcCer and SM are dependent and related to each other (Yamashita, 2011). We found that the levels of all sphingolipids in male d_7-C12- and d_7-C16-BAC-treated groups, as well as d_7-C16-BAC group in the female cohort, were significantly higher relative to controls. Interestingly, the d_7-C12-BAC

treated group in the female cohort revealed no significant changes in overall lipid class totals (Kojima *et al.*, 2016). This is supported by the lack of any GO terms identified within the d_7-C12-BAC female group in the RNA sequencing analysis.

To summarize, this work demonstrates that BAC exposure led to increased lipids in the livers of male d_7-C12- and d_7-C16-BAC-exposed mice, as well as the female d_7-C16-BAC-exposed group (**Figure 4.12**). Perturbation of lipid metabolism in the livers of has been associated in diabetes, hepatocellular carcinoma, steatosis and cirrhosis (Wang and Tontonoz, 2018; Ten Hove *et al.*, 2020), and in particular, accumulation of lipids in tissues has become increasingly recognized as a contributor to cellular dysfunction (Yoon *et al.*, 2021). Thus, depletion of PA, and accumulation of PC, PS, PG and PE point to a novel BAC-induced mechanism of toxicity. Lastly, this work further demonstrates the difference in the responses of male and female mice to BACs, as the males were more impacted by BAC exposure in their liver lipidomes.

4.2.4 Xenobiotic Metabolizing Capability of BAC-Exposed Mice Relative to Controls

To evaluate xenobiotic metabolizing capability between the livers of BAC-exposed and control mice, microsomes were isolated from all livers of each mouse (n=6 control male, n=6 control female, n=6 d_7-C12-BAC male, n=6 d_7-C12-BAC female, n=6 d_7-C16-BAC male, n=6 d_7-C16-BAC female). Metabolite formation of four separate CYP probes were measured after a 10 minute incubation (**Figure 4.13**). Cyp1a activity was probed with Phenacetin (20 uM), but the metabolite formation of acetaminophen (APAP) was not different between the d_7-C12- and d_7-C16-BAC treated male groups relative to controls (**Figure 4.14**). However, in the female cohort, increased formation of APAP was observed in the d_7-C16-BAC exposed group, relative to controls, suggesting increased Cyp1a activity (**Figure 4.15**). Interestingly, a recent study found increased

cyp1a1 expression in jejunum and colon of mice exposed to environmental toxicant PCB 126 (Petriello *et al.*, 2018). Cyp2 and Cyp3 activities were evaluated by cyp probes dextromethorphan and midazolam, respectively, but the formation of the metabolites dextrorphan and 1'-OH midazolam, respectively, were not impacted by BAC exposure (**Figures 4.14** and **4.15**). Cyp4 activity was probed by lauric acid and the formation of its metabolite 12'-OH LA (**Figures 4.14** and **4.15**). There was no significant difference in the formations of 12'-OH LA between the d_7-C12- and d_7-C16-BAC exposed groups and the controls in either male or female cohort. Interestingly, there were baseline sex differences between the control, d_7-C12-BAC and d_7-C16-BAC groups in metabolite formation of each of the four Cyp Probes (**Figure 4.16**)

Finally, to evaluate if BAC exposed mice had differences in metabolizing BACs themselves, MLMs were incubated with parent C12- and C16-BACs for 5 minutes and the formation of both the (ω-1)-OH and ω-OH metabolites of the C12 and C16-BAC structures were quantified. In both the male and female cohorts', formation of either (ω-1)-OH or ω-OH metabolite of C12-BAC was not different between control, d_7-C12-BAC and d_7-C16-BAC treated groups (**Figure 4.17** and **Figure 4.18**). However, in the female cohort, the rate formation of the ω-OH C16-BAC metabolite was significantly larger in the d_7-C16-BAC treated group relative to control (**Figure 4.18**).

This work is the first to elucidate the metabolizing capability CYPs in liver microsomes of mice that underwent the oral BAC exposure paradigm. We found that the d_7-C16-BAC female treatment group was significantly impacted in their ability to metabolize phenacetin and C16-BAC, suggesting BACs could upregulate or enhance the activities of Cyp1a and Cyp4F isoforms. More work is needed to elucidate the mechanisms through which BACs regulate these Cyps, for

example, the activation of nuclear receptors. This data also validates our previous findings (**Chapter 2**) that male and female mice have different responses to BAC exposure.

4.3 Experimental Procedure

Animals. The University of Washington Institutional Animal Care and Use Committee approved all animal protocols. All experiments followed the Guiding Principles in the Use of Animals in Toxicology. Seven to eight-week-old C57BL/6J male and female mice were purchased from Jackson Laboratories (Bar Harbor, Maine). Experiments were staggered, with male mice undergoing the exposure protocol first. Mice were acclimated to an untreated Nutra-Gel diet (Product F5769-KIT, Bio-Serv, Frenchtown, New Jersey) for 2 weeks before BAC exposure. Deuterated BACs were used to ensure prevention of interruption of accurate quantitation, as described in Herron et al., 2018. Mice were randomly assigned to exposure groups (n = 6) and housed into cages of two: control Nutra-Gel diet, or treatment with d_7-C12- BAC (120 µg/g/day) or d_7-C16- BAC (120 µg/g/day) for 1 week. At the end of the treatment period week, mice were sacrificed, and liver was flash-frozen in 2-methylbutane on dry ice and harvested. Samples were stored in -80 °C until subsequent analyses.

Chemicals. Optima LC/MS solvents (acetonitrile, chloroform, methanol, methylene chloride and water), 2-methylbutane, Ammonium Acetate (Optima LC/MS), sodium chloride and formic acid (Optima LC/MS) were purchased from Thermo Fisher Scientific (Grand Island, New York). d_7-C12-BAC and d_7-C16-BAC were prepared as described previously (Herron *et al.*, 2016), as well as deuterated d_7-sterol standard, d_7-7-dehydrocholesterol. d_7-cholesterol and C12 Sphingosyl PE (d17:1/12:0) were purchased from Avanti Polar Lipids (Alabaster, Alabama) and $^{13}C_3$-desmosterol and $^{13}C_3$-lanosterol were purchased from Kerafast (Boston, Massachusetts).

RNA Isolation, Sequencing and Data Analysis. RNA Isolation and RNA Sequencing and Data Analysis. Total RNA was extracted from the livers of male and female control, d_7-C12- and d_7-C16-BAC exposed mice using RNeasy Mini Kit (Qiagen, Germantown, Maryland) according to the manufacturer's protocol. The concentration of RNA was determined via microplate spectrophotometer (Bio-Tek, Winooski, Vermont). The RNA integrity was assessed by agarose gel electrophoresis to visualize the 18S and 28S rRNA bands. Novogene confirmed RNA concentrations and integrity before performing cDNA library construction sequencing on RNA isolates using the Illumina NovaSeq 6000 platform (150 base pairs paired-end, sequencing depth above 20 million reads per sample) (Chula Vista, California).

Raw RNA sequencing reads in FASTQ format were first mapped to the mouse genome using HISAT (HISAT (jhu.edu)) and then aligned to genome order using SamTools, as previously described (Herron *et al.*, 2019). FeatureCounts was utilized to count reads to genomic features, and then Deseq2 was used to determine differentially expressed genes (DEGs) between d_7-C12-BAC vs Control or d_7-C16-BAC vs Control in both the male and female cohorts (Liao *et al.*, 2014; Love *et al.*, 2014). Upstream Pathway Analysis was performed using the Core Analysis feature of Ingenuity Pathway Analysis (IPA, Ingenuity Systems), using an adjusted p value cutoff of 0.1.

Lipid Extraction. 50 mgs of liver tissue from male and female control, d_7-C12- and d_7-C16-BAC exposed groups were accurately weighed. Isotopically labeled sterol and lipid internal standards were added to tissue (5µg of d_7-cholesterol and d_7-7-dehydrocholesterol, 1 µg of $^{13}C_3$-lanosterol and $^{13}C_3$-desmosterol, and 100 µL of Sphingosyl PE). Folch solution (4 mL chloroform/methanol [2/1, v/v]), was added to each sample and they were homogenized by Precellys bead homogenizer. NaCl aqueous solution (0.9% [w/v], 1mL) was subsequently added to each sample and then briefly vortexed and then centrifuged for 5 minutes, at 4 °C, 2000 rpm. The organic (lower) phase was

recovered using 9" glass pastuer pipette, and solvent was removed in vacuo using SpeedVac (Thermo Fisher Savant). Lastly, samples were redissolved in 0.3 mL methylene chloride, as described in Herron et al., 2018.

Untargeted Lipidomics and Data Analysis. Lipid profiles were analyzed by ultra-high-performance liquid chromatography-tandem mass spectrometry (UHPLC-MS/MS) using a Waters Acquity FTN (Waters Corp, Milford, Massachusetts). Ion mobility-mass spectrometry (IM-MS) analysis was operated on a Waters Synapt G2-Si HDMS (Waters Corp) that contained an electrospray ionization (ESI) source in negative mode. Chromatographic separation was achieved with a hydrophilic interaction column (HILIC; Phenomenex Kinetex, 2.1 x 100 mm, 1.7 um). The inlet system was a Waters Acuity UPLC system and autosampler (Waters Corporation, Wilford, MA) that was utilized for mobile phase delivery and sample injection. Detailed conditions have been described previously (Hines *et al.*, 2017; Li *et al.*, 2020). Samples were injected at a 5 uL volume and the solvent flow rate was 0.5 mL/min. The solvents comprised of HILIC A: 95% ACN, 5% Water, 5mM ammonium acetate and HILIC B: 50% ACN, 50% Water, 5 mM ammonium acetate. Mass calibration was achieved for the range of m/z 50-1200 with sodium formate. Collision cross-section (ccs) was calibrated using PE CCS standard as described previously (Hines *et al.*, 2016).

Raw files were imported to Progenesis Q1 software (Nonlinear Dynamics). Data alignment was assigned to pooled sample as a reference for automatic peak detection of profile (continuum) data. Outputted data was filtered for anova p value < 0.05 between comparisons of either Male control vs d_7-C12-BAC, Male control vs d_7-C16-BAC, Female control vs d_7-C12-BAC or Female control vs d_7-C16-BAC. Resulting data were imported to Python software, LiPydomics which was used to identify lipids based on RT, m/z and CCS to known values (Ross *et al.*, 2020). Tolerances

inputted were 0.03 Da, 0.3 min. and 3.0 % respectively. Lipids outside of a 10% threshold of global trend Y were removed. When appropriate, lipids were further identified by LipidMaps database.

Targeted Sterolomics and Data Analysis. Sterol profiles were analyzed by UHPLC-MS/MS using a Waters Xevo TQ-XS (Waters Corp, Wilford, Massachusetts), utilizing an atmospheric pressure chemical ionization (Herron *et al.*, 2018; Weakly *et al.*, 2024). Chromatographic separations were achieved by utilization of reverse phase chromatography by Phenomenex Kinetex C18 column (100 x 2.1 mm, 1.7 um). The mobile phase was 90% MeOH, 10% Water and 0.1% Formic Acid (FA), as previously described. The TargetLynx software in MassLynx 4.1 version was utilized for peak integrations and data analysis. Sterols were quantified by use of peak area ratios relative to respective internal standards and a relative response factor (Herron *et al.*, 2018).

Mouse Liver Microsome Preparation. 800 mg of liver tissue was weighed from Male and Female Control, d_7-C12- and d_7-C16-BAC exposed mice. Over ice, livers were minced using razors. Cut liver were individually transferred to pestles using homogenization buffer, and were thoroughly homogenized using drill. For ultracentrifugation steps described below, we used a Beckman Type 70.1 Ti rotor and the Beckman Optima L-100K ultracentrifuge. Liver homogenates were transferred to spin tubes (Beckman Coulter, catalog number: 355603) and balanced within 0.010 grams before spinning for 20 minutes at 12,000 rpm at 4 °C to pellet mitochondria and cell debri. Supernatants were then transferred to clean tubes and balanced within 0.010 grams before spinning for 70 minutes at 38, 500 rpm at 4 °C to pellet microsomes. Supernatant was aspirated off and microsomal pellets were resuspended in KCl wash buffer. Tubes were balanced within 0.010 grams of eachother and then spun for 70 minutes at 38,500 rpm at 4 °C to pellet the washed microsomes. Pellets were resuspended in homogenizing buffer using disposable pellet pestles (Fischer brand,

catalog number: 12-141-368) and stored at -80 °C. Protein concentrations were determined by BCA and then all samples were diluted to 15 mg/mL.

DME Activity Assay and Analyzation. Microsomal incubations were run in the following conditions: 0.4 mg/mL MLM, 37 C water bath, 10 min. To evaluate CYP1 activity, phenacetin (20 μM) was used as the substrate; CYP2 was evaluated by dextromethorphan (10 μM); CYP3 activity was evaluated by midazolam, and CYP4 was evaluated by Lauric Acid. Internal standards used were d_3-APAP, d_3-DXO, d_3-1-OH MDZ and 15-OH PDA, respectively. Incubations were quenched with ACN and appropriate internal standard. Samples were rested on ice prior to centrifugation at 4000 rpm, 4 °C for 10 minutes. Lastly, 100 μL of the supernatant was transferred to a new 96-well plate and added to 100 μL of a 2:1 mixture of water/MeOH.

Metabolite formations was determined by UHPLC-MS/MS using a Synapt G2-XS ion mobility Q-TOF mass spectrometer equipped with electrospray ionization (Waters Corporation, Milford, MA). Reverse chromatographic separation was achieved by Thermo Hypersil GOLD C18 column (100 x 2.1 mm, 1.9 um). ACUITY UPLC system and autosampler (Waters Corporation, Wilford, WA) were used for mobile phase delivery and sample injection. The solvents were as follows: Mobile phase A: 0.1% formic acid, 2mM ammonium formate in water; solvent B: Acetonitrile. The quantification traces and retention times are described in **Table 4.2**.

4.4 Conclusions

In conclusion, this study provides significant and novel insight into benzalkonium chloride toxicity following an oral dose exposure. We demonstrate that BACs altered the transcriptomic profiles of the livers of mice exposed to BACs by an oral dosage model. Abundant data highlight necessity to study endogenous (Sterolomics and Lipidomics) as well as exogenous (DME Activity) metabolism. Through a targeted sterolomic analysis, we observed significant decreases in cholesterol in female BAC-exposed mice, and not in males. Lipidomic analysis reveals significant increases in lipid content in the livers of both Male and Female BAC-exposed mice. We observe a much more dramatic increase in changes of lipid class profiles within the male cohort between control and BAC-exposed groups. We believe this could be evidence of BACs impacting male and female subjects differently. Through DME activity assays, we observe evidence of BACs being capable of inducing cyp1a in female mice exposed to d_7-C16-BAC. Furthermore, we demonstrate the female d_7-C16-BAC group also had higher metabolizing capability of C16-BAC itself, potentially signaling an impact of BACs on the metabolism of longer chained structures. Overall, this work is substantial in its elucidation of BAC toxicity on endogenous and exogenous metabolism. Future work should consider NRs and their relationships to sex differences, sterol homeostasis, lipid metabolism and DMEs following BAC exposure.

Chapter 4 Figures

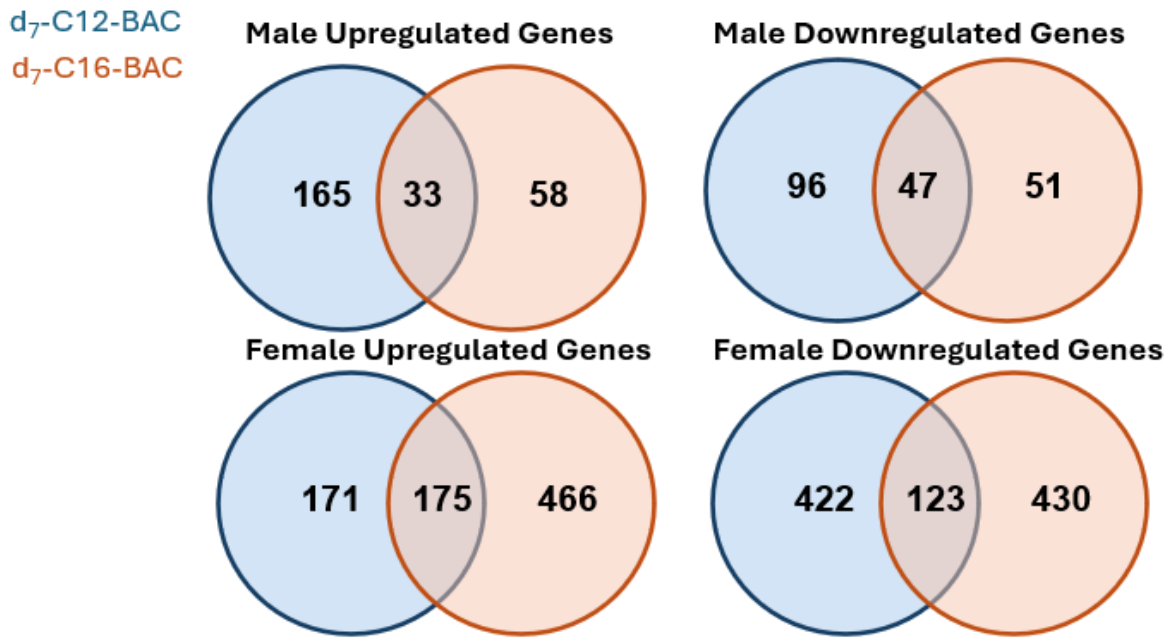

Figure 4.1 Up and Downregulated Genes in Male and Female d_7-C12-BAC vs Control, and d_7-C16-BAC vs Control Livers.

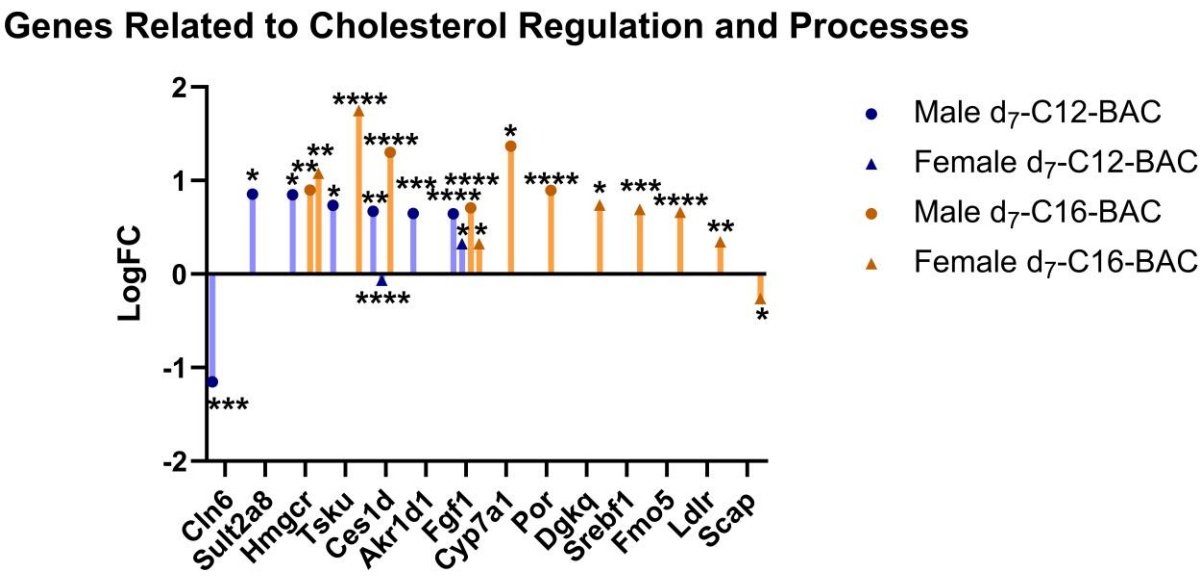

Figure 4.2 DEGs related to Cholesterol Regulation and Processes in Male and Female Cohorts.

P ≤ 0.1; ** P ≤ 0.05; *** P ≤ 0.01; **** P ≤ 0.001.

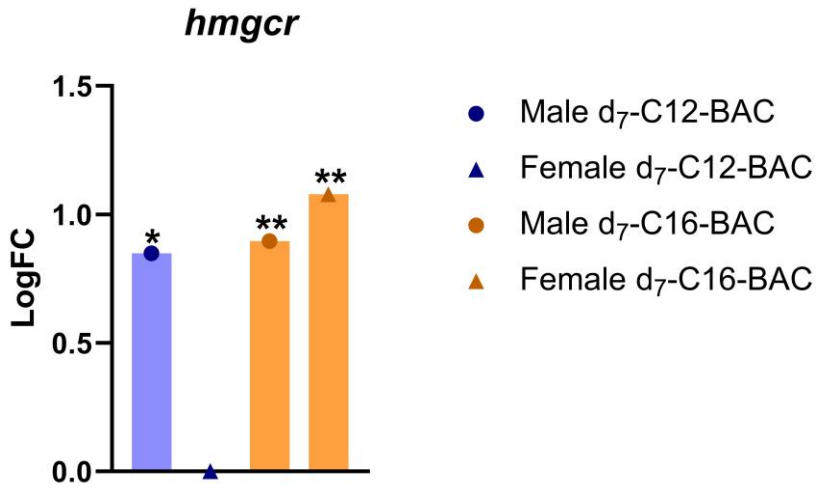

Figure 4.3 Differential *hmgcr* Gene Expression in Male and Female d_7-C12- and d_7-C16-BAC Treated mice Relative to Controls.

* $P \leq 0.05$; ** $P \leq 0.01$; *** $P \leq 0.001$; **** $P \leq 0.0001$.

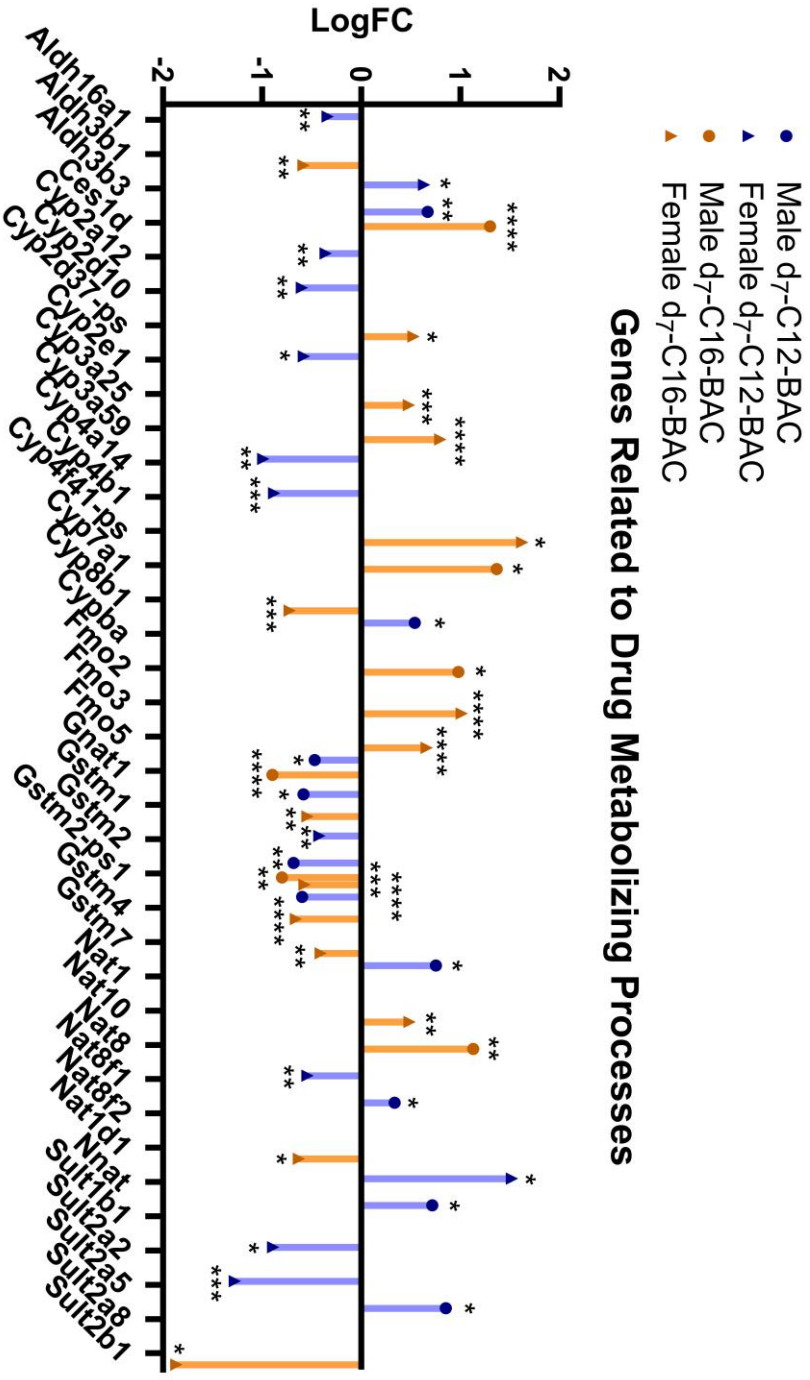

Figure 4.4 LogFC of DEGs Related to DMEs in BAC-Exposed Livers.

$P \leq 0.1$; ** $P \leq 0.05$; *** $P \leq 0.01$; **** $P \leq 0.001$.

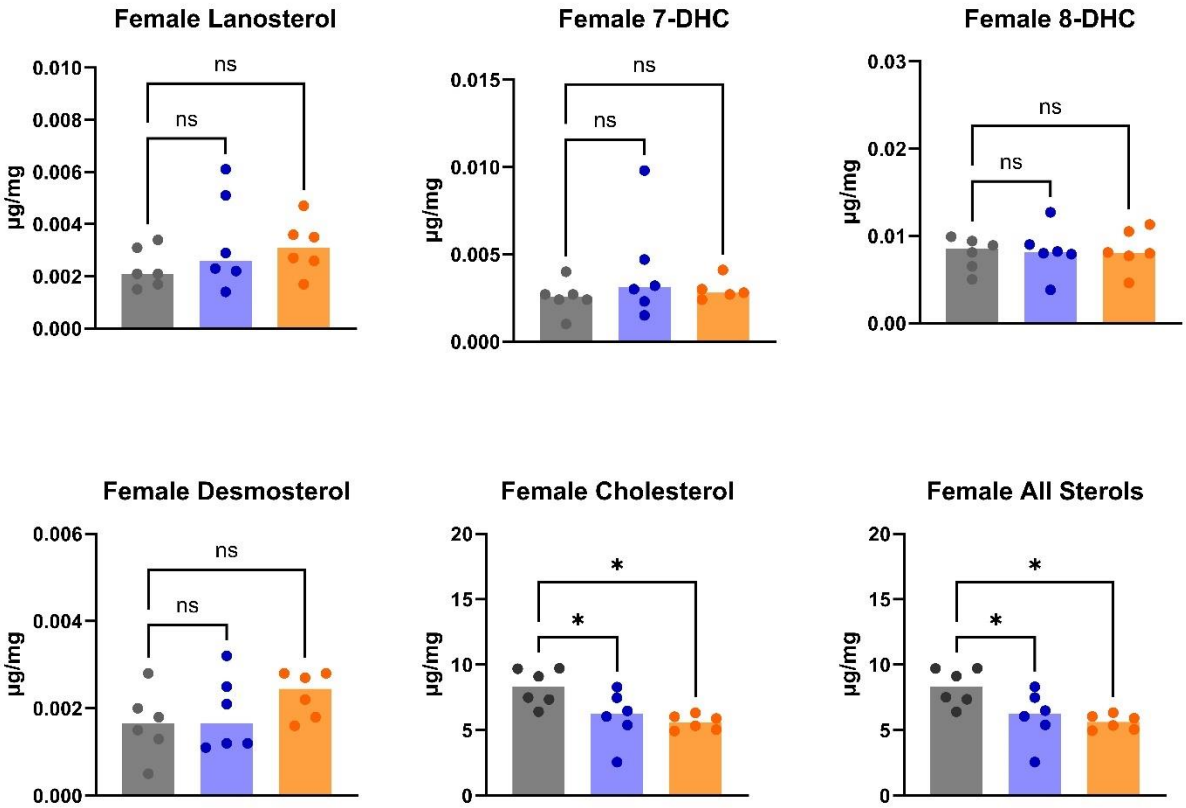

Figure 4.5 Quantified Sterol Levels in BAC-exposed mice relative to Controls in Female Cohort

* $P \leq 0.05$; ** $P \leq 0.01$; *** $P \leq 0.001$; **** $P \leq 0.0001$.

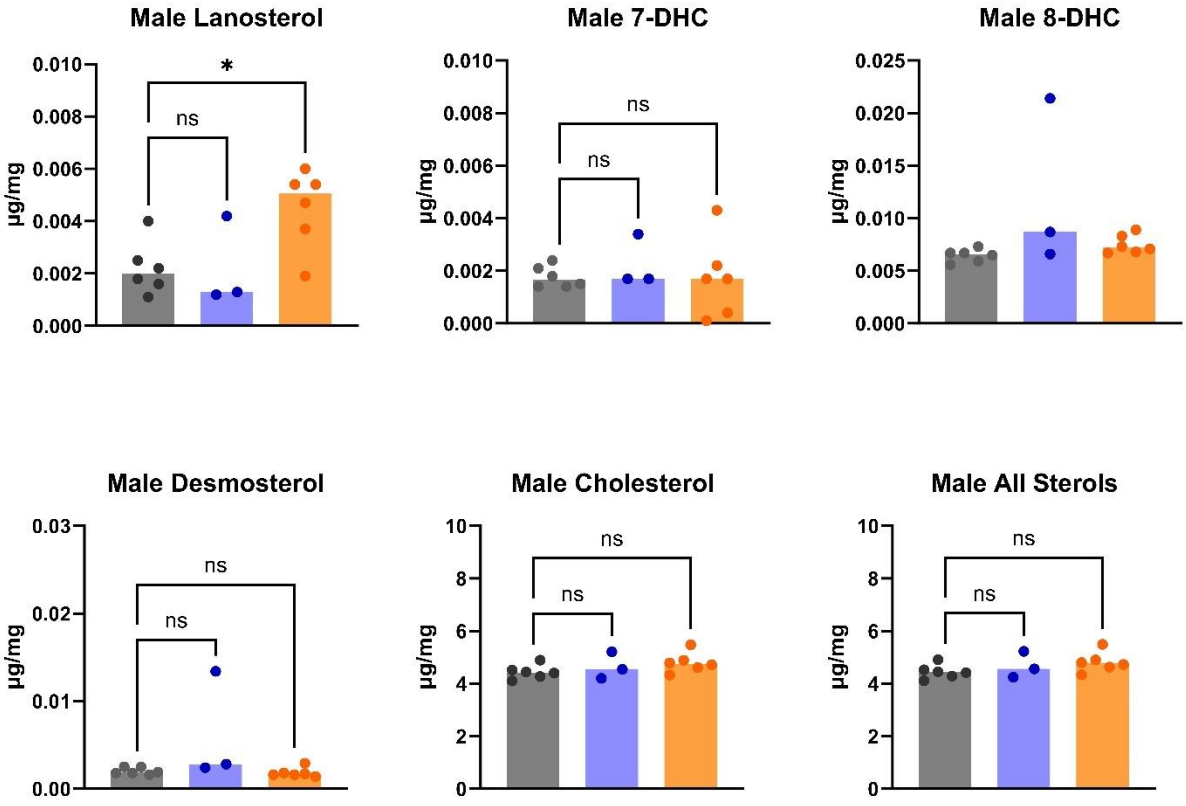

Figure 4.6 Quantified Sterol Levels in BAC-exposed mice relative to Controls in Male Cohort

* $P \leq 0.05$; ** $P \leq 0.01$; *** $P \leq 0.001$; **** $P \leq 0.0001$.

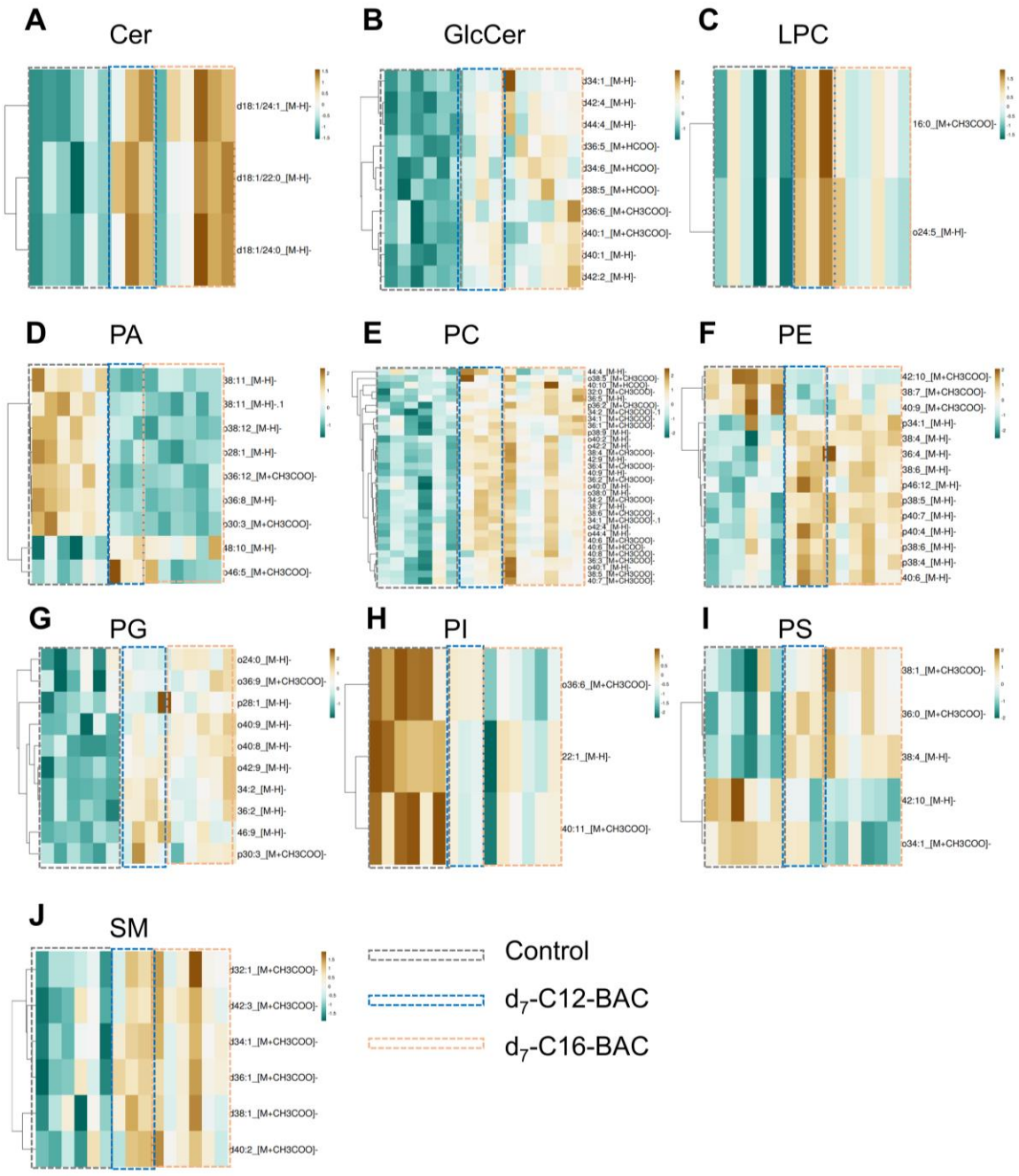

Figure 4.7 Heatmaps depicting Lipid Profiles in BAC-Exposed Male Livers.

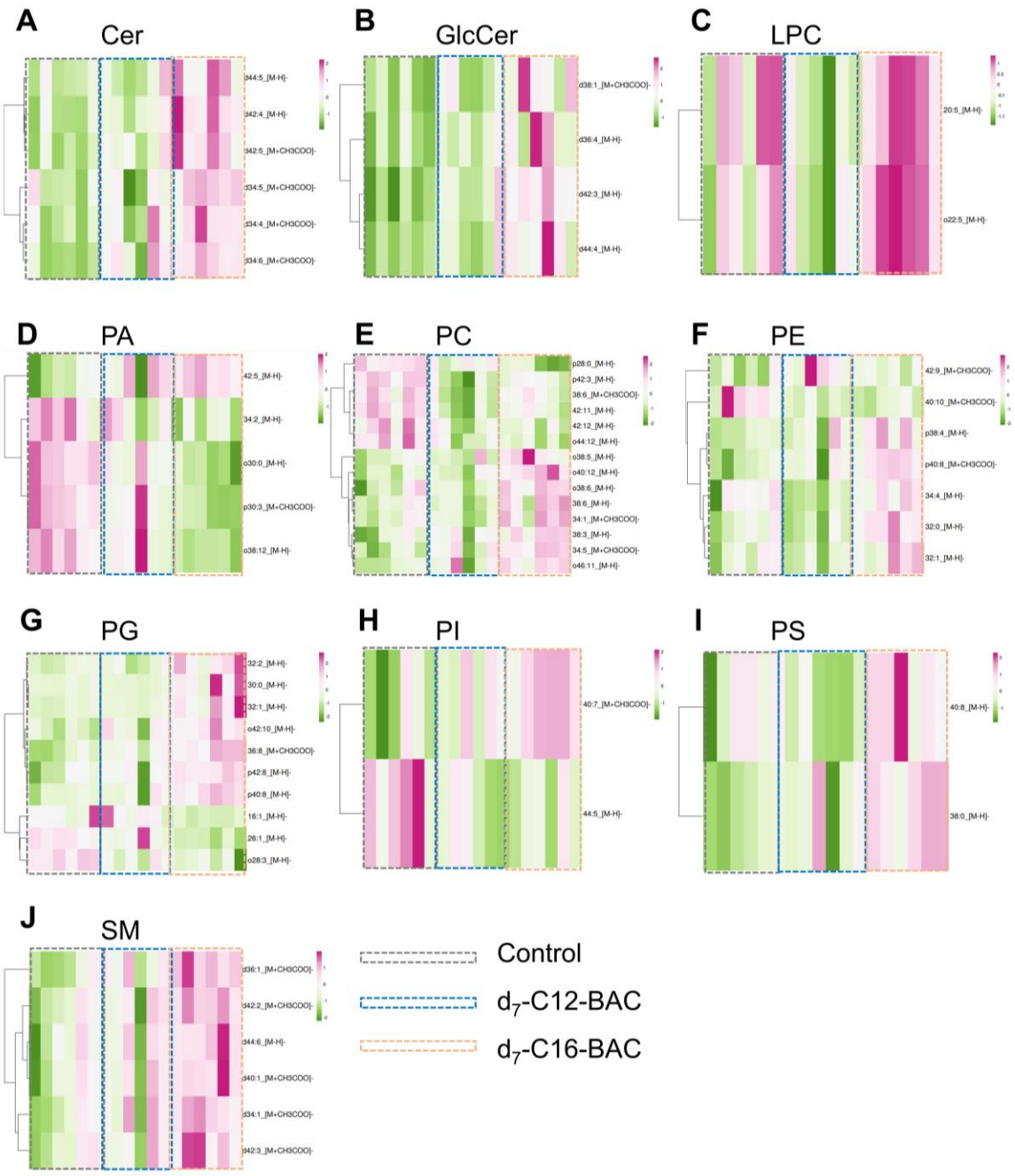

Figure 4.8 Heatmaps depicting Lipid Profiles in BAC-Exposed Male Livers.

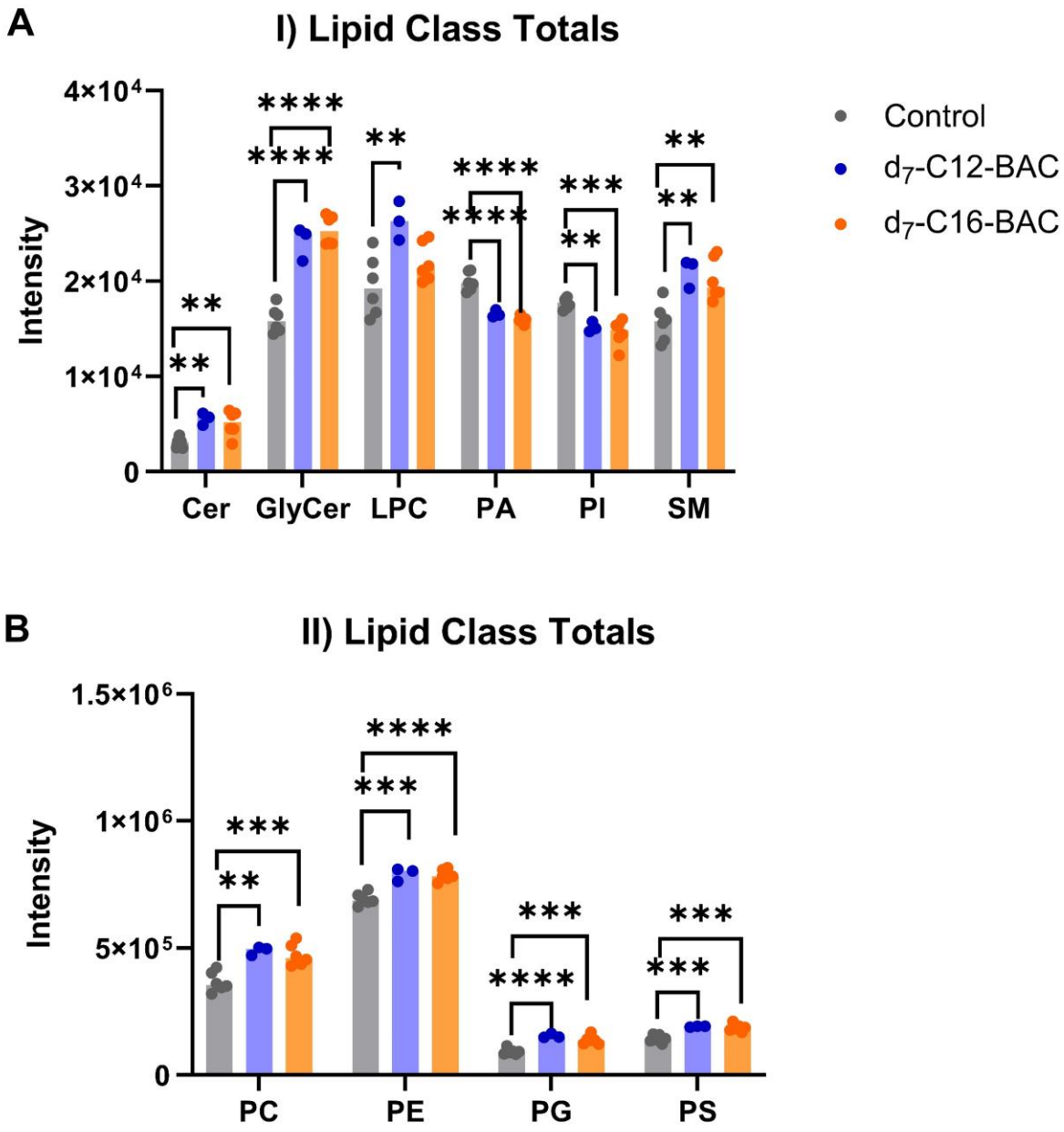

Figure 4.9 Lipid Class Totals between BAC-Exposed and Control Male Livers.

* $P \leq 0.05$; ** $P \leq 0.01$; *** $P \leq 0.001$; **** $P \leq 0.0001$.

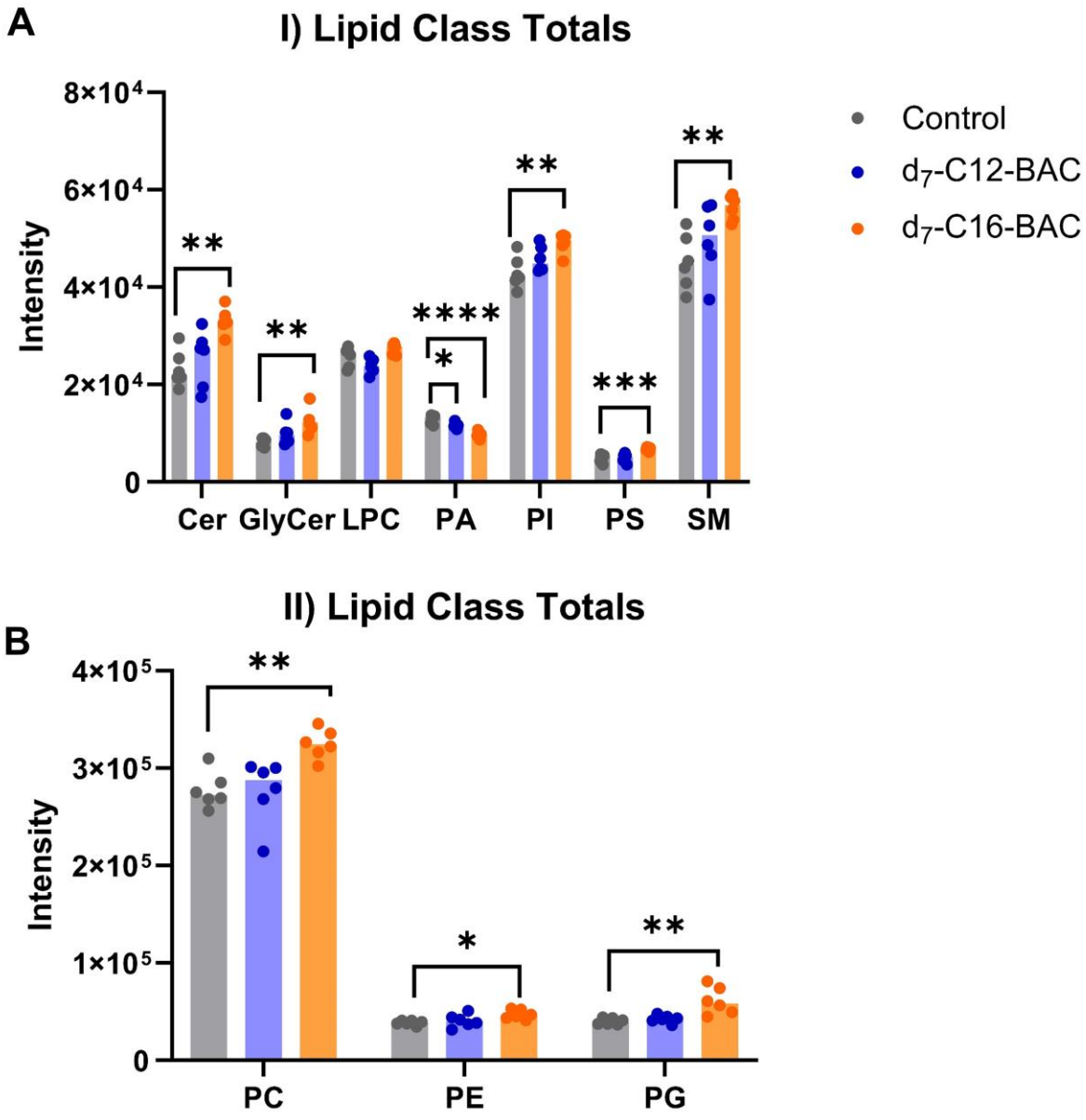

Figure 4.10 Lipid Class Totals between BAC-Exposed and Control Female Livers.

* $P \leq 0.05$; ** $P \leq 0.01$; *** $P \leq 0.001$; **** $P \leq 0.0001$.

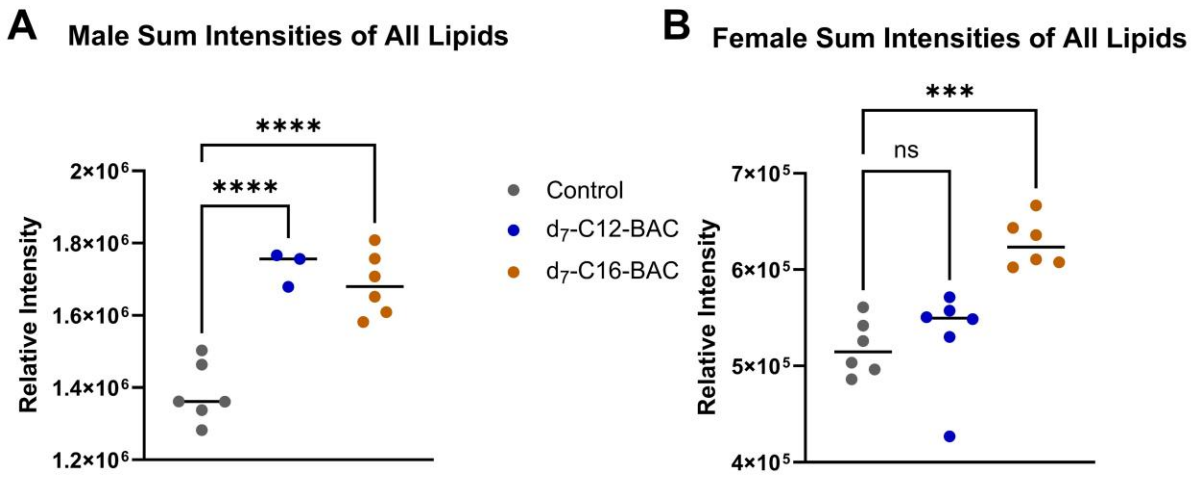

Figure 4.11 Sum Lipid Intensities between BAC-Exposed and Control Male and Female Liver Samples.

* $P \leq 0.05$; ** $P \leq 0.01$; *** $P \leq 0.001$; **** $P \leq 0.0001$.

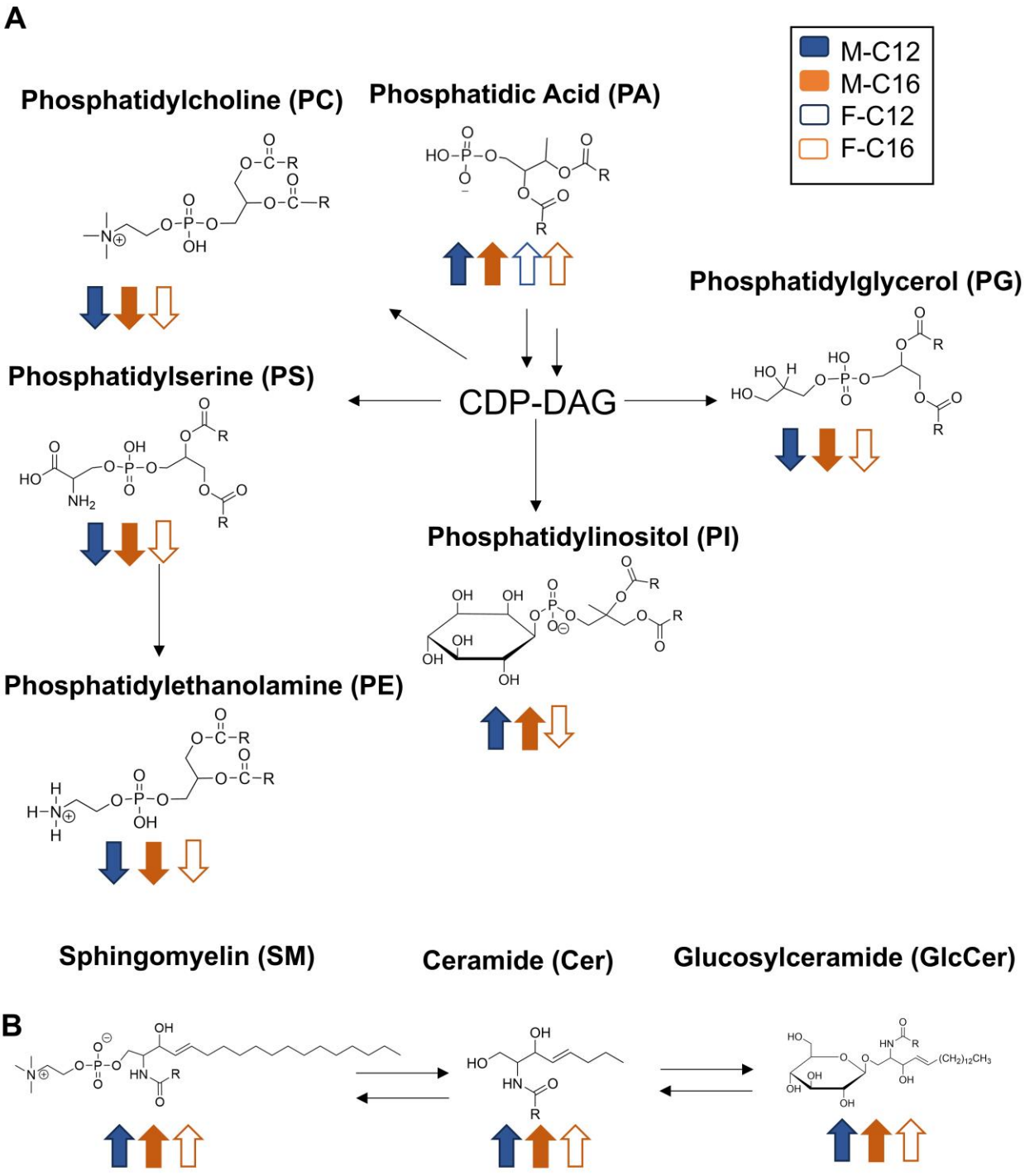

Figure 4.12 Schematic of Lipid Relationships and Class Alterations following BAC exposure relative to Controls.

Arrows depict whether sum totals of all lipids identified within lipid class were significantly increased or decreased relative to controls

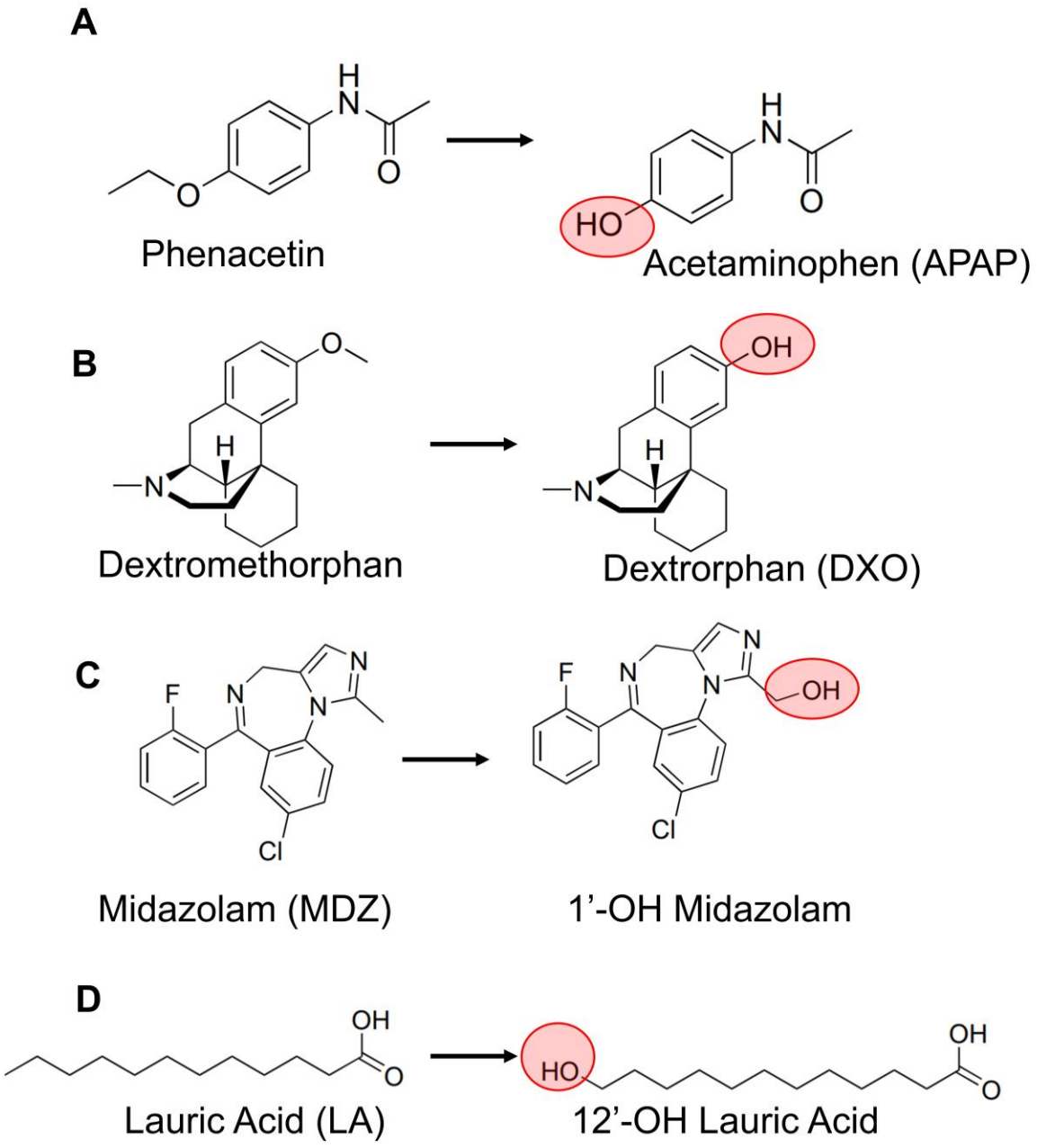

Figure 4.13 Schematic of DME Probes used in MLM Study.

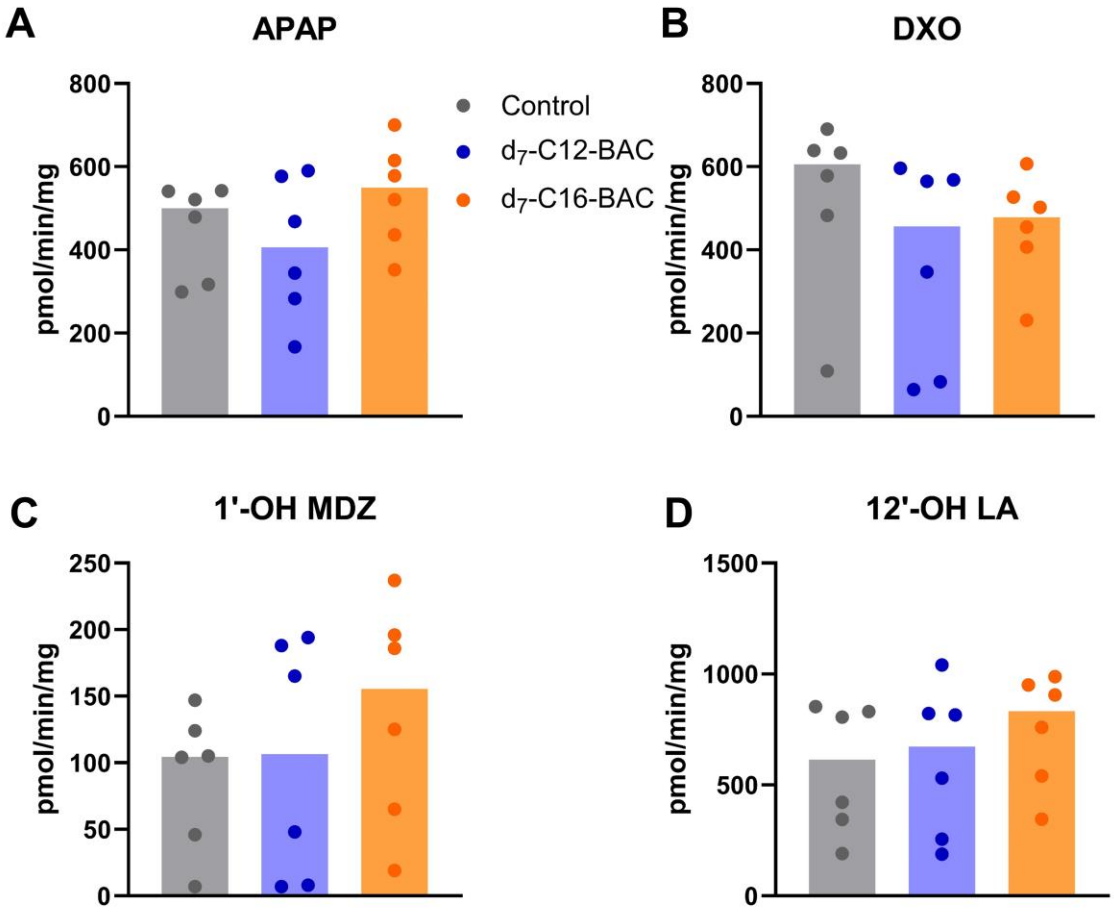

Figure 4.14 Metabolite Formation of Cyp Probes in Male MLMs.

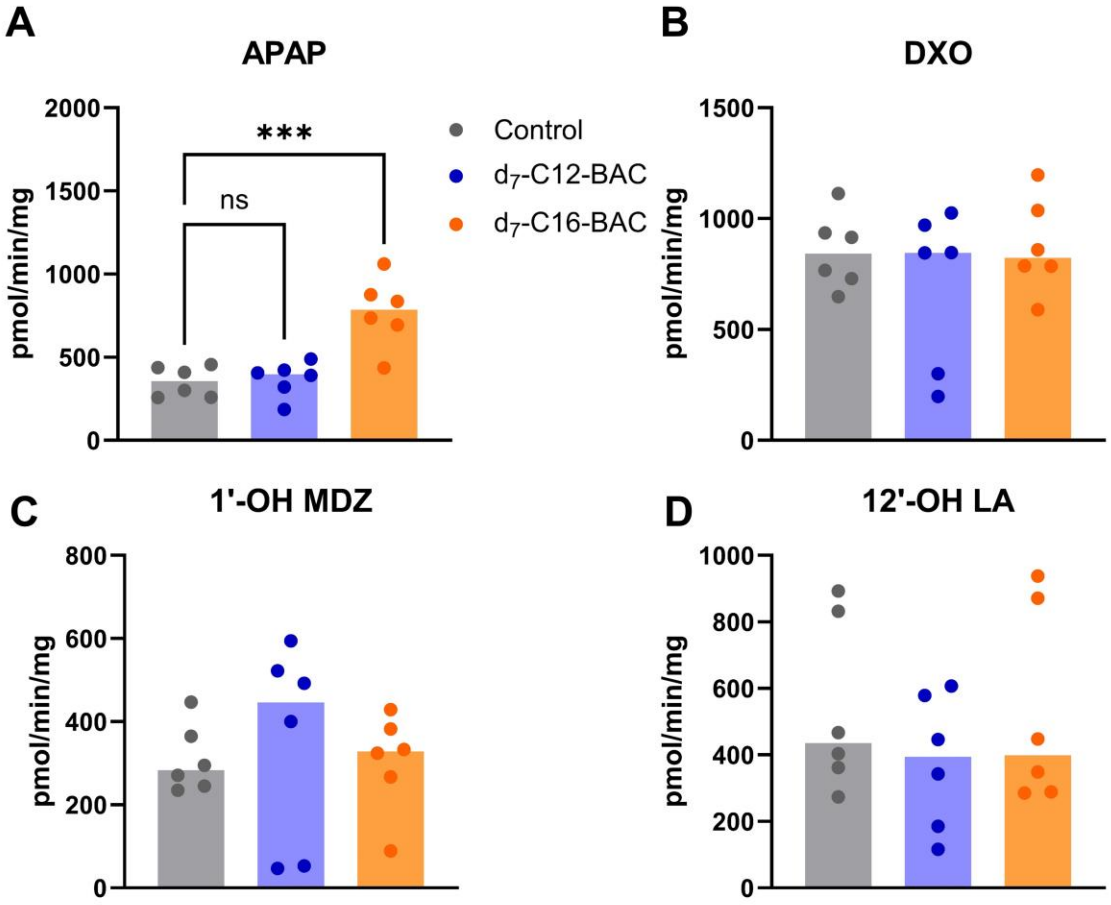

Figure 4.15 Metabolite Formation of Cyp Probes in Female MLMs.

* $P \leq 0.05$; ** $P \leq 0.01$; *** $P \leq 0.001$; **** $P \leq 0.0001$.

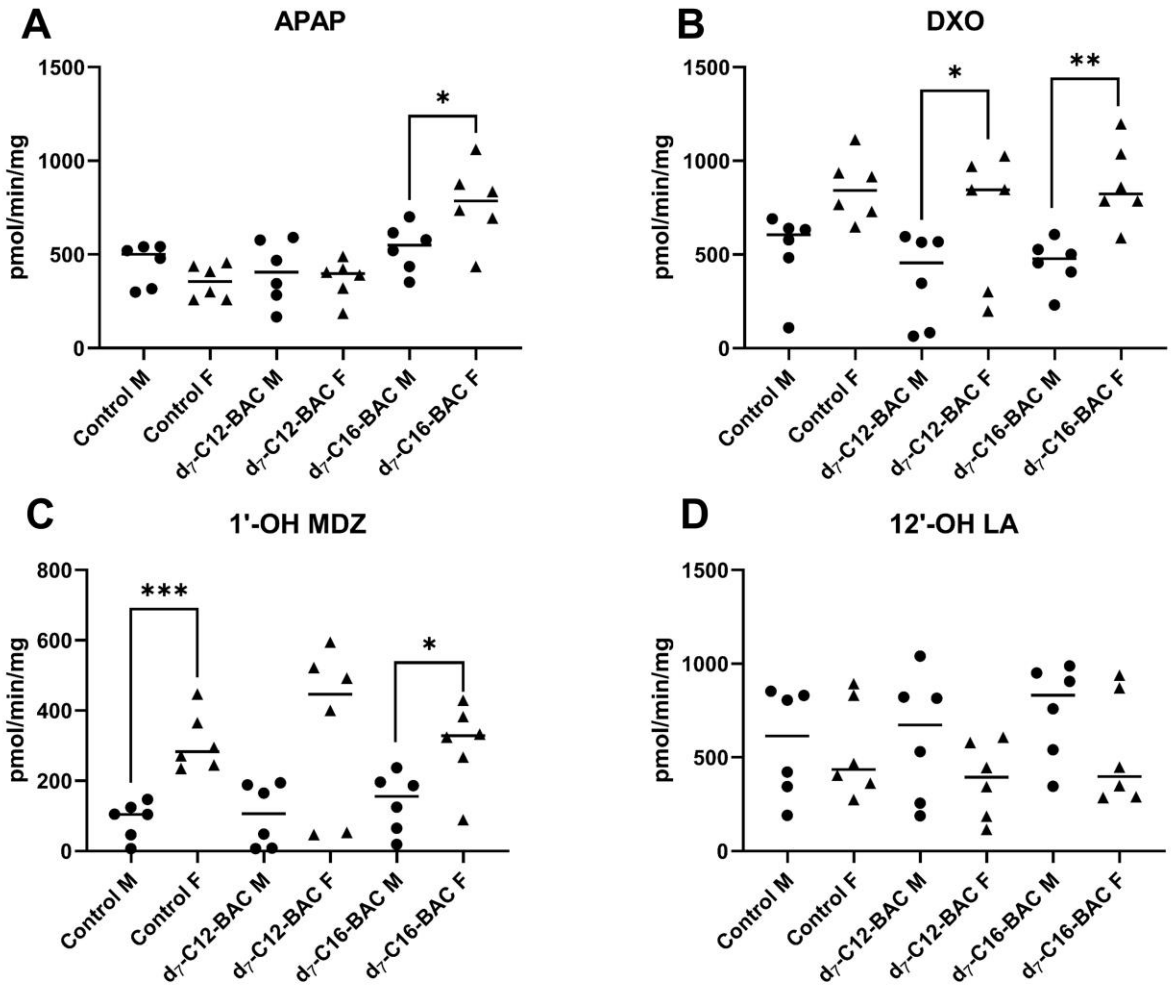

Figure 4.16 Comparison of Metabolite Formation Between Male and Female Control and BAC-Exposed Groups.

* $P \leq 0.05$; ** $P \leq 0.01$; *** $P \leq 0.001$; **** $P \leq 0.0001$.

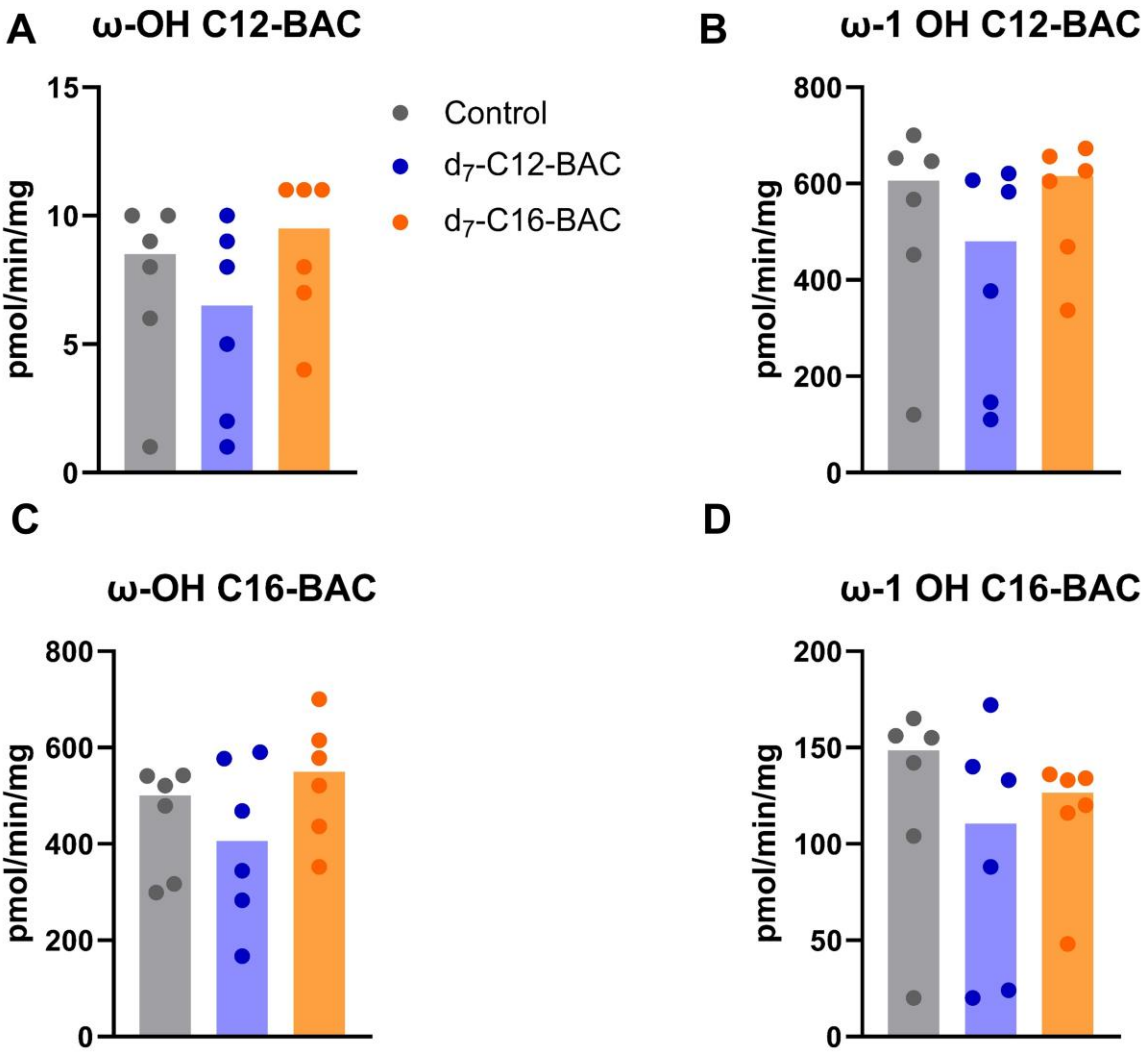

Figure 4.17 Hydroxylation Metabolite Formation of C12 and C16 BACs in Male MLMs.

* $P \leq 0.05$; ** $P \leq 0.01$; *** $P \leq 0.001$; **** $P \leq 0.0001$.

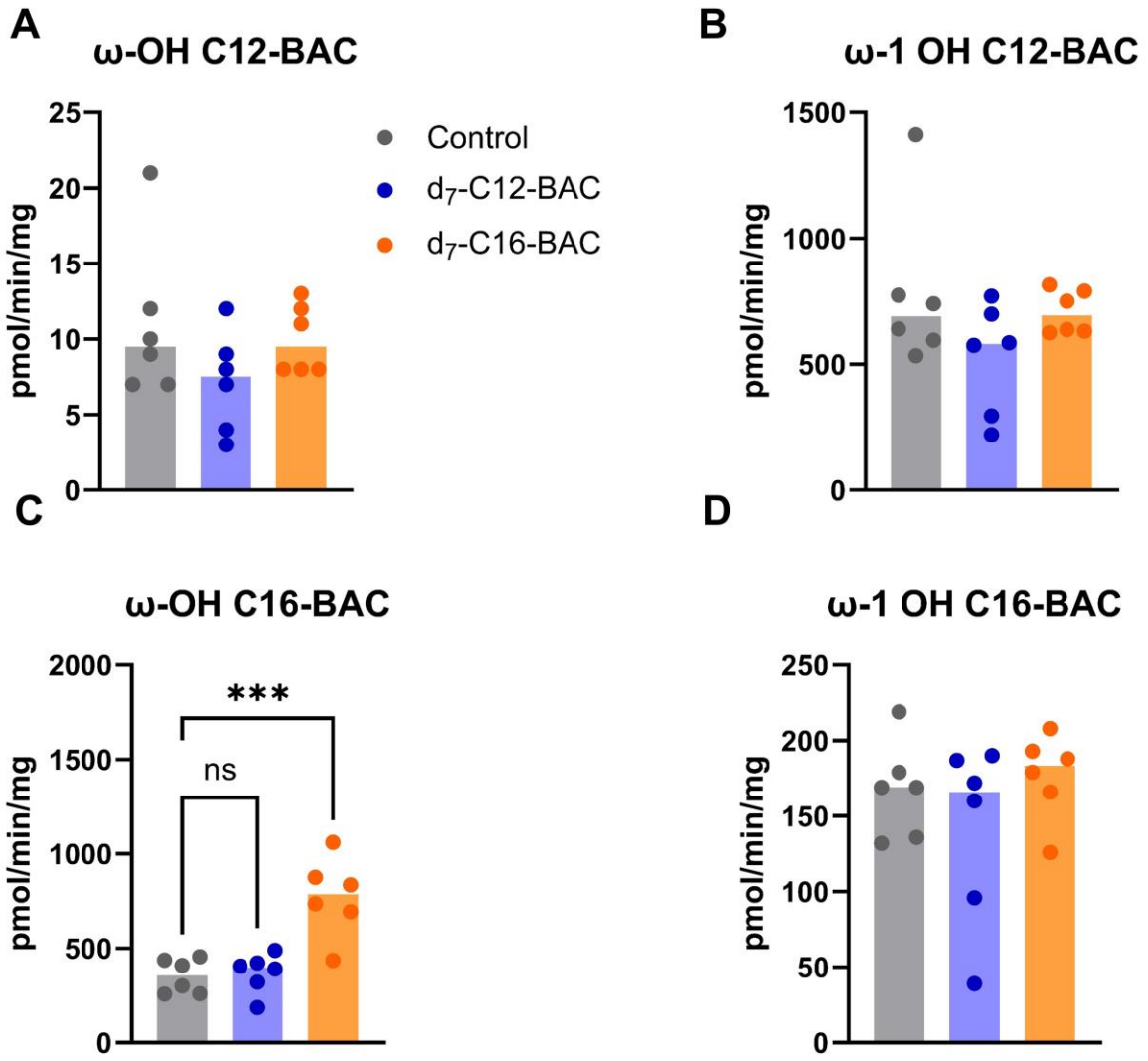

Figure 4.18 Hydroxylation Metabolite Formation of C12 and C16 BACs in Female MLMs.

* $P \leq 0.05$; ** $P \leq 0.01$; *** $P \leq 0.001$; **** $P \leq 0.0001$.

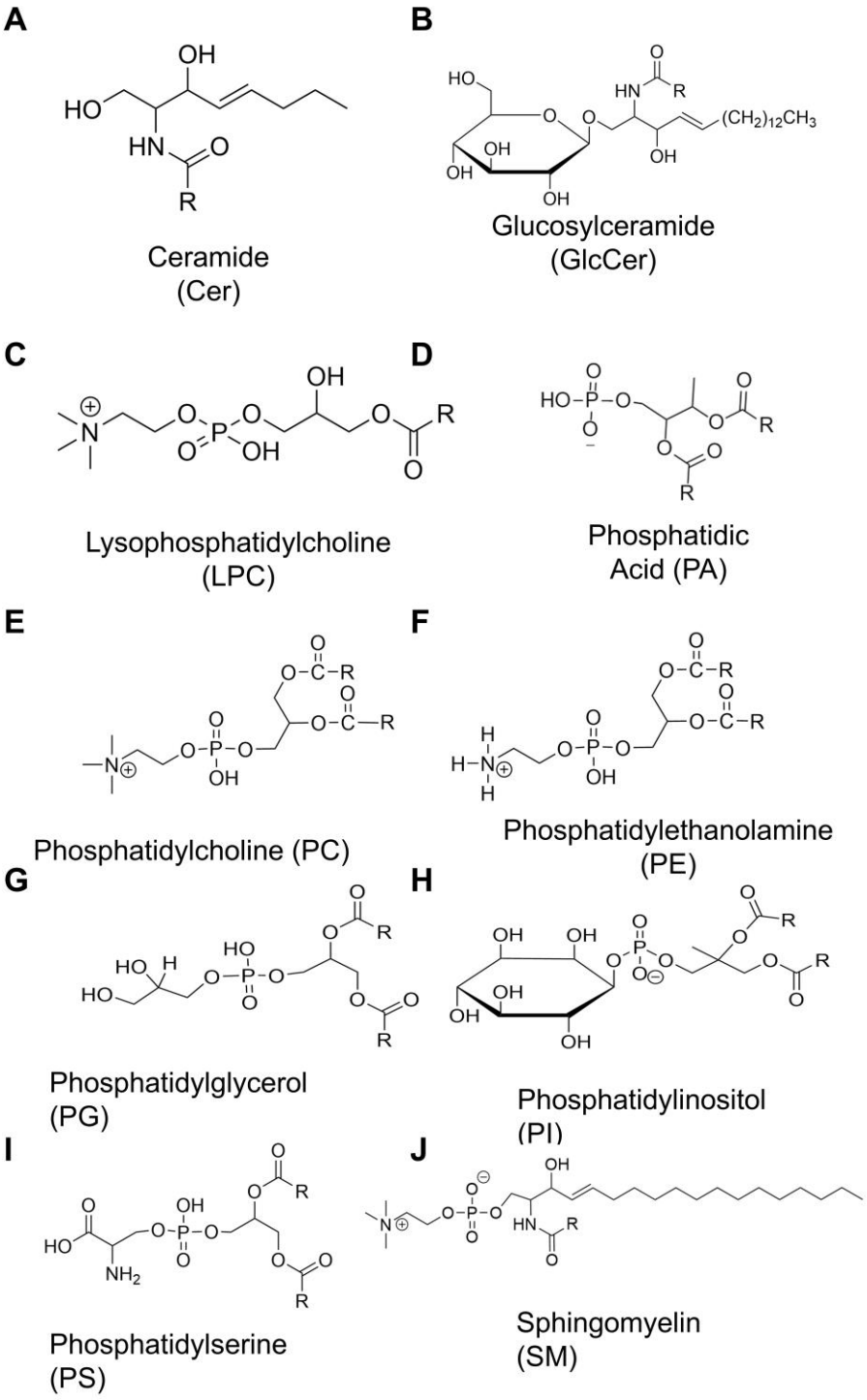

Schematic 4.1 Lipid Class Structures and Abbreviations.

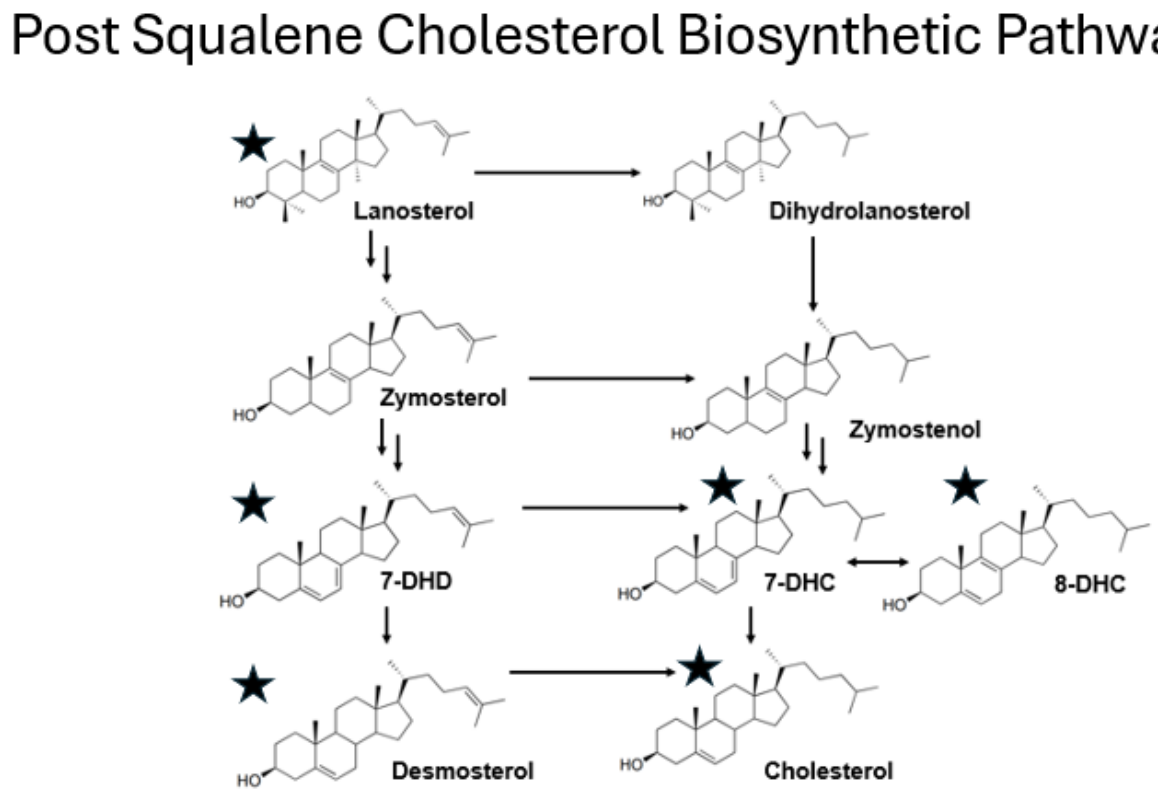

Schematic 4.2 Post Squalene Cholesterol Biosynthetic Pathway.

Starred sterols are those quantified in livers of Chapter 3.

Chapter 4 Tables

Table 4.1 Genes Related to Lipid Processes Impacted by BAC Exposure in Male and Female Cohorts.

P ≤ 0.1; ** P ≤ 0.05; *** P ≤ 0.01; **** P ≤ 0.001.

Gene	Male C12		Female C12		Male C16		Female C16	
	LogFC	adj. pval	LogFC	adj. pval	LogFC	adj. pval	LogFC	adj. pval
Abcb11	-0.4	***			-0.7	****	-0.5	**
Acsl3							0.6	**
Adm							-1.2	*
Adora1	-0.6	*						
Adora2b							-3.5	*
Adra1b							0.5	*
Ahr							0.4	*
Akap13			0.4	*			0.4	**
Akap8			0.6	*			0.7	***
Akr1c20	0.7	*						
Akr1c6	0.6	*						
Akr1d1	0.6	***						
Aqp1					-1.2	****	-0.7	*
Ar					0.9	**		
Atp1a2					3.4	**		
C1qtnf2					-0.9	**	-0.9	**
Capn2							-0.5	***
Ccn1					-0.8	*		
Cd36							-0.8	***
Cd74	-0.7	*					-0.7	*
Cdkn2nd							-0.7	**
Cdo1							-0.4	**
Ces1d	0.7	**	1.3	****				
Clk2							0.5	**
Cln3	-0.4	*						
Cln6	-1.2	***						
Cnr2			-1.4	***			-1.0	**
Crls1					0.8	*		
Crtc3	-0.4	*						
Cry1					0.9	**	1.0	****
Cxcl11							0.6	*
Cxcl13							-1.4	*
Cyb5a	0.5	*						
Cyp7a1					1.4	*		
Cyp8b1							-0.7	***

Dbi			-0.5	***			-0.4	***
Dddrgk1			-0.5	**			-0.3	*
Ddx5			0.4	***			0.4	****
Dgkq							0.7	*
Dnajc15	0.8	*			-0.4	**		
Egfr							0.9	***
Eif2ak3			0.6	**			0.5	**
Elovl3	-0.7	**						
Elovl5							-0.5	**
Ephx1	-0.4	*						
Esr1					0.9	*	0.8	****
Etfbkmt							0.4	*
Fabp2	0.6	*						
Fgf1	0.6	****			0.7	****	0.7	*
Fgf21	-1.9	***						
Fgfr4	-0.4	*						
Fmo5							0.7	***
Gimap5							-1.0	*
Gm2a	-0.4	*			-0.4	***		
Gm4969							-2.2	*
Gstm4	-0.6	****						
Heyl							-1.0	**
Hsd17b2							-0.4	**
Hsd3b2							0.6	***
Igfbp7							-0.6	**
Ill1rn	-1.3	**						
Irak3							-1.0	*
Irs2	-1.2	**			-1.4	**		
Kcnj8							-0.7	**
Klf9							-0.6	**
Ldlr							0.3	**
Lgals9					-0.5	*	-0.4	**
Lima1							-0.3	*
Lipg							0.8	***
Ly96							-0.7	**
Mapk3							-0.4	***
Mapkapk2							-0.4	*
Mapkapk3					-0.8	***		
Mfsd2a							1.1	****
Mrc1							-0.7	***
Mtln	0.7	*						
Noct							1.8	****
Nr1d1	-1.5	****			-2.2	****	-1.5	****
Ogt							0.4	*
Pck1							0.6	*

Pde3b							0.3	*
Pdgfrb							-0.7	**
Per1							1.0	****
Pf4							-0.8	*
Pik3r1							0.5	**
Plin5					0.7	*		
Por					0.9	****		
Ppara							0.5	***
Ppard							0.5	*
Ppargc1b							-0.8	**
Prdm2							-0.4	**
Prkcd	-0.7	****						
Prox1							0.4	*
Pycard							-0.7	*
Rcn3							-0.8	****
Ripk2							-0.4	**
Rorc	0.6	***			0.9	****	1.0	****
S100a9							-1.5	**
Safb							0.4	*
Sash1							-0.4	**
Scap							-0.3	*
Scnn1a							0.5	*
Sik1							1.1	****
Smad6							-0.4	*
Sox9	-0.6	*						
Spi1							-0.8	**
Spon2							-1.2	***
Srebf1							0.7	***
Sult1b1	0.7	*						
Sult2a8	0.9	*						
Synj2	-0.9	***						
Tab2							-0.3	*
Tat							0.8	****
Tfap4					-0.9	**		
Tgfb1							-0.6	***
Thra							-0.8	***
Thrsp	0.9	*						
Tnfrsf1b							0.5	**
Trib3	-0.8	**	-0.8	*			-1.5	****
Trim41							0.4	***
Trim63							-3.5	**
Tsku	0.7	*						
Ttc39aos1							2.4	***
Ufl1							0.4	***
Upf1							0.3	*

Vim							-0.5	*
Wdtc1	-0.4	*					-0.5	***
Zfp36							0.6	*
Zfp703							-0.5	**

Table 4.2 Quantification Traces and RTs of Cyp Probes

Analyte	Quantification Trace	rt
APAP	110.06 + 152.071	1.39
d_3-APAP	110.067 + 155.089	1.385
DXO	157.065	1.56
d_3-DXO	157.065	1.57
1-OH-MDZ	324.07	2.25
d_4-1-OH MDZ	328.095	2.20
12-OH LA	215.164	2.71
15-OH PDA	257.212	3.93

Chapter 4 References

Bhattacharya, A. *et al.* (2023) In vivo mouse models to study bile acid synthesis and signaling. *Hepatobiliary Pancreat. Dis. Int.*, **22**, 466–473.

Bond, P. (2017) Phosphatidic acid: biosynthesis, pharmacokinetics, mechanisms of action and effect on strength and body composition in resistance-trained individuals. *Nutr. Metab.*, **14**, 12.

Clayton, P.T. (1998) Disorders of cholesterol biosynthesis. *Arch Child*, **78**, 185–9.

Cook, D.N. *et al.* (2015) Retinoic Acid-Related Orphan Receptors (RORs): Regulatory Functions in Immunity, Development, Circadian Rhythm, and Metabolism. *Nucl. Recept. Res.*, **2**.

Dalhat, M.H. *et al.* (2022) NAT10: An RNA cytidine transferase regulates fatty acid metabolism in cancer cells. *Clin. Transl. Med.*, **12**, e1045.

Duan, Y. *et al.* (2022) Regulation of cholesterol homeostasis in health and diseases: from mechanisms to targeted therapeutics. *Signal Transduct. Target. Ther.*, **7**, 265.

Esteves, F. *et al.* (2021) The Central Role of Cytochrome P450 in Xenobiotic Metabolism—A Brief Review on a Fascinating Enzyme Family. *J. Xenobiotics*, **11**, 94–114.

Goldstein, J.L. *et al.* (2006) Protein sensors for membrane sterols. *Cell*, **124**, 35–46.

Guo, J. *et al.* (2024) Cholesterol metabolism: physiological regulation and diseases. *MedComm*, **5**, e476.

Herron, J. *et al.* (2018) Assessment of Altered Cholesterol Homeostasis by Xenobiotics Using Ultra-High Performance Liquid Chromatography-Tandem Mass Spectrometry. *Curr Protoc Toxicol*, **78**, e65.

Herron, J. *et al.* (2016) Identification of Environmental Quaternary Ammonium Compounds as Direct Inhibitors of Cholesterol Biosynthesis. *Toxicol Sci*, **151**, 261–270.

Herron, J.M. *et al.* (2019) Multiomics investigation reveals benzalkonium chloride disinfectants alter sterol and lipid homeostasis in the mouse neonatal brain. *Toxicol Sci*, **171**, 32–45.

Hines, K. *et al.* (2017) Assessment of Altered Lipid Homeostasis by HILIC-Ion Mobility-Mass Spectrometry-Based Lipidomics. *J Lipid Res*, **58**, 809–819.

Hines, K.M. *et al.* (2016) Evaluation of Collision Cross Section Calibrants for Structural Analysis of Lipids by Traveling Wave Ion Mobility-Mass Spectrometry. *Anal Chem*, **88**, 7329–36.

Klyushova, L.S. *et al.* (2022) The Role of CYP3A in Health and Disease. *Biomedicines*, **10**, 2686.

Kojima, R. *et al.* (2016) A phospholipid transfer function of ER-mitochondria encounter structure revealed in vitro. *Sci. Rep.*, **6**, 30777.

Li, A. *et al.* (2020) Lipidomics by HILIC-Ion Mobility-Mass Spectrometry. *Methods Mol. Biol.*, **2084**, 119–132.

Li, J. *et al.* (2024) TRIB3 promotes the progression of renal cell carcinoma by upregulating the lipid droplet-associated protein PLIN2. *Cell Death Dis.*, **15**, 240.

Li, S. *et al.* (2021) Cytochrome P450 Omega-Hydroxylase 4a14 Attenuates Cholestatic Liver Fibrosis. *Front. Physiol.*, **12**, 688259.

Liao, Y. *et al.* (2014) featureCounts: an efficient general purpose program for assigning sequence reads to genomic features. *Bioinformatics*, **30**, 923–930.

Love, M.I. *et al.* (2014) Moderated estimation of fold change and dispersion for RNA-seq data with DESeq2. *Genome Biol*, **15**, 550.

Minchin, R.F. *et al.* (2007) Arylamine N-acetyltransferase I. *Int. J. Biochem. Cell Biol.*, **39**, 1999–2005.

Patterson, A.D. *et al.* (2010) Xenobiotic Metabolism: A View through the Metabolometer. *Chem. Res. Toxicol.*, **23**, 851–860.

Petriello, M.C. *et al.* (2018) Dioxin-like PCB 126 increases intestinal inflammation and disrupts gut microbiota and metabolic homeostasis. *Environ. Pollut.*, **242**, 1022–1032.

Phillips, I.R. and Shephard, E.A. (2017) Drug metabolism by flavin-containing monooxygenases of human and mouse. *Expert Opin. Drug Metab. Toxicol.*, **13**, 167–181.

Prysyazhnyuk, V. *et al.* (2021) Glutathione-S-transferases genes-promising predictors of hepatic dysfunction. *World J. Hepatol.*, **13**, 620–633.

Qin, X. and Wang, X. (2019) Role of vitamin D receptor in the regulation of CYP3A gene expression. *Acta Pharm. Sin. B*, **9**, 1087–1098.

Röder, A. *et al.* (2023) Spotlight on CYP4B1. *Int. J. Mol. Sci.*, **24**, 2038.

Ross, D.H. *et al.* (2020) LiPydomics: A Python Package for Comprehensive Prediction of Lipid Collision Cross Sections and Retention Times and Analysis of Ion Mobility-Mass Spectrometry-Based Lipidomics Data. *Anal. Chem.*, **92**, 14967–14975.

Schwabe, R.F. and Maher, J.J. (2012) Lipids in liver disease: looking beyond steatosis. *Gastroenterology*, **142**, 8–11.

Seebacher, F. *et al.* (2020) Hepatic lipid droplet homeostasis and fatty liver disease. *Semin. Cell Dev. Biol.*, **108**, 72–81.

Seguin, R.P. *et al.* (2019) Metabolism of Benzalkonium Chlorides by Human Hepatic Cytochromes P450. *Chem Res Toxicol*, **32**, 2466–2478.

Sim, E. *et al.* (2014) Arylamine N-acetyltransferases: from drug metabolism and pharmacogenetics to drug discovery. *Br. J. Pharmacol.*, **171**, 2705–2725.

Struik, D. *et al.* (2019) Fibroblast growth factors in control of lipid metabolism: from biological function to clinical application. *Curr. Opin. Lipidol.*, **30**, 235–243.

Taylor, C. *et al.* (2020) A Review of the Important Role of CYP2D6 in Pharmacogenomics. *Genes*, **11**, 1295.

Ten Hove, M. *et al.* (2020) The hepatic lipidome: From basic science to clinical translation. *Adv. Drug Deliv. Rev.*, **159**, 180–197.

Trapani, L. (2012) Regulation and deregulation of cholesterol homeostasis: The liver as a metabolic "power station". *World J. Hepatol.*, **4**, 184.

Veiga-da-Cunha, M. *et al.* (2010) Molecular Identification of NAT8 as the Enzyme That Acetylates Cysteine S-Conjugates to Mercapturic Acids. *J. Biol. Chem.*, **285**, 18888–18898.

Wang, B. and Tontonoz, P. (2018) Liver X receptors in lipid signalling and membrane homeostasis. *Nat. Rev. Endocrinol.*, **14**, 452–463.

Weakly, H.M.J. *et al.* (2024) Several common methods of making vesicles (except an emulsion method) capture intended lipid ratios. *bioRxiv*, 2024.02.21.581444.

Xue, Y. *et al.* (2004) Distribution and disposition of benzalkonium chloride following various routes of administration in rats. *Toxicol Lett*, **148**, 113–23.

Xue, Y. *et al.* (2002) Sensitive determination of benzalkonium chloride in blood and tissues using high-performance liquid chromatography with solid-phase extraction. *Leg Med Tokyo*, **4**, 232–8.

Yamashita, T. (2011) Glycosphingolipid Modification: Structural Diversity, Functional and Mechanistic Integration of Diabetes. *Diabetes Metab. J.*, **35**, 309.

Yoon, H. *et al.* (2021) Lipid metabolism in sickness and in health: Emerging regulators of lipotoxicity. *Mol. Cell*, **81**, 3708–3730.

Zhang-sun, Z.-Y. *et al.* (2023) Targeting NR1D1 in organ injury: challenges and prospects. *Mil. Med. Res.*, **10**, 62.

Chapter 5: Conclusions and Future Directions

The findings of this work implicate the capability of BACs to alter gut microbiome composition, alter secondary BA formation, and affect endogenous and exogenous metabolism in the livers of BAC-exposed male and female mice. Chapter 2 described the phylum, family, and genera compositional shifts in the microbiomes of BAC-exposed mice relative to controls. We described significant shifts in bacteria like phylums: Firmicutes, Actinobacteria, Proteobacteria, and Verrucomicrobia; families: Akkermansiaceae, Bacteriodaceae, Lactobacillaceae, and Atopobiaceae; and genera: Parasutterella, Lactobacillus, Coriobacteriaceae UCG-002, and Akkermansia. Furthermore, we demonstrate that BAC-exposed mice had significant decreases in alpha diversity, and beta diversity analysis revealed BAC-exposed mice had microbiome communities statistically different from controls. The gut microbiome composition is significant in understanding human health because of the implications the gut microbiome has in the health and disease states. For example, variations in the gut microbiome can influence disease biomarker levels in the blood, and the gut microbiome is thought to have pivotal roles in the etiology of diseases like IBD, diabetes, and hypertension (Manor et al., 2020). Our study is significant in being the first to demonstrate the ability of environmental toxicants, BACs, to alter the gut microbiome in vivo. Future work should focus on identifying microbiome-dependent versus independent physiological changes in BA formation and endogenous and exogenous metabolism in the liver by utilizing a GF mouse model. Additionally, recovery of homeostasis in BA formation, microbiome composition and diversity, and endogenous and exogenous metabolism in the liver should be evaluated by enforcing timepoints of collection and sacrifice throughout a longer treatment period.

Follow-up experiments should also consider probing the BAC-mediated decreases in bacteria in culture systems. For example, microbial cells can be isolated and cultured to mimic the

microbiome of interest (Koontz et al., 2019). In Chapter 3, we demonstrated a cohesive understanding of BAC metabolism and distribution throughout harvested tissues of BAC-exposed mice. We revealed beta-oxidation to be a major route of metabolism, and we observed CYP-mediated BAC hydroxylation products. Notably, we demonstrated parent:metabolite profiles throughout the intestinal sections: duodenum, jejunum, ileum, and big intestine. Future work should investigate within the in vitro/cell culture systems a) the metabolism of parent BAC structures and b) the toxicity of the metabolites within the in vitro/cell culture systems. This work would give a unique understanding of BAC metabolism and, potentially, BAC-metabolite toxicity capability. Importantly, physiological gut microbiota variations have significant implications for intestinal and extra-intestinal disorders (Rinninella et al., 2019). Thus, follow-up studies should evaluate gut barrier integrity by measuring tight junction genes in the ileums of BAC-exposed mice relative to controls. This would provide an exciting opportunity to understand the physiological implications of BAC-induced disease state.

Chapter 2 also demonstrated decreased secondary BA formation in BAC-exposed mice relative to controls. BAs are potent modulators of lipid, carbohydrate, and protein (macronutrient) metabolism and systemic pro-inflammatory/anti-inflammatory balance (Fleishman and Kumar, 2024). When normal BA pool composition is disrupted, this results in an impaired ability to absorb nutrition. Furthermore, BAs have been implicated in disease states like cardiometabolic, intestinal, liver, and inflammatory diseases (Fleishman and Kumar, 2024; Shulpekova et al., 2022). Decreases in BA pool production lead to gut inflammation and bacterial burden increases, which decreases the integrity and increases the permeability of the mucosal barrier, triggering hepatic inflammation. Hepatic inflammation can then induce phenotypes associated with NAFLD and other liver disease states (Fleishman and Kumar, 2024). Furthermore, recent evidence warrants the suggestion that

some cholestatic liver diseases in adults may be due to an inherited defect in BA biosynthesis (Monte et al., 2009). Importantly, NRs FXR, VDR, LXR, GPBAR1, and TGR5 are all BA receptors (Shulpekova et al., 2022). Secondary BAs, DCA and LCA, are both agonists of FXR - a nuclear receptor that not only has a role in the metabolism of carbohydrates and lipids but also in BA synthesis (Jiang et al., 2021). Moreso, within the female cohort, there were significant decreases in DCA and LCA formation. Primary BAs, CDCA and CA are also agonists of FXR. Conjugated BAs, T-a-MCA and T-B-MCA, are agonists of FXR (Tian et al., 2022). Thus, future studies should evaluate NR expression to develop a better mechanistic understanding of BAC-induced changes to the BA pool and secondary BA formation. In addition, future studies should incorporate conjugated BAs and quantify them across liver, blood and feces. Furthermore, BA measuring across the intestinal sections would be an opportunistic chance to understand the BA profile and add to the above suggestions.

We observed baseline differences in microbiome composition between control male and control female mice. Importantly, the literature also reported that there were differences between the male and female gut microbiome composition and diversity in both human and mouse subjects (Siddiqui et al., 2022; Kim et al., 2020; Koliada et al., 2021). We also described decreases in secondary BA-forming bacteria like genus-Blautia, and families Ruminococcaceae and Lachnospiraceae, particularly in the female cohort. The differences we observed in BA profile and microbiome composition and diversity response between male and female cohorts provides an exciting opportunity for further investigation. An increasing amount of work demonstrates the role between sex hormones and the gut microbiome being bidirectional. Considerably, in female polycystic ovary syndrome (PCOS) patients, changes to their microbiome affected BA metabolism (Siddiqui et al., 2022). Furthermore, dysbiosis of the gut microbiota is observed in cancers affecting female

patients like breast, cervical, and ovarian cancers (Siddiqui et al., 2022). Bacteria are also capable of metabolizing sex hormones; for example, fecal bacteria carry out hydrolytic reductive and oxidative reactions of androgens and estrogen, and the gut microbiome influences estrogen levels (Siddiqui et al., 2022). Furthermore, the rate of BA synthesis and BA pool composition are sexually dimorphic (Phelps et al., 2019). Cholesterol homeostasis has long been recognized as an important modulatory aspect of the cardiovascular system in health and disease, and systemic cholesterol homeostasis is achieved by its synthesis and conversion to BAs in the liver as well as feedback mechanisms mediated by BAs (Phelps et al., 2019). Thus, future work should probe the mechanisms by which BACs may impact sex hormone synthesis and levels by using a) in vitro/culture techniques and co-dosing estrogen/androgen and BACs and evaluating metabolism and b) conventional versus GF mouse models and sex hormone analysis.

In Chapter 4, we described a comprehensive multiomics analysis of BAC-induced endogenous and exogenous shifts in the metabolism of the livers of BAC-exposed mice. When measuring the lipidome of BAC-exposed mice relative to controls, we observed distinct shifts in the lipid profiles of lipid classes, including PA, PC, PE, PI, PG, PS, and SM. Aside from acting as structural elements in biological membranes, storing energy, and functioning as signaling molecules, disruption in levels of lipid expression is seen in disease states like obesity, diabetes, and immune disorders (Finkelstein et al., 2014). Moreover, we observed a more potent response in lipid class shifts in the male cohort compared to the female cohort. For example, in both BAC-treated groups, lipid class totals in PC, PE, PG, and PS were all significantly increased relative to controls in the male cohort. Total intensities of all lipids identified were increased in both C12 and C16 male groups and in the female C16 group. Importantly, accumulation of lipids in the liver is observed in obesity and NAFLD (Holter et al., 2020). Additionally, we observed decreases in PA. NRs like TGR5 and LXR

play important roles in the regulation of lipid, glucose, and energy metabolism to maintain metabolic homeostasis. Additionally, Tgr5−/− mice exhibited increased lipid deposition in male mice compared to female mice, suggesting the effect of TGR5 signaling on liver lipid deposition may be influenced by sex (Holter et al., 2020). Thus, future work should consider validating the mechanisms by which BACs elicit their effect on endogenous lipid metabolism. To do this, more work could be completed within in vitro/culture systems, evaluating microbiome-independent versus microbiome-dependent lipid changes using a GF model, studying NRs TGR5 and LXR, and quantifying lipids versus using relative intensities. This would be especially useful in potentially mechanistically validating the result of the female C12-BAC-exposed group having little to no significant shift in lipid profile. Additionally, as described above, studying sex hormones within the BAC-exposed mice and their roles in lipid synthesis would be a great asset to understanding sex-related and specific responses to BACs.

Lastly, in Chapter 4, we described novel insight into BAC-induced shifts in DME capability. Specifically, in the C16 BAC-exposed female cohort, we provide preliminary evidence of Cyp1a induction. CYP1A is an important DME that participates in the biotransformation of up to 9% of clinical drugs and is additionally involved in biological activation or deactivation of pollutants like benzopyrene (Lu et al., 2020). Furthermore, CYP1A is important in the biotransformation of endogenous substances like linoleic acid, PC, estradiol, and testosterone (Lu et al., 2020). Additionally, CYP1A affects both male and female reproductive systems, and CYP1A-mediated metabolic disorders may lead to lower birth and survival rates (Lu et al., 2020). Thus, follow-up experiments should validate whether Cyp1a was induced in the C16 BAC-exposed female liver group. Additionally, through RNA sequencing analysis, we observed plenty of Cyp gene expression changes. However, through incubation studies, we did not observe changes in the

metabolism of Cyp2, Cyp3 or Cyp4 probes. Thus, it will be important first to validate RNA sequencing results by qPCR, and subsequently, in another animal study, it would be interesting to evaluate if a longer BAC exposure time would be necessary to observe the effects of the gene expression changes. Lastly, to evaluate the effect of BACs on the metabolizing capabilities of the MLMs, it should be considered to test the Cyp probes and BACs together.

Chapter 5 References

Finkelstein, J. *et al.* (2014) Lipids in health and disease. *Nature*, **510**, 47–47.

Fleishman, J.S. and Kumar, S. (2024) Bile acid metabolism and signaling in health and disease: molecular mechanisms and therapeutic targets. *Signal Transduct. Target. Ther.*, **9**, 97.

Holter, M.M. *et al.* (2020) TGR5 Signaling in Hepatic Metabolic Health. *Nutrients*, **12**, 2598.

Jiang, L. *et al.* (2021) Farnesoid X receptor (FXR): Structures and ligands. *Comput. Struct. Biotechnol. J.*, **19**, 2148–2159.

Kim, Y.S. *et al.* (2020) Sex Differences in Gut Microbiota. *World J. Mens Health*, **38**, 48.

Koliada, A. *et al.* (2021) Sex differences in the phylum-level human gut microbiota composition. *BMC Microbiol.*, **21**, 131.

Koontz, J.M. *et al.* (2019) The Role of the Human Microbiome in Chemical Toxicity. *Int. J. Toxicol.*, **38**, 251–264.

Lu, J. *et al.* (2020) New insights of CYP1A in endogenous metabolism: a focus on single nucleotide polymorphisms and diseases. *Acta Pharm. Sin. B*, **10**, 91–104.

Manor, O. *et al.* (2020) Health and disease markers correlate with gut microbiome composition across thousands of people. *Nat. Commun.*, **11**, 5206.

Monte, M.J. *et al.* (2009) Bile acids: Chemistry, physiology, and pathophysiology. *World J. Gastroenterol.*, **15**, 804.

Phelps, T. *et al.* (2019) The influence of biological sex and sex hormones on bile acid synthesis and cholesterol homeostasis. *Biol. Sex Differ.*, **10**, 52.

Rinninella, E. *et al.* (2019) What is the Healthy Gut Microbiota Composition? A Changing Ecosystem across Age, Environment, Diet, and Diseases. *Microorganisms*, **7**, 14.

Shulpekova, Y. *et al.* (2022) The Role of Bile Acids in the Human Body and in the Development of Diseases. *Molecules*, **27**, 3401.

Siddiqui, R. *et al.* (2022) The Gut Microbiome and Female Health. *Biology*, **11**, 1683.

Tian, S. *et al.* (2022) FXR: structures, biology, and drug development for NASH and fibrosis diseases. *Acta Pharmacol. Sin.*, **43**, 1120–1132.